JPRS L/8859

10 January 1980

USSR Report

ELECTRONICS AND ELECTRICAL ENGINEERING

(FOUO 1/80)

FBIS FOREIGN BROADCAST INFORMATION SERVICE

NOTE

JPRS publications contain information primarily from foreign newspapers, periodicals and books, but also from news agency transmissions and broadcasts. Materials from foreign-language sources are translated; those from English-language sources are transcribed or reprinted, with the original phrasing and other characteristics retained.

Headlines, editorial reports, and material enclosed in brackets [] are supplied by JPRS. Processing indicators such as [Text] or [Excerpt] in the first line of each item, or following the last line of a brief, indicate how the original information was processed. Where no processing indicator is given, the information was summarized or extracted.

Unfamiliar names rendered phonetically or transliterated are enclosed in parentheses. Words or names preceded by a question mark and enclosed in parentheses were not clear in the original but have been supplied as appropriate in context. Other unattributed parenthetical notes within the body of an item originate with the source. Times within items are as given by source.

The contents of this publication in no way represent the policies, views or attitudes of the U.S. Government.

For further information on report content call (703) 351-2938 (economic); 3468 (political, sociological, military); 2726 (life sciences); 2725 (physical sciences).

APPROVED FOR RELEASE: 2007/02/08: CIA-RDP82-00850R000200040025-8

JPRS L/8859

10 January 1980

USSR REPORT

ELECTRONICS AND ELECTRICAL ENGINEERING

(FOUO 1/80)

This serial publication contains articles, abstracts of articles and news items from USSR scientific and technical journals on the specific subjects reflected in the table of contents.

Photoduplications of foreign-language sources may be obtained from the Photoduplication Service, Library of Congress, Washington, D. C. 20540. Requests should provide adequate identification both as to the source and the individual article(s) desired.

CONTENTS PAGE

CONTENTS (Continued)

Antennas

UDC 621.396.677.8.001.5

CYLINDRICAL ANTENNA ARRAYS WITH COHERENT OPTICAL SIGNAL PROCESSING

Kiev IZVESTIYA VYSSHIKH UCHEBNYKH ZAUEDENIY RADIOELEKTRONIKA in Russian
Vol 22 No 5, May 79 pp 29-34

[Article A.Yu. Grinev and Ye.N. Voronin, manuscript received 30 Jun 78]

[Text] The specific features of the shaping of the receive beams of aplanar antenna arrays by radio-optical methods which allow for a parallel view of space in a broad sector of angles are treated. The possibility of the reduction of the coherent optical processor of a cylindrical antenna array is demonstrated and an example is adduced.

The shaping of the receive beams of aplanar antennas by coherent optical (KO) methods in an approximation of a continuous aperture was analyzed in [1]. The results of [1] are extended to discrete apertures in the form of antenna arrays [AR's] consisting of radiators arranged on an aplanar geometric or conducting surface.

The "radio value" image, as follows from [1], is generated in the form of a continuous fan of directional patterns (DN's) of the antenna F(K, K'), modulated by the angular spectrum of received radio waves:

$$\tilde{\vec{E}}(\vec{K}') = \iint_{4\pi} \vec{E}(\vec{K}) \vec{F}(\vec{K}, \vec{K}')\, d\Omega, \tag{1}$$

when the aperture response of the antenna is acted upon by the following operator:

$$\hat{L}\{\ldots\} = \iint_{\Sigma} \ldots \dot{J}_{opt}(\vec{R}, \vec{K}')\, d^2\vec{R}, \tag{2}$$

where $\dot{J}_{opt}(\vec{R}, \vec{K}')$ is the optimal (for example, in terms of the side lobe suppression, directional gain, etc.) amplitude-phase distribution (AFR) of the excitation of the aperture for the case of pencil-beam reception from the direction $\vec{K}'$ ($\vec{K}'$ is a wave vector); Σ is the aperture surface; $\vec{R}$ is the current point of the aperture.

In the case of an antenna array of N radiators, positioned at the points $\vec{R}_n$, the directional pattern in (1) has the form:

$$\vec{F}_{AP}(\vec{K}, \vec{K}') = \sum_{n=1}^{N} \vec{F}_э(\vec{K}, \vec{R}_n) \exp - i\vec{K}\vec{R}_n \dot{J}_{opt}(\vec{R}_n, \vec{K}'), \tag{3}$$

where $\vec{F}_э(\vec{K}, \vec{R}_n)\exp -i\vec{K}\vec{R}_n$ is the directional pattern of the n-th element, referenced to the origin of the coordinates.

On analogy with [1], by using (1) and (3) instead of (2), we obtain:

$$\hat{L}_{AP}\{\ldots\} = \sum_{n=1}^{N} \ldots \dot{J}_{opt}(\vec{R}_n, \vec{K}'). \tag{4}$$

We will note that similarly to algorithm (2), operator (4) has the equivalent alternative:

$$\hat{\dot{L}}_{AP}\{\ldots\} = \sum_{n=1}^{N} \ldots \dot{J}_{opt}(\vec{R}_n, \vec{K}') \tag{5}$$

(where the symbol * signifies the complex conjugate), which in contrast to (4), generates a focused image of the type (1) in the form of a first order diffraction negative [1].

It is expedient to express operator (4) in terms of operator (2) by making use of the Dirac function $\delta(\vec{R}, \vec{R}_n)$:

$$\hat{L}_{AP}\{\ldots\} = \hat{L}\left\{\ldots \sum_{n=1}^{N} \delta(\vec{R}, \vec{R}_n)\right\}. \tag{6}$$

As we see, the requisite coherent optical processing using algorithm (4) reduces to processing with algorithm (2), carried out by means of the corresponding KOP [coherent optical processor] for a continuous aperture [1], if in this case the input signal of the KOP is "weighted" with the "Dirac comb" $\sum_{n=1}^{N} \delta(\vec{R}, \vec{R}_n)$. It is obvious that an N-channel spatial-time light modulator (PVMS) can serve as the latter, where the modulator channels are arranged in accordance with the law governing the addressing of the original KOP.

It is appropriate to note that algorithm (6) encompasses all the special cases of antenna array radiator arrangement (equally spaced and nonequally spaced) in the surface of the aperture, something which indicates the invariance of algorithm (2), and this means also, that of the corresponding KOP with respect to the location of the radiators. It likewise follows from (6) that the properties of a ROAR [unknown type of antenna array], which were studied in a continuous aperture approximation [1], are also extended to a discrete aperture. However, along with the cited continuity, certain specific features are also observed:

a) In the case of processing using algorithm (6), auxiliary algorithm (2) and the KOP corresponding to it are not uniquely alike since one can take as the filtering property of the δ-function in place of operator (2) in (6) any other one:

$$\hat{L}'\{\ldots\} = {}_{\Sigma}\iint \ldots \dot{J}'_{opt}(\vec{R}, \vec{K}')\, d^2\vec{R} \neq \hat{L}\{\ldots\},$$

in which

$$\left.\begin{aligned} \dot{J}'_{opt}(\vec{R}, \vec{K}) &= \dot{J}_{opt}(\vec{R}, \vec{K}) \text{ при } \vec{R} = \vec{R}_n \\ \dot{J}'_{opt}(\vec{R}, \vec{K}) &\neq \dot{J}_{opt}(\vec{R}, \vec{K}) \text{ при } \vec{R} \neq \vec{R}_n \end{aligned}\right\}; \tag{7}$$

the circumstance cited here points to the fact that algorithm (2) is redundant with respect to operator (4), and this permits optimizing algorithm $\hat{L}'\{\ldots\}$, and consequently, also the KOP within the limits of that freedom in the selection of the amplitude-phase distribution which is permitted by expressions (7);

b) The "Dirac comb" model in the form of an N-channel PVMS is an approximate one, since each of its channels has a distributed structure and is not described by the δ-function, but rather by finite width pupil function $J_\delta(\vec{R}, \vec{R}_n)$ (for the sake of convenience, this function is tied to the coordinate system of the antenna array) and therefore, instead of (6) we have:

$$\tilde{\hat{L}}_{AP}\{\ldots\} = \hat{L}\left\{\sum_{n=1}^{N} \ldots J_\delta(\vec{R}, \vec{R}_n)\right\} = \sum_{n=1}^{N} \ldots \tilde{\dot{J}}_{opt}(\vec{R}, \vec{K}') \neq \tilde{L}_{AP}\{\ldots\}, \tag{8}$$

where

$$\tilde{\dot{J}}_{opt}(\vec{R}_n, \vec{K}') = \hat{L}\{J_\delta(\vec{R}, \vec{R}_n)\} \neq \dot{J}_{opt}(\vec{R}_n, \vec{K}') = \hat{L}\{\delta(\vec{R}, \vec{R}_n)\};$$

As we see, the approximation of the "comb" with the pupil function results in a distortion of the specified amplitude-phase distribution, and consequently, in the requisite algorithm for coherent optical processing, and for this reason, it is necessary in a number of cases to accordingly compensate for the pupil effect;

c) Inherent in the PVMS, as a system of N channels close together and controlled by an electrical field is the effect of mutual influence between the channels.

Only the first of the effects mentioned here is studied in the following using the example of a cylindrical ROAR.

A KOP was synthesized in [1, Figure 1] which reproduces algorithm (2) for a continuous cylindrical aperture of radius R_0:

$$\hat{L}\{\ldots\} = \hat{F}_{\varphi}^{-1}\{\hat{F}\{\ldots J(Z)\}\dot{T}(\Omega_{\varphi}, \Omega_Z')\}, \quad (9) \qquad (9)$$

where

$$\dot{T}(\Omega_{\varphi}, \Omega_Z') = \hat{F}_{\varphi}\{J_{\varphi}(\varphi)\exp(-iR_0\sqrt{K^2 - \Omega_Z'^2}\cos\varphi)\}, \quad (10) \qquad (10)$$

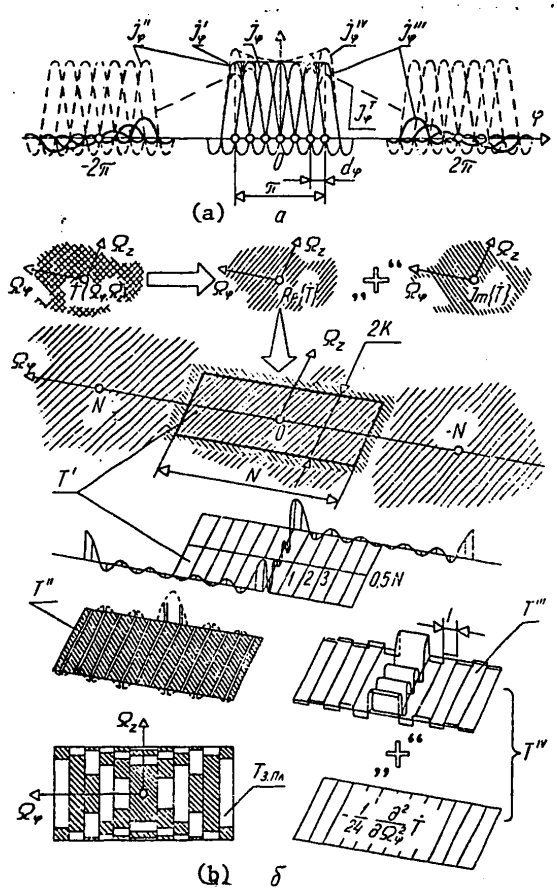

Figure 1.

$\hat{F}$, $\hat{F}_{\phi}$ are operators for two-dimensional and one-dimensional Fourier transforms respectively; $K = 2\pi/\Lambda$, Λ is the radio wavelength; $J(Z)$ and $J_{\phi}(\phi)$ are the partial amplitude-phase distributions; Ω_Z and Ω_{ϕ} are the spatial frequencies.

In accordance with (7), operator (9) permits a reduction. We shall demonstrate the reduction using the example of simplification of transparency (10), the structure of which is substantially determined by the form of the amplitude-phase response:

$$\dot{J}_\varphi(\varphi, \Omega_z) = J_\varphi(\varphi) \exp(-iR_0 \sqrt{K^2 - \Omega_z^2} \cos\varphi) \tag{11}$$

and consequently, is more susceptible to reduction. For a cylindrical antenna array with radiators at the nodes of a rectangular grid (Figure 1, [1]), in place of (11), we form a new amplitude-phase response (Figure 1a):

$$\dot{J}'_\varphi(\varphi, \Omega_z) = \sum_{n=-\infty}^{\infty} \dot{J}_\varphi(nd_\varphi, \Omega_z) \operatorname{sinc}(\varphi/d_\varphi - n), \tag{12}$$

where sinc(n) is the readout function [2]; $d_\phi = 2\pi/N$ is the azimuthal spacing of the grid (N is the number of elements in a ring). Since (12) satisfies (7), then instead of transparency (10), one can use a new transparency (Figure 2b):

$$\begin{aligned} \dot{T}'(\Omega_\varphi, \Omega_z) = \hat{F}_\varphi\{\dot{J}'_\varphi(\varphi, \Omega_z)\} = \sum_{n=-\infty}^{\infty} \dot{J}_\varphi(nd_\varphi, \Omega_z) \hat{F}_\varphi\{\operatorname{sinc}(\varphi/d_\varphi - n)\} = \\ = \operatorname{rect}(\Omega_\varphi/N) \frac{1}{N} \sum_{n=-\infty}^{\infty} \dot{J}(nd_\varphi, \Omega_z) \exp(i\Omega_\varphi n d_\varphi) = \\ = \operatorname{rect}(\Omega_\varphi/N) \sum_{n=-\infty}^{\infty} \dot{T}(\Omega_\varphi + nN, \Omega_z), \end{aligned} \tag{13}$$

where Poisson's summing formula is employed [2]. As we see, in contrast to (10), transparency (13) is finite and entirely located within the rectangular window (Figure 1b):

$$-\frac{N}{2} \leqslant \Omega_\varphi \leqslant \frac{N}{2}, \quad -K \leqslant \Omega_z \leqslant K,$$

where for the sake of clarity, the reduction of only the real part of the transparency transmittance is shown, which is also shown in Figure 5 in [1].

We shall continue the reduction of the transparency, forming a new amplitude-phase distribution of the following form (see Figure 1a) instead of (12):

$$\dot{J}''_\varphi(\varphi, \Omega_z) = \sum_{m=-\infty}^{\infty} \dot{J}'_\varphi(\varphi + 2\pi m, \Omega_z), \tag{14}$$

which likewise satisfies condition (7). For this reason, one can employ a transparency of the following form instead of (13):

$$\dot{T}''(\Omega_\varphi, \Omega_z) = \hat{F}_\varphi\{\dot{J}''_\varphi(\varphi, \Omega_z)\} = \operatorname{comb}(\Omega_\varphi) \dot{T}'(\Omega_\varphi, \Omega_z), \tag{15}$$

where $\operatorname{comb}(\Omega_\varphi) = \sum_{n=-\infty}^{\infty} \delta(\Omega_\varphi - n)$ is an equally spaced "Dirac comb".

Thus, transparency (13) does not necessarily have to be reproduced entirely, and it is sufficient to limit it to samples along the lines $\Omega_\phi = 0$, ± 1 ± 2, ... $\pm 0.5N$ (N + 1 lines in all). Transparency (15) is weighted with the "Dirac comb" and is physically not feasible. For this reason, we shall approximate it with the following transparency (Figure 1b):

$$\dot{T}^{III}(\Omega_\varphi, \Omega_z) = \sum_{n=-\infty}^{\infty} T_\delta(\Omega_\varphi - n)\,\dot{T}^{I}(n, \Omega_z), \tag{16}$$

where

$$T_\delta(\Omega_\varphi) = \begin{cases} 1, & \Omega_\varphi = 0, \\ 0, & |\Omega_\varphi| > 0{,}5. \end{cases}$$

Transparency (16) is physically feasible, however, in this case condition (7) is violated. In fact, according to (10), the following amplitude-phase distribution (Figure 1a) corresponds to transparency (16):

$$\dot{J}^{III}_\varphi(\varphi, \Omega_z) = \widehat{F}_\varphi^{-1}\{\dot{T}^{III}(\Omega_\varphi, \Omega_z)\} = J^T_\varphi(\varphi)\,\dot{J}^{II}_\varphi(\varphi, \Omega_z), \tag{17}$$

where $J^T_\varphi(\varphi) = \widehat{F}_\varphi^{-1}\{T_\delta(\Omega_\varphi)\}$.

If $J^T_\phi(\phi) \simeq 1$ when $-\pi/2 \leq \phi \leq \pi/2$, then amplitude-phase distribution (17) satisfies (7). In particular, when $T_\delta(\Omega_\phi) = \text{rect}\,(\Omega_\phi)$, we have $J^T_\phi(\phi) = \text{sinc}(\phi/2\pi) \simeq 1 - \phi^2/24 \geq 0.9$ throughout the entire range $|\phi| \leq \pi/2$. However, if the nonuniformity of the function $J^T_\phi(\phi)$ is unsatisfactory, for example, based on the resulting reduction in the directional gain, then one can narrow the envelope $T_\delta(\Omega_\phi)$ (however, this is unfavorable in a power engineering sense), or one can introduce in place of (17) the following corrected amplitude-phase distribution (Figure 1a):

$$\dot{J}^{IV}_\varphi(\varphi, \Omega_z) = \dot{J}^{III}_\varphi(\varphi, \Omega_z)/J^T_\varphi(\varphi) \cong \dot{J}^{III}_\varphi(\varphi, \Omega_z)\left(1 + \frac{\varphi^2}{24}\right),$$

to which the following transparency corresponds according to (10):

$$\dot{T}^{IV}(\Omega_\varphi, \Omega_z) = \sum_{n=-\infty}^{\infty} \text{rect}\,(\Omega_\varphi - n)\left[\dot{T}^{III}(n, \Omega_z) - \frac{1}{24}\frac{\partial^2}{\partial \Omega_\varphi^2}\dot{T}(\Omega_\varphi, \Omega_z)\big|_{\Omega_\varphi = n}\right]. \tag{18}$$

Transparencies of the type of (16) and (18) are structurally extremely simple and take the form of N + 1 parallel bands with a width of 1 and a length of 2 K, which are uniformly transparent along Ω_ϕ (Figure 1b). We will note that a transparency of such a structure is suitable only for an antenna array with a specified geometry for the placement of the radiators.

The proposed reduction of transparency (10), achieved as a result of an arbitrary selection of the amplitude-phase distribution within the framework

of expression (7) can be supplemented by a reduction of the redundancy of the analytical transmission function $\hat{T}$ as the Fourier transform of a finite amplitude-phase distribution [2]. For example, we shall reproduce the real part of function (10), $\mathrm{Re}\hat{T} = (1/2)(\hat{T} + \hat{T}^*)$, which according to (10) and (11), corresponds to an amplitude-phase distribution of the form:

$$\hat{F}_{\varphi}^{-1}\{\mathrm{Re}\,\hat{T}\} = \frac{1}{2}[\dot{J}_{\varphi}(\varphi, \Omega_z) + \dot{J}_{\varphi}^{*}(\varphi, \Omega_z)].$$

The amplitude-phase distributions obtained using (4) and (5) realize the following processing algorithm:

$$\hat{L}_{\mathrm{Re}}\{\ldots\} = \frac{1}{2}\hat{L}\{\ldots\} + \frac{1}{2}\hat{L}^{*}\{\ldots\},$$

which, in contrast to (9), generates the superposition of four images conjugate in pairs (a pair of focused ones F^{+1}, F^{-1}, and a pair of defocused ones, F^{+1}, F^{-1}) for the case of a two-band PVMS (Figure 2a) [3].

We shall estimate the level of defocusing of one of the $F^{\pm 1}$ images as compared to the focused one $F^{\pm 1}$. In accordance with the principle of an equivalent plane aperture, the following estimate is justified for the relative reduction in the directional gain:

$$D_{F^{\pm 1}}/D_0 \cong \left| \int_0^{\frac{\pi}{2}} \exp\,(i2KR_0 \sin\theta \cos\varphi) \cos\varphi\, d\varphi \right|^2 \cong \frac{0{,}125\,\Lambda}{|\sin\theta|\,R_0},$$

Where the steady-state phase method of [2] is used, taking into account the fact that $KR_0 >> 2\pi$. The latter function is shown in Figure 2b (a logarithmic scale is used along the horizontal axis). We will note that the estimate obtained actually characterizes the defocusing of the first order diffraction negative with operator (4) or the first order positive with operator (5).

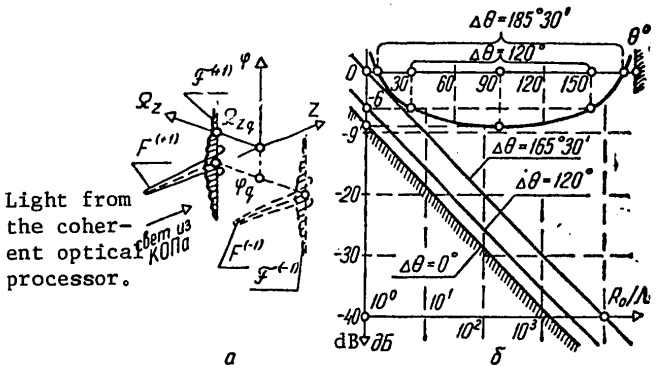

Figure 2.

The reduction of the complex transparency (10) - $\dot{T}$ (Figure 1b) carried out here is justified for the real transparency Re$\dot{T}$. By using an analytical expression for transparency (10), derived in [1] for the case of $J_\phi(\phi) = \text{reet}(\phi/\pi)$, we shall find the real part of (16):

$$\operatorname{Re}\left[\dot{T}^{III}(\Omega_1, \Omega_2)\frac{1}{\pi}\exp -\frac{i\pi}{2}\Omega_\varphi\right] \cong J_{-\text{entier}\Omega_\varphi}(\sqrt{K^2-\Omega_z^2}R_0), \tag{19}$$

where it is taken into account that when $\Omega_\phi = \text{entier}\Omega_\phi = n$, the Anger function (18) [1] degenerates into a Bessel function $J_{-n}(...)$. One section of the resulting function $J_0(\sqrt{K^2-\Omega_z^2}R_0)$ where $KR_0 = 10$ is shown in Figure 1b.

BIBLIOGRAPHY

1. Grinev A.Yu., Voronin Ye.N., "Formirovaniye priyemnykh luchey neploskikh antenn radiooptycheskimi metodami" ["The Shaping of the Receive Beams of Aplanar Antennas by Radio-optical Methods"], IZV. VUZOV - RADIOELEKTRONIKA [PROCEEDINGS OF THE HIGHER EDUCATIONAL INSTITUTES, RADIOELECTRONICS], 1979, 22, No 2, p 25.

2. Papulis A., "Teoriya sistem i preobrazovaniy v optike" ["Transformations and Systems Theory in Optics"], Moscow, Mir Publishers, 1971.

3. Grinev A.Yu., Voronin Ye.N., "Preobrazovaniye prostranstvenno-vremennogo spektra antennymi reshetkami s obrabotkoy signala metodami kogerentnoy optiki" ["Spatial-Time Spectral Conversion by Antenna Arrays with Signal Processing Using the Methods of Coherent Optics"], IZV. VUZOV - RADIOELEKTRONIKA, 1798, 21, No 2, p 74.

8225
CSO:1870

ELECTRONIC SYNTHESIS OF TV PICTURES

Moscow ELEKTRONYY SINTEZ TELEVIZIONNYCH IZOBRAZHEMIY in Russian 1979 pp 3, 256

[Annotation and table of contents from book by Il'ya Naumovich Guglin, Izdatel'stvo Sovetskoye Radio, 256 pages]

[Text] This book considers the physical bases of forming TV pictures without a camera. Devices designed on the basis of analog, digital and combined methods are described. The principles of forming primary signals as well as static and dynamic complex pictures are considered in detail. Considerable attention is devoted to questions of forming test signals, synchronizing signals, visual TV indications, visual imitation arrangements and devices for multipoint monitoring. Examples of the use of electronic synthesis in automatic TV computer devices are cited.

The book is intended for a wide circle of specialists interested in questions of electronic synthesis in TV, automatic TV computer devices, systems of visual presentation of data, remote, computer techniques, etc. It may be useful also to students and instructors of corresponding vuz.

14 tables, 130 pictures, 229 bibliography titles.

Table of Contents

Table of Contents

Table of Contents

[28-2291]

2291
CSO: 1860

Communications, Communications Equipment;
Networks; Data Transmission and Processing

UDC 621.31.5•2.029.5

WAVEGUIDE TRANSMISSION LINES

Moscow VOLNOVODNYYE LINII PEREDACHI (Waveguide Transmission Lines) in Russian 1979 signed to press 22 Feb 79 pp 2, 23-231

[Annotation and table of contents from book by Ivan Yefimovich and Galina Arsen'yevna Shermina, Izdatel'stvo Svyaz', 3,600 copies 232 pages]

[Text] This book examines modern types of waveguide systems: waveguides of rectangular, round cross-section, channel-bar waveguide and H sections, elliptical and dielectric waveguides, surface wave transmission lines and lightguides. The authors present design and electrical characteristics of various types of transmission lines and methods of calculating them.

This book is intended for communications engineers and technicians in the cable and radio electronics industry.

Contents

[264-3024]

3024
CSO: 1860

UDC 621.374.32:519.218

AVERAGE RECURRENCE FREQUENCY OF NOISE OVERSHOOTING IN A DIGITAL REVERSIBLE MEMORY

Moscow RADIOTEKHNIKA in Russian Vol 34, No 7 pp 53-54

[Article by N. A. Bol'shakov, submitted 4 Sep 1978]

[Text] The digital reversible memory (TsRN) containing a reversible counter in which binary signals 1 and 0 are summed in the form of digital signals $s \geqslant 1$ and $v = -1$, respectively, as was shown by experimental studies [1], is effective in detecting and measuring signal parameters. Unlike the moving-window binary memory, the TsRN is simpler in realization, because it does not contain a shift register for storing the readout in the window. The frequency of false solutions in it is determined by the recurrence frequency of noise overshooting [2]

$$F_в = F_д \frac{W(n \geqslant L)}{\overline{K}}, \qquad (1)$$

where $F_д$ -- sampling frequency; R -- average length of overshooting; $W(n \geqslant L)$ -- probability of exceeding the threshold L by the accumulated sum n.

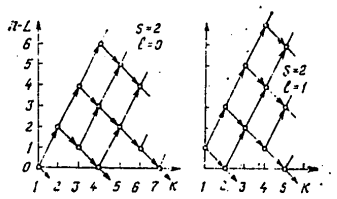

In order to define $\overline{K}$, it is necessary to obtain the distribution of the lengths of overshooting. The figure gives examples of transition trees illustrating the behavior of the sum above the threshold L if the accumulated signals are uncorrelated. The transitions of the sum upward to s occur with probability p or downward to 1 with probability q=1-p, where p is the probability of the appearance of the signal s. In summing a number $s > 1$, the overshooting can begin with the state $L+l$, where $l = 0, 1, 2, \ldots, s-1$. The probability of the formation of overshooting with a length of k steps from

the first entry of the sum into above-threshold states to the first entery into the below-threshold state is determined by summing the probabilities of all moves over the transition tree leading to the termination of the overshooting at the k-th step. The summing of the probabilities leads to the formation of infinite series given in the table.

Searching for the rule of the formation of the terms of the series obtained on the basis of transition trees showed that the terms of the series can be computed with the aid of the following normalized expression

$$W(k, l) = \frac{1+l}{k} C_k^{\frac{k-l-1}{s+1}} p^{\frac{k-l-1}{s+1}} q^{\frac{sk+l+1}{s+1}}, \quad (2)$$

where $k = (1+l),\ (1+l)+(1+s),\ (1+l)+2(1+s), \ldots, (1+l)+m(1+s), \ldots, \infty$.

s	l	k									
		1	2	3	4	5	6	7	8	9	10...
1	0	q	0	rq^3	0	$2p^2q^3$	0	$5p^3q^4$	0	$14p^4q^5$	0...
2	0	q	0	0	rq^3	0	0	$3p^2q^5$	0	0	$12p^3q^7$
	1	0	q^2	0	0	$2pq^4$	0	0	$5p^2q^6$	0	0...

By using the induction method it is possible to show that expression (2) is applicable for $s \geqslant 0$. When s = 0, the distribution (2) changes to the Pascal law. The distribution W(k) is obtained from (2) by averaging over a random value l. As a result of weight addition of nonoverlapping lattices W(k, l), the W(k) distribution also is a lattice in which nonzero terms are obtained when k = (1+s)(1+m), where m=0, 1, ..., ∞. The average length of overshotting is equal to

$$\overline{K} = \sum_{k=1+l}^{k=\infty} kW(k) = \sum_{l=0}^{l=s-1} \overline{k}(l) W(l) \Big/ \sum_{l=0}^{l=s-1} W(l), \quad (3)$$

where

$$\overline{k}(l) = \sum_{k=1+l}^{k=\infty} kW(k, l). \quad (4)$$

Direct computation by (4) shows that $\overline{K}(l) = (1+l)/[1-p(s+1)] = 1+q)/(q-ps)$, $s \geqslant 0$. The value of $\overline{K}$ is determined by the numerical method.

In order to determine the probabilities W(n $\geqslant$ L) and W(l), it is necessary to find the distribution W(n) of the sum in the TsRN. The W(n) distribution can be calculated through solving the matrix equation [3]

$$W(n)(B-I)=0, \tag{5}$$

where B is the matrix of the probabilities of transitions of the sum; I is the unit matrix.

For the ergodic Markov chain, solution (5), which can be converted to an algebraic system of difference equations with constant coefficients has the following form when s=1:

$$W(n)=\left(1-\frac{p}{q}\right)\left(\frac{p}{q}\right)^{n},$$

and for $s>1$, the solution can be expressed approximately through the exponential rule. For the exponential rule of W(n), average lengths and the recurrence frequency of noise overshooting are equal to:

$$\overline{K}=1/(q-ps); \quad F_B=F_L qW(n=L). \tag{6}$$

Expressions (6) are exact at s=1 and are approximate at $s>1$. The simulation of TsRN on a digital computer by the Monte-Carlo method showed that at $s\leq 4$ the accuracy of the determination of the value F_B by (6) is not worse than one percent. It can be shown that the expression for F_B at s=1 remains exact even if the capacity of the reversible counter is limited, which results in the limitation of the amplitude of overshooting, and that at $s>1$ its accuracy, as was shown by simulation, is retained regardless of the capacity of the counter.

Bibliography

1. Minguzzi, B., and Picardi, G. ALTA FREQUENZA, Vol 39, No 11, 1970.

2. Likharev, V. A. "Tsifrovyye metody i ustroystva v radiolokatsii" [Digital Methods and Devices in Radar], Sovetskoye radio, Moscow, 1973.

3. Kemeni, Dzh., and Snell, Dzh. "Konechnyye tsepi Markova" [Finite Markov Chains], Nauka, Moscow, 1970.

10,233
CSO: 1860

UDC 621.391.2

EPXERIMENTAL STUDY OF SPACE-TWO-CHANNEL DETECTION RECEIVER--INTERFERENCE COMPENSATOR

Kiev IZVESTIYA VYSSHIKH UCHEBNYKY ZADEDENIY: RADIOELEKTRONIKA in Russian No 7, 79 signed to press 10 May 78; after revision 10 Oct 79 pp 98-100

[Article by B. A. Lazutkin, A. B. Lazutkin, V. V. Mansurov, B. B. Pospelov]

[Text] In [1] was obtained the structural arrangement of an optimal receiver with respect to the criterion of the maximum ratio of probability, and a two-channel version of such a receiver was studied analytically. The possibility was shown as, a result of such a study, of the possibility of full compensation of stationary interferences, created by an external source, located at an arbitrary point of a remote zone. It was assumed in the analytical study that averaging multipliers (correlators), multipliers, band filters, summing and subtracting devices are ideal and, further more, phenomena of limiting interferences and useful signals in various receiver components were not taken into account. The characteristics of actual devices differ from the ideal ones, therefore, to check the degree of compensation of interferences in a space-two-channel receiver [1], an experimental device was assembled, with a structural arrangement as shown in Fig. 1, where G4-1A$_1$,G4-1A$_2$ are standard signal oscillators used to initiate the high frequency voltages of interferences and the useful signal at the outputs of a two-channel antenna with phase channel centers spaced by value d; G2-37 -- noise oscillator to produce amplitude modulation of the output voltage of oscillator G4-1A, by noise; M_1, M_2 -- pulse modulators of interference and useful signal voltages respectively; φ -- regulated phase rotator used to provide a phase difference

$$\psi = \frac{2\pi}{\lambda} d \sin \Theta$$

between high frequency interference oscillations in the first and second channels of the receiver (θ -- angular displacement of the interference source with respect to the reference direction of the two-channel antenna); C_1-54 -- monitoring oscillograph; EP -- emitter repeater to provide matching of modulator M_1, M_2 outputs to inputs of the two-channel receiver; PRM -- space-two-channel receiver (without antennas) in which, instead of single-dimensional filters matched to the spectrum of the useful signal, single-dimensional filters matched to the width of useful signal are used.

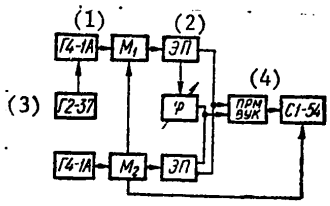

Fig. 1

1. G4-1A
2. EP
3. G2-37
4. PRM-VUK

The PRM operation is shown in Fig. 2 [1] .

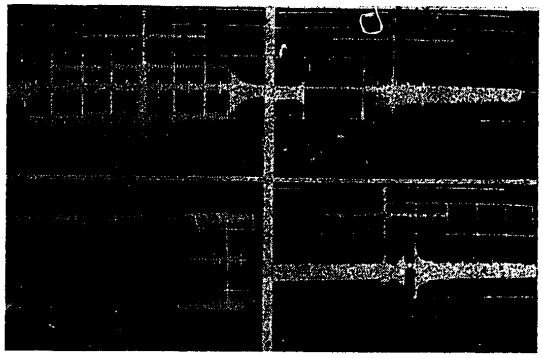

Fig. 2

The PRM was assembled with ordinary parts used in household equipment. For example, phase detectors are used as averaging multipliers and broadcasting receiver filters are used as band filters, retuned for the working frequency of the installation f_0 = 500kHz. The following signals were sent to the inputs of the two-channel PRM (Fig. 1) during the experiment:

1) useful signals in the form of a sequence of simple radio pulses with a frequency of high frequency oscillations equal to f_0=500kHz, pulse length τ_c considerably smaller and the period of following $T_н$ considerably greater than the time constants T_2 of the averaging amplifiers [1] ($\tau_c \ll T_2 \ll T_н$);

2) interferences -- long pulses of narrow band quasiharmonic fluctuations ($\tau_п \gg T_2$) with an average frequency equal to f_0;

3) a mixture of a sequence of radio pulses of the useful signals ($\tau_c \ll T_2 \ll T_н$) and pulses of narrow band quasi-harmonic fluctuations ($\tau_п \gg T_2$) overlapping in time. The frequency of high frequency oscillations f_0 of the radio pulses was equal to the average frequency of the narrow band fluctuations.

In the process of the experiment, phases of the high frequency oscillations of the useful signals at both inputs of the two-channel PRM were equal at each moment of time, which conformed to the coincidence of the direction of the useful signal source with the maximum of the total radiation pattern of the two-channel antenna. The oscillation phase of the narrow band of the quasi-harmonic fluctuations at one of the PRM inputs was changed in the process of the experiment by means of a phase rotator φ (Fig. 1), which corresponded to the shifting of the interference source with respect to a direction corresponding to the maximum of the total radiation pattern of the two-channel antenna.

Experimental investigations have indicated that in the installation per Fig. 1, when there is a useful signal, it is comparatively easy to compensate narrow band quasi-harmonic fluctuations, created by the source located at an arbitrary angle, of 15 to 30db. Compensation by 25 to 30db was achieved for a width of the interference fluctuations spectrum

$$\Delta f \approx (0{,}15 \div 0{,}10)\Delta f_s,$$

when Δf_s is the width of the useful signal spectrum at the half power level. When the interference spectrum widens to

$$\Delta f \approx 0{,}3\Delta f_s$$

the compensation efficiency fell to 12-13db.

Fig. 2 shows oscillograms of the input (Fig. 2a) and output (Fig. 2b) PRM voltages in the case where the duration of interference pulses $\tau_п$ is considerably greater than time constant T_2 of the averaging-multiplier (Fig. 2 [1]).

It follows from Fig. 2 that interference compensation is provided in the settled mode. The time of process settling in the PRM is proportional to time constant T_2. Beats are formed when there is a time overlap between interferences and useful signals at the PRM output.

The moment of the appearance of these beats coincides with the moment of arrival of the useful signal, while the duration is almost equal to the duration of the useful signal. The power of the useful signal and interference beats at the PRM output is greater than the power of the useful signal alone.

Fig. 2c and 2d represent oscillograms of the input (Fig. 2c) and output (Fig. 2d) PRM voltages for the case when the useful signal pulses are overlapped by continuous stationary narrow band fluctuations. The oscillograms of Fig. 2c and 2d correspond to the case when the useful signal to noise ratio q at the PRM (Fig. 1) input is equal to approximately 0.2db, while the useful signal to internal noise ratio q_o of the PRM is approximately 40db.

The nature of the useful signal and the interference beats at the PRM output depends on the ratios of q, q_o and the width of the fluctuation spectrum. Thus, for example, for $q \approx$ 40db and $\Delta f \approx 0.3\Delta f_c$, beats occur if the useful signal to noise ratio of the external source at the PRM inputs is within

$$-9\text{db} \lesssim q \lesssim 12\text{db}$$

for $q < -10$ db and $q_o \gtrsim 40$ db, it is practically impossible to detect the PRM output voltage and, thus, the installation in Fig. 1 compensates, in this case, for the useful signal together with the interferences.

For $q > 15$ db and $q_o < 40$ db, the beats of useful signals and the interferences practically do not differ from the output voltage of the interferences when there is no useful signal.

The results of the experimental investigation of the installation in Fig. 1 confirms in principle the possibility of compensating stationary narrow band fluctuations created by one source, positioned at an arbitrary angle θ to the reference direction (to the optical axis of the two-channel antenna).

The distinguishing feature of the system, corresponding to Fig. 1, is the possibility of compensating stationary narrow band interferences, the source of which is combined with the source of the useful signal. In this case, unlike well-known compensating arrangements, there is a possibility in principle of determining not only the bearing of the interference source, but also the distance to this source.

BIBLIOGRAPHY

1. Lazutkin, B. A. "On Some Additional Possibilities of Multichannel Detecting Systems." RADIOTEKHNIKA I ELEKTRONIKA, 1972, No 10, pp-2189-1291 [?].

[269-2291]

2291
CSO: 1860

UDC 621.391.2

OPTIMUM RECEPTION OF COMPLEX SIGNALS WITH UNDETERMINED MODULATION CHARACTERISTICS

Moscow RADIOTEKHNIKA I ELEKTRONIKA in Russian No 7 1979 pp 1360-1366

[Article by V. A. Cherdyntsev: "On Optimum Reception of Complex Signals with Undetermined Modulation Characteristics"]

[Text] The problem of reception of signals whose modulation characteristics are unknown at the receiving end is considered. On the basis of equations for simultaneous nonlinear filtering of discrete and continuous Markov processes is constructed a structural diagram of a receiver for a complex signal with an unknown phase modulation characteristic amplitude-modulated with binary information digits.

Introduction

In known studies on the reception of complex signals, the signal modulation characteristics are presumed to be known. Thus, for instance, in studies (1, 2) a pseudorandom sequence (PSP) is considered by which phase or frequency modulation of the carrier is accomplished. In this case, the optimum receiver is a unit which accomplishes tracking over the continuous parameters of the signal (phase, frequency, delay). When there is additional modulation of the signal with information digits, the latter may be extracted by a comparator whose reference signal is formed by a generator incorporated in a tracking circuit for the continuous parameters (3-5).

In a number of radio systems the receiver is operated under conditions where the structure of the received complex signal is partially or completely unknown. Specifically, with complex phase-modulated (FM) signals the signal modulating the PSP may be unknown. The problem of optimum reception of such signals has not been investigated before, although several circuits have been described which were obtained using aheuristic approach (6, 7).

In this study an unknown PSP modulating a complex signal is considered with a Markov circuit and information digits which modulate the signal further by a discrete Markov process. Under these conditions based on equations for simultaneous filtering of discrete and continuous Markov processes, a structural synthesis for an optimum receiver is produced.

1. Statement of the Problem.

A mixture r(t) of signal and noise is observed at the receiver input:

$$r(t)=s(t, \lambda, Z, X)+n(t).$$

Here n(t) is white noise with zero average value and a correlation function $\langle n(t_1)n(t_2)\rangle = 1/2N_0\delta(t_2 - t_1)$; the signal s(t) depends on the vector of the continuous parameters $\lambda = \{\lambda_1(t), \lambda_2(t), \ldots, \lambda_n(t)\}$, the components of which are described by stochastic differential equations

$$\frac{d\lambda_\beta(t)}{dt}=a_\beta(\lambda, t)+n_\beta(t), \quad \beta=\overline{1, n},$$

where $n_\beta(t)$ is whitenoise with the characteristics $\langle n_\beta(t)\rangle = 0$; $\langle n_\beta(t_1)n_\alpha(t_2)\rangle = \frac{1}{2}N_{\beta\alpha}\delta(t_2 - t_1)$; $a_\beta(\lambda, t)$ is the known function. The discrete parameter Z represents a single-type symmetrical Markov chain with m possible states $\zeta_1, \zeta_2, \ldots, \zeta_m$. Conversions from one state to another take place over a minimum interval τ_n which corresponds to the durations of the components modulating the PSP. A Markov process X with possible states $x_1, x_2, \ldots, x_i$ characterizes the sequence of information digits in accordance with which the parameters of the complex signal are varied. Probabilities P_j of the states of the Markov process X are given by the Chapman-Kolmogorov equation

$$(1) \qquad \frac{dP_j}{dt}=\sum_{r=1}^{l}\eta_{rj}P_r, \quad j=\overline{1, l},$$

where n_{rj} are the local probabilities of conversion of the X process from the state x_r to the state x_j (4). The X process under actual conditions proves to be "slower" than the Z of the PSP, i. e. in the limits of one information digit is contained $M \gg 1$ of the PSP components. The continuous processes λ_β (t), $\beta = 1,n$ have a correlation time of $\tau_{K\lambda}$ which satisfies the inequality

$$(2) \qquad \tau_{M\lambda} \gg \tau_n.$$

Hereinafter a statistical independence is assumed for the processes λ, Z and X.

The receiving unit should accomplish the extraction of information digits x_j with concurrent filtering of the vector of continuous parameters λ. The Markov properties of parameter Z impart specific qualities to the reception problem which will be noted in the further presentation.

2. Simultaneous Filtering Equations

As is known from (4), an optimum receiver forms an a posteriori density of distribution of the signal parameters. The equation which describes the combined distribution density $W(\lambda_{K+1}, Z_{K+1}, X_{K+1} | r_0^{K+1})$ for the moment t_{K+1} allowing for the observation at interval $(0, t_{K+1})$, r_0^{K+1} can be written as follows:

$$(3) \qquad W(\lambda_{k+1}, Z_{k+1}, X_{k+1}|r_0^{k+1}) = \frac{1}{W(\xi_k^{k+1}|r_0^k)} \exp\left[\int_{k\tau_n}^{(k+1)\tau_n} F(\lambda_{k+1}, Z_{k+1}, X_{k+1})\, dt\right] \sum_{Z_k} \sum_{X_k} \int_{\lambda_k} W(\lambda_k, Z_k, X_k|r_0^k)\, p(\lambda_{k+1}, Z_{k+1}, X_{k+1}|\lambda_k, Z_k, X_k)\, d\lambda_k.$$

where

$$F(\lambda_{k+1}, Z_{k+1}, X_{k+1}) = -\frac{1}{N_0}[r(t) - s(t, \lambda_{k+1}, Z_{k+1}, X_{k+1})]^2.$$

The probability of conversion $p(\lambda_{K+1} | \lambda_K)$ satisfies the equation (4)

$$(4) \qquad p(\lambda_{k+1}|\lambda_k) = \delta(\lambda_{k+1} - \lambda_k) + \tau_n L\delta(\lambda_{k+1} - \lambda_k) + \tau_n^2 \ldots,$$

where L is the Fokker-Planck-Kolmogorov operator and the probability of conversion $p(Z_{K+1} | Z_K)$ is the equation

$$(5) \qquad \sum_{Z_k} p(Z_k|r_0^k)\, p(Z_{k+1}|Z_k) = p(Z_{k+1}|r_0^k).$$

Taking into account (4), (5) and also the independence of parameters λ, Z, X and focusing attention on condition (1) after integration of equation (3) by λ_K, we write the equation for combined distribution density

$$(6) \qquad W(\lambda_{k+1}, Z_{k+1}=\zeta_i, X=x_j|r_0^{k+1}) = K_{k+1} \exp\left[\int_{k\tau_n}^{(k+1)\tau_n} F(\lambda_{k+1}, Z_{k+1}= \right.$$
$$= \zeta_i, X=x_j)\, dt\Big] \Big\{ W(\lambda_{k+1}, Z_{k+1}=\zeta_i, X=x_j|r_0^k) +$$
$$+ \tau_n L W(\lambda_{k+1}, Z_{k+1}=\zeta_i, X=x_j|r_0^k) +$$
$$\left. + \sum_{\gamma=1}^{l} \eta_{ij} W(\lambda_{k+1}, Z_{k+1}=\zeta_i, X=x_\gamma|r_0^k) \right\},$$

where $K_{K+1} = 1/W(r_K^{K+1} \quad r_0^K)$

Let us introduce for consideration the functional #3)

$$V_{ij}=\frac{1}{\tau_{\text{н}}}\left\{\exp\left[\int_{h\tau_{\text{н}}}^{(h+1)\tau_{\text{н}}} F(\lambda_{h+1}, Z_{h+1}=\zeta_i; X=x_j)\,dt\right]-1\right\};$$

Then taking into account the expansion $K_{K+1} = -\gamma\tau_n + \gamma\tau_n^2\ldots$, valid in executing the inequality (2), on the basis of (6) it is possible to write the equation in finite differences, disregarding here the terms on the order of τ_n^2 and higher. Further, having in view condition (2) we will convert from the equation in finite differences to the following differential equation for combined a posteriori density $W(\lambda, Z=\zeta_1, X=x_j, t) = W_{ij}(\lambda t)$:

$$\frac{\partial W_{ij}(\lambda, t)}{\partial t}=LW_{ij}(\lambda, t)+(V_{ij}-\gamma_0)W_{ij}(\lambda, t)+\sum_{\gamma=1}^{l}\eta_{\gamma j}W_{ij}(\lambda, t). \tag{7}$$

Here the coefficient γ_0 is determined from the condition of normalization

$$\gamma_0=\sum_{i=1}^{m}\sum_{j=1}^{l}\int_{\lambda} V_{ij}W_{ij}(\lambda, t)\,d\lambda.$$

By adding up the left and right sides of the equation (7) with all possible values of i, j it is not difficult to obtain the equation for unconditional a posteriori density of distribution $W(\lambda, t)$, of the continuous parameters:

$$\frac{\partial W(\lambda, t)}{\partial t}=LW(\lambda, t)+[\langle V\rangle_{zx}-\gamma_0]W(\lambda, t), \tag{8}$$

where

$$\langle V\rangle_{zx}=\frac{1}{\tau_{\text{н}}}\left\{\sum_{i=1}^{m}\sum_{j=1}^{l}p_{ij}\exp\left[\int_{h\tau_{\text{н}}}^{(h+1)\tau_{\text{н}}} F_{ij}\,dt\right]-1\right\}, \tag{9}$$

$p_{ij} = p(Z=\zeta_i, X=x_j)$ is the a posteriori probability of states $Z=\zeta_i$, $X=x_j$ and the notation $F_{ij} = F(\lambda, Z=\zeta_i, X=x_j, t)$ is introduced.

Strictly speaking, the probabilities p_{ij} have a conditional nature, but for problems of structural synthesis it is possible to restrict the case of independence of p_{ij} from parameters λ (5).

Considering the a posteriori density $W(\lambda, t)$ which is valid for the condition of applicability of Gaussian approximation, it is possible to convert from equation (8) to equations for the estimated values λ_β^* of the components of vector λ and of the cumulants $h_{\alpha,\beta}$:

$$(10)\qquad \frac{d\lambda_\beta^*}{dt}=a_\beta(\lambda^*,t)+\sum_{\alpha=1}^{n}h_{\beta\alpha}\frac{\partial\langle V\rangle_{zx}^*}{\partial\lambda_\alpha^*},$$

$$(11)\qquad \frac{dh_{\alpha\beta}}{dt}=\sum_{\nu=1}^{n}\left[\frac{\partial a_\alpha(\lambda^*,t)}{\partial\lambda_\nu^*}h_{\nu\beta}+\frac{\partial a_\beta(\lambda^*,t)}{\partial\lambda_\nu^*}h_{\alpha\nu}\right]+$$

$$+\frac{N_{\alpha\beta}}{2}+\sum_{\nu,\mu=1}^{n}h_{\alpha\nu}\frac{\partial^2\langle V\rangle_{zx}^*}{\partial\lambda_\nu^*\partial\lambda_\mu^*}h_{\mu\beta}.$$

Here $\langle V\rangle_{zx}^*$ is calculated by formula (9) with $F_{ij}=F_{ij}^*$ for $\lambda=\lambda^*$.

To complete the system of equations (10) and (11), equations for a posteriori probabilities p_{ij} inserted in $\langle V\rangle_{zx}^*$ must be added to it. Let us consider first the a posteriori conditional probabilities $p_j(i)=p(Z=\zeta_i \mid X=x_j)$. They can be expressed through nonnormalized probabilities $\tilde{p}_j(i)$ as follows:

$$(12)\qquad p_j(i)=\frac{\tilde{p}_j(i)}{\sum_{\alpha=1}^{m}\tilde{p}_j(\alpha)},$$

where

$$\tilde{p}_j(i)=\exp\left[\int_{k\tau_H}^{(k+1)\tau_H}F_{ij}^*dt\right].$$

To determine the right and left sides of the equation (7) for the a posteriori probabilities $P(j)=p(X=x_j)$ we add the possible values of $i=1,m$ and, keeping in mind the a posteriori independence of parameters λ and X and taking into account the Gaussian distribution $W(\lambda,t)$ we obtain

$$(13)\qquad \frac{dP(j)}{dt}=\sum_{\gamma=1}^{l}\eta_{\gamma j}P(\gamma)+P(j)\left[\langle V_j\rangle_z^*-\sum_{\gamma=1}^{l}P(\gamma)\langle V_\gamma\rangle_z^*\right],$$

where

$$(14)\qquad \langle V_j\rangle_z^*=\frac{1}{\tau_H}\left[\sum_{i=1}^{m}p_j(i)\exp\left(\int_{k\tau_H}^{(k+1)\tau_H}F_{ij}^*dt\right)-1\right].$$

The solution of the value of parameter X is produced by the maximum a posteriori probability P(j).

In designing a structural diagram equation (11) may be excluded, inserting into (10) the values $\bar{h}_{\alpha\beta}$ obtained for the stationary mode. Here $dh_{\alpha\beta}/dt = 0$ and equation (11) converts to the algebraic form from which, using a time averaging operation, $\bar{h}_{\alpha\beta}$ is determined. Thus, the structural diagram of the receiver is described with the set of equations (10), (12) and (13).

Reception of Binary Signals

Let us specify the obtained equations for the case of signal reception where the Z parameter receives two values ζ_1 and ζ_2, which corresponds, for instance, to modulation of the carrier phase with a pseudorandom sequence. Let the information parameter X also take on two values x_1 and x_2 with which the signals are differentiated in amplitude, delay, form of components and so on. Specifically, with $X = x_2$ the signal may be absent which is characteristic of information transmission with a passive pause. We will consider the signal dependent on a continuous parameter $\lambda_1(t)$ which determines the random delay (phase) and represents one of the components of vector λ. To be definite, we will use $a_1(\lambda, t) = 0$, i.e. $\lambda_1(t)$ is considered a Wiener process (4).

With the indicated assumptions it is adviseable ti onsert varieties of a posteriori probabilities in the consideration:

$$(15)\qquad \begin{aligned} z_{zj} &= p(Z=\zeta_1 | X=x_j) - p(Z=\zeta_2 | X=x_j),\ j=1,2;\\ z_x &= p(X=x_1) - p(X=x_2). \end{aligned}$$

Allowing for (15) the expression $\langle V \rangle_{zx}$ * is rewritten as follows:

$$(16)\qquad \begin{aligned} \langle V\rangle_{zx^*} = \frac{1}{\tau_н}\Bigg\{ &\frac{1}{2}(1+z_x)\left[\frac{1}{2}(1+z_{z1})\exp\left(\int\limits_{k\tau_н}^{(k+1)\tau_н} F_{11}^{*}dt\right)+\right.\\ &\left.+\frac{1}{2}(1-z_{z1})\exp\left(\int\limits_{k\tau_н}^{(k+1)\tau_н} F_{21}^{*}dt\right)-1\right]+\\ &+\frac{1}{2}(1-z_x)\left[\frac{1}{2}(1+z_{z2})\exp\left(\int\limits_{k\tau_н}^{(k+1)\tau_н} F_{12}^{*}dt\right)+\right.\\ &\left.+\frac{1}{2}(1-z_{z2})\exp\left(\int\limits_{k\tau_н}^{(k+1)\tau_н} F_{22}^{*}dt\right)-1\right]\Bigg\}. \end{aligned}$$

Here in accordance with (12) and (15) the difference Z_{zj} is determined by the formula

$$(17)\qquad z_{zj} = \mathrm{th}\left\{\frac{1}{2}\int\limits_{k\tau_н}^{(k+1)\tau_н}[F_{1j}^{*} - F_{2j}^{*}]dt\right\},\quad j=1,2.$$

According to (13) the difference Z_x satisfies the following equation

$$\frac{dz_x}{dt}=\frac{1}{2}(1-z_x^2)[\langle V_1\rangle_z^*-\langle V_2\rangle_z^*]-(\eta_{12}+\eta_{22})+(\eta_{22}-\eta_{12})z_x, \tag{18}$$

where $\langle V_j\rangle^*$ is determined from the ratio (14) with m = 2 and j = 1,2. Solution of the value x* of the parameter X is done on the basis of the rule

$$x^*=\operatorname{sign} z_x.$$

Inserting the entry $\sigma_\lambda^2 = \bar{h}_{11}$ for the stationary value of deviation of reproduction error of the parameter λ_i, we rewrite equation (10) in the form

$$\frac{d\lambda_i^*}{dt}=\sigma_\lambda^2\frac{\partial\langle V\rangle_{zx}^*}{\partial\lambda_i^*}. \tag{19}$$

The set of equations (17), (18) and (19) allowing for (16) describes the structural diagram of a receiver for binary signals, the modulation characteristic of which is unknown. It should be noted that the signals are discernible with x_1 and x_2 if the condition of inequality with zero differences $\langle V_1\rangle_z^* - \langle V_2\rangle_z^*$ inserted into the right side of the equation (18) is fulfilled. This means that the known components (elements) of the signal s(t) with x_1 and x_2 should be different in form.

Let us consider, for instance, the reception of a complex FM signal for which the characteristic Z of the phase modulation is unknown. We will calculate that the duration of the component of the unknown PSP equals $\tau_н$. The discrete information is included in the amplitude modulation of the FM signal by binary process X. We calculate the delay τ (t) of the signal to be a Wiener process generated by white noise with the spectral density N_τ. The phase modulation of the carrier corresponds to the equality $F_{11}^* = -F_{21}^*$ and the presence of a passibe pause if $F_{12}^* = 0$, i = 1,2. We calculate that in the band $\Delta f = 1/\tau_н$ the signal-to-noise ratio is relatively small and holds the approximate ratio

$$\exp\left(\int_{k\tau_н}^{(k+1)\tau_н} F_{11}^*\,dt\right)\simeq 1+\int_{k\tau_н}^{(k+1)\tau_н} F_{11}^*\,dt.$$

With the indicated conditions of the equation describing the structural diagram of the receiver, the following forms are adopted:

$$\frac{d\tau^*}{dt}=\frac{2\sigma_\tau^2}{N_0^2\tau_н}(1+z_x)\int_{k\tau_н}^{(k+1)\tau_н} r(t)f(t,\tau^*)\,dt\int_{k\tau_н}^{(k+1)\tau_н} r(t)\frac{\partial f(t,\tau^*)}{\partial\tau^*}\,dt, \tag{20}$$

$$\frac{dz_x}{dt}=\frac{1}{N_0^2\tau_н}(1-z_x^2)\left[\int_{k\tau_н}^{(k+1)\tau_н} r(t)f(t,\tau^*)\,dt\right]^2- \tag{21}$$

$$-(\eta_{12}+\eta_{22})+(\eta_{22}-\eta_{12})z_x,$$

where $f(t,\tau)$ is the function which describes the known characteristic of the signal component.

The structural diagram which corresponds to equations (20) and (21) is given in the illustration. The estimation of τ^* is done in the tracking circuit whose operation is described by equation (20). The discrimination characteristic (DKh) of the tracking unit's discriminator is formed as the result of multiplication of the outputs of the correlation (multiplier P_1) and differential (multiplier P_2) channels.

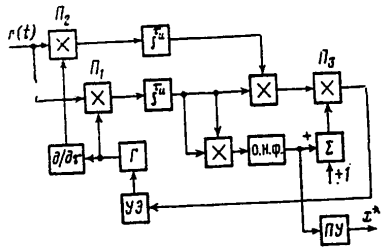

Due to multiplication of the channels, the DKh is invariant to variation of the states of the Z process (the FM signal phases). In accordance with the estimated value of τ^* the control component (UE) produces tuning of the generator G which generates voltage $f(t, \tau^*)$. The channel for extraction of the discrete parameter contains an optimum nonlinear filter (o.n.f.) described by equation (21) and a cut-off unit (PU). The output of the o.n.f. is used to control the coefficient of transmission of the tracking circuit (see multiplier P_3) which is varied depending on the presence or absence of signals in the mixture r(t).

Using the known procedure (3,4) it is possible to estimate the values of the deviation $\delta\tau^2$ and theprobabilities P_e of the spurious reproduction of digits x_j. The question of noise-immunity of the receiver for unknown signals would be better covered in more detail in another place.

In conclusion let us note that the equations given in the article have a rather general nature and may also be used in solving problems of reception of signals in a background of pulse noise of the Markov type.

BIBLIOGRAPHY

1. Detinov, A. N. RADIOTEKHNIKA I ELEKTRONIKA, 13, 3, 1968.

2. Tuzov, G. I. "Statisticheskaya teoriya priyema slozhnykh signalov" [Statistical Theory of Complex Signal Reception], Izd. Sovetskoye radio, 1977.

3. Smirnov, V. A. IZV. VUZOV MVSSO SSSR (RADIOELEKTRONIKA), 17, 4, 1974.

4. Tikhonov, B. I.: and Kul'man, N. K. "Nelineynaya filtratsiya i kvasikogerentnyy priyem signalov" [Nonlinear Filtering and Quasicoherent Signal Reception], Izd. Sovetskoye radio, 1975.

5. Shakhgil'dyana, V. V.; and Belyustinly, L. N. (ed.) "Fazovaya sinkhronizatsiya" [Phase Synchronization], Izd. Svyaz', 1975.

6. Cherdyntsev, V. A.; and Khodasevich, P. G. RADIOTEKHNIKA I ELEKTRONIKA, 20, 2, 1975.

7. Cherdyntsev, V. A. RADIOTEKHNIKA I ELEKTRONIKA, 22, 6, 1977.

[272-8945]

8945
CSO: 1860

UDC 621.391.019.4

OPTIMAL RECEPTION OF DISCRETE SIGNALS AGAINST THE BACKGROUND OF RANDOM PULSED NOISE

Moscow RADIOTEKHNIKA in Russian No 7, 1979 pp 46-50

[Article by V. A. Smirnov, V. N. Kharisov, and L. A. Yershov, submitted 24 May 1978]

[Text] In [1-3], the method of Markov's theory of nonlinear filtration was used to solve the problem of optimal processing of continuous signals containing useful information which are observed against the background of additive pulsed interference and stationery white noise. This is important in developing various radio engineering systems operating in the conditions of the influence of pulsed interference. Messages in such systems can be continuous and discrete. It is interesting to develop the results of [1-3] for a case of the reception of discrete (digital) messages characteristic of systems for transmission of digital information. An algorithm was obtained below for combined filtration of discrete messages against the background of pulsed interference and stationery white noise.

Let us assume that at the observation interval (0, t) we receive the realization of a randon process $\xi(t)$ which is an additive mixture of a useful signal $S[t, \theta(t), \bar{\lambda}(t)]$, pulsed noise $\chi[t, \eta(t), \bar{\mu}(t)]$, and normal white noise n(t) with known statistical characteristics

$$<n(t)>=0, \quad <n(t_1)n(t_2)> = \frac{N_0}{2}\delta(t_2-t_1).$$

The pulsed noise $\chi(t)$ depends on the discrete parameter $\eta(t)$ which is a discrete Markov's process with m states and is described by the following equation for state probabilities [4]:

$$\dot{p}(\eta_r) = \sum_{l=1}^{m} b_{lr}(t)\, p(\eta_l) \tag{1}$$

(for m=2, the process $\eta(t)$ is a sequence of video pulses with an exponential distribution of the lengths of pulses and intervals) and on the Markov diffusion process $\bar{\mu}(t)$ which allows for the random nature of the change in the continuous parameters of the interfering radio pulses (amplitude, phase,

etc) and is described by the following equation for the a priori probability density:

$$\dot{W}(\bar{\mu}) = L_{pr\mu}\{W(\bar{\mu})\}, \tag{2}$$

where $L_{pr\mu}$ is the Fokker-Planck operator.

The useful signal s(t) depends on the Markov diffusion process $\lambda(t)$ which allows for randon changes in the continuous parameters of the signal (amplitude, frequency, phase, etc) and is also described by an equation of the type of (2) with operator $L_{pr\lambda}$ and, moreover, on the discrete parameter $\theta(t)$. The discrete process $\theta(t)$ is constant at time intervals (t_k, t_k+1) with lengths T_0 and values equal to the state of the information parameter $\theta(k)$ at a given interval. The values of $\theta(k)$, k=0, 1, ... at various time intervals form a discrete Markov chain with "n" states which is fully characterized by the transition probability matrix $\prod = \overline{\pi_{ij}}, i, j = \overline{1,n}$ and the vector of probabilities of initial states $p(0) = \{p_i(0)\}$, i - $\overline{1, n}$. The probabilities of states of $\theta(k)$ are now defined by the formula [6]

$$p(k) = (\Pi^T)^k p(0), \tag{3}$$

where $\prod^T$ is the transposed matrix of $\prod$.

In its nature, the $\theta(t)$ process will be substantially different from the $\eta(t)$ process in which the transition moments are stochastic. However, it is possible to show that $\theta(t)$ is a special (limiting) case of discrete Markov processes in continuous time described by (1).

In fact, let us examine the Markov process in continuous time defined by the following matrix equation: p(t) = A(t)p(t) with the initial conditions

$$p(t_0) = p_i(t_0) \text{ for } i = \overline{1, n}. \tag{4}$$

If A(t) matrix is selected in the form of

$$A(t) = A\sum_{l=0}^{\infty}\delta(t - t_l) \tag{5}$$

(where A is a constant matrix, $A = a_{ij}$, $i, j = \overline{1, n}$), then the solution of equation (4) will have the following form

$$p(t) = \exp\left\{\int_0^t A(\tau)\,d\tau\right\} p(t_0) = \exp\{Ak\}\,p(t_0) = (\Pi^T)^k p(t_0) \tag{6}$$

at $t \in (t_k, t_{k+1})$, i.e., in the interval (0, t) there are k points of permitted transition and the elements of matrix A are selected in such a way that

$$\exp\{A\} = \Pi^T. \tag{7}$$

As can be seen, expression (6) fully coincides with (3). Thus, the selection of A(t) matrix in accordance with (5), (7) makes it possible to define the process in continuous time whose probability states in interval (t_k, t_k+1) coincide with the corresponding probabilities for the k-th step of the discrete Markov chain, i.e., the process is statistically equivalent to process $\theta(t)$. This makes it possible to directly transfer the results obtained from the general case of a mixed Markov process to the case of receiving signals with a constant length of elementary sending. To achieve this, it is sufficient to determine the mixed a posteriori probability density of the continuous and discrete parameters of the signal and the interference $W(t, \theta_i, \eta_r, \bar{\lambda}, \bar{\mu})$. On the basis of [1], in application to the case in question, let us write

$$\dot{W}(t, \theta_i, \eta_r, \bar{\lambda}, \bar{\mu}) = L_{pr\lambda}\{W_{i,r}\} + L_{pr\mu}\{W_{i,r}\} + \sum_{j=1}^{n} a_{ji}(t) W_{j,r} + \\ + \sum_{l=1}^{m} b_{lr}(t) W_{i,l} + W_{i,r}(F_{i,r} - \langle F_i \rangle), \tag{8}$$

where

$$F_{i,r} = F(t, \theta_i, \eta_r, \bar{\lambda}, \bar{\mu}) = \frac{1}{N_0}[\xi(t) - S(t, \theta_i, \bar{\lambda}) - \chi(t, \eta_r, \bar{\mu})]^2;$$

$$\langle F_{i,r} \rangle = \sum_r \sum_i \int_{\bar{\lambda}} \int_{\bar{\mu}} F_{i,r} W_{i,r} d\bar{\lambda}\, d\bar{\mu}; \quad W_{p,q} = W(t, \theta_p, \eta_q, \bar{\lambda}, \bar{\mu}).$$

Considering the kind of $a_{ji}(t)$ in (5), for $t \in (t_k, t_{k+1})$, let us write the expression (8) in the form of

$$W_{i,r} = L_{pr\lambda}\{W_{ir}\} + L_{pr\mu}\{W_{i,r}\} + \sum_{l=1}^{m} b_{lr} W_{i,l} + W_{i,r}\{F_{i,r} - \langle F_{i,r} \rangle\}. \tag{9}$$

In points t_k, all addends in the right part of (8) are negligibly small in comparison with the term $\Sigma a_{j,i} W_{jr}$, which contains the δ function and with consideration for (7) in a certain small neighborhood of the transition point $(t_k - \Delta, t_k + \Delta)$, where Δ is the as-much-as-desired small positive value, the equation (9) is equivalent to the following:

$$W_{i,r}(t_k + \Delta) = \sum_{j=1}^{n} \pi_{ji} W_{j,r}(t_k - \Delta). \tag{10}$$

Equations (9) and (10) describe fully the changes in the mixed a posteriori density of $W_{i,r}$ in time.

In order to find the algorithms of the filtration of the parameters of the signal and the interference, let us represent the joint density of the probability of $W_{i,r}$ in the form of

$$W(t, \theta_i, \eta_r, \bar{\lambda}, \bar{\mu}) = P(t, \theta_i, \eta_r/\bar{\lambda}, \bar{\mu}) W(t, \bar{\lambda}, \bar{\mu}). \tag{11}$$

Having substituted (11) in (8) and having summed with respect to θ_i and η_r, we shall obtain an expression for a joint a prosteriori density of probability of continuous parameters which is true for all t:

$$\dot{W}(t, \bar{\lambda}, \bar{\mu}) = \dot{W} = L_{pr\lambda}(W) + L_{pr\mu}(W) + W[F_{cp}(t, \bar{\lambda}, \bar{\mu}) - \langle F_{t,r} \rangle], \tag{12}$$

where $F_{cp}(t, \bar{\lambda}, \bar{\mu}) = \sum_{i=1}^{n} \sum_{r=1}^{m} F_{i,r} P_{i,r}$; $P_{i,r} = P(t, \theta_i, \eta_r/\bar{\lambda}, \bar{\mu})$.

Substituting (11) and (12) in (9) and considering the slowness of the changes of $\bar{\lambda}$, $\bar{\mu}$ which is typical in practice, we shall obtain the algorithm of the filtration of discrete parameters for

$$t \in (t_k, t_{k+1})$$

$$P_{i,r} = \sum_{l=1}^{m} b_{lr} P_{i,l} + P_{i,r}[F_{i,r} - F_{cp}(t, \bar{\lambda}, \bar{\mu})]. \tag{13}$$

For the moments of transition $t=t_k$, having substituted in advance (11) in (10), we have

$$P_{i,r}(t_k + \Delta) = \sum_{j=1}^{n} \pi_{j,i} P_{j,r}(t_k - \Delta). \tag{14}$$

Under the conditions of good filtration $(\bar{\lambda} \approx \bar{\lambda}^*, \bar{\mu} \approx \bar{\mu}^*)$, as an evaluation of the informational discrete parameter (by the criterion of the minimum probability of error), it is necessary to take the value of θ_i corresponding to the maximum of the a posteriori probability at the end of the time interval being considered [5]

$$\theta^*(k) = \max_i [P(t_{k+1}, \theta_i | \bar{\lambda}^*, \bar{\mu}^*)] = \max_i \left\{ \sum_r P(t_{k+1}, \theta_i, \eta_l | \bar{\lambda}^*, \bar{\mu}^*) \right\}. \tag{15}$$

Expressions (12), (13) and (15) give the algorithms of the evaluation of the informational parameter of the signal with consideration for the effect of pulsed interference.

Let us examine the widespread case of digital information transmission when the probabilities of transitions for the sequence $\{\theta(k)\}$ do not depend on the value of θ at the preceding time interval, i.e.,

$$\pi_{j,i} = p_i \text{ at } i, j = \overline{1, n}. \tag{16}$$

Let us represent the joint probability of discrete parameters in the form of

$$P(t, \theta_l, \eta_r/\bar{\lambda}^*, \bar{\mu}^*) = P(t, \theta_l/\bar{\lambda}^*, \bar{\mu}^*)\, P(t, \eta_r/\theta_l, \bar{\lambda}^*, \bar{\mu}^*). \tag{17}$$

Having substituted (17) in (13), summarized over r, and solved the obtained equation, we shall obtain for $t \in (t_k, t_{k+1})$:

$$P(t, \theta_l/\bar{\lambda}^*, \bar{\mu}^*) = \frac{p_l \exp\left\{\int_{t_k}^{t} \sum_r F_{l,r}(\tau)\, P(\tau, \eta_r/\theta_l, \bar{\lambda}^*, \bar{\mu}^*)\, d\tau\right\}}{\sum_l p_l \exp\left\{\int_{t_k}^{t} \sum_r F_{l,r}(\tau)\, P(\tau, \eta_r/\theta_l, \bar{\lambda}^*, \bar{\mu}^*)\, d\tau\right\}}. \tag{18}$$

In this case, at the beginning of the time interval $P(t_k + \Delta, \theta_l/\bar{\lambda}^*, \bar{\mu}^*) = p_l$ and the expression (14) is not used.

The algorithm of the evaluation of the discrete parameter (15) assumes a simpler form

$$\theta(k) = \max_i{}^{-1}\left\{\int_{t_k}^{t_{k+1}} \sum_r F(\tau, \theta_l, \eta_r, \bar{\lambda}^*, \bar{\mu}^*)\, P(\tau, \eta_r/\theta_l, \bar{\lambda}^*, \bar{\mu}^*)\, d\tau + \ln p_l\right\}. \tag{19}$$

Equations for the a posteriori probability of the discrete parameter of the interference are obtained by substituting (16)-(18) in (13) and (14). For $t \in (t_k, t_k+1)$ we find

$$\dot{P}(t, \eta_r/\theta_l, \bar{\lambda}^*, \bar{\mu}^*) = \sum_l b_{lr}(t)\, P(t, \eta_l/\theta_l, \bar{\lambda}^*, \bar{\mu}^*) +$$

$$+ P(t, \eta_r/\theta_l, \bar{\lambda}^*, \bar{\mu}^*)\left[F_{l,r} - \sum_r F_{l,r}\, P(t, \eta_r/\theta_l, \bar{\lambda}^*, \bar{\mu}^*)\right], \tag{20}$$

for $t = t_k$

$$P(t_k + \Delta, \eta_r/\theta_l, \bar{\lambda}^*, \bar{\mu}^*) = \sum_j P(t_k - \Delta, \theta_j/\bar{\lambda}^*, \bar{\mu}^*)\, P(t_k - \Delta, \eta_r/\theta_l, \bar{\lambda}^*, \bar{\mu}^*). \tag{21}$$

Expressions (18)-(21) make it possible to obtain simple algorithms of technical realization in some extreme cases. For example, in the cases of large signal/noise and interference/noise ratios, it is possible to write the following for the a posteriori probabilities of the discrete parameters of the signal and interference:

$$p(t, \theta_l) = \delta(\theta_l, \theta^*) + \varepsilon_l; \quad p(t, \theta_l/\xi_j) = \delta(\theta_l, \theta^*) + \varepsilon'_l,$$

where $\delta(\theta_i, \theta^*)$ is the Kronecker symbol; ε_i, ε'_i are certain small values, i.e., $|\varepsilon_i|\ |\varepsilon'_i| \ll 1$.

In this case the algorithm (19)-(21) changes to an approximate algorithm of filtration:

$$\left.\begin{aligned}
&\theta^*(t) = \max_l{}^{-1}\left\{\int_{t_k}^{t_{k+1}} F(\tau, \theta_l, \eta^*, \bar{\lambda}^*, \bar{\mu}^*)d\tau + \ln p_l\right\};\\
&\theta^*(k) = \theta^*(t_{k+1}),\ \eta^*(t) = \max_r{}^{-1}\{P(t, \eta_r/\bar{\lambda}^*, \bar{\mu}^*)\};\\
&\dot{P}(t, \eta_r/\bar{\lambda}^*, \bar{\mu}^*) = \sum_l b_{lr} P(t, \eta_l/\bar{\lambda}^*, \bar{\mu}^*) +\\
&+ P(t, \eta_r/\bar{\lambda}^*, \bar{\mu}^*)[F(t, \theta^*, \eta_r, \bar{\lambda}^*, \bar{\mu}^*) - F(t, \theta^*, \eta^*, \bar{\lambda}^*, \bar{\mu}^*)].
\end{aligned}\right\} \qquad (22)$$

The physical sense of the algorithm (22) is explicit. The filtration of the signal is accomplished with a compensated interference, for which a current evaluation of the interference is selected. The filtration of the interference is done in the same way, i.e., in this case, optimal algorithms lead to the so-called compensation circuits which found practical application.

For an example, let us examine the reception of binary signals against the background of random pulsed interference (KhIP) and white noise, when

$$s(t, \theta, \bar{\lambda}) = A\theta(t) f(t) = \begin{cases} A\theta(t) & \text{for } 0 \leqslant t \leqslant \tau_u; \\ 0 & \text{for } \tau_u < t < T, \end{cases} \qquad (23)$$

where f(t)=f(t+kT), θ(t) assumes with a probability of 1/2($\overline{\eta_{ji}}$=1/2) values of 0 or 1 at intervals [kT, (k+1)T].

Let us write KhIP in the form of

$$\chi(t, \eta, \bar{\mu}) = \eta(t)\cos\varphi(t), \qquad (24)$$

where the discrete process $\eta(t)$ assumes the values of 0 or 1 and is described by the equation (1) for the probability of states

$$\dot{p}(t, \eta = 0) = -\dot{p}(t, \eta = 1) = -\mu p(t, \eta = 0) + \nu p(t, \eta = 1), \qquad (25)$$

where μ -- intensity of transition from 0 to 1, v -- from 1 to 0.

The continuous parameter $\varphi(t)$ has an equiprobable distribution at the interval $[0, 2\pi]$. Such a model describes the process at the output of a synchronous detector when the phase of the signal is known. The concretization of the algorithm (22), in this case with consideration for (23)-(25), leads to the expressions

$$\left.\begin{aligned} q &= \int_{kT}^{t}\left[\xi(\tau)-\cos\varphi(\tau)\,\eta^{*}(\tau)-\frac{1}{2}A\right]d\tau \gtrless 0 \quad \begin{cases}\theta^{*}=1 & \text{for } q>0,\\ \theta^{*}=0 & \text{for } q<0;\end{cases}\\ \dot{z} &= (\mu-\nu)-(\mu+\nu)z+\frac{1}{2N_0}(1-z^{2})\left\{[\xi(t)-A\theta^{*}(t)]\cos\varphi(t)-\frac{1}{2}\cos^{2}\varphi(t)\right\};\\ \theta_k^{*} &= \theta^{*}(kT+\tau_{\text{н}}), \quad z(t)=p(t,\ \eta=1)-p(t,\ \eta=0). \end{aligned}\right\} \tag{26}$$

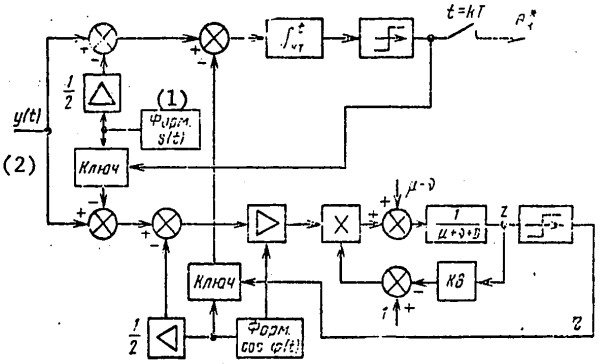

Figure 1

Key: 1. Form
2. Key

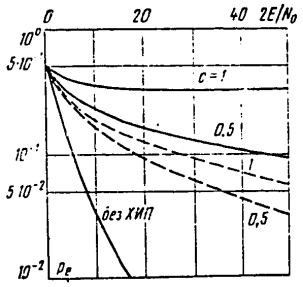

Figure 2

Key: 1. Without KhIP

The block diagram of the device realizing (26) (Figure 1) is a combination of two devices: a correlation receiver for detecting signals and a known circuit for optimal evaluation of random interference examined, for example, in [6].

Figure 2 shows the probabilities of errors under the effect of n(t), signal (23), and interference (24) depending on the signal/noise ratio $2E/N_0=2A^2\tau_и/N_0$ for various ratios of the amplitudes of the interference and signal c (interference parameters $\mu\tau_и = 6.577$, $\sqrt{\tau_и} = 0.143$) for an optimal receiver only against the white noise background (solid lines) and an optimal receiver with allowance for KhIP (broken lines). As can be seen, the application of optimal methods of reception (Figure 1) with compensation for KhIP makes it possible to improve considerably the characteristics of receivers of discrete signals under the conditions of interference.

Bibliography

1. Tikhonov, V. I., and Stepanov, A. S. RADIOTEKHNIKA I ELEKTRONIKA (Radio Engineering and Electronics], Vol 18, No 7, 1973.

2. Smirnov, V. A., and Yakovlev, A. I. IZVESTIYA VUZOV SSSR, SERIYA RADIOELEKTRONIKA [News of USSR Vuzes, Radio Electronics Series], Vol 19, No 11, 1976.

3. Yarlykov, M. S.; Smirnov, V. A.; and Yakovlev, A. I. RADIOTEKHNIKA I ELEKTRONIKA, Vol 21, No 2, 1976.

4. Tikhonov, V. I., and Mironov, M. A. "Markovskiye protsessy" [The Markov Processes], Sovetskoye radio, Moscow, 1977.

5. Middleton, D. "Vvedeniye v statisticheskuyu teoriyu svyazi" [Introduction to the Statistical Theory of Communication], Vol 2, Sovetskoye radio, Moscow, 1962.

6. Kul'man, N. K., and Stratonovich, R. L. RADIOTEKHNIKA I ELEKTRONIKA, Vol VI, No 9, 1961.

10,233
CSO: 1860

UDC: 621.391.8

AN OPTIMUM TWO-STAGE PROCEDURE FOR DETECTING A SIGNAL IN NOISE

Moscow RADIOTEKHNIKA I ELEKTRONIKA in Russian No 7 1979 pp 1447-1449

[Article by A. I. Shatilov: "An Optimum Two-Stage Procedure for Detecting a Signal in a NOise Background"]

[Text] In study (1) two-stage procedures for signal detection in a noise background were considered and the effectiveness of these procedures for receiving a fluctuating signal with undetermined phase and amplitude was evaluated. However, closed-state relationships convenient in a computer connection were not obtained.

The purpose of the present study is actualization of the general relationships obtained in (2) for the problem of detecting a fluctuating signal with undetermined amplitude and phase(3) with independent fluctuations at the first and second stages which permit the parameters of the optimum procedures to be effectively determined.

The conditional probability distribution densities for the logarithms of the probability coefficients v_k at each of the stages (k = k,2) equal (3)

$$(1) \qquad f_1^i(v_k)=\frac{1+c_i}{c_i}\exp\left(-\frac{1+c_i}{c_i}[v_k+\ln(1+c_i)]\right)$$

in the absence of a signal (hypothesis H_1) and

$$(2) \qquad f_2^i(v_k)=\frac{1}{c_i}\exp\left(-\frac{1}{c_i}[v_k+\ln(1+c_i)]\right)$$

in the presence of a signal (hypothesis H_2). In (1) and (2) c_i stands for the signal-to-noise ratio for many types of experiments i = 1, $\sum$ ($v_k \geqslant -$| n(1+ c_i)). In what follows we will assume that at the first stage the signal-to-noise ratio equals c_1 and at the second (if it is given) depending on the observed value of v_1 it equals c_1 or c_2 ($c_2 \rangle c_1$).

It is necessary to determine the minimum average power outlays $\beta_1(D_1^2) = c_1+E_1(c_1)+E_1(c_2)$ when there is no signal (hypothesis H_1). In this case the probability of a spurious response $\alpha_{12}(D_1^2)$, the probability of absence of a signal $\alpha_{21}(D_1^2)$ and the average power outlays (hypothesis H_2) $\beta_2(D_1^2) = c_1+c_2(c_1)+E_2(c_2)$ are limited at the top by the assigned constants α_{12}^*, α_{21}^* and β_2^*. $E_j(\cdot)$ and D_1^2 stand for the conditional mathematical expectation of the corresponding magnitude and the two-stage sequential procedure.

The existence of the probability densities (1) and (2) ensure the capability of substituting the direct problem with its double (2). The Lagrange function in the given case has the form

$$D(D_1^2, \vec{\lambda}) = \beta_1(D_1^2) + \lambda_1[\alpha_{12}(D_1^2) - \alpha_{12}^*] + \lambda_2[\alpha_{21}(D_1^2) - \alpha_{21}^*] + \lambda_3[\beta_2(D_1^2) - \beta_2^*]. \quad (3)$$

Solution of the dobuel problem assumes solution of the problems related to each other (2)

$$\varphi(\vec{\lambda}) = \min_{D_1^2 \in D_{12}^*} L(D_1^2, \vec{\lambda}), \quad (4)$$

$$\varphi(\vec{\lambda}^0) = \max_{\vec{\lambda} \in \Lambda} \varphi(\vec{\lambda}). \quad (5)$$

As was shown in study (2), the optimum two-stage procedure for the assigned vector $\vec{\lambda}$ may be found from the recurrence equation for Bayes's risk (4) and the mutually unequivocal correspondence between the Lagrange multipliers λ_1, λ_2 and λ_3 and the a priori probabilities p_j^0 of hypotheses H_j ($j = 1,2$) and the arrays W_{ji} behind the error solutions (hypothesis H_i is used when H_j is real) is expressed by the formulas ($j \neq i$)

$$\lambda_1 = W_{12}; \quad \lambda_2 = \frac{1-p_1^0}{p_1^0} W_{21}; \quad \lambda_3 = \frac{1-p_1^0}{p_1^0}. \quad (6)$$

The sequential procedure constructed this way is optimum for the assigned parameters W_{12}, W_{21} and p_1^0 or for the assigned Lagrange multipliers λ_1, λ_2 and λ_3 which are the same.

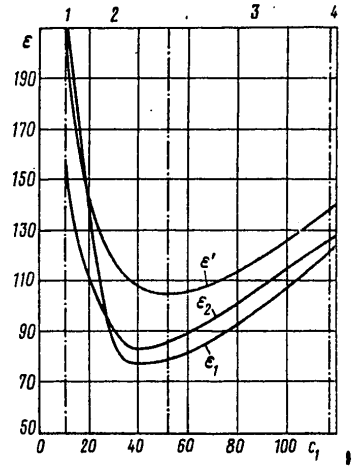

Figure 1. Graphs of $E_1(c_1)$, $E_2(c_1)$ and $E'(c_1)$ when $c_2 = 200$, $a_{12}^* = 10^{-5}$, $a_{21}^* = 3 \cdot 10^{-2}$

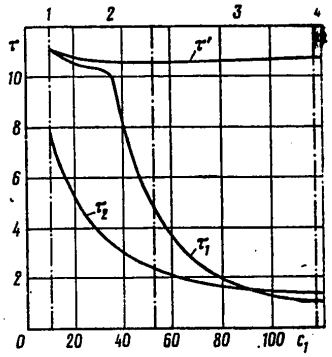

Figure 2. Graphs $\tau_1(c_1)$, $\tau_2(c_1)$ and $\tau'(c_1)$ when $T = 10T_2$, $a_{12}^* = 10^{-5}$, $a_{21}^* = 3 \cdot 10^{-2}$

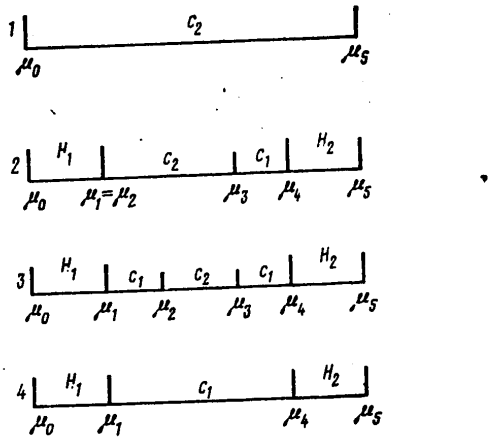

Figure 3. Sequence of Logic Circuits for Adopting Decisions for Optimum Two-stage Sequential Procedures $^0D_1^2$

The function $\phi(\lambda)$ is concave and its maximum is easily computed by the method of directed excess since the limits of the set $\Lambda(2)$ are determined by means of a Neumann-Pearson criterion.

In figure 1 is given a graph of the dependence of the average power outlays E' for a block of signals (two pulses) from c_1 necessary for the Neumann-Pearson criterion of the same power. The numerical calculations were done with the following parameter values: $c_2 = 200$; $\alpha_{12} = 10^{-5}$; $\alpha_{21} = 3 \cdot 10^{-2}$.

From figure 1 it is apparent that there exists an optimum from the point of view of power outlays ratio between c_1 and c_2 for which the optimum procedure ${}^{0}D_1{}^{2}$ provides a power gain 27 percent higher than the Neumann-Pearson criterion when a signal is absent.

On the other hand the gain in average detection time including the interval between pulses T_1 compared with the detection time required for the Neumann-Pearson criterion with an assigned α_{12}^* and α_{21}^* may achieve a considerable magnitude.

In fact, assume that the signal-to-noise ratio c_1 is proportional to the pulse duration T_i $(i = 1,2)$ and the fixed interval of time T is sufficiently large compared to $T_2 (T_2 > T_1)$ that the amplitudes and phases of the pulses may be considered statistically independent.

In figure 2 the dependence is shown of the average detection time $\tau_i = T_1 + E_j(T_1) + E_i(T_2)$ necessary for the procedure considered above ${}^{0}D_1{}^{2}$ from c_1 $(T = 10T_2)$.

For comparison, in figure 2 is shown the detection time τ' for a block of signals (two pulses) as a function of c_1 necessary for the Neumann-Pearson criterion with assigned α_{12}^* and α_{21}^*.

From figures 1 and 2 we see that the choice of value c_1 for which the average power outlays do not exceed the minimum outlays needed for the Neumann-Pearson criterion provides a gain in the average detection time of more than 84 percent for both hypotheses.

In figures 1 and 2 the entire set of considered values c_1 $(10 < c_1 < 120)$ is carried out to four numbered places separated in these illustrations by dot and dash lines. The sequence of ligic circuits corresponding to these numbers for adopting solutions in the detection process is shwon in figure 3.

Since it is possible to interpret the Lagrange function as the average risk with an accuracy up to a linear transform (2) and the a priori probabilities of the hypotheses are directly computed in accordance with the ratios (4)-(6) it is convenient to use the a posteriori probability $p_1{}^{1}(v_1)$ of the actuality of hypothesis H_1 instead of v_1 for adopting solutions after the first stage.

The first zone is confluent at the point where $c_1 = 10.05$. In thise case the sequential procedure is confluent at a nonconsecutive point (the Neumann-Pearson criterion). By μ_0 and μ_5 are meant respectively the lower and upper limits of $p_i(v_1)$.

The remaining zones of values c_1 correspond to various logic circuits for optimum sequential procedures obtained as a result of the calculations.

If $\mu_0 \leq p_i(v_1) \leq \mu_1$ or $\mu_4 \leq p_i(v_1) \leq \mu_5$, then the process of observation is terminated by adopting hypotensis H_2 or H_1 respectively.

If $\mu_i < p_i(v_1) < \mu_{i+1}$ and $c = c_j$ $(j = 1,2)$, then it is necessary to perform the second stage in the detection process using power satisying the signal-to-noise ratio c_j.

It should be noted that the fourth zones of the values $c_1 (c_1 > 117.5)$ corresponds to a logic circuit for trur ated sequential analysis when only one type of experiment is used.

With a further increase in c_1 the logic circuit for truncated sequential analysis converts to a logic circuit for a single-pulse Neumann-Pearson criterion.

BIBLIOGRAPHY

1. Sindler, Yu. B. RADIOTEKHNIKA I ELEKTRONIKA, 11, 6, 1966.

2. Shatilov, A. I. RADIOTEKHNIKA I ELEKTRONIKA, 23, 8, 1978.

3. Vaynshteyn, L A.; and Subakov, V. D. "Vydeleniye signalov na fone sluchaynykh pomekh" [Detection of Signals in a Random Noise Background], Izd. Sovetskoye radio, 1960.

[272-8945]

8945
CSO: 1860

UDC 621.391:53.08

THEORY OF SIGNAL RESTORATION

Moscos TEORIYA VOSSTANOVLENIYA SIGNALOV in Russian, 1979 pp 271-272

[Annotation and Table of Contents From Book by Georgiy Ivanovich Izdatez'stvo Sovetskoye Radio, 272 pages]

[Text] The theory of signal restoration is described in its general form which is scientifically aimed at developing methods of an a posteriori elimination of distortions introduced by actual devices and environment as a result of observing some processes or phenomena. Signal restoration is considered an incorrectly posed problem of mathematical physics. Efficient ways of signal restoration are studied on the basis of general methods for solving such problems. Practical restoration algorithms obtained by computers and methods of optical processing of data and holography are described.

Signal restoration methods considered in this book find use in radar, communications, measuring equipment, acoustics, optics, spectroscopy, X-rays, electron microscopy etc.

The book is intended for scientific workers and research engineers working in various fields of physics and engineering.

Forty-four pictures, 4 tables, bibliography of 130 titles.

Table of Contents

2291
CSO: 1860

UDC 621.391.278

A STUDY ON THE TRANSMISSION OF AN OPTICAL SIGNAL WITH MULTIPOSITION PULSE-TIME MODULATION OVER A COMMUNICATION LINE WITH REPEATERS

Moscow RADIOTEKHNIKA I ELEKTRONIKA in Russian No 7 1979 pp 1332-1338

[Article by Yu. A. Gol'dshteyn and B. Ya. Frezinskiy: "A Study on the Transmission of an Optical Signal with Multiposition Pulse-Time Modulation over a Communication Line with Repeaters"]

[Text] Optimum and quasi-optimum algorithms for reception of an optical signal with multiposition pulse-time modulation (VIM) transmitted via a communication line with repeaters are considered. The power loss of the quasi-optimum algorithm is estimated. It is established that synchronization should be accomplished by means of short periodic pulse trains. Dependence of noise-immunity of the reception on the distribution frequency of the repeaters is considered.

Let us consider the transmission of discrete information via a line with repeaters by means of multiposition pulse-time modulation (VIM) of an optical signal. In designing such lines several problems arise: determination of the structure and noise-immunity of the receiver, the number of repeaters and their respective positioning, synchronization and so on. From the mathematical point of view this set of problems is sufficient for the following rather general task.

Suppose that to a line consisting of R repeaters is applied a train consisting of m periodic pulses with duration τ each also having a sequence period of $T = N\tau$ and also a train of successive nonperiodic pulses of the same duration representing an information-bearing sequence with multiposition pulse-time modulation (fig. 1).

The position of the whole train on a time axis is defined by the vector

$$\vec{\alpha}=\{i, j_1, j_2, \ldots, j_l\},$$

where i = 1,2,...,N defines the positions of the synchronization pulses and j_s = 1,2,...,N (s = 1,2,...,l) is the position of the S information pulse.

At the output of the final receiver of the line, the luminous flux is converted into photoelectric current. We represent the results of measuring the number of photoelectrons in the form of a matrix

$$\{n_{si}\}, \quad \begin{matrix} s=1, 2, \ldots, m+l, \\ i=1, 2, \ldots, N, \end{matrix}$$

where n_{si} is the number of photoelectrons recorded in subinterval τ_i of interval T_s.

The problem lies in calculating the vector $\vec{d}$ in terms of the measured values of $\{n_{si}\}$.

For a communication line without repeaters the overall multiple-alternative task of detecting signals in noise is investigated in such studies as (1). In the case of communication systems with repeaters the optimum algorithm for processing a signal at the terminal point (OAOKP) depends, generally speaking, on the operation of the repeaters. Due to the criterion of maximum probability, however, it can be shown that in implementing the condition

$$(1) \qquad \prod_{r=1}^{R} (P_r^{(1)} - P_r^{(0)}) > 0,$$

where $P_r^{(1)}$ is the probability of accurate relay and $P_r^{(0)}$ is the probability of a certain error in relaying a train with r repeaters.* Detection of the synchronizing pulse and each of the information pulses is accomplished independently. In this case OAOKP coincides in essence with the algorithm for known from the theory of multiple-alternative signal detection in noise (1), namely, the synchronizing pulses hold position i corresponding to

$$(2) \qquad \text{макс}_i \prod_{i=1}^{m} p_1(n_{si})/p_0(n_{si}) \quad (i=1, 2, \ldots, N),$$

while position j_s of the information pulse s corresponds to

$$(3) \qquad \text{макс}_{j_s} p_1(n_{m+sj_s})/p_0(n_{m+sj_s}) \quad \begin{pmatrix} s=1, 2, \ldots, l \\ j_s=1, 2, \ldots, N \end{pmatrix},$$

*In communication systems of practical interest, $P_r^{(1)} \quad P_r^{(0)}$ which is why (1) is done.

where $p_0(n)$ and $p_1(n)$ are the probabilities of recording n photoelectrons at time $\tilde{t}$ in the absence and presence of a signal respectively. Thus, in implementing condition (1) OAOKP does not depend on the number, structure and nature of the repeater operation. With m = 1, (3) coincides with (2); for this reason only algorithm (2) is considered below.

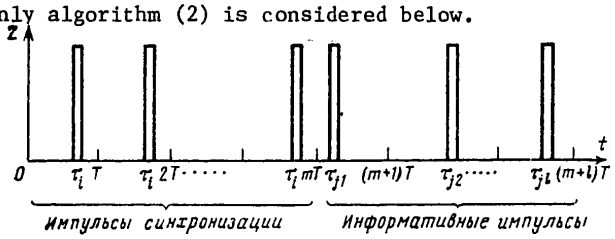

Figure 1. Transmitted Pulse Train

Synchronization Pulse Information Pulses

OAOKP (2) does not determine unambiguously the structure of the receivers in the repeaters, but since this structure has a significant effect on the noise-immunity of the entire line's reception, it is necessary that the receivers in the repeaters provide maximum noise-immunity for the communication line.

The probability of accurate reception at the end of the line equals

$$F_{\text{прав}}=F_1\prod_{r=1}^{R}P_r^{(1)}+F, \tag{4}$$

where F_1 is the conditional probability of accurate reception of the periodic train assuming its correct relay and F contributes mutually compensated errors to $F_{\text{прав}}$. Analysis of formula (4) shows that the requirement for maximum noise-immunity of the reception of the entire line makes it impossible to implement receivers in the repeaters based on algorithms which are optimum in the sense of having maximum $P_r^{(1)}$. In this case it may be calculated with an adequate degree of accuracy that

$$F_{\text{прав}}=F_1\prod_{r=1}^{R}P_r^{(1)}. \tag{5}$$

Specifically, if the transmission to the repeaters is doen in the optical range, reception at the repeater must be performed by (2) with $P_r^{(1)}$ calculated the same as F_1.

The probability F_1 is equal to the probability of the inequality

$$\lambda(\vec{n}_{mi}^{\text{см}})>\lambda(\vec{n}_{mk}^{\text{ш}}), \tag{6}$$

where

$$\vec{n}_{mi}=\{n_{1i}, n_{2i}, \ldots, n_{mi}\}; \quad \lambda(\vec{n}_{mi})=$$

$$=\prod_{s=1}^{m} p_1(n_{si})/p_0(n_{si}),$$

and the values $\vec{n}^{ш}$ and $\vec{n}^{сш}$ are only caused by noise and signal plus noise respectively.

Inserting the set $D(\vec{n}_{mi}^{сш})$ of values $\vec{n}_{mk}^{ш}$ which satisfy (6), we write F_1 in the form

$$F_1=\sum_{\vec{n}_{mi}^{сш}=0}^{\infty} P_1(\vec{n}_{mi}^{сш})\left[\sum_{\vec{n}_{mk}^{ш}\in D(\vec{n}_{mi}^{сш})} P_0(\vec{n}_{mk}^{ш})\right]^{N-1}, \tag{7}$$

where

$$P_0(\vec{n}_{mk}^{ш})=\prod_{s=1}^{m} p_0(n_{sk}); \quad P_1(\vec{n}_{mi}^{сш})=\prod_{s=1}^{m} p_1(n_{si}).$$

Addition by $\vec{n}^{ш}$ in (7) means addition by all m coordinates of $\vec{n}^{ш}$ in the range of the set D. Addition by the first coordinate of $n^{сш}$ results in from 1 to ∞ and by the other coordinates of $\vec{n}^{сш}$ results in from 0 to ∞. The optimum spatial distribution of the repeaters may be ascertained by solving the system

$$\frac{\partial F_{прав}}{\partial x_r}=0, \quad r=1,2,\ldots,R, \tag{8}$$

where x_r is the distance between adjacent repeaters. With a fixed length of the entire line $X=\sum_{r=1}^{R+1} x_r$ of system (8) virtue of (5) will take the form

$$\frac{\partial P_r^{(1)}}{\partial x_r}F_1-P_r^{(1)}\frac{\partial F_1}{\partial x_{R+1}}=0; \quad r=1,2,\ldots,R. \tag{9}$$

Solving (9) we obtain the values $x_1, x_2, \ldots, x_r$ which yield the maximum $F_{прав}$ which we designate $F_{опт.R}$. If $F_{опт R}$ does not reach maximum in terms of R, the number of repeaters for reliable operation of the communication line must be looked for from the condition

$$F_{опт,R}\geqslant F_0,$$

where F_0 is the assigned value of noise-immunity of reception. If all the transmitters of the system radiate in one and the same range and have equal power and the properties of all the intermediate channels are identical, then the uniform distribution of the repeaters ($x_1 = x_2 = \ldots x_r = X/R+1$) is optimum, being in this case $P_1^{(1)} = P_2^{(1)} = \ldots = P_R^{(1)} = F_1$.

To obtain quantitative results it is necessary to know the principles of distribution of the noise photoelectrons $p_0(n)$ and the convolution of the distribution of signal and noise photoelectrons $p_1(n)$. As is known, the problem of calculating the different kinds of noise in optical communications has not been solved (2); the form $p_0(n)$ and $p_1(n)$ is found only in a number of limited cases. Inasmuch as a rather general problem is considered here (specifically, open and enclosed lines). we are limited to detecting the greatest and least of the possible values of reception noise-immunity for arbitrary communication lines and the noise properties of a photoreceiver (as regards the photoreceiver, it is assumed only that it operates in a mode such that the single-electron pulses are discernible). For this purpose the calculations are performed at two extremes in the sense of deviation in the distribution of the cases: for Poisson distribution (PR)

$$p_0(n)=\frac{(\gamma_m\tau)^n}{n!}\exp(-\gamma_m\tau);\quad p_1(n)=\frac{((\gamma_m+\gamma_c)\tau)^n}{n!}\exp(-\gamma_m-\gamma_c)\tau, \tag{10}$$

which has the least deviation and for the distribution

$$p_0(n)=\frac{(\gamma_m\tau)^n}{(1+\gamma_m\tau)^{n+1}};\quad p_1(n)=\frac{(\gamma_m\tau)^n}{(1+\gamma_m\tau)^{n+1}}\times\exp\left(\frac{-\gamma_c\tau}{1+\gamma_m\tau}\right)L_n\left(\frac{-\gamma_c}{\gamma_m(1+\gamma_m\tau)}\right), \tag{11}$$

which has the greatest deviation and represents the convolution of a single-mode Gaussian noise with a Poisson signal (2) (γ_ω and γ_c in (10) and (11) are the average intensities of the noise and signal photoelectrons; $L_n(x)$ is the Laguerre polynomial). As is shwon in (2), other variations of the distribution including multimode sound radiation, shot noise and so on have intermediate deviation in comparison with (10) and (11).

In (10), algorithm (2) stands for detection by maximum cumulative number of photoelectrons

$$\sum_{i=1}^{m} n_{i,i}=\text{макс}_i, \tag{12}$$

and, due to the additivity of the Poisson distribution, (7) is considerably simplified:

$$F_1=\sum_{n=1}^{\infty}\frac{((\gamma_m+\gamma_c)m\tau)^n}{n!}\exp(-\gamma_m-\gamma_c)m\tau\times \times\left[\sum_{k=0}^{n-1}\frac{(\gamma_m m\tau)^k}{k!}\exp(-\gamma_m m\tau)\right]^{N-1}. \tag{13}$$

In (11) algorithm (2) has the form

$$\prod_{s=1}^{m}L_{n_{si}}\left(-\frac{\gamma_c}{\gamma_m(1+\gamma_m\tau)}\right)=\max_i \tag{14}$$

and with m = 1 in virtue of the monotony of $L_n(x)$ with respect to n, (14) also signifies reception with the maximum number of photoelectrons. In (11) inequality (6) has the form

$$\prod_{s=1}^{m}L_{n_{cm}}(x)>\prod_{s=1}^{m}L_{k_{sm}}(x),$$

where

$$x=-\gamma_c/\gamma_m(1+\gamma_m\tau).$$

Inserting the function $x = U_n(y)$, in inverse ratio to $y = L_n(x)$, and calculating that $L_0(x) = 1$, we write (7) in the form

$$F_1=\frac{1}{(1+\gamma_m\tau)^{mN}}\exp\left(\frac{-\gamma_c m\tau}{1+\gamma_m\tau}\right)\times \times\sum_{n_1=1}^{\infty}\sum_{n_2=0}^{\infty}\cdots\sum_{n_m=0}^{\infty}\left(\frac{\gamma_m\tau}{1+\gamma_m\tau}\right)^{\sum_{s=1}^{m}n_s}\prod_{s=1}^{m}L_{n_s}(x)\times \times\left[\sum_{k_1=0}^{U_{k_1}\left(\prod_{s=1}^{m}L_{n_s}\right)-1}\ \sum_{k_2=0}^{U_{k_2}\left(\prod_{s=1}^{m}L_{n_s}/L_{k_1}\right)-1}\cdots \cdots\sum_{k_m=0}^{U_{k_m}\left(\prod_{s=1}^{m}L_{n_s}\Big/\prod_{s=1}^{m-1}L_{k_s}\right)-1}\left(\frac{\gamma_m\tau}{1+\gamma_m\tau}\right)^{\sum_{s=1}^{m}n_{k_s}}\right]^{N-1}. \tag{15}$$

The optimum reception algorithm (2), practically unrealizeable due to

equipment difficulty, may serve as the standard of quality for quasi-optimum algorithms.

Reception with the maximum number of excesses of a certain threshold n, when the position of the pulses of the train is determined from the condition

$$g_i=\sum_{s=1}^{m}\varkappa(n_{si})n_{si}=\text{макс},$$

where

$$\varkappa(n)=\begin{cases}0, & n<\hat{n},\\ 1/n, & n\geqslant\hat{n}.\end{cases}$$

is a conveniently implemented version for simplification of the optimum algorithm (12).

Essentially, the numbers g_i differ from zero only for a small number of positions $i_1,i_2,\ldots,i_k$ and the number of these positions k is an arbitrary magnitude the numerical distribution characteristics of which, according to (3), satisfy the inequality

$$\sigma_k^2<\bar{k}<m \quad \text{при} \quad p_0=\sum_{n=\hat{n}}^{\infty}p_0(n)<\frac{1}{N}.$$

The conditional probability F_1 in this case is calculated according to (3) by the formula

$$F_1=\sum_{k=1}^{N}C_{N-1}^{k-1}\sum_{s=\varepsilon_{k-1}}^{m}C_m^s p_1^s q_1^{m-s}\left[\sum_{l=1}^{s-1}C_m^l p_0^l q_0^{m-l}\right]^{k-1} q_0^{m(N-k)}, \tag{16}$$

where

$$p_1=\sum_{n=\hat{n}}^{\infty}p_1(n), \quad q_1=1-p_1, \quad q_0=1-p_0, \quad \varepsilon_{k-1}=\begin{cases}1, & k=1,\\ 2, & k>1.\end{cases}$$

The optimum threshold $\hat{n}$ is determined from the condition of maximum F_1. Calculations by formula (16) have been performed for distributions (10) and (11).

Results of the calculations make the following conclusions possible:

1. With reception of a single pulse, the conditional probability of error

$1 - F_1$ decreases both with an increase in $\gamma_c / \gamma_ш$ and with a decrease in $\gamma_ш$ while in the latter case the ratio $\gamma_c / \gamma_ш$ which fulfills a fixed error probability is increased (fig. 2). In the case of distribution (11) the curves in figure 2 are positioned higher and are more concave than the corresponding curves for PR. The value of the power loss in reception with the quasi-optimum algorithm compared to the optimum in the case of PR is considerably less then

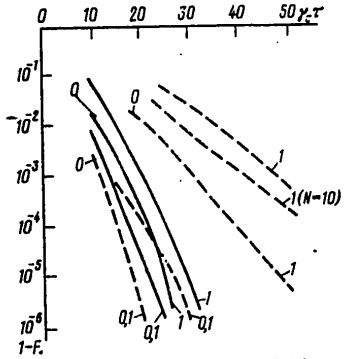

Figure 2. Dependnece of the Error Probability $1 - F_1$ in Pulse Reception by the Optimum (o) and Quasi-optimum Algorithms for Various $\gamma_ш r$: Unbroken Curves --Poisson Distribution; Broken-- Calculation of Thermal Noise (11), N = 100.

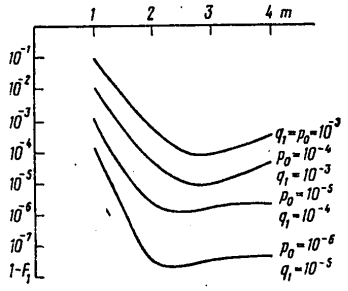

Figure 3. Dependence of the Error Probability $1 - F_1$ in Pulse Train Reception by the Quasi-optimum Algorithm from the Train Size m (N = 100).

with (11), while with a reduction in $\gamma_ш$ the absolute value of the power loss is decreased for both distributions.

2. As figure 3 shows, there exists an optimum in the sense of minimum error probability $1 - F_1$ size of the periodic train m equal in the cases considered to two to three pulses. With a reduction in p_0 and q_1 the optimum train

size is reduced. Note that the presence of a minimum $1 - F_1$ with respect to m is a result of the random nature of the signal. It is significant that with the conversion from transmitting a single pulse to transmitting two pulses $1 - F_1$ is reduced by several factors. Thus, for synchronization it is necessary to send short periodic pulse trains.

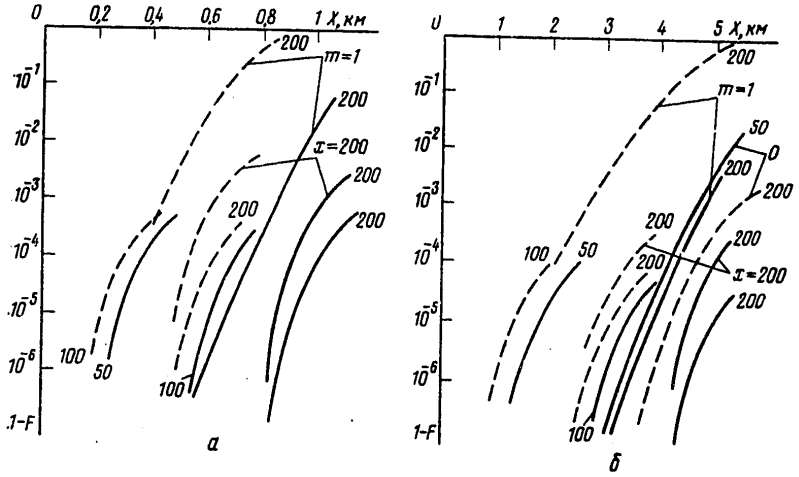

Figure 4. Dependence of the Error Probability 1 - F in Pulse Train Reception of Optimum Size by Optimum (o) and Quasi-optimum Algorithms from Distance X for Various q_c N = 100; X = 20 km; $\gamma_ш \tau$ = 1. Unbroken Curves -- Poisson Distribution; Broken -- Calculation of Thermal Noise (11): a -- μ = db/km; b -- μ = 2 db/km.

3. In calculating the error probability $1 - F_{трав}$ for an entire line, the exponential attenuation of the signal $\gamma_c = d_c \exp(-ux)$ has been taken into account. With convergence of the repeaters the probability of error $1 - F_{трав}$ diminishes monotonally (fig. 4). The curves in figure 4 represent the dependence of $1 - F_{трав}$ for Q_c and $\gamma_ш$.

Increasing the length of the line, of course, leads to an increase in the error probability which may, however, be compensated for easily with a small convergence of the repeaters (such as in the case of μ - 2 db/km, $d_c\tau$ = 200, $1 - F_{трав} = 10^{-5}$ with X - 20 km x = 3.2 km and with X = 200 km x = 3 with (11). The transmission of optimum-sized pulse trains ensures a considerably greater noise-immunity than transmission of a single pulse.

As figure 4 shows, the quasi-optimum circuit as opposed to the optimum provides a definite reduction in the number of repeaters, less significant the stronger the signal.

BIBLIOGRAPHY

1. Middleton, D. "Introduction to Statistical Communications Theory", 2, Izd. Sovetskoye radio, 1960.

2. Sheremet'yev, A. G. "Statisticheskaya teoriya laxernoy svyazi" [Statistical Theory of Laser Communications], Izd. Svyaz', 1971.

3. Gol'dshteyn, Yu. A.; and Frezinskiy, B. Ya. RADIOTEKHNIKA, 33, 10, 1978.

[]72-2845]

8945
CSO: 1860

UDC 621.391.278

OPTIMIZATION OF A PROCEDURE FOR SEQUENTIAL DETECTION OF THE DELAY IN A RECEIVED SIGNAL

Moscow RADIOTEKHNIKA I ELEKTRONIKA in Russian No 7 1979 pp 1351-1359

[Article by V. N. Naumov, L. N. Barannikov and A. I. Zhodzishchskiy:
"Optimization of a Procedure for Sequential Detection of the Delay in a Received Signal"]

[Text] A procedure for detecting the delay in a signal received in a background of normal white noise is considered. It is assumed that information about the delay is extracted by a comparator and the detection procedure consists of measuring the comparison of the received and reference signals and the corresponding shift in the delay of the reference signal.

For a known received signal envelope, an algorithm for variation of the delay in the reference signal is found at each detection stage. Examples of detection algorithms are given for several signal envelopes.

Introduction

One of the main problems in operating digital radio lines using signals with a complex envelope is establishing synchronization(1). This process consists, as a rule, of differencing the delay in the reference $\tau_{оп}$ and received $\tau_{пр}$ signals.

The synchronizing process consists of the stage of detecting the value of the received signal delay relative to the reference signal with error not exceeding the capture range of the tracking system and the tracking stage. The primary focus of the article is on the detection stage.

At present various methods are known for detecting the delay in $\tau_{пр}$ (1-4). When there is no limit to the number of receiver channels in the detection

unit, a multichannel comparator is best from the point of view of minimum detection time. The number of channels M in such a comparator equals the ratio of the detection range for delay T to the required accuracy :

$$M = \text{integer } (T/\tau_{ош}).$$

A significant increase in the amount of equipment in this unit, proportional to the number of channels, is a defect in a multichannel detection unit with a large M value. For this reason a comparator with one channel is often used in practice for establishing synchronization.

To detect the $\tau_{пр}$ value in a single-channel detection unit, the delay of the reference signal is varied according to a certain principle. The principle for varying the delay of the reference signal is usually selected either linearly or randomly. However, these principles of variation of $\tau_{оп}$ are not optimum for all signal envelopes.

In general form, a single-channel detection unit with a comparator may be presented in the form of a functional circuit (fig. 1). A single-channel comparator is the input block of the detection unit. To this input is applied a signal y(t) which is an additive mixture of the received signal $s(t-\tau_{пр})$ with the unknown delay in and standard white noise n(t). The comparator produces measurements X_i from the input signal in discrete time:

$$(1) \qquad X_i = \frac{1}{p_c T_i}\int_0^{T_i} y(t)s(t-\tau_{оп i})dt = R(\tau_i)+n_i = R(\tau_{пр}-\tau_{оп i})+n_i,$$

where P_c is the power of the received signal, T_i is the time for producing the i measurement, $\tau_{оп}$ is the delay in the reference signal during production of the i measurement, $R(\tau_i) = R(\tau_{пр} - \tau_{оп i})$ is the function of autocorrelation of the received signal, n_i is the noise component of the measurement distributed normally with deviation σ_i.

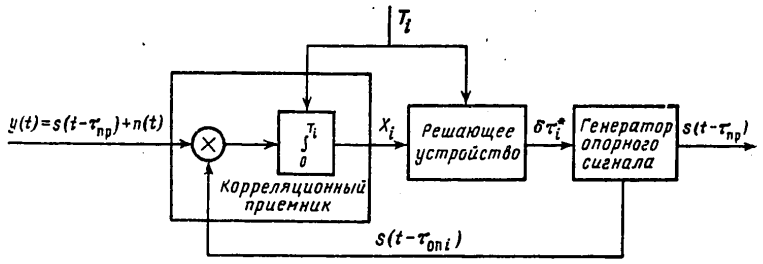

Figure 1. Functional Circuit of Detection Unit

During detection it is assumed that the power of the received signal and noise as well as the value of the delay $\tau_{пр}$ remain constant. Detection of the value of the delay $\tau_{пр}$ relative to $\tau_{оп}$ is done by varying the reference signal delay. The algorithm for varying the reference signal delay (the

detection algorithm) is incorporated in the decision unit which according to the information contained in the preceding measurements makes a decision on the magnitude of the delay in the reference signal for the next measurement and also a decision on the termination of detection. The decision to terminate detection is made when the absolute value of the error in determination of $\tau_{пр}$ does not exceed $\tau_{доп}$ with the assigned probability P. Thus, the detection procedure consists of a certain number of stages of the same type. Each stage includes production of a measurement X, the adoption of a decision on the magnitude of the reference signal delay for the next measurement and accordingly the shift of the delay in the reference signal generator as well as the adoption of a decision on termination of detection.

1. Optimum Detection Algorithm

Let us consider an optimum algorithm for varying the delay $\tau_{опт}$ which makes it possible on the average to minimize the overall detection time. To determine the value of the delay of a received signal in the T range with a given accuracy $\tau_{доп}$ it is necessary to extract a certain amount of information on the delay I_{Σ}. Inasmuch as a large detection time is required on the average for extracting a large I_{Σ}, minimizing the average detection time is equivalent to maximizing the average amount of information extracted in a certain number of detection stages n. The greater the overall amount of information on $\tau_{пр}$ extracted in n detection stages, the greater the information extracted at each detection stage. Thus, the optimum detection algorithm can be defined from the condition of maximization of the average amount of information extracted at each detection stage. Note that in a number of studies (5,6,7) an information criterion is also used in optimizing synchronization systems.

The average amount of information according to Shannon (6) consisting of an i measurement relative to the delay in the received signal under the condition that the values of the first produced measurementd equal $X_1,\ldots,X_{i-1}$ is determined by the formula

$$(2)\qquad I_{срi}=\int\limits_{(\tau_{пр},X_i)} W(X_i,\tau_{пр}/X_1,\ldots,X_{i-1})\times \times\ln\frac{W(X_i,\tau_{пр}/X_1,\ldots,X_{i-1})}{W(X_i/X_1,\ldots,X_{i-1})W(\tau_{пр}/X_1,\ldots,X_{i-1})}dX_i d\tau_{пр},$$

where $W(X_i,\tau_{пр}/X_1,\ldots,X_{i-1})$ is a two-dimensional conditional density of the probability that the produced measurement i has the value X_i and the delay in the received signal equals if the first produced measurements have the values $X_1,\ldots,X_{i-1}$; $W(X_i/X_1,\ldots,X_{i-1})$ is the conditional probability density that the produced measurement i has the value X_i if i-1 of the first produced measurements have the values $X_1,\ldots,X_{i-1}$; $W(\tau_{пр}/X_1,\ldots,X_{i-1})$ is the conditional density of the probability of the presence of the given value $\tau_{пр}$ on condition that i-1 of the first produced measurements have the values $X_1,\ldots,X_{i-1}$.

The limits of integration in (2) are determined by the range of occurrence of $\tau_{пр}$ and the admissible probability of error P.

Let us consider the case of the application of signals having the monotonic function $R(|\tau|)$ with a uniform a priori distribution principle for $\tau_{пр}$. We will use a piecewise approximation R( ) where the maximum length $|\tau_1 - \tau_2|$ of any linear section of $R(\tau)$ is determined from the equations

$$X_i - \alpha\sigma_i = R(\tau_1),$$
$$X_i + \alpha\sigma_i = R(\tau_2),$$

and $q\sigma_i$ is fould from the admissible probability P of the accurate detection of the magnitude of the delay:

$$P = 2\int_0^{\alpha\sigma_i} \frac{1}{\sqrt{2\pi}\sigma_i} \exp\left[-\frac{X^2}{2\sigma_i^2}\right] dX.$$

In this case it can be shown that the expression for the average amount of information has the approximate form

$$(3) \qquad I_{cpi} \simeq \frac{1}{2}\int_{(X_i)} \ln\left[1 + \frac{1}{A_{i-1}}\left(\frac{R'(X_i)}{\sigma_i}\right)^2\right] \times \frac{\exp\left\{-\frac{[X_i - R(\tau_{oni} - B_{i-1}/A_{i-1})]^2}{2\sigma_i^2[1+(1/A_{i-1})(R'(X_i)/\sigma_i)^2]}\right\}}{\sqrt{2\pi\sigma_i^2[1+(1/A_{i-1})(R'(X_i)/\sigma_i)^2]}} dX_i.$$

In (3) the values A_i and B_i respectively are found from the formulas

$$A_i = \sum_{k=1}^{i}\left(\frac{R'(X_k)}{\sigma_i}\right)^2 = A_{i-1} + \left(\frac{R'(X_i)}{\sigma_i}\right)^2,$$

$$B_i = \sum_{k=1}^{i}\left(\frac{R'(X_k)}{\sigma_k}\right)^2 [\tau(X_k) + \tau_{onk}] = B_{i-1} + \left(\frac{R'(X_i)}{\sigma_i}\right)^2 [\tau(X_i) + \tau_{oni}],$$

and $R'(X_i) = R'(\tau(X_i))$ is the value of the derivative function of autocorrelation at the point $\tau(X_i)$ where $\tau(X_i)$ is the value of the inverse function $R(\tau)$ with $R(\gamma) = X_i$. From (3) it is apparent that only the value of the component $R(\tau_{oni} - B_{i-1}/A_{i-1})$ depends on the choice of $\tau_{оп}$.

We will designate by τ_{o}, the value of the independent variable of this component by which the maximum $I_{cp\,i}$ is provided. Then the optimum value of the reference signal delay $\tau_{опт\,i}$ at this detection stage is determined as follows:

$$\dot{\tau}_{опт\,i}=\frac{B_{i-1}}{A_{i-1}}+\tau_{оi}. \tag{4}$$

We will substitute in (4) the expression for B_{i-1}. After conversion we obtain

$$\dot{\tau}_{опт\,i}=\dot{\tau}_{опт\,i-1}+\frac{[R'(X_{i-1})/\sigma_i]^2[\tau(X_{i-1})+\tau_{оi-1}]}{A_{i-1}}+\tau_{оi}-\tau_{оi-1}. \tag{5}$$

From (5) it is apparent that the shift in the delay of the reference signal $\delta\tau_{опт}{}^{*}=\tau_{опт\,i}{}^{*}-\tau_{опт\,i-1}^{*}$ at the i detection stage depends on the squares of the characteristic slope of the correlation function which correspond to the values of the preceding measurements.

The dependence $\tau_0(A)$ should be calculated in (5) up to the accomplishment of detection. If $|R'(\tau)|$ is the monotonic function of $|\tau|$, then considering that it may only be a monotonally nonprogressive function as follows from (3), with any value of A and σ we obtain $\tau_0 = 0$.

The optimum detection algorithm described by equation (5) is rather complicated in its practical implementation. This algorithm may be simplified if information consisting only of the last measurement is used in determining $\tau^{*}_{опт}$. With this assumption, as (5) shows, the value of the reference signal delay in a quasi-optimum algorithm is determined by the equation

$$\dot{\tau}_{опт\,i}=\dot{\tau}_{опт\,i-1}+\tau(X_{i-1})+\tau_{оi}. \tag{6}$$

The functional circuit of the unit which implements the quasi-optimum algorithm for sequential detection is illustrated in figure 2.

In computing the signs with τ (X) it is not known that it results in am ambiguous definition of the direction of shift in τ. To eliminate the ambiguity it is necessary to determine the direction of shift of the reference signal delay at the beginning of detection and if $\tau_0 < q\sigma$ then not to pass the peak of the autocorrelation function to subsequent stages with probability P.

To rule out the possibility of passing the peak because of errors in producing the measurements it is necessary to decrease the value of the shift by the delay. In figure 3 a typical dependence of $R(\tau)$ it shown which elucidates this requirement. The actual value of $R(\tau)$ with probability P differs from the value of the produced measurement X by no more than $q\sigma$.

For this reason, to exclude the possibility of passing the optimum value of the delay τ_{c_i}, it is necessary to reduce the value of the shift by τ to

$$\Delta\tau_i=\tau(X_{i-1})-\tau(X_{i-1}+\alpha\sigma_{i-1}). \tag{7}$$

If not only the last measurement is considered, then it is possible to show that $\Delta\tau_i$ will be equal to

$$\Delta\tau_i=\frac{\alpha}{\sqrt{A_{i-1}}}.$$

Note that in the article is not considered the question of distribution of the measurement production time between the detection stages. The principle of distribution of T_i is determined by the form of the autocorrelation function and is not successfully obtained in general form. It is possible to find it by solving the variation problem for n detection stages where the magnitude of error during detection and the probability P will act as the limits.

2. Examples of Detection Algorithms

For examples let us consider detection algorithms for the delay in a pseudonoise video signal constrcuted on the basis of an M-train and a composite video signal constructed of two pseudonoise signals with multiple cadence frequencies.

For both signals, in order for the tracking system capture to take place, it is necessary to determine the delay of the received signal relative to the reference signal with error no greater than $\tau_{\text{н}}$. Here $\tau_{\text{н}}$ is the minimum duration of the symbol of the pseudonoise signal. However, since the decision to terminate detection is made in the presence of an excess in $R(\tau)$ of the threshold value $X_{\text{пор}}=\alpha\sigma$, the magnitude of error should be no greater than $\tau_{\text{доп}}=\tau_{\text{н}}(1-\alpha\sigma)$. Standardized autocorrelation functions of the pseudonoise signal (PShS) and the composite signal are represented in figures 4 and 5 respectively. These autocorrelation functions are not smooth and consequently they cannot be approximated in the entire range of τ linearly. Since for PDhS in the entire range of τ for exclusion of the range where cessation of detection is produced $R'(\tau)=0$, equation (5) for determining $\tau^*_{\text{опт}i}$ is expressed in (6).

The actual value of R( ) for each of the produced measurements of X_i falls within probability P in the range from $X-\alpha\sigma$ to $X+\alpha\sigma$. For this reason, as demonstrated earlier, in order to prevent passing $\tau_{\text{пр}}$ it is necessary to decrease the magnitude of the shift in comparison with (6) to Δ t, shifting $\tau_{\text{опт}}$ in one direction.

At the same time it is possible to increase the magnitude of shift of the delay to accelerate the detection procedure as the result of an additional

shift in the referende signal delay to $\tau_{cш}$ since during detection error in the delay is permissible. Thus, for the reasons indicated above, in calculating the correction for the magnitude of shift of $\tau_{cш}$ expression (6) may be given the form

$$\delta\tau^{*}_{оп i}=\tau_{оп i+1}-\tau^{*}_{оп i}=\tau(X_i)+\tau_0-\Delta\tau+\tau_{оп}. \quad (8)$$

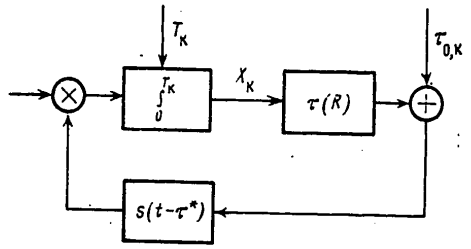

Figure 2. Functional Circuit of Quasi-optimum Detection Unit

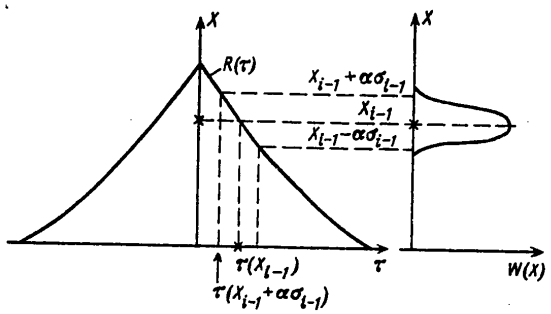

Figure 3

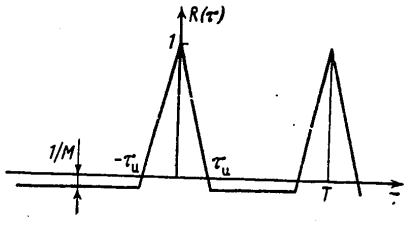

Figure 4. Autocorrelation Function of Pseudonoise Signal

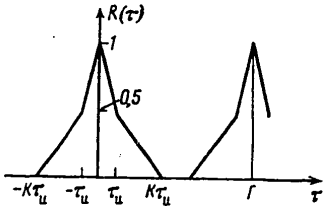

Figure 5. Autocorrelation Function of Composite Signal

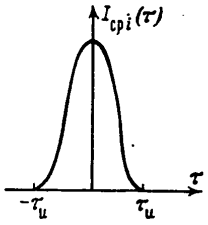

Figure 6. Average Amount of Information Contained in One Measurement

We find the value $\tilde{\tau}_0$ for PShS from the condition of maximization of the amount of information extracted at each detection stage. The qualitative dependence $I_{cp}(\ )$ for PShS calculated by formula (3) is presented in figure 6. As figure 6 shows, $\tilde{\tau}_0 = 0$.

Since all the measurements produced outside of the peak of the autocorrelation function carry, on the average, an identical amount of information about $\tau_{пр}$, the time for producing them should be identical at all detection stages, i.e. $T_i = T_j = T_1$ and therefore $\sigma_i = \sigma_j = \sigma$.

Since for PShS of figure 4 in the limits of peak

$$R(\tau_i)=1-\frac{\tau_i}{\tau_и}\left(1+\frac{1}{M}\right)=X_i,$$

then taking (7) into account we obtain

$$\tau(X_i)=\frac{(1-X_i)\tau_и}{1+\frac{1}{M}},$$

$$\Delta\tau=\frac{\alpha\sigma\tau_и}{1+\frac{1}{M}},$$

where M is the number of symbols in the PShS period.

We determine τ_{om} from the condition of accurate adoption of a decision to terminate detection with probability P, i.e.

$$\tau_{om}=\frac{(1-2\alpha\sigma)\tau_{и}}{1+\frac{1}{M}}.$$

Finally we obtain

$$\delta\tau^{\cdot}_{oиi}=\tau^{\cdot}_{oиi+1}-\tau^{\cdot}_{oиi}=\frac{(2-X_i-3\alpha\sigma)\tau_{и}}{1+\frac{1}{M}}. \tag{9}$$

In order to find the optimum time for producing measurements it is necessary to minimize with respect to σ the average detection time

$$T_{ср}=\frac{M\tau_{и}T_1}{2\delta\bar{\tau}_{oи}}, \tag{10}$$

where T_1 is the time for producing one measurement; $\delta\bar{\tau}_{om}$ is the average magnitude of shift of the reference signal delay.

Calculating (1), the value T_1 may be written in the form

$$T_1=G_0/P_c\sigma^2, \tag{11}$$

where G_0 is the spectral density of the power of the random process at the input of the meter; P_c is the power of the signal.

Assuming $M \gg 1$ after neutralizing $\delta\bar{\tau}^{*}_{oиi}$ with respect to X, we obtain

$$\delta\bar{\tau}_{oи}=(2-3\alpha\sigma)\tau_{и}. \tag{12}$$

Substituting (11) and (12) in (10) and minimizing $T_{ср}$ with respect to σ we obtain what is the optimum value $\sigma = 4/9$.

Then with $M \gg 1$ the equation for shift of the reference signal delay finally may be written as:

$$\delta\tau^{\cdot}_{oиi}\simeq\left(\frac{2}{3}-X_i\right)\tau_{и}. \tag{13}$$

Thus, the magnitude of shift of the delay $\tau_{oи}$ with detection of $\tau_{иp}$ of the PShS depends on the result of the preceding measurement and depends practically none on the probability P necessary for accomplishing detection. The final expression for the average detection time has the form

$$T_{ср}\simeq 3{,}8M\frac{G_0\alpha^2}{P_c}. \qquad (14)$$

For illustration we will compare $T_{ср}$ of the optimum detection algorithm with the often encountered in practice sequential linear detection. With linear scanning the shift of $\tau_{оп}$ is accomplished discretely at each detection stage at a constant magnitude. For this algorithm it can be shown that the optimum magnitude of shift of the delay $\tau_{оп}$ and $a\sigma$ are equal respectively to $2/3\,\tau_и$ and 1/3. Then the minimum average detection time for linear scanning is found from the formula

$$T_{ср\ лин}=6{,}75M\frac{G_0\alpha^2}{P_c}. \qquad (15)$$

From comparison of expressions (14) and (15) it is apparent that with the optimum algorithm the average detection time is 1.75 times less than with linear scanning.

For the second example of detection algorithms let us consider the detection algorithm for a composite signal. As figure 5 shows, an autocorrelation function of the composite signal taken as the example has three characteristic sections in which it is linear. In the first section in the range of delay $K\tau_и \leq |\tau| \leq T/2$ the optimum detection algorithm for $\tau_{пр}$ coincides with the one considered earlier for PShS. As studies have shown, the components in equation (8) for the given form of $R(\tau)$ are determined from the formulas $\sigma_i = \sigma_j = \sigma$, $\tau_{ош} = K\tau_и(1 - 2a\sigma)$, $\tau_0 = 0$ and $\tau_{пр} = 4Ka\sigma\tau_и$. Finding the optimum value of σ, we obtain $a\sigma = 2/9$ while equation (13) for a composite signal will have the form

$$\delta\tau_{1i}^{*}=2K\tau_и\left(\frac{1}{3}-X_i\right). \qquad (16)$$

The average detection time of the peak of the autocorrelation function in this section is accordingly equal to

$$T_{ср}\simeq 15{,}2\frac{M}{K}\frac{G_0\alpha^2}{P_c}.. \qquad (17)$$

After adopting a decision on the detection of the peak of the autocorrelation function with an excess in the magnitude of X of the threshold 2/9, it is necessary to produce an additional measurement shifted by the delay relative to the last in magnitude $K\tau_и/3$ in the direction opposite to that in which detection in the first delay section was done. Analyzing the ratio of the measurements of the last two measurements, it is possible to determine correctly the direction of further shift of $\tau_{оп}$.

In the second delay section $\tau_и \leq |\tau| \leq K\tau_и$ the derivative of the autocorrelation function is different from zero and therefore the detection algorithm should

calculate the information contained in all of the measurements produced in this section. Since the derivative of the autocorrelation function in this delay section is constant, the time for producing the measurements should not depend on their number in the series. As the studies have shown, the following ratios hold true for the detection information in the second delay section:

$$\tau_{om}=(1-\alpha\sigma)\tau_{\text{н}};\quad \tau_{i}=2K\tau_{\text{н}}\alpha\sigma/\sqrt{i}.$$

According to (5), taking into account $\tau_{0\text{ш}}$ and $\Delta\tau$ and assuming $M\gg 1$, it can be shown that the algorithm for a shift in the delay $\tau_{0\text{ш}}$ is described by the equation

$$(18)\qquad \delta\tau_{\text{оп}i}^{\cdot}\simeq\frac{K\tau_{\text{н}}}{i}\left[1-2X_{i}-\frac{\alpha\sigma}{\sqrt{i+1}}\right]+(1-\alpha\sigma)\tau_{\text{н}}.$$

The decision to terminate detectin is made when there is an excess in the magnitude of X_i for the threshold value $X_{\text{пр}}\rho=0.5+\alpha\sigma$. Minimizing the average detection time by σ it is possible to find the optimum magnitude of the threshold $X_{\text{опф}}$ and the optimum time for producing the measurements.

Conclusions

1. An optimum algorithm is found for detecting the delay in a received signal with a single-channel comparator synthesized according to the criterion of the maximum average amount of information extracted from measurements.

2. For signals with monotonic dependence, the autocorrelation function from the modulus of its independent variable is obtained by the simple expressions (5) and (6) for calculating the magnitude of shift of the reference signal delay.

3. An optimum detection algorithm is given for pseudonoise and composite signals. Comparison of the average time for detecting the delay in a pseudonoise signal with the optimum algorithm and with a linear scanning algorithm has shown that with the optimum algorithm, detection is accomplished 1.75 times more rapidly on the average.

BIBLIOGRAPHY

1. Toplyakov, I. M.: Kalashnikov, I. D.; and Roshchin, B. V. "Radiolinii kosmicheskikh sistem peradachi informatsii" [Radiolines for Space Information Transmission Systems], Izd. Sovetskoye radio, 1975.

2. Golomb, S. "Tsifrovyye metody v kosmicheskoy svyazi" [Digital Methods in Space Communications], Izd. Svyaz', 1969.

3. Uord. "Discrimination of Pseudonoise Signals by the Sequential Analysis Method", 8, ZARUBEZHNAYA RADIOELEKTRONIKA, 1966.

4. Pestryakov, V. B. "Shymopodobniyye signaly v sistemakh peredachi informatsii" [Noise-type Signals in Information Transmission Systems], Izd. Sovetskoye radio, 1973.

5. Levin, B. R. "Teoreticheskiye osnovy statisticheskoy radiotekhniki" [Theoretical Bases of Statistical Radio Engineering], Izd. Sovetskoye radio, 1966.

6. Klyuyev, N. I. "Informatsionnyye osnovy peredachi soobshcheniy" [Information Fundamentals of Communications Transmission], Izd. Sovetskoye radio, 1966.

7. Sviridenko, S. S. "Osnovy sinkhronizatsii pri priyeme diskretnikh signalov" [Fundamentals of Synchronization in the Reception of Discrete Signals], Izd. Svyaz', 1974.

[272-8945]

8945
CSO: 1860

UDC 621.391.812

GROUND AND SPACE MICROWAVE LINK RADIO WAVE PROPAGATION

Moscow RASPROSTRANENIYE RADIOVOLN NA TRASSAKH NAZEMNYKH I KOSMICHESKIKH RADIOLINIY (Propagation of RAdio Waves on Ground and Space Radio Links) in Russian 1979 signed to press 27 Dec 78 pp 2, 290-293

[Annotation and table of contents from book by Anatoliy Ivanovich Kalinin, Svyaz', 3,600 copies, 296 pages]

[Text] This book examines the laws governing propagation of microwaves on line-of-sight microwave relay links, tropospheric microwave relay links, and satellite communication links and presents methods of calculating the statistical characteristics of signals. The author also presents data on propagation of microwaves, requisite for solving problems of electromagnetic compatibility of different radio systems using common frequency bands.

This book is intended for engineers and technicians working on the development and design of ground and space radio links; it can also be useful to upper-division students enrolled at communications electrical engineering institutes.

Contents Page

3024
CSO: 1860

UDC: 621.396.4

RADIO RELAY COMMUNICATIONS

Moscow RADIORELEYNAYA SVYAZ' in Russian 1979

[Annotation and Table of Contents from Book by V. V. Markov, Izdatel'stvo "Svyaz', 368 pages]

[Text] This textbook is intended for tekhnikum students taking the radio relay communications course on specialty 0706 "TV equipment and radio relay communications." The book describes the principles of designing direct visual range radio relay lines, and tropospheric and satellite communications lines. Basically, radio relay lines with frequency division of channels and frequency modulation are considered. Apparatus design principles on examples of radio relay lines being operated at present are considered.

Table of Contents

[267-2291]

2291
CSO: 1860

UDC 621.396.96

INTERFERENCE OF SIDE LOBES OF A LINEAR-FREQUENCY SIGNAL FROM A NEAR TARGET

Kiev IZVESTIYA VYSSHIKH UCHEBNYKH ZAVEDENIY: RADIOELEKTRONIKA in Russian No 7, 79 signed to press 24 Mar 78 pp 93-95

[Article by P. M. Golubev]

[Text] The possibility of using 2 LChM [linear-frequency modulated] signal depends to a great extent on the interference action of side lobes. The interference is determined not only by the level of the side lobes, but also by the nature of the relationship between this level and time. This is demonstrated especially when remote targets are detected on the background of side lobes of the signal from a near target. The relative position of signals in this case is shown in Fig. 1. In this figure, τ is the delay time of signal 1, reflected from the near target.

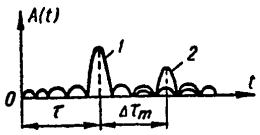

Fig. 1

We will find the signal to lobe ratio

$$q_m = \frac{A_2}{A_{БЛ1}},$$

where A_2 is the amplitude of signal 2, reflected from the remote target; $A_{БЛ1}$ is the amplitude of the side lobe of signal 1. We will seek this ratio for those time intervals between signals $\Delta\tau_m$ in which the side lobes of signal 1 are maximum.

We will assume, first, that the LChM signal processing is done by means of a matched filter. Then the signal envelope at the filter output may be represented in form [1].

$$A(\Delta\tau) = A\left|\frac{\sin \pi\Delta f\Delta\tau\left(1-\frac{|\Delta\tau|}{T}\right)}{\pi\Delta f\Delta\tau}\right|,$$

$$\text{for} \quad |\Delta\tau| \leqslant T, \tag{1}$$

where Δf, T are, respectively, frequency deviations and the duration of the LChM signal.

The distribution of side lobe maxima along the time axis depends on the value of the base $B = \Delta fT$. The analysis of expression (1) shows that side lobes with clearly expressed maxima take place at $B \geqslant 4$. If, for simplicity of the analysis, we assume that B is an even number, then with sufficient accuracy, it may be considered that the maxima of the side lobes correspond to the moments when the sine in expression (1) is equal to unity. Then on the basis of (1), we will obtain for moments that determine the position of maxima.

$$\Delta\tau_m\Delta f = 3{,}4 \quad \text{for} \quad m = 1,\ B = 4,$$

$$\Delta\tau_m\Delta f = \begin{cases} \frac{B}{2}\left[1-\sqrt{1-\frac{2(2m+1)}{B}}\right] & \text{for} \quad 1 \leqslant m \leqslant \frac{B}{4}-\frac{1}{2}, \\ \frac{B}{2}\left|1+\sqrt{\frac{2(2m+1)}{B}-1}\right| & \text{for} \quad \frac{B}{4}+\frac{1}{2} \leqslant m \leqslant \frac{B}{2}-1, \end{cases} \tag{2'}$$

where $B \geqslant 6$ and B/2 is an odd number;

$$\Delta\tau_m\Delta f = \begin{cases} \frac{B}{2}\left[1-\sqrt{1-\frac{2(2m+1)}{B}}\right] & \text{for} \quad 1 \leqslant m \leqslant \frac{B}{4}-1, \\ \frac{B}{2}\left[1+\sqrt{\frac{2(2m+3)}{B}-1}\right] & \text{for} \quad \frac{B}{4} \leqslant m \leqslant \frac{B}{2}-2, \end{cases} \tag{2''}$$

where $B \geqslant 8$ and B/2 is an even number.

In expression (2), m is the number of the side lobe. It follows from (2) that for an even base and B $\geqslant$ 6

$$\frac{B}{2}\left(1-\sqrt{1-\frac{6}{B}}\right)\leqslant\Delta\tau_m\Delta f\leqslant\frac{B}{2}\left(1+\sqrt{1-\frac{2}{B}}\right). \qquad (3)$$

For these limits on the basis of (1), we will obtain the amplitude of side lobes of signal 1

$$A_{\text{БЛ1}}=\frac{A_1}{\pi\Delta f\Delta\tau_m}.$$

The signal from target 2 may be expressed through the signal from target 1, if the relationship between the amplitudes and the effective dispersion area (EPR) of the target and the distance are taken into account

$$A_2=A_1\sqrt{\frac{S_2}{S_1}}\frac{\tau^2}{(\tau+\Delta\tau_m)^2}, \qquad (4)$$

where S is the EPR of the target. Then we obtain for the signal to lobe ratio

$$q_m=\frac{\pi\sqrt{\frac{S_2}{S_1}}\Delta f\Delta\tau_m}{\left(1+\frac{\Delta\tau_m}{\tau}\right)^2} \qquad (5)$$

when condition (3) is met.

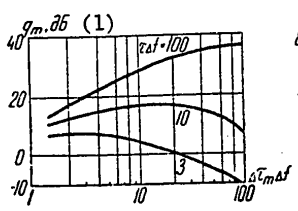

Fig. 2

1. Db

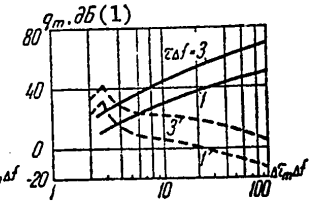

Fig. 3

1. Db

In Fig. 2 are shown the q distributions in the side lobe zone of action for various distances from the near target, expressed by the number of resolution sections. These distributions were calculated from (5) on the assumption that target EOR are equal. By taking into account condition (3), it is possible to use the curves of Fig. 2 for various signal bases. It is then found that the interference of side lobes increases with the decrease in the distance to the near target. The interference by more remote lobes increases especially strongly.

Inasmuch as the very last lobe appears for $\Delta\tau_m \simeq T$, , then for $\tau_{min} \ll T$ on the basis of (5) we will obtain

$$q_\tau \simeq \frac{\pi \sqrt{\frac{S_2}{S_1}}\, \tau_{min}^2 \Delta f}{T},$$

where τ_{min} is the delay time corresponding to the minimum distance to the near target.

It follows from here that to reduce the interference of remote side lobes it is necessary to increase the frequency deviation and decrease the duration of the signals.

It follows from the curves that for $\tau\Delta f < 10$, detecting targets in the action zone of side lobes will be unreliable, especially if the EPR of the near target is greater. Therefore, additional measures for reducing the side lobes are necessary.

Usually, a frequency weighted processing [1] is used for reducing the side lobes in the receiver after compressing the LChM signal.

We will assume that after weighted processing, the spectrum of the compressed signal may be approximated by a curve of form

$$G(\omega) = k + (1-k)\cos^2 \frac{\pi(\omega - \omega_0)}{\Delta\omega}, \qquad (6)$$

where $0 \leqslant k \leqslant 1$. Expression (6) for a rectangular LChM signal spectrum describes the frequency characteristic of the weighted processing filter. On the basis of the Fourier transformations, we will obtain the following expression for the signal envelope at the output

$$A(\Delta\tau) = A\left|\frac{1 - \frac{2k}{1+k}(\Delta f \Delta\tau)^2}{1-(\Delta f\Delta\tau)^2} \frac{\sin \pi\Delta f\Delta\tau}{\pi\Delta f\Delta\tau}\right|. \qquad (7)$$

It follows from (7) that when k=o there is a sharp decrease in the side lobe amplitudes in the far zone and that when k=0.08 the smallest peak level of side lobes is obtained. Both cases are characterized by small losses for mismatching and a small reduction in the resolution capacity [1].

Fig. 3 shows distributions of q_m at various distances to the nearest target calculated on bases (4) and (7) on the assumption that the EPR of targets are equal (solid lines for k=1, broken lines at k=0.08).

It follows from Fig. 3 that weighted processing at k=o makes it possible to reduce sharply the interference of the remote side lobes. As a result, favorable conditions are provided for detecting remote targets at practically any distances to the nearest target. The greatest interference in this case is due to the near side lobes.

Weighted processing at k=0.08, conversely, provides the best conditions for detection on the background of the near side lobes, while remote lobes provide the greatest interference.

The analysis above makes it possible to conclude that the best detection conditions in the entire side lobe zone at minimal losses for mismatching, and a small reduction in the resolution capacity may be obtained by the combined utilization of the indicated weighted processing devices.

BIBLIOGRAPHY

1. Kuk, Ch.; Bernfel'd, M. "Radar Signals." Moscow SOVETSKOYE RADIO, 1971

[269-2291]

2291
CSO: 1860

UDC 621.396.931

ON THE EFFECTIVENESS OF CIRCULAR POLARIZATION ANTENNAS IN SYSTEMS OF RADIO COMMUNICATION WITH MOVING OBJECTS

Moscow RADIOTEKHNIKA in Russian Vol 34, No 1, 1979, pp 72-75

[Article by E. S. Golovin]

[Text] A number of methods of increasing reliability and noise stability of communication systems working under the conditions of multipath propagation of radio waves of the meter and decimeter ranges [1], for example, adaptive and spaced reception, developed for tropospheric radio lines, due to the complexity of instrument solutions and the necessity of expanding the spectrum of woking frequencies, still cannot be realized in systems of communication with moving ground objects.

The searching for the ways of further lowering the intensity of multipath interference led to the idea of using radio waves with circular polarization in systems of mobile radio communication, and the results of the first experimental work [2,3] are already encouraging. The purpose of this work is to give a theoretical evaluation of the gain in the suppression of multipath interference in switching from the linear polarization of radio waves to circular polarization.

Let us assume that a stationery transmitter emits a monochromatic wave with circular polarization which can be represented in the form of a sum of waves with orthogonal (vertical and horizontal) linear polarizations

$$E_k = E_{oz}\exp i\varphi_0 + E_{ox}\exp i\left(\varphi_0+\frac{\pi}{2}\right),\ E_{oz} = E_{ox}.$$

The field at the point of reception is formed by a direct wave from the transmitter and N reflected waves arriving chiefly in a horizontal plane from reradiators, for example, from the walls of artificial structures arbitrarily situated around the route of the movement of the object, i.e.,

$$E_0 = E_{np} + E_{otp} = \left[E_z\exp i\varphi_1 + E_x\exp i\left(\varphi_1+\frac{\pi}{2}\right)\right] + \\ + \left[E_{1z}\sum_{n=1}^{N}K_{nz}\exp i\varphi_n + E_{1x}\sum_{n=1}^{N}K_{nx}\exp i\left(\varphi_n+\frac{\pi}{2}\right)\right], \quad (1)$$

where E_z, E_x, φ_1; E_{1z}, E_{1x}, φ_n are the amplitudes and phases of the orthogonal components, respectively, of the direct and reflected waves ($E_z=E_x$, $E_{1z}=E_{1x}$); K_{nz}, K_{nx} are the reflection coefficients for the waves, respectively, with vertical and horizontal orthogonal polarizations of the field.

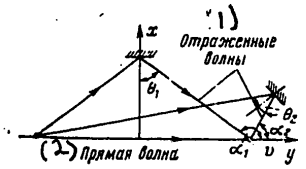

Figure 1
Key: 1. Reflected waves
2. Direct waves

In the general case, coefficients K_{nz} and K_{nx} are complex values and are defined by the known Frenel formulas. Since we are going to solve the problem not of an absolute but a relative evaluation of the suppression of multipath interference in switching from linear polarization to circular polarization, it is possible to simplify the analysis and consider the reflectors as ideal dielectrics, particularly because a number of concrete and brick structures have similar properties for the waves of the metric and decimetric ranges.

Then K_{nz} and K_{nx} are independent of the frequency and electric conductance of the reflecting surfaces, i.e.,

$$K_{nz}=K_z(\theta_n)=\frac{\cos\theta_n-\sqrt{\varepsilon-\sin^2\theta_n}}{\cos\theta_n+\sqrt{\varepsilon-\sin^2\theta_n}};\quad K_{nx}=K_x(\theta_n)=\frac{\varepsilon\cos\theta_n-\sqrt{\varepsilon-\sin^2\theta_n}}{\varepsilon\cos\theta_n+\sqrt{\varepsilon-\sin^2\theta_n}}. \qquad (2)$$

where θ_n is the angle of incidence (reflection) of the n-th wave (Figure 1), and ε is the dielectric constant of the material of the reflectors.

Since the orthogonal components of waves have different reflection coefficients, each reflected wave at the reception point has now an elliptic polarization and not circular polarization, and at $0<\theta_n<\theta_б$ the directions of the rotation of the vector of the electric field and the vector of the direct wave are opposite, and at $\theta_б<\theta_n<\pi/2$ they coincide. The angle θ (Brewster angle) is equal to $\theta_б=\arccos(1/\sqrt{1+\varepsilon})$.

Any wave with elliptic polarization can be represented in the form of two waves with circular polarization of mutually opposite rotation

$$E=E_1\exp i\varphi_0+E_2\exp i\left(\varphi_0+\frac{\pi}{2}\right)=\left[\frac{E_1+E_2}{2}\exp i\varphi_0+\right.$$
$$\left.+\frac{E_1+E_2}{2}\exp i\left(\varphi_0+\frac{\pi}{2}\right)\right]+\left[\frac{E_1-E_2}{2}\exp i\varphi_0+\frac{E_1-E_2}{2}\exp i\left(\varphi_0-\frac{\pi}{2}\right)\right].$$

Applying this rule to all reflected waves and switching from orthogonal scanning of each wave to the usual recording, we have the following for the field components at the point of reception instead of (1):

$$E_{\Sigma} = \underset{(1)}{E_{\text{пр}}} + \underset{(2)}{E_{\text{отр1}}} + E_{\text{отр2}} = E_0 \exp i\varphi_1 + 0{,}5E_1 \sum_{n=1}^{N} [K_z(\theta_n) + K_x(\theta_n)] \exp i\varphi_n + 0{,}5E_1 \sum_{n=1}^{N} [K_z(\theta_n) - K_x(\theta_n)] \exp i\varphi_n.$$

Key: 1. Direct
2. Reflected1

If the moving object has a circular-polarization nondirectional antenna matched with the direct wave of the transmitter E_{dir}, then the electromotive force at its output is created only by the direct wave and the first field component of the reflected waves $E_{reflected1}$. However, the second component $E_{reflected2}$ are not received, because the reflected waves forming it have the opposite direction of rotation of the planes of polarization to E_{dir} and $E_{reflected1}$.

The total power of the reflected waves received by the antenna and creating interference to reception will be determined with the aid of the expression for the function of spatial correlation of the field at the point of reception. For this, we shall make up the product

$$E^{*}_{\text{отр1}} E'_{\text{отр1}} = 0{,}25E_1^2 \sum_{n=1}^{N} [K_z(\theta_n) + K_x(\theta_n)] \exp(-i\varphi_n) \times \times \sum_{n=1}^{N} [K_z(\theta_n) + K_x(\theta_n)] \exp i\left(\varphi_n + \frac{2\pi}{\lambda} r \cos\alpha_n\right), \quad (3)$$

where $E^{*}_{reflected1}$ is the value of complex conjugate of $E_{reflected1}$; $E'_{reflected1}$ is the field at the point removed from the initial point by the value of spatial separation r, and the phase of the n-th wave at this point changes by $2\pi/\lambda \; r \cos\alpha_n$; α_n is the azimuthal angle of the arrival of the n-th wave at the point of reception; λ is the wave length. In order to obtain the correlation function, it is necessary to perform averaging in (3) over the ensemble of possible statistical values of random geometric (θ_n and α_n) and phase (φ_n) angles:

$$\langle E^{*}_{\text{отр1}} E'_{\text{отр1}} \rangle = 0{,}25E_1^2 \Big\langle \sum_{n=1}^{N} \sum_{m=1}^{N} [K_z(\theta_n) + K_x(\theta_n)] [K_z(\theta_m) + K_x(\theta_m)] \exp i(\varphi_m - \varphi_n) \exp i\frac{2\pi}{\lambda} r \cos\alpha_m \Big\rangle. \quad (4)$$

It is evident that there exists a definite dependence between θ_n and α_n, therefore, having expressed $\alpha = f(\theta)$, it is sufficient to perform averaging only over θ_n. Since the time delays τ_n of reflected waves are independent, and their root-mean-square deviation on real routes are greater than the period of oscillation of the metric and decimetric ranges [5] then it is possible to consider that the random phase angles $\varphi_n = \omega_0 \tau_n$ are statistically independent from one another and of θ_n. Then the right part of (4) can be represented in the form of two separate averages over θ_n and φ.

$$\langle E^*_{\text{отр}} E'_{\text{отр}} \rangle = 0{,}25E_1^2 \sum_{n=1}^{N} \left\langle [K_z(\theta_n) + K_x(\theta_n)]^2 \exp\left[i \frac{2\pi}{\lambda} r \cos\alpha(\theta_n) \right] \right\rangle +$$
$$+ 0{,}25E_1^2 \sum_{\substack{n=1 \\ n \neq m}}^{N} \sum_{m=1}^{N} \left\langle [K_z(\theta_n) + K_x(\theta_n)] [K_z(\theta_m) + K_x(\theta_m)] \exp\left[i \frac{2\pi}{\lambda} r \cos\alpha(\theta_m) \right] \right\rangle \left\langle \exp i(\varphi_m - \varphi_n) \right\rangle.$$

The slow nature of the variations of τ_n along the movement routes makes it possible to speak of the constancy of the distribution density $\omega_0(\tau_m - \tau_n)$ in each 2π interval for any values of $K_{z,x}(\theta_n)$ and $K_{z,x}(\theta_m)$. Consequently, the value of $\omega_0(\tau_m - \tau_n)$ is evenly distributed in the interval $0\text{-}2\pi$ and is independent of $K_{z,x}(\theta_n)$ and $K_{z,x}(\theta_m)$, which is in agreement with the data given in [4,5]. Then $\langle \exp i(\varphi_m - \varphi_n) \rangle = 0$ and we have for the spatial correlation function

$$B_{\text{отр}}(r) = 0{,}25NE_1^2 \int_0^{\pi/2} [K_z(\theta) + K_x(\theta)]^2 \exp\left[i \frac{2\pi}{\lambda} r \cos\alpha(\theta) \right] W(\theta)\, d\theta,$$

where $W(\theta)$ is the distribution density of angles θ.

The solution of this integral would make it possible to determine not only the spatial correlation function of the electric field, but also, by using the relation $r = v\tau$ (v -- speed of movement), to go over to the time correlation function and the energy spectrum of the multipath signal in the antenna of the mobile receiver matched with the direct wave with respect to polarization. The difficulty lies in the absence of experimental data on the functional dependence between the geometric angles $\alpha = f(\theta)$. However, in order to solve this problem, it is sufficient to know the dispersion of the reflected waves, and this does not require the clarification of the above dependence. In fact,

$$\sigma_k^2 = B_{\text{отр}}(0) = 0{,}25NE_1^2 \int_0^{\pi/2} [K_z(\theta) + K_x(\theta)]^2 W(\theta)\, d\theta. \qquad (5)$$

The reradiators are concentrated arbitrarily around the moving object, therefore it is expedient to consider that angles θ are evenly distributed in the interval $0—\theta_0$, i.e., $W(\theta) = 1/\theta_0$. Moreover, the maximum value of $\theta < \pi/2$

(at $\theta \to \pi/2$, the reradiators must be arranged directly along the route of movement), and for concrete and brick reflectors $\varepsilon > 3 \div 4$, then the value of $\sin^2\theta$ under the radical in formulas (2) can be disregarded. The integral obtained as a result of the substitution of the $W(\theta)$ law and simplified expressions for $K_Z(\theta)$ and $K_X(\theta)$ in (5) is reduced to a tabular integral, and its solution is written in the form

$$\sigma_x^2 = \frac{0{,}25NE_1^2}{\theta_0}\left[4\theta_0 - \frac{2\varepsilon \sin 2\theta_0}{(\sqrt{\varepsilon} + \varepsilon\cos\theta_0)(\sqrt{\varepsilon} + \cos\theta_0)} - \right.$$
$$\left. - \frac{8\varepsilon\sqrt{\varepsilon}\operatorname{arctg} A}{(\varepsilon-1)\sqrt{\varepsilon-1}} + \frac{4\ln|B|}{(\varepsilon-1)\sqrt{\varepsilon-1}}\right]. \qquad (6)$$

where

$$A = \frac{\sqrt{\varepsilon}-1}{\sqrt{\varepsilon-1}}\operatorname{tg}\frac{\theta_0}{2};\quad B = \frac{(\sqrt{\varepsilon}-1)\operatorname{tg}\frac{\theta_0}{2} + \sqrt{\varepsilon-1}}{(\sqrt{\varepsilon}-1)\operatorname{tg}\frac{\theta_0}{2} - \sqrt{\varepsilon-1}}.$$

For comparison, let us determine the dispersion of the field of the reflected waves when nondirectional linear antennas are used in the transmitter and the receiver (for example, vertical dipoles). In this case, (5) has the form

$$\sigma_z^2 = B_{отр}(0) = NE_1^2\int_0^{\pi/2} K_z^2(\theta)\,W(\theta)\,d\theta.$$

Solving the integral with consideration for the assumption introduced above, we obtain

$$\sigma_z^2 = \frac{NE_1^2}{\theta_0}\left[\theta_0 + \frac{8\sqrt{\varepsilon}}{(\varepsilon-1)\sqrt{\varepsilon-1}}\operatorname{arctg} A - \frac{4\varepsilon\sin\theta_0}{(\varepsilon-1)(\sqrt{\varepsilon}+\cos\theta_0)}\right]. \qquad (7)$$

In order to evaluate the effectiveness of the circular polarization antennas which, unlike linear antennas, receive only a part of the energy of the reflected waves, let us make up the relation

$$\frac{\sigma_z^2}{\sigma_x^2} = \frac{\theta_0 + \frac{8\sqrt{\varepsilon}}{(\varepsilon-1)\sqrt{\varepsilon-1}}\operatorname{arctg} A - \frac{4\varepsilon\sin\theta_0}{(\varepsilon-1)(\sqrt{\varepsilon}+\cos\theta_0)}}{0{,}25\left[4\theta_0 - \frac{2\varepsilon\sin 2\theta_0}{(\sqrt{\varepsilon}+\varepsilon\cos\theta_0)(\sqrt{\varepsilon}+\cos\theta_0)} - \frac{8\varepsilon\sqrt{\varepsilon}\operatorname{arctg} A}{(\varepsilon-1)\sqrt{\varepsilon-1}} + \frac{4\ln|B|}{(\varepsilon-1)\sqrt{\varepsilon-1}}\right]}. \qquad (8)$$

The dependence diagram of $\sigma_z^2/\sigma_x^2 = f(\theta_0)$ (Figure 2) plotted with the aid of (8) makes it possible to make the following conclusions.

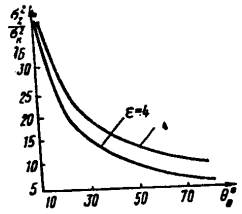

Figure 2

1. The dispersion of the field of reflected waves received by a circular-polarization antenna is considerably smaller than the dispersion of the total field of the waves received by a linear-polarization antenna. This is explained by the peculiarities of the rereflection mechanism of waves and the property of circular-polarization antennas to accomplish the wave polarization selection.

In fact, waves from a transmitter, for example, with counterclockwise rotation of the vector of the electric field, when reflecting from a system of independent reradiators along the route due to different moduli and phases of reflection coefficients K_{nz} and K_{nx}, change to a set of elliptically polarized waves each of which has a depolarized component with clockwise rotation of the vector of the electric field. If the receiving antenna matched with the direct wave from the transmitter has counterclockwise circular polarization, then the depolarized component of the reflected waves will not induce an electromotive force in it and, consequently, the power of the multipath interference at the input of the receiver will decrease.

2. The intensity of the depolarized components unmatched with the receiving antenna depends on the angle of reflection (incidence) θ_n increasing as it decreases (it is known that at $\theta_n = 0$, i.e., during normal incidence of a wave on a dielectric plane, the direction of the rotation of the vector of the electric field changes to opposite). Therefore the relation σ_z^2/σ_x^2, and, consequently, the effectiveness of circular-polarization antennas from the viewpoint of the selection of multipath interference increases sharply at narrow beams of reflected waves (the range of angles θ_o is small) which can be formed by reradiators situated in the vicinity of the transmitter and follow the moving object or by reradiators ahead of the object along its route and come toward it from the opposite direction. This situation occurs frequently along real routes, particularly when communicating with automobiles on country highways and trains in electrified sections of railroads, as well as when receiving signals with a stationary receiver whose antenna is situated considerably higher than local reradiators.

3. There exists a definite dependence of the relation σ_z^2/σ_x^2 on the dielectric constant of the material of reradiators. As $\hat{\varepsilon}$ increases, the

effectiveness of circular-polarization antennas also increases, which, evidently, is explained by less sharp changes in the reflection coefficient within a wide range of the angles of incidence of waves and increase in the power of waves unmatched with the antenna with respect to polarization.

Bibliography

1. Nimirovskiy, A. S. ELEKTROSVYAZ' [Telecommunications], No 5, 1970.

2. Cunningham, M. L. TRANS IEEE, Vol com-21, No 11, 1973.

3. Lee, C. Y., Yeh, Y. S. TRANS IEEE, Vol com-20, No 5, 1972.

4. Clarke, R. H. BSTJ, Vol 47, No 6, 1968.

5. Gans, M. J. TRANS IEEE, VT-21, No 1, 1972.

10,233
CSO: 1860

UDC 621.396.931

ACTUAL NOISE-IMMUNITY OF AUTOMATIC SELECTION DEVICES IN MOBILE RADIO COMMUNICATIONS SYSTEMS

Kiev IZVESTIYA VYSSHIKH UCHEBNYKH ZADEDENIY: RADIOELEKTRONIKA in Russian No 7, 79 manuscript received 19 June 78 pp 75-78

[Article by E. S. Golovin]

[Text] When designing mobile line radio communications system for main transport lines, the problem arises of providing continuity of information exchange between subscribers of the central office (TsS) and the mobile radio station (MS) when the station moves from the zone of action of one line office (LS) to the zone of action of another. There are two basic groups of radio systems depending upon the method of their solution. In the first group [1], transmitters of adjacent LS, connected to each other and to the TsS by a line communications channel, operate simultaneously on different carrying frequencies, while in an equal-signal zone in the MR receiver is implemented by an automatic selection signal of the transmitter of that LS, that provides a greater signal to noise ratio n in the channel at a given moment. In the reverse direction of communications (MR → TsS) an LS receiver, also with a high value of n, is connected to the line channel, while a receiver for other LS is disconnected in the TsS apparatus to avoid interference signals.

The second group includes systems in which transmitters of adjacent LS have equal carrying frequencies, however, a transceiver of only one LS is always connected to the line and the radio-channels. The connecting signal is formed in a special TsS device after an analysis is made of n ratios at the receiver outputs of all LS. To implement such systems which save the number of channels between LS and TsS, it is necessary to provide additional control channels [2].

In these and other systems, devices for automatic selection of the best branch LS ⇄ MR that solve the problem of the information exchange continuity are used and, moreover, with proper selection of parameters, raise the reliability of communications in an equal-signal zone when signals fade due to the multibeam propagation of radio waves. Automatic

selection devices are also provided in TsS and MR receivers of radial communications networks for organizing space-diversity reception.

The advantages of automatic selection over separate reception, from the viewpoint of raising the reliability of communications and improving the signal to noise ratio in a channel with a fading signal, are well-known [3]. However, retuning the MR receiver in an equal-signal zone in line communications systems or switching antennas with diverse reception in radial communications systems are accompanied by the origination of switching noises, because the processes in branches, in the first case, differ in frequencies and, in the second case, are not synphase. This paper evaluates the powers of the indicated kinds of noises and determines the conditions when the power approaches the minimum value.

As is well known, two types of automatic selections are available -- simple and optimal. In optimal automatic selection, at any moment of time, communications are implemented over a branch with the maximum ratio of n and requires continuous comparative analysis of n in both branches, which requires the use of two receiving channels. The latter is very undesirable in the apparatus of mobile radio systems, therefore, a simple automatic selection is usually used instead of the optimal one in which communications are implemented over a branch with a ratio n, exceeding a given threshold level n_0, switching to the other branch every time that condition $n > n_0$ is violated.

We will consider a radio communications line system in which transmitters of adjacent LS radiate monochromatic signals with different frequencies Ω_1 and Ω_2, while simple automatic selection in receiver MR is reduced to retuning the latter from frequency Ω_1 to frequency Ω_2 and back according to a signal of the analyzing threshold device, connected to the output of the UPCh [Intermediate frequency amplifier] channel. Then the signal at the input of the converter will be a random process $\xi(t)$ with a sudden change in frequency, which assumes one of two independent values Ω_1 and Ω_2 and remains constant in a finite segment of time -- equal frequency interval $\Delta\tau$, the length of which is determined by the statistics of fading and the threshold level of the analysing device. In analysing such a process, the behavior of its phase and frequency is of great importance, while changes in amplitude, important only for the operation of the analyzer, may be neglected and the following can be written

$$\xi(t) = \sqrt{2}\cos[\omega_k t + \varphi_k],$$

where φ_k -- are, in the general case, initial random phase signals in the diversity branches, constant in interval .

An expression is obtained in [4] for the normalized average correlation function of a similar process with a frequency assuming N possible values, which for our case assumes form

$$R(\tau)=\overline{\xi(t)\,\xi(t-\tau)}=P_0(\tau)\sum_{m=1}^{2}P(\Omega_m)\,[1-\gamma P(\Omega_m)]\cos\Omega_m\tau+$$

$$+\sum_{m=1}^{2}P^2(\Omega_m)\,\gamma\cos\Omega_m\tau, \qquad (1)$$

where $P(\Omega_m)$ -- probability of $\omega_k=\Omega_m$, $\gamma=\overline{\cos(\varphi_1-\varphi_2)}$; $P_0(\tau)$ -- probability of moments t and t-τ being located in an equal frequency interval.

Statistical signal parameters in branches in an equal-signal zone may be considered equal, therefore, we will assume that $P(\Omega_1)=P(\Omega_2)=0{,}5$, while equal frequency intervals $\Delta\tau$ coincide in length and are equal to the average interval length between blips $\overline{\Delta\tau}$ of the envelope of the narrow band process above level C_0 coinciding with the threshold level of the analyzer. In Rice's model of fading, which is true, if, at the receiving point, there is a direct wave from the stationary transmitter with amplitude A_0 and M-reflected waves, forming a normal process with dispersion σ_0^2, we have [5]

$$\overline{\Delta\tau}=\frac{1}{m_0}\sqrt{\frac{2\pi}{-\rho_0''}}\exp\left(\frac{A_{01}^2+m_0^2}{2}\right)\frac{B}{I_{01}(A_{01}m_0)}, \qquad (2)$$

where

$$B=\int_0^{m_0}x\exp\left(-\frac{A_{01}^2+x^2}{2}\right)I_0(A_{01}x)\,dx,\ m_0=\frac{c_0}{\sigma_0}>0,\ A_{01}=\frac{A_0}{\sigma_0},\ \rho_0''$$

-- second derivative of the autocorrelation function of the normal process at τ = 0. Then

$$P_0(\tau)=\begin{cases}1-|\tau|/\overline{\Delta\tau} & \text{for } |\tau|\leqslant\overline{\Delta\tau}\\ 0 & \text{for } |\tau|>\overline{\Delta\tau}.\end{cases} \qquad (3)$$

Taking into account (1), we can write

$$R(\tau)=0{,}5\,[1-0{,}5\gamma]\,[1-|\tau|/\overline{\Delta\tau}]\,[\cos\Omega_1\tau+\cos\Omega_2\tau]+$$
$$+0{,}25\gamma\,[\cos\Omega_1\tau+\cos\Omega_2\tau]. \qquad (4)$$

Normalized spectral density of the average power of process $\xi(t)$ is equal to

$$S(\omega) = 2\int_0^{\infty} R(\tau)\cos\omega\tau d\tau = (1-0{,}5\gamma)\overline{\Delta\tau}\left[\frac{\sin^2[(\omega-\Omega_1)\overline{\Delta\tau}/2]}{(\omega-\Omega_1)^2\Delta\tau^2}+\frac{\sin^2[(\omega-\Omega_2)\Delta\overline{\tau}/2]}{(\omega-\Omega_2)^2\overline{\Delta\tau}^2}\right]+$$
$$+0{,}25\pi\gamma[\delta(\omega-\Omega_1)+\delta(\omega-\Omega_2)]. \qquad (5)$$

Frequency components $\omega+\Omega_1$ and $\omega+\Omega_2$ are not considered here because the width of the power spectrum of the fluctuating process is much smaller than the values of received frequencies Ω_1 and Ω_2. The first two addends of (5) characterize the continuous (noise) part of the process, while the last two are discrete (signal) components.

We can calculate the power of the noise and signal components at the UPCh output with an ideal filter and a $2\Delta\omega$ bandpass by formula

$$P_k = \frac{1}{\pi}\int_{\Omega_0-\Delta\omega}^{\Omega_0+\Delta\omega} S(\omega)\,d\omega,$$

where $\Omega_0 = \Omega_1 - \Omega_r' = \Omega_2 - \Omega_r''$ is the intermediate frequency of the receiver. The solution of this integral taking into account (5) has the form

$$P_k = \frac{2(1-0{,}5\gamma)}{\pi\Delta\omega\overline{\Delta\tau}}[\cos(\Delta\omega\overline{\Delta\tau}-1)]+\frac{2}{\pi}(1-0{,}5\gamma)\,\mathrm{Si}(\Delta\omega\overline{\Delta\tau})+0{,}5\gamma, \qquad (6)$$

where Si (z) is the integral sine .

The quotient of dividing the last addend by the sum of the first two gives the signal-to-noise ratio at the modulator input. Calculations according to formulas (2) and (6), presented as curves in Figs. 1a and 1b, make it possible to draw the following conclusions.

For a given UPCh $\Delta\omega$ bandpass, the signal-to-noise ratio of switching decreases when interval $\Delta\overline{\tau}$ increases (Fig. 1a), because the percentage of time increases during which the level of the received signal is lower than the analyzer threshold in the automatic selection circuit and the switching speed of the communications branches increases. In case $\Delta\omega$ and $\Delta\overline{\tau}$ are constant, ratio $P_c/P_{шк}$ reaches the maximum value when phases of signals in branches are (γ = 1) and decreases when the correct phase is absent ($\gamma < 1$).

The length of interval $\Delta\overline{\tau}$, according to (2) and Fig. 1b, depends on the analyzer threshold (C_0/σ_0), the ratio of direct and reflected waves (A_0/σ_c), as well as their statistical parameters ρ_0''. As shown in

[6], in mobile radio communications systems ρ_0'' is determined by the nature of the multiwires and type of antenna system and is in the order of $\rho_0'' = -\omega_д^2$, where $\omega_д = \omega_0 \frac{V}{C}$ is the doppler frequency.

It is possible to increase ratio $P_c/P_{шк}$ for given communications conditions by reducing the threshold level of the analyzer. However, in this case, the automatic selection loses its advantages from the viewpoint of increasing the reliability of communications during signal fading and raising the signal to thermal noise ratio

$$n = \frac{P_c}{P_{шт}}.$$

Actually, the distribution density of this ratio for a doubled automatic selection with the Rayleigh type of signal fading is determined by expression [3]

$$W(n) = \frac{1}{n_м}\left[1 - \exp\left(-\frac{n_м}{n_0}\right)\right]\exp\left(-\frac{n}{n_м}\right) + \frac{1}{n_м}\exp\left(-\frac{n}{n_м}\right)E(n - n_0 \ldots \quad (7)$$

where n_M -- ratio of medium value of signal to the noise dispersion,

$$n_м = A_м^2/\sigma_ш^2;$$

n_o -- ratio of threshold level of the analyzer to the noise dispersion

$$n_0 = C_0^2/\sigma_ш^2;\ E(n - n_0) = 1$$

$E(n-n_o) = 1$ at $n > n_o$ and 0 at $n < n_o$. Average value of n on the basis of (7) is equal to

$$\frac{P_в}{P_{шт}} = n_м\left[1 + \frac{n_0}{n_м}\exp\left(-\frac{n_0}{n_м}\right)\right].$$

The value obtained approaches the maximum value at $n_0 \to n_{0opt} = n_м$, while the ratio

$$\frac{P_c}{P_{шк}} \to \max \quad \text{at} \quad \frac{C_0}{\sigma_0} \to 0.$$

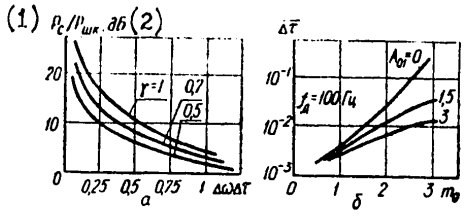

Fig. 1

1. $P_c/P_{шк}$ 2.db

It follows, therefore, that there exists an optimal value of the threshold level of the analyzer at which the noise resistance of the receiver will be maximal for two kinds of noises.

It was assumed previously that the length of equal frequency intervals $\Delta\tau$ in the equal signal zone is constant and is equal to the average interval between the blips of the narrow band process. This limitation may be removed if the distribution density of such intervals $W(\Delta\tau)$ is known. Then, instead of (3), it is necessary to write

$$P_0(\tau)=\int_{|\tau|}^{\infty}(1-|\tau|/\Delta\tau)\,W(\Delta\tau)\,d\Delta\tau$$

and make similar calculations. Regrettably, no expression fo $W(\Delta\tau)$ convenient for calculation has been published even for a Rayleigh model of fading.

The relationships obtained in the paper may be used also for evaluating the actual noise resistance of an automatic selection installation when organizing the usual space-diversity reception. In this case, the reception frequency is constant $P(\Omega_1)=P(\Omega_2)=1$ and multiplier 0.5 in front of coefficient γ disappears in expression (6). Then, for a full inphase state of signals in branches ($\gamma=1$), independently of threshold level

$$\frac{P_c}{P_{шк}}\to\infty,$$

which was to be expected.

BIBLIOGRAPHY

1. Sakata Tatsuporr. Communications system for running trains. Jap. Railway Eng., 1970, 20, No 10, p 25.

2. Bilenko, A. P.; Morgunov, L. N.; Kuz'min, V. I. "Multichannel System of the 'Altay' Mobile System of the Ultra-Shortwave Radio Communications." ELEKTROSVYAZ'. 1972, No 1, p 1.

3. Zyuko, A. G. "Interference Resistance and Efficiency of Communications Systems." Moscow, "Svyaz'," 1972.

4. Barsukov, Yu. K. "Correlation Function and Spectrum of Sinusoidal Oscillations for Sudden Random Changes of Frequency and Phase. " RADIOTEKHNIKA I ELEKTRONIKA, 1965, 10, No 4, p 595.

5. Tikhonov, V. I. "Blips in Random Processes." Moscow, "Nauka," 1970.

6. Golovin, E. S. "On Antenna Effect on Statistical Characteristics of the Signal Envelope in Communications Systems with Mobile Objects." RADIOTEKHNIKA, 1977, 32, No 2, p 32.

[269-2291]

2291
CSO: 1860

ELECTROCOMMUNICATIONS EQUIPMENT AND ITS PRODUCTION

Moscow APPARATURA ELEKTROSVYAZI I EE PROIZVODSTVO in Russian 1979 signed to press 25 Oct 78 pp 2, 326-328

[Annotation and table of contents from book by Anatoliy Filippovich Gryzlov; Aristid L'vovich Meytin'sh; and Yuris Petrovich Pone, Izdatel'stvo "Vysshaya shkola," 17,000 copies, 328 pages]

[Text] The technology of assembly and wiring operations during production of electrocommunications equipment is examined in the book. Particular attention is devoted to the switching and electroradio elements which form the basis for switching and channel-forming equipment. Information on telephony and telegraphy, as well as the principles of multichannel communications are presented, and power-supply devices are described. Individual chapters are devoted to interchangeability. tolerances and play, technical and electrotechnical measurements, quality control and labor safety procedures.

Table of Contents

9194
CSO: 1860

UDC 535

ELECTRONIC-OPTICAL CONVERTERS AND THEIR USE IN SCIENTIFIC RESEARCH

Moscow ELEKTRONNO-OPTICHESKIYE PREOBRAZOVATEL I IKH PRIMENENIYE V NAUCHNYKH ISSLEDOVANIYAKH in Russian, 1979 pp 432

[Annotation and table of contents from book by Mikhail Mikhaylovich Butslov; Boris Mikhaylovich Stepanov; and Sergey Dmitriyevich Fanchenko, Izdatel'stvo "Nauka," 432 pages]

[Text] This book considers a broad calss of devices for spectral conversion, amplification and analysis of pictures. The first section presents the physical principles of forming and tramsmitting pictures. It also considers certain general properties of pictures with brightness near the threshold and of short duration. The second section of rhe book describes electronic-optical converters and brightness amplifiers of various systems, while the last two chapters of the fourth section describe experimental apparatus and apparatus manufactured by industry for electronic-optical high-speed photography.

The third and fourth sections present a detailed review of the use of electronic-optical devices and apparatus in physical research (including laser and thermonuclear), in astronomy, biology and medicine.

Table of Contents

Table of Contents

Table of Contents

Table of Contents

2291
CSO: 1860

621.317.4

ELECTRICAL CONDUCTIVITY SENSORS

Moscow DATCHIKI ELEKTROPROVODNOSTI in Russian 1979 signed to press 19 Dec 78 pp 2, 156-167

[Annotation and table of contents from menograph by Mikhail Matveyevich Zakharov, Izdatel'stvo "Nauka", 1800 copies, 156 pp]

[Text] This menograph discusses sensors based on inductive windings and ring magnets and also sensors in the form of systems of electrodes of various configurations. A theory of sensors is presented, taking account of the nature of interaction of a quasistationary electromagnetic field with a semiconductor, and problems of analysis of sensor characteristics are solved.

The book is intended for scientific, engineering and technical workers.

Contents Page

8480
CSO: 1860

UDC 621.371.5.[Illegible] 11

MATHEMATICAL SIMULATION OF EXTERNAL ELECTROMAGNETIC FIELDS OF SOURCES

Minsk IZVESTIYAVYSSHIKH UCHEBNYKH ZAVEDENIY: ENERGETIKA in Russian No 6, 1979 pp 34-38

[Article by Docent S. M. Apollonskiy, Candidate in Technical Sciences]

[Text] At the present time various methods of passive shielding are used for lowering external electromagnetic fields of electric equipment. The determination of electromagnetic fields and calculation of shields present certain difficulties.

However, the solution of problems of shielding can be simplified substantially if the real sources of electromagnetic fields are replaced by their equivalent models which are a set of dipoles. As was shown in [1], it is possible to create them if there are available data about the nature of the distribution of the fields over some geometric surface of the second order covering the sources of the fields. The distribution of the fields of real sources is presented in the form of the sum of electromagnetic fields of dipoles arbitrarily oriented and arranged within the above-mentioned surface. The dipoles used in modeling

$$D^{i}(\vec{M}^{(i)}(t),\ \vec{r}_0^{(i)}),$$

where i=1, 2, ..., 6 is the number of dipoles, are defined by six parameters: the components of the moment $\vec{M}^{(i)}(t)$ of the dipole along the axis of the coordinates and $\vec{r}^{(i)}_0$ -- coordinates of the center of the dipole. The moment of the dipole $\vec{M}^{(i)}(t)$ is the time function and in quasi-stationary approximation can be written in the form of

$$\vec{M}^{(i)}(t) = \vec{M}^{(i)}_m \exp[j(\omega t - \alpha\xi)],$$

where $\vec{M}^{(i)}_m$ is the dipole moment modulus; ω is the frequency of the electromagnetic field; α -- is the coefficient; and ξ is the coordinate.

For a rotating field: $\alpha = \frac{\pi}{\tau}$, $\varepsilon = \varphi$; for a traveling field: $\alpha = \frac{\pi}{\tau}$, $\varepsilon = x$; and for a pulsating field: $\alpha = 0$. Here, τ is the pole pitch.

In order to determine the parameters of the dipoles of an equivalent model, it is necessary to have information about the arrangement of the sources and their geometry. Therefore, in their analysis it is assumed that the

arrangement of the sources and their form are known and, consequently, the approximate arrangement of the dipoles is also known. In addition, it is also assumed that the frequency spectrum of a real electromagnetic field does not exceed 5000 Hz, which makes it possible to use the quasi-stationary approximation in solving a system of Maxwellian equations.

This article gives a method of numerical determination of the parameters of specially oriented dipoles with whose aid it is possible to replace a real field of a source at any distance from its surface.

1. The problem of the determination of the parameters of dipoles approximating a prescribed field is formulated in the following way. Let us assume that normal electric or magnetic intensities of the electromagnetic field $F_{n|k}$* are known at points Q_k(k=1, 2, ..., N) which are evenly distributed over a second-order surface S (of a sphere, circular cylinder, ellipsoid, etc), $\Phi_{n|k}$ are the corresponding normal intensities of electromagnetic fields of dipoles which approximate the external field of the source. The problem is solved if the parameters of the dipoles are determined in such a way that the error δ, when the field of the source is replaced by the field of the model,

$$\delta = \sum_{k=1}^{N} [F_n(Q) - \Phi_n(Q)]_k \qquad (1)$$

is smaller than the prescribed number $\varepsilon(\delta < \varepsilon)$.

In order to solve the problem, the normal electric or magnetic intensities of the electromagnetic field known at the points of the surface must be compared with the corresponding intensities of a field arbitrarily located and oriented in relation to the center of the coordinates of the dipole.

In order to determine the electric or magnetic intensity of the electromagnetic field of the dipoles, it is possible to use the expression for a scalar dipole potential in the form of [2]:

$$V(Q) = -\frac{\vec{M}(L)\vec{R}_{QL}}{4\pi(\mu, \varepsilon)\vec{R}_{QL}}, \qquad (2)$$

where $\vec{M}(L)$ is the vector of the magnetic or electric dipole moment; (μ, ε) are the relative magnetic and electric permeability of the medium, respectively; R_{QL} is the distance from the point L of the location of the dipole to the observation point Q

$$R_{QL} = \sqrt{(x_L - x_Q)^2 + (y_L - y_Q)^2 + (z_L - z_Q)^2}.$$

*If the distribution $F_{n|k}$ is prescribed on a closed surface, then the field outside the surface S is fully determined. This follows from the uniqueness of the solution of the external Neumann problem.

With consideration for (2), the intensities $\vec{F}(Q)$ on the surface S are determined from the expression

$$\vec{F}(Q) = \frac{1}{4\pi(\mu, \varepsilon)} \left[3 \frac{\vec{R}_{QL}}{R_{QL}^5} (\vec{M}(L) R_{QL}) - \frac{\vec{M}(L)}{R_{QL}^3} \right]. \quad (3)$$

In order to find the dipole parameters

$$M_x^{(i)}(L),\ M_y^{(i)}(L),\ M_z^{(i)}(L),\ x_{Li},\ y_{Li},\ z_{Li},$$

where $M_x^{(i)}(L),\ M_y^{(i)}(L),\ M_z^{(i)}(L)$ are the components of the moment of the i-th dipole; $x_{Li},\ y_{Li},\ z_{Li}$ are the coordinates of the center of the i-th dipole (i=1, 2, ..., G -- the number of dipoles, equivalentizing fields of the source), a system of algebraic equations is constructed:

$$F_n(Q)|_k = \left\{ \frac{1}{4\pi(\mu, \varepsilon)} \left[3 \frac{\vec{R}_{QL}}{R_{QL}^5} (\vec{M}(L) \vec{R}_{QL}) - \frac{\vec{M}(L)}{R_{QL}^3} \right] \right\}_k. \quad (4)$$

If $F_n(Q)|_k$ are known, the system of equations (4) makes it possible to determine the parameters of each of the G dipoles. To do this, it is necessary to solve a system of equations for $N \gg 6G$. Due to the fact that the equations of the system are nonlinear, the most effective method is that of differentiation with respect to the parameter [3,4]. The latter can be considered as an approximate method of solving a system of nonlinear equations.

2. The determination of the parameters of dipoles of a model of an electromagnetic field of a source is carried out in the following sequence. First, we find the parameters of the first dipole satisfying normal intensities of the field on the surface S at a certain number of points Q_k. As a rule, a dipole creating maximum known field intensities on S is selected. On the same surface, normal field intensities created by the dipole at points Q_k - $\Phi_n(Q)|_k$ are calculated, and then the error $\delta^{(1)}$ and the remanent field with intensity $F^{(1)}{}_n(Q)|_k$ are calculated. Then, the intensities of the remanent field are used to determine parameters of the second dipole of the model, the error $\delta^{(2)}$ and the second remanent field with intensity $F^{(2)}{}_n(Q)|_k$. If necessary, the parameters of the third dipole, the value of the remanent field and $\delta^{(3)}$ are calculated. Calculations are continued until the error $\delta^{(i)}$ becomes less than ε ($\delta^{(i)} < \varepsilon$).

Thus, the problem of the replacement of a real external field of a source by a field of a system of dipoles can be solved if the investigator has the necessary information about intensities $F_n(Q)|_k$ of the electromagnetic field at points Q_k on one of the surfaces of the second order. When approximating external fields of working electrical equipment, information about normal intensities $F_n(Q)|_k$ can be obtained in the process of the experiment.

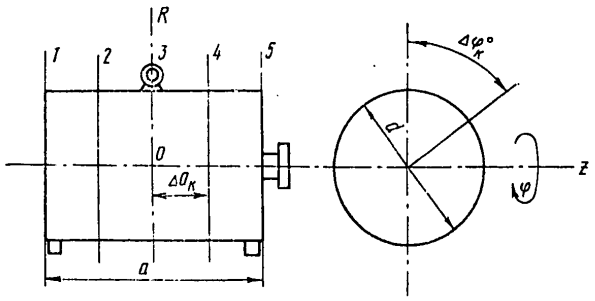

Figure 1

An example of the approximation of the magnetic field of an asynchronous motor is given below.

3. For a fixed moment of time, normal intensities of the field at points Q_k evenly distributed over the surface are measured on the body of the motor or in the immediate vicinity of it and points with the maximum intensity are determined. It is assumed that the direction of the axis of the dipole and its position are determined by the line connecting the points with the maximum intensity, and the modulus of its moment $M^{(1)}_m$ is found by solving only two equations from (4). Having determined the parameters of the first dipole, we find that intensities created by it at points Q_k on S, and the first remanent field, where points with the maximum intensity are also isolated, and by them we find the second dipole $M^{(2)}_m$ and the second remanent field. The process of approximation continues until the required accuracy is reached.

Example. In order to construct a dipole model of an asynchronous squirrel-cage motor of the type A-42-4 with the following principal data (delta connection of stator phases):

$$P_H=2.8 \text{ kW}; \ \omega=314 \text{ c}^{-1}; \ p=2; \ n-1420 \text{ rpm}; \ a - 0.20 \text{ m}; \ d=0.22 \text{ m}$$

normal intensities $H_R|_k$ of a variable magnetic field are measured at points Q_k uniformly distributed over the surface of a circular cylinder (coordinates R, φ, z) through $\Delta a_k=0.05$ m, $\Delta \varphi_k=90$ degrees (Figure 1).

The table gives the results of measurements of intensities $H_R(Q)|_k$ in A/m made with the aid of equipment of the firm Bryuĭ' and K'yer while idling ($U_{xx}=230$ V, $I_{xx}=5.0$ A) and in the short-circuit mode ($U_{кз}=80$ V, $I_{кз}=10.0$ A).

Table

φ_k° \ a_k	(1) Холостой ход					(2) Короткое замыкание				
	1	2	3	4	5	1	2	3	4	5
0	450	775	640	770	500	14,0	21,0	22,0	25,0	12,5
90	320	720	680	700	312	15,0	20,5	23,0	22,5	13,0
180	640	1200	1150	1320	780	13,0	21,0	21,0	22,0	12,0
270	280	630	770	700	350	12,5	22,5	23,0	20,5	10,0

Key: 1. Idling
2. Short circuit

Radial dipoles are constructed (with an error of up to 10 percent).

While idling

D_1 $M_m^{(1)} = 0{,}32$ Ам², $z_{10} = 0{,}05$ м, $R_{10} = 0{,}01$ м, $\varphi_{10} = 180°$;
D_2 $M_m^{(2)} = 0{,}32$ Ам², $z_{20} = -0{,}05$ м, $R_{20} = 0{,}01$ м, $\varphi_{20} = 180°$;
D_3 $M_m^{(3)} = 0{,}095$ Ам², $z_{30} = 0{,}04$ м, $R_{30} = 0{,}004$ м, $\varphi_{30} = 90°$;
D_4 $M_m^{(4)} = 0{,}095$ Ам², $z_{40} = -0{,}05$ м, $R_{40} = 0{,}004$ м, $\varphi_{40} = 90°$.

In short-circuit mode

D_1 $M_m^{(1)} = 0{,}009$ Ам², $z_{10} = 0{,}04$ м, $R_{10} = 0$, $\varphi_{10} = 180°$;
D_2 $M_m^{(2)} = 0{,}009$ Ам², $z_{20} = -0{,}04$ м, $R_{20} = 0$, $\varphi_{20} = 180°$;
D_3 $M_m^{(3)} = 0{,}0028$ Ам², $z_{30} = 0{,}04$ м, $R_{30} = 0$, $\varphi_{30} = 90°$;
D_4 $M_m^{(4)} = 0{,}0028$ Ам², $z_{40} = -0{,}04$ м, $R_{40} = 0$, $\varphi_{40} = 90°$.

Here, $M_m^{(1)}$, $M_m^{(2)}$, $M_m^{(3)}$, $M_m^{(4)}$ are understood to be the moduli of the dipole moments. In the instances when, as a result of solving the problems, it is required to know not so much the structure of the field as its maximum value, the number of dipoles can be reduced to a minimum (one or two).

Conclusion

The proposed method for approximating external electromagnetic fields with the aid of fields of dipoles is suitable for using at any distance from the source and makes it possible to simplify the analysis of external electromagnetic fields of electrical equipment by using analytical methods both in calculating passive shielding shells, and active compensating systems.

Bibliography

1. Apollonskiy, S. M. "Dipole Representation of the External Magnetic Field of an Induction Magnetohydrodynamic Pump," MAGNITNAYA GIDRODINAMIKA [Magnetic Hydrodynamics], No 3, 1976.

2. Tozoni,O. V. "Metod vtorichnykh istochnikov v elektrotekhniki" [Method of Secondary Sources in Electrical Engineering], Moscow, Energiya, 1975.

3. Davidenko, D. E. "On a Method of Numerical Solution of a System of Nonlinear Equations," DOKL AN SSSR, Vol 88, 1953.

4. Davidenko, D. F. "On Approximate Solution of Systems of Nonlinear Equations," UKRAINSKIY MATEMATICHESKIY ZHURNAL [Ukrainian Mathematical Journal], Vol 5, 1953.

10,233
CSO: 1860

Electromagnetic Wave Propagation; Ionosphere, Troposphere; Electrodynamics

UDC 621.372

ON THE ELECTROMAGNETIC FIELD IN THE VICINITY OF THE EDGE OF A CONDUCTING HALF-PLANE

Moscow RADIOTEKHNIKA in Russian Vol 34, No 7, 1979 pp 66-69

[Article by Veselov, G. I.; Platonov, N. I.; and Acheyev, V. Ye., submitted 9 Jan 79]

[Text] Analyses of electrodynamic characteristics of a number of microwave devices are often done on models containing, apart from smooth boundary surfaces, the so-called "geometric singularities", for example, sharp edges. It is very important to have an accurate description of the electromagnetic field (EMP) in the vicinity of the points of geometric singularity, particularly for developing effective algorithms for the calculation of complex electrodynamic structures [1,2]. Analyzed below is the behavior of the field in the vicinity of the edge of an ideally conducting half-plane for its different orientation in relation to the flat interface of media with different relative permeabilities ε_1, μ_1, and ε_2, μ_2 (Figure 1a)[1].

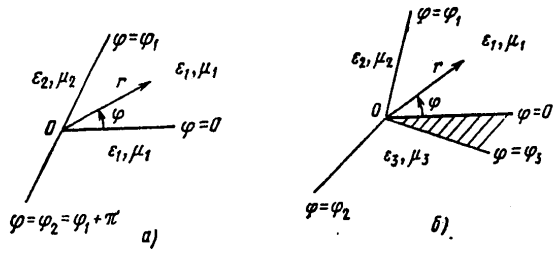

Figure 1

1. This work was prepared in connection with the discussion regarding the report of A. A. Kirilenko et al "Analysis and Optimization of the Parameters of Polarization Converters in the Form of Waveguide-Type Arrays with cones for Scanning Antenna Systems" at the meeting of the All-Union Seminar on Scientific Methods of Higher Schools on Applied Electrodynamics held on 16 Feb 1978 at MEI [Moscow Power Engineering Institute].

Investigation of the EMP in the vicinity of the point of geometric singularity can be done by means of the Meixner method [3] which is based on the expansion of the field components into generalized power series with their subsequent substitution in Maxwell's equations and imposition of appropriate boundary conditions. In [4], analysis of the field is carried out in the vicinity of the edge of an ideally conducting wedge surrounded by three sectorial regions characterized by different scalar permeability (Figure 1b). However, the field was not studied for a number of configurations occurring frequently in solving applied problems. For example, no analysis was done of a geometrical model shown in Figure 1a which is a concrete modification of the generalized model of Figure 1b for $\varphi_2 = \varphi_1 + \pi$, $\varphi_3 = 2\pi$, $\varepsilon_3 = \varepsilon_1$, $\mu_3 = \mu_1$. (axis z is normal to the plane of the drawing of Figure 1 and coincides with the edge of the wedge).

In order to analyze the EMP in the vicinity of the edge, we make up a superposition of two solutions:

1) H_z, $E_z = O(r^\tau)$; $E_t = O(r^{1+\tau})$; $H_t = O(r^{-1+\tau})$ for $r \to 0$, where $\tau > 0$ is the smallest positive root of the equation

$$F_\mu(\tau) = \left(1 - \frac{\mu_1}{\mu_2}\right)\cos(2\varphi_1 - \pi)\tau - \left(1 + \frac{\mu_1}{\mu_2}\right)\cos\pi\tau = 0. \qquad (1)$$

The solution is characterized by the presence of singularities in the vicinity of the edge of an ideally conducting half-plane only in the transverse components of the magnetic field H_t.

2) E_z, $H_z = O(r^\tau)$; $H = O(r^{1+\tau})$; $E_t = O(r^{-1+\tau})$ for $r \to 0$.

Here, τ is the lowest positive root of the equation[2]

$$F_\varepsilon(\tau) = \left(1 - \frac{\varepsilon_1}{\varepsilon_2}\right)\cos(2\varphi_1 - \pi)\tau + \left(1 + \frac{\varepsilon_1}{\varepsilon_2}\right)\cos\pi\tau = 0. \qquad (2)$$

In this case, the singularities are in the transfers components of the electric field Et.

In addition to these two solutions, in the general case, there is a possibility of another solution which was not taken into consideration in the analysis of fields in [4] (see Table 1.1):

3) $E_t, H_t = O(r)$; $E_z = O(r^\tau)$; $H_z = C_0 + O(r^\tau)$ for $r \to 0$.

2. There is a mistake in the formula (1.3.14c) in work [4] for the general case. The correct expression for $F_\varepsilon(\tau)$ has the form

$$F_\varepsilon(\tau) = \left(1 - \frac{\varepsilon_1}{\varepsilon_2}\right)\left[\cos\varphi_2\tau\cos(\varphi_2 - \varphi_1)\tau - \frac{\varepsilon_1}{\varepsilon_2}\sin\varphi_2\tau\sin(\varphi_2 - \varphi_1)\tau\right] - \ldots$$

As can be seen, the field in this case does not have any singularities, however, it is important to note that the longitudinal component of the magnetic field in the vicinity of the edge is a nonzero constant, which was pointed out in [5].

In the general case, the field in the vicinity of the point of geometric singularity is determined by the superposition of fields corresponding to the three solutions mentioned above. Naturally, the nature of the behavior of any field component is determined by that component of the superposition which has the smallest index in the functional dependence on the coordinate r.

Henceforth, it is practical to introduce the following parameters into equations (1) and (2): $\theta = \varphi_1$ and $\zeta = \mu_2/\mu_1$ or $\varepsilon_1/\varepsilon_2$. Then we obtain a generalized equation

$$F(\tau) = (1-\zeta)\cos(2\theta-\pi)\tau - (1+\zeta)\cos\pi\tau = 0. \qquad (3)$$

It follows from (3) that when $\theta = 0$, the lowest root of the equation $\tau = 0.5$ and does not depend on the parameter ζ; when $\zeta = 1$, $\tau = 0.5$ and does not depend on the angle θ. In the extreme case $\zeta \to \infty$, it is easy to obtain an explicit expression for the lowest root of equation (3)

$$\tau_\infty = \lim_{\zeta\to\infty}\tau = \frac{\pi}{2(\pi-\theta)} \quad \text{for} \quad 0 \leqslant \theta \leqslant \frac{\pi}{2}.$$

In another extreme case ($\zeta = 0$), we have $\tau_0 = \lim_{\zeta\to 0}\tau = 0.$

In a special case $\pi - 2\theta = \frac{\pi}{m}$ (m -- integral number), explicit analytic expressions are obtained for τ from the transcendental equation (3) when values m are definite. Having used the formula of multiple angles of trigonometric functions, we obtain an algebraic equation in relation to $\cos \pi\tau/m$. Let us write the final formulas for different θ:

$$\theta = 0 \quad (m=1)\ \tau = 0,5;$$

$$\theta = \frac{\pi}{4} \quad (m=2)\ \tau = \frac{2}{\pi}\arccos\frac{1-\zeta+\sqrt{(1-\zeta)^2+8(1+\zeta)^2}}{4(1+\zeta)};$$

$$\theta = \frac{\pi}{3} \quad (m=3)\ \tau = \frac{3}{\pi}\arccos\frac{1}{2}\sqrt{\frac{2(2+\zeta)}{1+\zeta}};$$

$$\theta = \frac{2}{5}\pi \quad (m=5)\ \tau = \frac{5}{\pi}\arccos\frac{1}{2\sqrt{2}}\sqrt{5+\sqrt{\frac{9+\zeta}{1+\zeta}}}.$$

Other relations obtained for m = 4, 7, and 9 are not cited due to their awkwardness.

Analysis of equation (3) shows that $\frac{\partial\tau}{\partial\theta} = 0$ for $\theta = \pi/2$, i.e., the roots of the equation acquire extreme values defined by the formula

$$\tau_0 = \tau\Big|_{\theta=\frac{\pi}{2}} = \frac{1}{\pi}\arccos\frac{1-\zeta}{1+\zeta}.$$

Thus, the value of τ for a fixed value of ζ is defined explicitly for at least five values of the angle θ. Using them as zero approximations, it is possible to find solutions of equation (3) by the known numerical methods in the entire range of changes of the angle θ.

1 θ [град] \ ζ	0,01—0,4	0,4—2,5	2,5—50	50—100
0—20	0,5	0,5	0,5	τ_∞
20—50	τ_0	0,5	0,5	τ_∞
50—90	τ_0	0,5	τ_0	τ_∞

Key: 1. Degrees

For example, by using the Newton method according to which

$$\tau_{n+1} = \tau_n + F(\tau_n)/F'(\tau_n),$$

it is possible to obtain a high degree of accuracy in computing τ with a relatively small number of steps (iterations). Calculations showed that for achieving an accuracy of 10^{-4} it is possible to limit oneself to three approximations when the parameter ζ changes within a sufficiently wide interval: from 0.01 to 100. One of the three following values was selected as a zero approximation: $\tau = 0.5$, $\tau = \tau_0$ or $\tau = \tau_\infty$.

The table gives the values of τ which it is expedient to use as a zero approximation when calculating the roots of equation (3) by the Newton method (depending on the parameters ζ and θ). In order to achieve the necessary degree of accuracy, a minimal number of iterations is required.

Figure 2 shows curves of the dependence of the lowest root of equation (3) on the angle θ in a broad range of changes of the parameter ζ. As we can see, the value of τ changes most sharply at small angles θ (0-20°) in the range of values of $\zeta \ll 1$; as θ increases, the values of τ change insignificantly; when $\zeta > 1$, the function $\tau(\theta)$ increases steadily in the entire interval of changes of the angle θ.

Let us note one interesting singularity of the behavior of the field in the vicinity of an infinitely thin metallic edge: at $\zeta < 1$, the components of the EMP can have a singularity of a higher order in comparison with the known cases: when a conducting half-plane is in a homogeneous medium or directly at the interface of heterogeneous media (as is known, in this case $\tau = 0.5$).

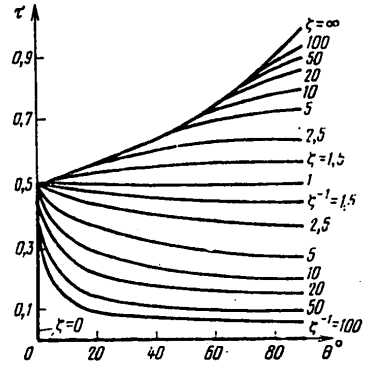

Figure 2

In the case under consideration, for example, when $\zeta = 0.01$ and $\theta = 90^{\circ}$, the characteristic index decreases to the value $\tau = 0.06345$, i.e., the transverse components of the EMP behave in the vicinity of the edge as $O(r^{-0.93655})$. It is evident that such extremely sharp increase in the degree of singularity of the field components in the neighborhood of the edge should be taken into consideration in creating stable algorithms for computing microwave devices.

Bibliography

1. Veselov, G. I., and Platonov, N. I. SBORNIK NAUCHNYKH TRUDOV PO PROBLEMAM MIKROELEKTRONIKI [Collected Scientific Papers on the Problems of Microelectronics] (Microwave and Measuring Techniques), No 32, Moscow, MIET [Moscow Institute of Electronic Engineering], 1976.

2. Veselov, G. I.; Platonov, N. I.; and Bogolyubova, G. V. SBORNIK NAUCHNYKH TRUDOV PO PROBLEMAM MIKROELEKTRONIKI (Microwave and Measuring Techniques in Microelectronics), No 37, Moscow, MIET, 1978.

3. Meixner, J. TRANS IEEE, Vol AP-20, No 7, 1972.

4. Mittra, R., and Li, S. "Analiticheskiye metody teorii volnovodov" [Analytical Methods of the Waveguide Theory], Mir, Moscow, 1974.

5. Veselov, G. I., and Platonov, N. I. SBORNIK NAUCHNYKH TRUDOV PO PROBLEMAM MIKROELEKTRONIKI (Microwave and Measuring Techniques in Microelectronics), No 37, MIET, Moscow, 1978.

10,233
CSO: 1860

UDC 621.391.81:551.510.535:621.3.029.42

MEASUREMENT OF VLF SIGNALS REFLECTED FROM THE IONOSPHERE

Moscow RADIOTEKHNIKA I ELEKTRONIKA in Russian No 7 1979 pp 1316-1322

[Article by Yu. V. Kashpar, A. A. Nikitin and A. B. Orlov: "Measurement of VLF Signals Reflected from the Ionosphere"]

[Text] A brief description is given of the measurement of the field component of near-field region VLF signals. The set-up of an experiment is considered and some of the results obtained in 1971-1974 in the European section of the USSR are shown.

Introduction

Measurements of the ionospheric field components of VLF signals on short paths are known mainly through the studies of the Cavendish laboratory in Cambridge (1-4). Such measurements have been made in the USA and Canada (5-7) but to a lesser extent. It must be noted that in setting up the experiment, the authors of the studies (1-5) rested on a priori assumptions of constance of amplitude of an ionospheric signal over a day's time. The position of the antenna intended to receive the ionospheric wave was adjusted to conform with these assumptions. The results of the studies of various groups of researcher reveal some differences for which the reasons are not altogether clear (3,5,6,8).

For this reason further experimental research, particularly in new geographical areas, is of unquestionable interest.

1. Organization of the Experiment

The measurement System. Two vertical loop antennas perpendicular to each other areused to separate the ionospheric and ground waves. Antenna $L_{\parallel}$ inclined in the propagation plane picks up the transverse magnetic component $H_{\parallel}$ of the total field, determined almost entirely by the ground wave and used as the reference signal. Antenna $L_{\perp}$ mounted perpendicularly to the propagation plane picks up the anomalous component of the field $H_{\perp}$.

It should be noted that under actual conditions the existence of the $H_{\perp}$ component may be caused not only by varying the polarization of the wave during reflection from the ionosphere but also by distortions of the field structure at the point of reception due to the effect of local conditions.

The amplitudes and phase differences of the two signals received at the loop antennas $L_{\perp}$ and $L_{//}$ are recorded by measuring set-up consisting of two receivers, a phase compensator, recorders of the amplitudes and phase differences of the signals and also auxiliary units. During recording, the input circuits of the receivers are periodically switched over to deliver a calibration signal which makes it possible to reduce instrument error. For relative calibration of the two loop antennas, antenna $L_{\perp}$ rotates 90° counterclockwise from the operating position and is aligned parallel to the reference antenna $L_{//}$. Readings of the amplitudes and phase differences in this position make it possible to determine the difference of the phase shifts in the antennas and the ratio of their effective heights.

Experimental Errors. The instrument error which results during measurement of the ratio of components $H_{\perp}/H_{//}$ with allowance made for errors in the relative claibration of the antennas, amounts to no more than 15 percent in ratio and 0.03 of cycle in phase. However, these errors do not completely characterize the accuracy in the determination of the reflection coefficient from the ionosphere. The combination of the measured magnitudes $\dot{H}_{\perp}$ and $\dot{H}_{//}$ with the standard H_1 and anomalous H_2 components of the ionospheric wave falling on the ground surface and with the ground (surface) wave H_0 has a simple form in several hypotheses valid for short paths with a well-conducting ground surface: $\dot{H}_{\perp} = 2\dot{H}_2 \cos I$, $\dot{H}_{//} = \dot{H}_0 + 2\dot{H}_1$ where I is the angle of incidence on the ground of a wave reflected from the ionosphere once. If the angle of incidence I is known (or the equivalent altitude of the reflection h = 0.5 ctg I where d is the length of the path, then in a single-hop approach, the crossing reflection coefficient $_{//}R_{\perp}$ referred to the height h_1 is found by the formula

$$|_{//}R_{\perp}| = H_2/(H_0 \sin^2 I) = H_{\perp}/(2H_0 \cos I \sin^2 I),$$
$$\arg {}_{//}R_{\perp} = \varphi_2 - \varphi_0 - kd(\operatorname{cosec} I - 1).$$

where φ_2 and φ_0 are the complete phases of components H_2 and H_0 respectively. Since the standard component of the ionospheric wave H_1 is not directly measured in the given experimental set-up, $\dot{H}_{//} \approx \dot{H}_0$ is usually assumed which may lead to errors on the order of 10-20 percent for $|_{//}R_{\perp}|$ and 0.1-0.2 rad for the magnitude of $\arg_{//} R_{\perp}$. Accuracy in determining $\arg_{//} R_{\perp}$ (and to a lesser degree the magnitude of $|_{//}R_{\perp}|$) depends also on the correct choice of the angle of incidence (9). The possible effect of a double reflection of an ionospheric wave at night at distances of 150 km and more must also be kept in mind. Due to the indicated circumstances, for more accurate determination of the shape of the lower ionosphere it is more adviseable to take the directly measured magnitudes $\dot{H}_{\perp}/\dot{H}_{//}$ as the source experimental data rather than the reflection coefficients which are usually given in the literature.

The Effect of Local Conditions. Estimation and calculation of distortions of the field caused by local features of the terrain located in the vicinity of the receiving antennas is usually a rather complicated task. However, without such estimation it is difficult in some cases to establish unambiguously whether the observed properties of the behavior of the $H_{\perp}$ field component have physical significance. Since $H_{\perp}/H_{\parallel} \sim 10^{-1}$, the components reradiated by local features of the terrain, negligible in relationship to the total field and unnoticeable in measuring $H_{\parallel}$, may prove to be comparable in magnitude to the ionospheric component $2H_2 \cos I$. For this reason the effect of the reradiated fields has been investigated by measuring the ratio of the linear components of the field $\dot{H}_{\perp}(\vec{r})$ and $\dot{H}_{\perp}(\vec{r}_0)$ at different points of the site chosen for the antenna installation:

$$D(\vec{r}, \vec{r}_0) = \dot{H}_{\perp}(\vec{r})/\dot{H}_{\perp}(\vec{r}_0).$$

For this are used mobile and stationary loop antennas oriented perpendicularly to the propagation plane ($\vec{r}$ and $\vec{r}_0$ are the radius-vectors which define the position corresponding to the mobile and stationary antennas in a certain local system of coordinates).

The difference between $D(\vec{r},\vec{r}_0)$ and the unit and dependence $D(\vec{r},\vec{r}_0)$ and the position of the observation point $\vec{r}$ are signs that a linear magnetic component exists which is reradiated by local landmarks. The absence of such a dependence in the distance interval r comparable to the characteristic size of the obstacle can be considered an adequate indication of the negligible effect of local features of the terrain whose dimensions are much less than the length of the wave.

For illustration, the results of measurement of the ratio $D(\vec{r},\vec{r}_0)$ are given in figure 1 for different distances from a van about 4 m high (fig. 1a) and from a telegraph line suspended at a height of about 6 m (fig. 1b). During measurement in the vicinity of the van, the distance was calculated from the middle of the rear wall of the van (r = 0) and the mobiel antenna (oriented exactly perpendicular to the propagation plane) was moved from the van toward the transmitter composing an angle of about 45° from the longitudinal axis of the van. The stationary antenna was located at a distance r_0 = 9 m from the rear wall of the van. In measuring near the telegraph line which extended at an angle of about 45° to the direction of propagation, the stationary antenna was located at the distance r_0 = 24 m from it and the mobile antenna was moved perpendicularly to the line.

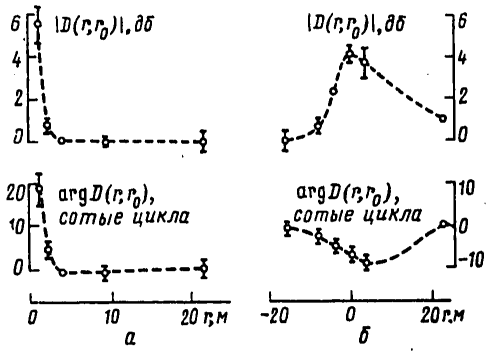

Figure 1. Nature of the Distortions of the Anomalous Component of a VLF Field by Local Objects

As figure 1 shows, the magnetic antennas for receiving the anomalous component of a near-filed VLF signal should be placed at a distance of at least four to five times the height of suspension of the line from overhead communications lines and power transmission lines. The effect of low, solitary landmarks at distances of as much as three times the height of the landmark may be disregarded. Similar results were obtained in (10) for a total field in a farfield region.

The loop antenna $L_{\perp}$, the accuracy of whose placement very significantly effects the error in the experiment, was oriented in a certain direction toward the source without subsequent correction of the antenna position according to the results of trail measurements of daily variations in the signal used in (1-5). The error in the antenna installation in a given direction did not exceed 0°,3. Corresponding errors in the measured magnitudes should not have exceeded 0.005 for the ratio $H_{\perp}/H_{\parallel}$ and 0.5 rad for the phase difference $\Delta\varphi = \varphi_{\perp} - \varphi_{\parallel}$ (here $\varphi_{\perp}$ is the phase applied at antenna $L_{\perp}$ with the magnetic component $H_{\parallel}$ applied at antenna $L_{\parallel}$).

The performed evaluations of the effect of local features of the terrain and the orientation of the loop antenna $L_{\perp}$ show that accuracy in measuring the magnitude of $2H_2\cos I/H_0 + 2H_1$) under the conditions of this experiment was determined by the instrument error of the measuring equipment indicated above.

2. Results of Measurement

Measurements of the anomalous component of a near-field VLF signal at the frequencies 14.9 kHz and 11.9 kHz were performed in the Krasnodar rayon on a path 95 km in length (direction of propagation was north to south). The first measurements in this rayon were made in July to October 1972. Similar measurements were made to a small extent at the frequency 17.1 kHz in October 1971 on a path 133 km in length (direction of propagation was east to west).

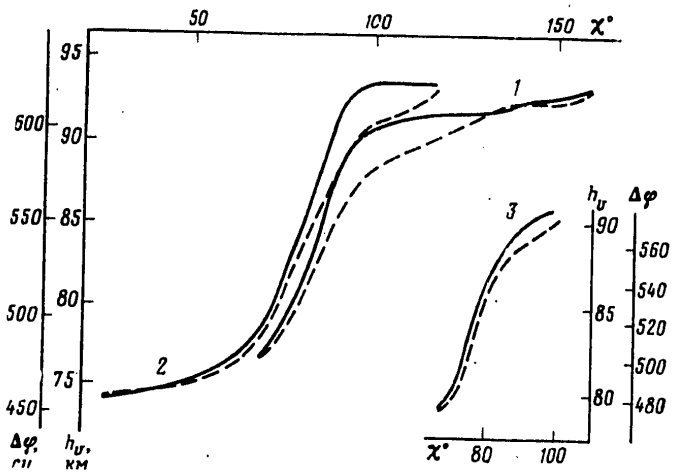

Figure 2. Daily Variation of Phase Difference $\Delta\varphi$ Depending on the Zenith Angle of the Sun. The measurements were made at the frequency 14.9 kHz in December 1973 (curve 1) and in May 1974 (curve 2) and also at the frequency 17.1 kHz in October 1971 (curve 3); the unbroken line indicates the phase variation before noon; the broken line is the variation after noon.

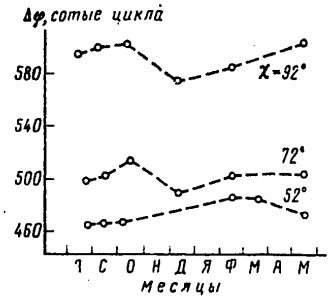

Figure 3. Seasonal Variations in the Relative Phase $\Delta\varphi$ of the Anomalous Component of a VLF field at the Frequency 14.9 kHz.

Phase of the Anomalous Component. The strongest dependence of phase difference $\Delta\varphi$ on the zenith angle of the Sun X is observed in the interval of the zenith angles 70-90° (fig. 2). Assymetry is noticeable in the curve of daily variations.

For X > 45° the forenoon value exceeds the postnoon with identical values of X. The assymetry with X > 90° indicates a slow increase in the reflection altitude during the night. In December with X > 130° the assymetry practically disappears while the phase dependence on X is retained. In figure 3 values of $\Delta\varphi$ for several months at the frequency 14.9 kHz corresponding to the indicated fixed X values are shown. They make it possible to judge the overall nature of the seasonal variation which proves to be similar to that described in (11).

Equivalent reflection altitudes may be compared by the measured values of the phase of a reflected wave. Using the concept of virtual height (12) according to the results of measurements at two frequencies f_1 and f_2 we define the equivalent reflection height to be $h_v = 0.5\ d\ \mathrm{ctg}\ I_v$, finding the corresponding angle of incidence I_v from the ratio $\mathrm{cosec}\ I_v = 1 + c\tau/d$, when $\tau = [\Delta\varphi(f_2) - \Delta\varphi(f_1) + 2\pi n] / 2\pi(f_2 - f_1)$.

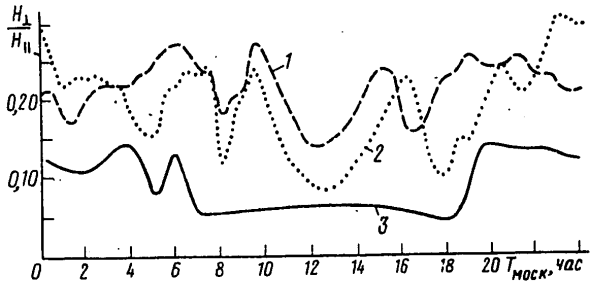

Figure 4. Variations in the Relative Value $H_\perp / H_\parallel$ of the Anomalous Component at the Frequency 14.9 kHz during a Day: 1 -- December 1973, 2 -- February 1974, 3 -- May 1974.

The integer n is determined on the basis of a priori information on the height of the reflecting region. The integers of the phase cycles at each frequency $N(f_1)$ and $N(f_2) = N(f_1) + n$ and also the value of $\arg_\parallel R_\perp$ (at the interval $0 - 2\pi$) are found from the equation

$$\arg_\parallel R_\perp = \Delta\varphi(f) + 2\pi N(f) - 2\pi f\tau.$$

The ranges of heights h_v shown in figure 3 correspond to $\arg_\parallel R_\perp = 1.1.\pi$ This magnitude is obtsined by measurement at the frequencies 11.9 kHz and 14.9 kHz with $X \simeq 52°$ and corresponds to n = 1. The noon values of virtual height were 74-75 km in May to September, 75.5 km in December and 76.2 km in February. At night with X > 110° the height h_v was found at the interval 89-94 km. The greatest seasonal variation of reflection height with fixed zenith angles of 72° and 92° was observed from October to December and was about 3km.

mplitude of the Anomalous Component. Typical dependences of the relative amplitude $H_{\perp}/H_{\parallel}$ of the anomalous component of a field over a day's time for summer and winter months are shown in figure 4. During the night the amplitude of a wave reflected from the ionosphere undergoes significant variations (a standard deviation on the order of 30 percent for hourly intervals) and averages 1.5-3 times greater than the noon level. After the Sun rises in the summer a comparatively rapid decrease takes place in the amplitude which is not varied significantly throughout the day. In the winter at the frequency 14.9 kHz a noticeable variation in amplitude also occurs during the daylight hours with zenith angles of $X \leq 75°$ while at the frequency 11.9 kHz at this time the amplitude is constant. At sunrise with $X \simeq 92\text{-}86°$ at both frequencies in both winter and summer minimum amplitudes are observed. At sunset apparent minimums of the field with these zenith angles can be noticed only in winter.

In summer (and also in October 1971 with observations at the frequency 17.1 kHz) with $X \simeq 70\text{-}77°$ a decrease was also observed in the field amplitude both in the morning and in the evening hours. The maximum amplitude occurs in winter at the zenith angle intervals 73-78° at the frequency 14.9 kHz.

Measurement of Values $H_{\perp}/H_{\parallel}$

Months	f, kHz	$H_{\perp}/H_{\parallel}$	
		Noon	Night
May - September	11.9 and 14.9	0.07±0.03	0.15±0.03
October	17.1	0.11±0,03	0.36±0.05
December	14.9	0.14±0.01	0.21±0.06
February	11.9	0.17±0.03	0.22±0.04
	14.9	0.08±0.02	0.27±0.03

These characteristics of the variations of a reflected field during the sunrise hours are consistent with concepts (13) of the "double-layered" structure of the reflecting region with $X \simeq 70\text{-}90°$. Here the parameters of the lower layer after sunrise are varied little compared to the variations of the upper part (14,15). Judging by the magnitude of the field variations, the double-layered structure is expressed more in winter. It should be noted that in the measurements at Cambridge at the frequency 16 kHz, as far as it is possible to judge by the mean curbes from (3), significant variations of amplitude were not detected during the day in winter either.

The noon and night (for a two hour interval around thelocal midnight) values of $H_{\perp}/H_{\parallel}$ are given in the table.

Conclusion

The given procedure for experimental analysis of distortions of polarization of a VLF field in the vicinity of the receiving antennas may be used in setting up an experiment for observing the ionospheric component of a near-field VLF radio station for the purpose of studying the D-region of the lower ionosphere. The given results of the observations may be of interest in improving models of electron concentration distribution in the lower ionosphere of middle latitudes as well as for direct evaluation of the contribution of an ionospheric wave to a total VLF field at distances on the order of 100 km from the transmitter.

BIBLIOGRAPHY

1. Best, J. E. et al. PROC. ROY. SOC., 156A, 889, London, 1936.

2. Budden, K. G. et al. PROC ROY. SOC., 171A, 945, London, 1939.

3. Bracewell, R. N. et al. PROC. I.E.E., pt III, 98, 1951.

4. Straker, T. W. PROC. I.E.E., 102C, 1955.

5. Belrose, J. S.; and Ross, D. B. "Proc. Conf. on Ground Based Radio Waves Propag. Studies of the Lower Ionosphere", DRB Publication, Ottawa, 1967.

6. Hayes, D. P.; and Sales, G. S. "Ibid".

7. Chilton, C. J. et al. "Propagation of Radio Waves at Frequencies Below 300 kc/s", ed. Blackband, W. T., Pergamon Press, Oxford, 1964.

8. Hopkins, H. G.; and Reynolds, B. A. PROC. I.E.E., pt III, 101, 1953.

9. Orlov, A. B.; and Pronin, A. E. IZV. VUZOV MVCCO SSSP (RADIOFIZIKA), 18, 12, 1975.

10. Demykin, S. M.; Nikitin, A. A.; and Orlov, A. B. RADIOTEKHNIKA I ELEKTRONIKA 19, 10, 1974.

11. Belrose, J. S. "low and Very Low Frequency Radio Wave Propagation. Radio Wave Propagation", AGARD Lecture Series XXIX, London, 1968.

12. Piggot, P. W. et al. PHILOS. TRANS. ROY. SOC., pt A, 257, 1965.

13. Bain, W. C. PROC I.E.E., pt IV, 99, 1952.

14. Krasnyshkin, P. E.; and Knyazeva, T. A. GEOMAGNETIZM I AERONOMIYA, 10, 6, 1970.

15. Azarnin, G. V.; Orlov, A. B.; and Sazayeva, N. N. GEOMAGNETIZM I AERONOMIYA, 15, 3, 1975.

[272-8945]

8945
CSO: 1860

UDC 537.533.32

MAGNETIC PERIODIC QUADRUPOLE FOCUSING OF INTENSIVE ELECTRON BEAMS

Moscow RADIOTEKHNIKA I ELEKTRONIKA in Russian No 6, 1979 signed to press 26 May 78 pp 1187-1193

[Article by L. E. Bakhrakh, S. P. Kudryavtseva, V. V. Murzin, M. B. Khlebtsova]

[Text] Abstract

An analytical relationship was established between boundary pulsations of a stretched beam, and conditions for its introduction into a magnetic periodic quadrupole focusing system MPKFS and conditions for optimal focusing were determined. It was proposed to use a thin quadrupole electrostatic lens for matching the cylindrical beam to the quadrupole magnetic field.

Introduction

Focusing high energy charged particle beams by means of magnetic periodic quadrupole focusing beams (MPKFS) has been well explored and described in papers, whose bibliography is cited in monographs [1, 2]. It is shown in [3] that the use of electrostatic quadrupole lenses instead of axial-symmetric lenses is very promising for forming electron beams with micro-perviousness greater than unity. Focusing electron beams by using magnetic quadrupole systems for microwave devices were considered in a comparatively small number of mainly theoretical investigations [4-7] with a number of essential simplifying assumptions. In these papers, the effect of the space charge was either neglected [4] or its effect was determined without taking into account changes in the elliptical cross section of the beam [5]. In [6], where the effect of the space charge is taken into stricter account, the effect of the conditions for introducing the beam into the MPKFS on its geometric parameters was not considered, while the calculation method proposed in [7] may be used only in the case of approximating the MPKFS magnetic field by a "square wave," i.e., on the assumption that transverse magnetic

fields in quadrupole cells do not depend on the longitudinal coordinate. Therefore, the conclusions drawn in these papers on the possibility of the successful use of MPKFS for focusing comparatively low energy beams, used in microwave devices, require a more thorough analysis.

This paper describes an approximate analytical consideration of the magnetic quadrupole focusing of intense electron beams that makes it possible to clarify the basic special features of MPKFS formation, compare it with other ways of focusing and establish the necessary requirements for conditions for introducing the beam into the focusing system. The possibility is considered of the practical implementation of these conditions by means of a thin quadrupole electrostatic lens located between the electron gun and the MPKFS.

1. Initial Relationships

Let the electron beam, moving along axis Z, pass through a sequence of magnetic quadrupole lenses turned by 90° with respect to each other. In the case of magnetic lenses with hyperbolic shape poles, the magnetic field distribution near the focusing system axis may be described in the form [5]

$$(1)\qquad \begin{aligned} B_x &= -\frac{B_0}{a} y \cos\frac{2\pi}{L} z, \\ B_y &= -\frac{B_0}{a} x \cos\frac{2\pi}{L} z, \\ B_z &= \frac{2\pi}{L}\frac{B_0}{a} xy \sin\frac{2\pi}{L} z. \end{aligned}$$

Here B_0/a -- magnetic field gradient at the center of the lens; L -- period of the magnetic field. We will describe the changes in the geometric dimensions of the beam on the basis of an analysis of the motion of two boundary electrons, lying on axes x and y, which are the main axes of the elliptical transverse cross section of the beam [8]. Taking into account (1) and assuming that the transverse velocities of electrons v_x and v_y are considerably smaller than longitudinal velocity v_z, the paraxial motion equations of the boundary electrons being considered are written in the form [6].

$$(2)\qquad \begin{cases} \dfrac{d^2X}{dZ^2} + \dfrac{\alpha}{\beta_0} X\cos Z = \dfrac{2\beta}{X+Y}, \\ \dfrac{d^2Y}{dZ^2} - \dfrac{\alpha}{\beta_0} Y\cos Z = \dfrac{2\beta}{X+Y}, \end{cases}$$

where

$$\alpha=\sqrt{\frac{2\eta}{U_0}}\frac{B_0}{a}\frac{Lr_0}{4\pi};\quad \beta=\frac{I}{4\pi\varepsilon_0\sqrt{2\eta U_0^3}\beta_0^2};\quad \beta_0=\frac{2\pi r_0}{L};$$
$$X=\frac{x}{r_0};\quad Y=\frac{y}{r_0};\quad Z=\frac{2\pi}{L}z;$$

r_0 -- average radius of the beam; U_0 -- accelerating voltage; I -- total beam current; η = e/m -- ratio of electron charge to its mass; ε_0 -- electrical constant.

We will solve system (2) by the method of gradual approximation [9, 2]. According to this method and in accordance with the proposed physical picture, in which longwave pulsations at its boundaries and undulations with a period of the focusing field must be observed, we will assume

$$\begin{aligned} X(Z)&=R_x(Z)[1+q_x(Z)],\\ Y(Z)&=R_y(Z)[1+q_y(Z)], \end{aligned} \tag{3}$$

where

$$q_x(Z)=\frac{\alpha}{\beta_0}\cos Z;\quad q_y(Z)=-\frac{\alpha}{\beta_0}\cos Z. \tag{4}$$

There, following [2], we obtain for functions R_x and R_y a system of equations

$$\begin{cases} \dfrac{d^2R_x}{dZ^2}+k^2R_x=\dfrac{2\beta}{R_x+R_y},\\ \dfrac{d^2R_y}{dZ^2}+k^2R_y=\dfrac{2\beta}{R_x+R_y}, \end{cases} \tag{5}$$

where $k^2 =$.

2. Conditions for Optimal Focusing Pulsations of Beam Boundaries

The system of equations (5) describes the anharmonic oscillations of the boundary electrons of the beam in the general case. At small pulsation amplitudes, these oscillations may be considered harmonic and assume

$$(6) \qquad \begin{aligned} R_x(Z) &= 1+\delta(Z), \\ R_y(Z) &= 1-\delta(Z), \end{aligned}$$

where $\delta(Z)$ -- harmonic function of small amplitude. Substituting these relationships into (5) under a condition of a state of equilibrium of motion of boundary electrons $d^2\delta/dZ^2 = 0$, we find the necessary optimal relation between parameters α, β_0 and β, that provides at certain initial conditions minimal changes in transverse dimensions of the beam:

$$(7) \qquad \frac{\alpha}{\beta_0} = \sqrt{2\beta}.$$

We will note that relationship (7) determines the value of the average radius r_0:

$$(8) \qquad r_0^2 = \frac{8\pi I}{\sqrt{(2\eta)^3 U_0 e_0 (B_0/a)^2 L^2}}$$

The solution of system (2), taking into account relationships (3), (4), (6) and (7) for the case of introducing the beam into the maximum of the magnetic field, has the form

$$(9)\qquad \begin{aligned} X(Z)&=\left[1+\frac{X_0'}{\sqrt{\beta}}\sin\sqrt{\beta}Z+\left(\frac{X_0}{1+\sqrt{2\beta}}-1\right)\cos\sqrt{\beta}Z\right]\times\\ &\times[1+\sqrt{2\beta}\cos Z],\\ Y(Z)&=\left[1+\frac{Y_0'}{\sqrt{\beta}}\sin\sqrt{\beta}Z+\left(\frac{Y_0}{1-\sqrt{2\beta}}-1\right)\cos\sqrt{\beta}Z\right][1+\sqrt{2\beta}\cos Z], \end{aligned}$$

where X_0, Y_0, X_0^1, Y_0^1 -- initial conditions of the introduction. In the case when the beam is introduced into the zero of the magneti, field, the solution of system (2) will be

$$(10)\qquad \begin{aligned} X(Z)&=\left[1+\frac{X_0'-\sqrt{2\beta}\,X_0}{\sqrt{\beta}}\sin\sqrt{\beta}Z+(X_0-1)\cos\sqrt{\beta}Z\right][1+\sqrt{2\beta}\sin Z],\\ Y(Z)&=\left[1+\frac{Y_0'+\sqrt{2\beta}\,Y_0}{\sqrt{\beta}}\sin\sqrt{\beta}Z+(Y_0-1)\cos\sqrt{\beta}Z\right][1-\sqrt{2\beta}\sin Z]. \end{aligned}$$

The obtained relationships (9) and (10) describe the contour of the electron beam in two mutually perpendicular planes in the periodic quadrupole magnetic field.

A comparison of the trajectories of the boundary electrons, obtained on the basis of the analytical solution of (9) and (10) and on the basis of solving system (2) on the computer, shows that even at trajectory deviations from the average radius $\delta \sim 0.5$ the spread in results is not greater than 20%. Fig. 1 shows the relationship between transverse coordinates X and Y of the boundary electrons of the beam, moving in planes (XZ) and (YZ) respectively, and longitudinal coordinate Z for a beam that has initial input parameters which differ from the optimal ones.

Value $\sqrt{2\beta}$, in relationships (9) and (10) and characterizing the amplitude of the undulation of the beam boundaries, depends on the perviousness, as well as on the ratio of the beam radius to the period of the system. Fig. 2 shows the relationship between the relative amplitude of the undulation of the beam boundaries $\Delta_B = (X_{max} - X_{min})/(X_{max} + X_{min})$ at optimal initial conditions and the parameter of space charge β. From the similar relationships for periodic electrostatic focusing and periodic magnetic focusing shown in this figure,

it may be seen for comparison that in its focusing properties quadrupole focusing systems are close to the systems of periodic electrostatic focusing and may find application in microwave devices of the 0 type.

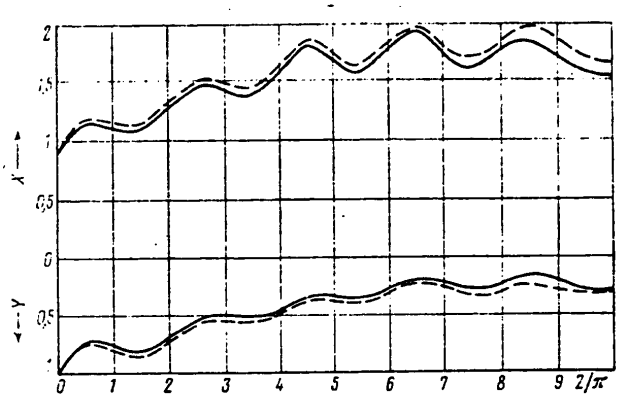

Fig. 1. Trajectory of boundary electrons X and Y in the MPKFS with parameters $\alpha/\beta_0 = 0.1$; $\beta = 0.005$ when introducing the beam into the zero of the magnetic field with initial conditions $X_0 = 0.9$; $Y_0 = 1.1$; $X_0^1 = 0.15$; $Y_0^1 = -0.15$: exact solution by computer -- solid curves; calculation by relationships (10) -- broken lines.

One considerable shortcoming of quadrupole focusing is the complexity of the practical implementation of the required conditions for introducing the beam into the MPKFS. Thus, it may be seen from equations (9) and (10) that to obtain a beam with minimum pulsation of boundaries when it is introduced into the maximum of the magnetic field, it is necessary to satisfy initial conditions

$$(11) \qquad X_0=1+\gamma\overline{2\beta},\ Y_0=1-\gamma\overline{2\beta},\ X_0'=Y_0'=0,$$

and when introducing the beam into the zero of the magnetic field

$$X_0=Y_0=1,\ X_0'=\sqrt{2\beta},\ Y_0'=-\sqrt{2\beta}. \tag{12}$$

The implementation of conditions (11) (introduction of a parallel beam with an elliptical transverse cross section) and conditions (12) (introduction of a round beam with such a distribution of slope angles of electrons that they are positive in the plane (XZ) and negative in plane (YZ), is quite difficult. The relationship between the absolute values of the initial slope of the boundary electrons of the beam $|\gamma|$, expressed in degrees, when it is introduced into the zero of the magnetic field and the microperviousness of beam P_μ is shown in Fig. 3. We will note that conditions (11) and (12) differ from those shown in [6], where they were obtained with rougher assumptions and do not correspond to the physical picture of focusing.

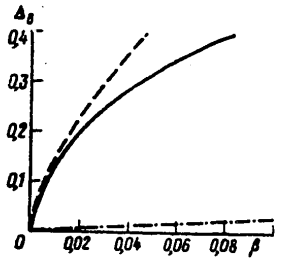

Fig. 2. Relationship between the relative amplitude of the undulation of the boundary of beam Δ_b and the parameter of space charge β for three kinds of periodic focusing: electrostatic -- dash; magnetic quadrupole -- solid curves; magnetic with axial field -- dash-dot.

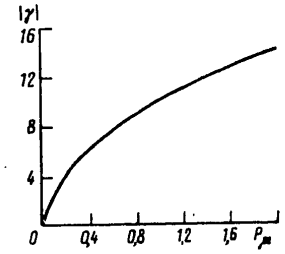

Fig. 3. Relationship between the absolute value of the slope angle of boundary electrons of the beam $|\gamma|$, located in coordinate planes (XY) and (YZ), when introducing the beam into the zero of the magnetic beam, and the microperviousness P_μ.

3. Matching the Electron Beam with the MPKFS by Means of a Quadrupole Electrostatic Lens

The practical implementation of conditions for introducing the beam, determined by relationships (12), is possible by means of a thin electrostatic quadrupole lens located in front of a magnetic periodic quadrupole system. Such a lens must preserve a round transverse cross section of the beam when slope angles of electron trajectories change by values near optimal. To determine the slope angles of electron trajectories when issuing from the electrostatic lens, we will start with the equation of the boundary electron motion in the "equivalent" lens [1] with a constant gradient of electric field intensity G and effective length $l_э$:

$$\text{(13)} \qquad \begin{cases} \dfrac{d^2X}{dZ^2} - \dfrac{\mu}{\beta_0} X = \dfrac{2\beta}{X+Y}, \\ \dfrac{d^2Y}{dZ^2} + \dfrac{\mu}{\beta_0} Y = \dfrac{2\beta}{X+Y}, \end{cases}$$

where $\mu = GLr_0/4\pi U_0$; $G = 2V/r_E^2$; V -- potential of lens electrodes. Considering that the electric beam has a round cross section at the entrance to the lens and that zero slope angles and coordinates X and Y of boundary electrons remain constant along the length of the lens, we have from system (13):

$$(14)\qquad X'(l_э)=\left(\beta+\frac{\mu}{\beta_0}\right)l_э,\quad Y'(l_э)=\left(\beta-\frac{\mu}{\beta_0}\right)l_э.$$

Comparing the values of $X^1(l_э)$ and $Y^1(l_э)$ at the electrostatic lens output, determined by equations (14), with optimal values of X_0^1 and Y_0^1 at the magnetic quadrupole input, determined by equations (12), it is obvious that their precise coincidence is impossible, since it may be achieved only at $\beta l_э = 0$. Thus, after passing the electrostatic lens, the boundary electrons of the beam have the following angles in the MPKFS input.

$$(15)\qquad X'_{опт}=\frac{\mu}{\beta_0}l_э=\sqrt{2\beta},\quad Y'_{опт}=-\frac{\mu}{\beta_0}l_э=-\sqrt{2\beta},\quad \Delta X=\Delta Y=\beta l_э.$$

0 П Т = opt

As may be seen from equations (10), deviations in the introduction angles of the boundary electrons from optimal values will lead to pulses originating in the MPKFS. For $\sqrt{2\beta} \ll 1$ the relative value of pulsations $\Delta_п$ is equal to

$$(16)\qquad \Delta_п=\frac{X_{макс}-X_{мин}}{X_{макс}+X_{мин}}\simeq\frac{\Delta X}{\sqrt{\beta}}=2\pi\sqrt{\beta}\,\frac{l_э}{L}.$$

The effective length of the lens will be minimal when the dimensions of the lens electrons are negligibly small, and it may be considered as consisting of point charges. Based on the potential distribution in such a lens [10], we have for its effective lens

$$l_{э\,мин}={}^4/_3 r_E.$$

Therefore, for a given value of β, the value of the pulsations in the MPKFS cannot be made smaller than a certain value.

$$\Delta_{\text{п мин}} = \frac{8\pi}{3}\frac{r_E}{L}\sqrt{\beta}.$$

Using relationships (15) and (16), it is possible to obtain a relationship between electrostatic lens parameters V and $l_э$ and parameters β and β_0 for a given relative value of MPKFS pulsations $\Delta_п$:

$$\frac{V}{U_0} = \frac{\sqrt{2}\gamma^2}{\Delta_п}\beta_0^2\beta, \tag{17}$$

$$\frac{l_э}{r_E} = \frac{\Delta_п}{\gamma}\frac{1}{\beta_0\sqrt{\beta}}, \tag{18}$$

where $\gamma = r_E/r_0$. We will note that the electrostatic lens parameters must have values that satisfy the condition of the thinnesss of the lens [1] , which, in our case, has the form

$$\gamma\frac{V}{U_0}\frac{l_э}{r_E} \ll \frac{1}{\beta_0}.$$

Conclusions

1. On the basis of an analytical consideration of the magnetic periodic quadrupole focusing of elongated electron beams in the mode of small pulsations of their boundaries, a relationship was established between the pulsations of the beam boundaries and the conditions for its introduction into the MPKFS, and conditions were determined for optimal focusing. It was shown that magnetic periodic quadrupole focusing in its focusing properties is close to periodic electrostatic focusing.

2. To match the beam to the MPKFS, the use of a single thin quadrupole electrostatic lens is proposed. Relationships were established between the effective length and electrode voltage of the lens and the parameters of the beam being focused in the MPKFS.

BIBLIOGRAPHY

1. Yavor, S. Ya. "Focusing Charged Particles by Quadrupole Lenses," Atomizdat, 1968.

2. Kapchinskiy, I. M. "Dynamics of Particles in Resonant Accelerators," Atomizdat, 1966.

3. Danilov, V. N.' Romanova, N. V. "Synthesis of Electrostatic Quadrupole Lenses, Forming Dense Electron Beams. Methods for Calculating Electron-Optical Systems," Izd. Nauka, 1977, pp 50-60.

4. Pierce, J. R. "Theory and Calculation of Electron Beams," Izd. Sovetskoye radio, 1956.

5. Glogston, A. M.; Hefner, H. J. Appl. Phys, 1954, 25, 436.

6. Glance, V. Fifth Congress Internationale, Section 3, Paris, 1964, 355.

7. Burnot, G. Nucl. Instr. Methods, 1964, 27, 1, 7.

8. Bick, J. N. IEEE Trans., 1965, ED-12, 7, 408.

9. Bogolyubov, N. N.; Mitropol'skiy, Yu. A. "Asymptotic Methods in the Theory of Nonlinear Oscillations," Fizmatgiz, 1958.

10. Strashkevich, A. M. "Electron Optics of Electrostatic Fields That Do Not Have Axial Symmetry," Fizmatgiz, 1959

[245-2291]

2291
CSO: 1860

UDC 621.384.63.2

ANALYSIS OF NONLINEAR SIGNAL DISTORTIONS IN TRAVELING-WAVE TUBES

Moscow RADIOTEKHNIKA I ELEKTRONIKA in Russian No 6, 1979 signed to press 6 Dec 77 pp 1153-1158

[Article by Ye. D. Belyavskiy, V. V. Gel'ner]

[Text] Abstract

A simplified method was developed for calculating the signal shape and spectrum in an O-type traveling wave tube (LBV-O). An analysis of nonlinear signal distortions as it passes through the LBV was made on the basis of this method.

Examples of numerical calculations of the signal shape and spectrum are given.

Introduction

In [1] a nonlinear theory was developed of amplification in a LBV of nonperiodic signals with a narrow frequency band, which makes it possible, by means of computer, to calculate the transformation of the signal spectrum when it passes through the LBV.

An analysis of nonlinear signal distortions in the LBV-O was made in this paper on the basis of equations formulated in [1].

1. Initial Conditions

According to [1] the VCh [High frequency] field in the decelerating system at point z and in moment of time t is described by the following formula:

$$(1) \qquad E_0(z,t)=\int_{-\infty}^{\infty}\dot{E}(z,\omega)e^{j\omega t}d\omega,$$

where

$$\dot{E}(z,\omega)=\frac{1}{2\pi}\int_{-\infty}^{\infty}[\mathrm{Re}\,\dot{E}(z,\varphi_0)e^{j\omega_0 t(z,\varphi_0)}]\frac{\partial t(z,\varphi_0)}{\partial t_0}e^{-j\omega t(z,\varphi_0)}dt_0$$
$$(\omega_н\leqslant|\omega|\leqslant\omega_в).$$

Here $\dot{E}(z,\omega)$ -- complex spectral density of the VCh field in the decelerating system at point z along the axis of the device; $\varphi_0=\omega_0 t_0$; t_0 -- initial and t -- current time; ω_0 -- average frequency of the input signal band;

$$(2)\qquad \dot{E}(z,\varphi_0)=\dot{E}[z,\dot{E}_0(\varphi_0)];\ t(z,\varphi_0)=t[z,\varphi_0,\dot{E}_0(\varphi_0)];$$

$\dot{E}[z,\dot{E}_0]$, $t[z,\varphi_0,\dot{E}_0]$ -- complex amplitude of the VCh field and the current time of an electron with an initial phase φ_0 in the LBV when amplifying the monochromatic signal with a frequency ω_0 and an initial amplitude (at z = o) complex amplitude $\dot{E}_0$; $\dot{E}_0(\varphi_0)$ -- slowly changing function $t_0(\varphi_0)$; $\omega_н$ -- lower and $\omega_в$ -- upper limit of the declerating system bandpass.

Formula (1) was obtained on the assumption that the input signal spectrum is not very wide ($\Delta\omega/2\omega_0\leqslant$ 0.1 - 0.2), while frequencies 2ω , 3ω ..., where ω belongs to the bandpass of the decelerating system, lie outside the limits of this band.

2. Separation of Slow and Fast Changing Values in (1)

Formula (1) includes both slow and fast changing values which complicates calculations on the computer. To separate these values we will write $\dot{E}(z,\omega)$ thus:

$$(3)\qquad \dot{E}(z,\omega)=\frac{1}{4\pi}\int_{-\infty}^{\infty}\left[\frac{\dot{E}(z,\varphi_0)}{j(\omega_0-\omega)}\frac{\partial}{\partial t_0}e^{j(\omega_0-\omega)t(z,\varphi_0)}-\right.$$
$$\left.-\frac{\dot{E}^*(z,\varphi_0)}{j(\omega_0+\omega)}\frac{\partial}{\partial t_0}e^{-j(\omega_0+\omega)t(z,\varphi_0)}\right]dt_0$$
$$(\omega_н\leqslant|\omega|\leqslant\omega_в).$$

We will expand values $\exp\{j(\omega_0-\omega)(t-t_0)\}$ and $\exp\{-j(\omega_0+\omega)(t-t_0)\}$ into a Fourier series with respect to φ_0, i.e., according to fast changing values. This expansion, according to [1] has the form

$$\exp\{j(\omega_0-\omega)(t-t_0)\}=\sum_{n=-\infty}^{\infty}G_n(z,\varphi_0,\omega-\omega_0)e^{jn\varphi_0},$$

$$\exp\{-j(\omega_0+\omega)(t-t_0)\}=\sum_{n=-\infty}^{\infty}G_n(z,\varphi_0,\omega+\omega_0)e^{jn\varphi_0}, \tag{4}$$

where

$$G_n(z,\varphi_0,\Omega)=G_n[z,\dot{E}_0(\varphi_0),\Omega];$$

$$G_n[z,\dot{E}_0,\Omega]=\frac{1}{2\pi}\int_0^{2\pi}\exp\{-j\Omega(t[z,\varphi_0,\dot{E}_0]-t_0)\}e^{-jn\varphi_0}d\varphi_0. \tag{5}$$

Substituting (4) into (3) and taking into account that spectral density $\dot{E}(z,\varphi_0)e^{j\omega_0 t_0}$ is different from zero only within limits $(\omega_н\leqslant\omega\leqslant\omega_в)$, while the value of $\dot{E}^*(z,\varphi_0)e^{-j\omega_0 t_0}$ is different from zero only within $(-\omega_в\leqslant\omega\leqslant-\omega_н)$, we obtain

$$\dot{E}(z,\omega)=\frac{1}{4\pi}\int_{-\infty}^{\infty}\left\{\frac{\partial\dot{E}(z,\varphi_0)}{\partial t_0}\frac{G_0(z,\varphi_0,\omega-\omega_0)}{j(\omega-\omega_0)}e^{-j(\omega-\omega_0)t_0}+\right.$$

$$\left.+\frac{\partial\dot{E}^*(z,\varphi_0)}{\partial t_0}\frac{G_0(z,\varphi_0,\omega+\omega_0)}{j(\omega+\omega_0)}e^{-j(\omega+\omega_0)t_0}\right\}dt_0 \tag{6}$$

$$(\omega_н\leqslant|\omega|\leqslant\omega_в).$$

In (6) only slowly changing values are under the integral sign which simplifies the calculation of the spectrum considerably.

3. Separation of the Frequency Dependence

There is another difficulty in (6), namely the necessity of calculating $G_0(z, \varphi_0, \Omega)$ for arbitrary values of Ω from interval $\omega_n+\omega_0 \geqslant \Omega \geqslant -\omega_n-\omega_0$. This difficulty, however, may be avoided by expanding $G_0(z, \varphi_0, \Omega)$ into a Taylor series with respect to Ω/ω_0 (such an operation is proper, because in the above indicated limits for changing Ω the value of $|\Omega|/\omega_0$ is limited). Here v_0 is the velocity of the undisturbed flow. In this case,

$$\dot{E}(z,\omega)=\frac{1}{4\pi}\int_{-\infty}^{\infty}\left\{\frac{\partial \dot{E}(z,\varphi_0)}{\partial t_0}\sum_{n=0}^{\infty}\frac{\left[-j\left(\frac{\omega}{\omega_0}-1\right)\right]^n}{j(\omega-\omega_0)n!}\Phi_n(z,\varphi_0)\times\right.$$
$$\times\exp\left\{-j\left[(\omega-\omega_0)\left(t_0+\frac{z}{v_0}\right)\right]\right\}+\frac{\partial \dot{E}^*(z,\varphi_0)}{\partial t_0}\times$$
$$\times\sum_{n=0}^{\infty}\frac{\left[-j\left(\frac{\omega}{\omega_0}+1\right)\right]^n}{j(\omega+\omega_0)n!}\Phi_n(z,\varphi_0)\exp\left\{-j\left[(\omega+\omega_0)\times\right.\right.$$
$$\left.\left.\left.\times\left(t_0+\frac{z}{v_0}\right)\right]\right\}\right\}dt_0 \tag{7}$$
$$(\omega_n\leqslant|\omega|\leqslant\omega_n).$$

Here

$$\Phi_n(z,\varphi_0)=\Phi_n[z,\dot{E}_0(\varphi_0)];$$
$$\Phi_n[z,\dot{E}_0]=\frac{1}{2\pi}\int_0^{2\pi}\left\{\omega_0 t[z,\varphi_0,\dot{E}_0]-\omega_0 t_0-\frac{\omega_0 z}{v_0}\right\}^n d\varphi_0 \tag{8}$$
$$(\Phi_0=1).$$

In calculating the spectrum in the sum with respect to n, it is possible to limit oneself to a finite number of members because of the rapid decrease of the latter with an increase in n for the frequencies lying within the bandpass of the decelerating system. Values of Φ_n are calculated, according to (8), from the nonlinear theory for a monochromatic input signal.

Taking into account (7), (8) initial relationship (1) may be written thus:

$$(9) \qquad E_c(z,t)=\frac{1}{2\pi}\int_{S_\omega}\left[e^{j\omega t}d\omega\int_{-\infty}^{\infty}e^{-j\omega t_1}f(z,t_1)\,dt_1\right],$$

where S_ω -- region of changing ω $(\omega_н\leqslant|\omega|\leqslant\omega_в)$;

$$(10) \qquad f(z,t)=\mathrm{Re}\,e^{j\omega_0\tau}\left\{\dot{E}[z,\dot{E}_0(\tau)]+\right.$$
$$+\sum_{n=1}^{\infty}(-1)^n\frac{1}{n!}\frac{\partial^{n-1}}{\omega_0{}^n\partial\tau^{n-1}}\left(\frac{\partial\dot{E}[z,\dot{E}_0(\tau)]}{\partial\tau}\times\right.$$
$$\left.\left.\times\Phi_n[z,\dot{E}_0(\tau)]\right)\right\}_{\tau=t-z/v_0}.$$

Thus, $E_c(z,t)$ coincides with $f(z,t)$ to a precision up to frequencies lying outside the bandpass of the decelerating system (these frequencies have a noticeable effect on the signal shape when operating near the bandpass limits).

4. Analysis of Nonlinear Signal Distortions

When the input signal spectrum is very narrow and the electron flight time is considerably smaller than the periods of differential signal frequencies, it is possible to neglect in expression (1) the signal delay ($\tau\simeq t$) and omit members under the summation sign with respect to n. In this case,

$$E_c(z,t)\simeq f(z,t)\simeq\mathrm{Re}\,\dot{E}[z,\dot{E}_0(t)]\,e^{j\omega_0 t},$$

i.e., the signal at the output may be obtained from a quasi-stationary approximation (i.e., as in a low-frequency amplifier -- in accordance with its amplitude characteristic), which coincides with results in [2].

As the spectrum of the input signal is broadened, signal delay ($\tau = t - (z\ v_0)$) in (10) has a greater effect and members with respect to n under the summation sign, related to the nonstationarity of the operation mode (finiteness of the signal propagation time, flight time of electrons and their nonlinear dependence on the value of the field and the velocity of its change), cannot be neglected, which was not taken into account in [2].

5. Simplification of Relationship

As already noted above, to calculate spectrum and signal shape distortions it is necessary to know the solution of the LBV equation for the monochromatic signal as a function of the complex amplitude of the input signal. This solution may be taken, for example, from the rigid LBV theory [3] or from approximate theories [4, 5], etc.

The greatest simplification of calculations is achieved by using the analytical nonlinear L3V theory [4]. Actually, within the framework of this theory values of $\dot{E}[z, \dot{E}_0]$ and $G_0[z, \dot{E}_0, \Omega]$ have the form

$$\begin{aligned} \dot{E}[z, \dot{E}_0] &= -4\beta_* U_0 C^2 \exp\{-j(\beta_* z - \delta - y_1 C\beta_* z)\} \times \\ &\times \dot{F}_0 \sum_{s=0}^{\infty} \frac{(-1)^s F_0^{2s} (D_1/2)^{2s+1}}{s!(s+1)![j(b+y_1)+(2s+1)x_1+d]}, \\ G_0[z, \dot{E}_0, \Omega] &= \exp\left\{-j\Omega \frac{z}{v_0}\right\} J_0\left(\frac{\Omega}{\omega_0} D_1 F_0\right) = \\ &= e^{-j\Omega(z/v_0)} \sum_{s=0}^{\infty} \frac{(-1)^s (D_1/2)^{2s} F_0^{2s}}{(s!)^2} \left(\frac{\Omega}{\omega_0}\right)^{2s}, \end{aligned} \tag{11}$$

where

$$\dot{F}_0 = \frac{\dot{E}_0}{2\beta_* U_0 C^2}; \quad F_0 = |\dot{F}|;$$

U_0 -- accelerating voltage; C -- amplification parameter; $\beta_* = \omega_0/v_0$;

$$D_1 = AR \exp(x_1 \beta_0 Cz);$$
$$R = [(x_1^2 - y_1^2 + q)^2 + 4x_1^2 y_1^2]^{-1/2};$$
$$\operatorname{tg}\delta = \frac{x_1^2 - y_1^2 + q}{2x_1 y_1};$$

x_1 and y_1 are the real and imaginary parts of the square root of the LBV characteristic equation for a rising wave; b -- parameter of non-synchronism; q -- parameter of space change; d -- parameter of attenuation; A -- parameter of initial losses [4].

Taking into account (11), we obtain

$$(12) \quad f(z,t) = -4\beta_0 U_0 C^2 \operatorname{Re} \times \left\{ e^{j\omega_0 \tau} \left[\sum_{n=0}^{\infty} \frac{(-1)^n (D_1/2)^{2n+1} \dot{F}_0(\tau) F_0^{2n}(\tau) e^{j(b+y_1\beta_0 Cz)}}{n!(n+1)![j(b+y_1)+(2n+1)x_1+d]} + \right.\right.$$
$$+ \sum_{s=1}^{\infty} \sum_{n=0} \frac{(-1)^n (D_1/2)^{2(n+s)+1} e^{j(b+y_1\beta_0 Cz)}}{(s!)^2 n!(n+1)![j(b+y_1)+(2n+1)x_1+d]} \times$$
$$\left.\left. \times \frac{1}{\omega_0^{2s}} \frac{d^{2s-1}}{d\tau^{2s-1}} \left(F_0^{2s}(\tau) \frac{d}{d\tau} \dot{F}_0(\tau) F_0^{2n}(\tau) \right) \right] \right\}_{\tau = t - \frac{z}{v_0}}.$$

In this form f(z,t) obviously depends on $\dot{F}_0$ which simplifies calculations considerably.

We will consider examples of propagation of concrete nonperiodic signals in LBV.

6. Quantitative Analysis

An analysis of the signal shape and spectrum distortion during its passing through the LBV is most convenient to make on the example when the envelope of input VCh signal ($\dot{E}_0(t_0)$) is a bell-shaped pulse

$$(13) \quad \dot{E}_0(t_0) = 2\beta_0 U_0 C^2 F e^{-t_0^2/2\tau_0^2};$$

where F -- nondimensional amplitude of the pulse; $\tau_и^2$ -- constant characterizing the velocity of the decrease in the function. The results of calculating the envelope of the VCh signal (E (z,t) and the signal spectrum at the LBV output (at point $z_н$ of VCh power saturation for $F_o = 0.9F_{omax}$) are shown in Figs. 1 and 2. Calculations were made at an average frequency of the bandpass of the decelerating system and at $\omega_в - \omega_н = 1.6\,\omega_o$.

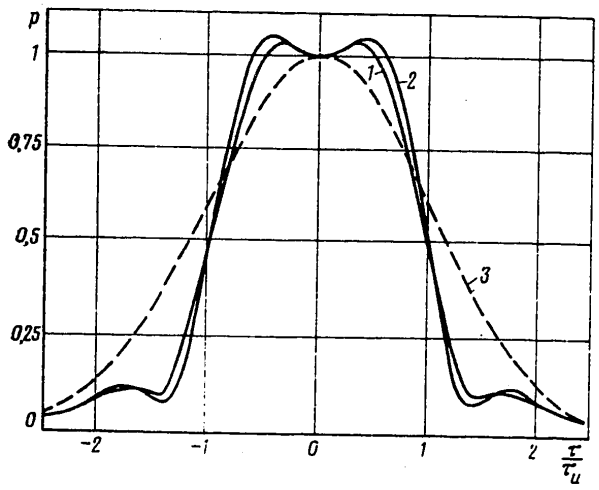

Fig. 1. Curves of relationships between p and relation time $\tau/\tau_и$: $\omega \geq 10$, $z = z_н$ -- curve 1; $\omega = 6$, $z = z_н$ -- curve 2; for input signal, z = o -- curve 3.

Fig. 1 shows relationships between $p = E(z,t)/E(z,o)$ and relative time $\tau/\tau_и = [t - (z/v_o)]/\tau_и$ at point $z = z_н$ for two values of parameter $w = \omega_o\tau_и$: $w \geq 10$ -- first curve; $w = 6$ -- second surve. For comparison Fig. 1 shows relationship between $p = E_o(t)/E_o(0)$ (for input signal)and $\tau/\tau_и$ at point z = o -- third curve (bell-shaped pulse with a single amplitude).

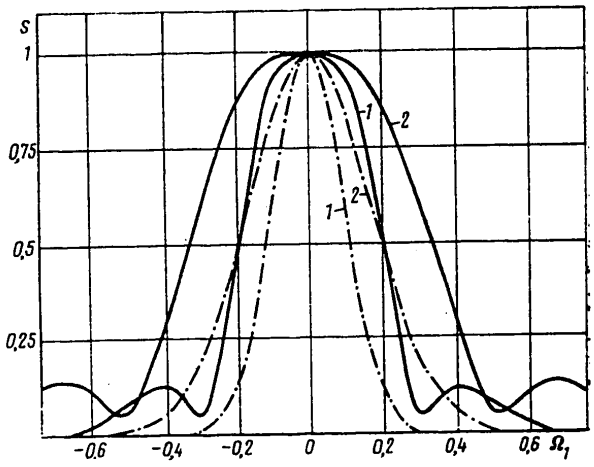

Fig. 2. Curves of relationships between s(ω) and relative frequency deviation Ω = (ω/ω_0) -1 (at point z = z_H, $\tau\omega$ = 10 -- solid curve 1, $\tau\omega$ = 6 -- solid curve 2; at point z = o, $\tau\omega$ = 10 -- dash-dot curve 1, $\tau\omega$=6 -- dash-dot curve 2) for $\omega > 0$.

The first curve corresponds to the envelope in a quasi-stationary mode ($\tau\omega \to \infty$), while, as shown by calculations, quasi-stationary approximation differs noticeably from the nonstationary calculation at $\tau\omega < 10$. A comparison of the first curve with the third curve in Fig. 1 shows that in a quasi-stationary mode nonlinear distortions are manifested by an increase in the steepness of the bell-shaped pulse and the formation of a pulse ledge. The shape of the pulse approaches the rectangular.

As parameter $\tau\omega$ decreases, transit effects related to members containing derivatives of F_0 (τ) in (12) begin to be manifested, leading to a further increase in the steepness of the pulse and increasing of the ledge width (see Fig. 1 -- second curve; $\tau\omega$ = 6).

Fig. 2 shows relationships between $s = |\dot{E}(z, \omega)/\dot{E}(z, \omega_0)|$ and the relative deviation of frequency $\Omega_1 = (\omega/\omega_0) - 1$ at point z = z_H for $\omega > o$ and two values of parameter $\tau\omega = \omega_0\tau$ ($\tau\omega$ = 10 -- first solid curve; $\tau\omega$ = 6 -- second solid surve). Dash-dot curve in Fig. 2 shows the relationship between s and Ω for the input signal (respectively first curve -- for $\tau\omega$ = 10 and second -- for $\tau\omega$ = 6); it may be seen from Fig. 2 that the signal spectrum at the output of the LBV is considerably wider than at the input.

BIBLIOGRAPHY

L. Belyavskiy, Ye. D. Radiotekhnika i elektronika, 1978, 23, 1, 211.

2. Malyshenko, V. I.; Solntsev, V. A. Elektronnaya tekhnika, Series 1, Elektronika SVCh, 1969, 10, 72.

3. Vaynshteyn, L. A. Radiotekhnika i elektronika, 1957, 2, 7, 883.

4. Man'kin, I. A. Elektronnaya tekhnika, Series 1, Eketronika SVCh, 1966, 4, 15.

5. Ovcharov, V. T.; Solntsev, V. A. Radiotekhnika i elektronika, 1962, 7, 11, 1931.

[245-2291]

2291
CSO: 1860

UDC 621.372.061.3

DETERMINATION OF KINDS OF COMBINATION INTERFERENCE WITH A POLYHARMONIC EFFECT ON A NONLINEAR DEVICE

Moscow RADIOTEKHNIKA in Russian No 6, 1979 pp 42-43 manuscript received 7 Apr 78

[Article by N.D. Vorob'yev and B.P. Krekoten']

[Text] A number of studies have been devoted to questions of analyzing polyharmonic effects on nonlinear circuits and devices [1-4]. Expressions gotten in them for the spectrum of the output signal make it possible to calculate the amplitudes (phases) of all signal and combination components. Practically all radio equipment devices have a limited passband; therefore, in calculating the spectrum of the output signal it is advisable to take into account only those combination components which fall within the device's passband. We will call these combination components combination interference. It is convenient to specify the kind of combination interference as $|\pm a_1 f_1 \pm a_2 f_2 \pm \ldots \pm a_n f_n|$, where f_1 f_2 ..., f_n are values of the frequencies of input signals, by a set of factors (a_1, a_2, ..., a_n) taking on values of numbers of the natural series or of zeroes [4]. The determination of kinds of combination interference represents an independent and general problem in analysis of polyharmonic effects on devices with any characteristics, the solution of which will make it possible considerably to reduce the amount of computations in the calculation of output spectra.

The only known method is that of calculating the values of frequencies and the order of magnitude of combination components falling within a given band with known values of the frequencies of input signals [5]. However, this method, based on solving linear Diophanthine equations with integral coefficients, is suitable only for analyzing the effect of a quite limited number of signals ($n \leq 3$) in view of its unwieldiness.

Let us consider the case of the effect of n narrow-band radio signals with a priori unknown values of carrier frequencies, $f_1, f_2, \ldots, f_n$, on a nonlinear device with a passband width of $\Delta f = f_{max} - f_{min}$, where f_{min} and f_{max} are respectively the lower- and upper-limit frequencies of the passband. This case is typical of the operation of broadband microwave radio receiving equipment. It is necessary to determine the kinds of combination components which will fall or potentially can fall within the passband, $\Delta f = f_{max} - f_{min}$.

Mathematically, the problem can be formulated in the following manner. Let us represent the values of the carrier frequencies of the radio signals by continuous random magnitudes $\xi_1, \xi_2, \ldots, \xi_n$, distributed equally probably over the interval $[1, K_f]$, where $K_f = f_{max}/f_{min}$ is the frequency overlap factor. Then the values of the frequencies of combination components are determined by the equation:

$$|\pm a_1\xi_1 \pm a_2\xi_2 \pm \ldots \pm a_n\xi_n|. \tag{1}$$

It is necessary to find factors $a_1, a_2, \ldots, a_n$ with which the following condition is fulfilled:

$$|\pm a_1\xi_1 \pm a_2\xi_2 \pm \ldots \pm a_n\xi_n| \in [1, K_f]. \tag{2}$$

i.e., to determine the kind of combination interference (a_1 a_2 ..., a_n). Since $\xi_1, \xi_2, \ldots, \xi_n$ are random values, then the values of frequencies of combination components determined in (1) will also be random, and condition (2) will be of a probabilistic nature, i.e., for each set of factors ($a_1, a_2, \ldots, a_n$) it is possible to determine the probability of the fulfillment of condition (2), corresponding to the probability of the appearance of combination interference of a given kind.

An analytical solution to this problem presents considerable difficulty with $n \geq 3$. Therefore, calculations of probability were performed by means of mathematical modeling by the Monte Carlo method using a "Vesna" computer.

Curves for the dependence of the probability of the appearance of combination interference of different kinds (up to the seventh order of magnitude inclusive) on the frequency overlap factor, K_f, plotted from the results of modeling are given in figs 1 and 2.

An analysis of these curves demonstrates the following:

The number of kinds and the probability of occurrence of combination interference increase with an increase in the frequency overlap factor (the width of the passband).

With two signals, the most probable ($p = 0.666$) is the occurrence of combination interference of type (1, 2).

With an odd number of signals ($n \geq 3$) combination interference of type (1, 1,...1) will certainly be present.

With an even number of signals ($n \geq 4$) combination interference of type (1, 1, ..., 1, 2) will certainly be present.

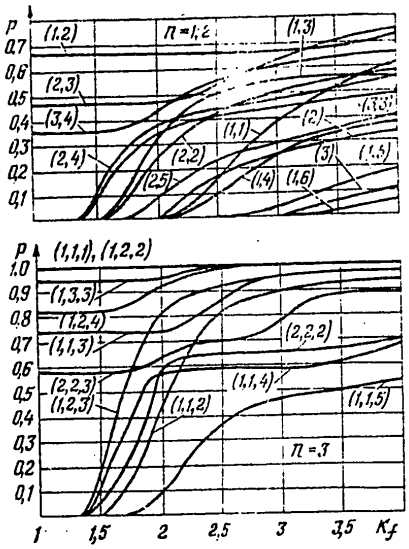

Figure 1.

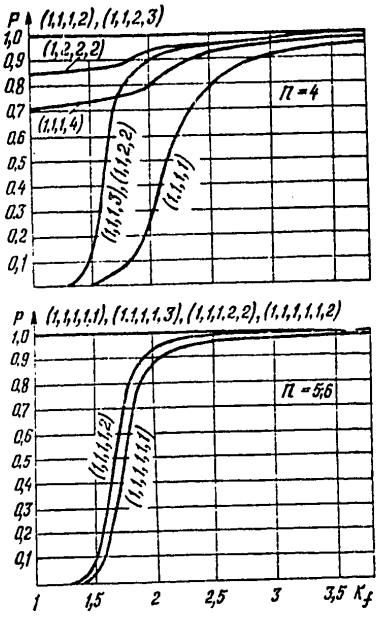

Figure 2.

Taking into account the fact that for the majority of nonlinear devices the amplitudes of combination interference diminish with an increase in their order of magnitude [6], it is possible to draw the following conclusions: With a frequency overlap factor of less than an octave and a random number of signals, the most dangerous is combination interference of the third order of magnitude of type (1, 1, 1) and (1, 2); with a frequency overlap factor of greater than an octave, the most dangerous is combination interference of the second order, of types (1, 1) and (2).

Therefore, for the purpose of eliminating combination interference of lower orders, it is advisable to select the frequency overlap factor at less than an octave.

The results gotten and these recommendations can be utilized in calculating the technical characteristics of devices (in particular, n-signal dynamic microwave ranges) and for the purpose of optimizing their passband.

Bibliography

1. Kotel'nikov, V.A. NAUCHO-TEKHNICHESKIY SBORNIK, LEIS, No 14, 1936.

2. Antonov, O.Ye. and Ponkratov, V.S. RADIOTEKHNIKA, Vol 18, No 11, 1963.

3. Shaft, P.D. "IEEE Int. Conv. Record," Part 2, Nos 22-26, 1965.

4. Sverkunov, Yu.D. RADIOTEKHNIKA, Vol 27, No 8, 1972.

5. Nikolayev, Ye.N. RADIOTEKHNIKA, Vol 28, No 2, 1973.

6. Sverkunov, Yu.D. RADIOTEKHNIKA, Vol 29, No 9, 1974.

[255-8831]

8831
CSO: 1860

UDC 621.3.049.77.002.002.5

CHEMICAL INDUSTRY EQUIPMENT IN MICROELECTRONICS MANUFACTURE

Moscow KHIMIKO-TEKHOLOGICHESKAYA APPARATURA MIKROELEKTRONIKI (Chemical Industrial Process Equipment in Microelectronics) in Russian 1979 signed to press 24 Jan 79 pp 2, 311-312

[Annotation and table of contents from book by Aleksey Tikhonovich Myagkov and Yevgeniy Mikhaylovich Korsetov, Energiya, 3,500 copies, 312 pages]

[Text] This book discusses designs, basic specifications and method of engineering and designing of equipment for monitoring and controlling chemical industrial processes, equipment for dispersion and atmization of aggressive media, equipment for preparation and batching of an aggressive liquid and piping systems.

This book is intended for engineers and technicians working in the area of design and operation of chemical process equipment in microelectronics manufacture.

Contents

[263-3024]

3024
CSO: 1860

UDC 621.382.2/.5

MEASUREMENT COMPONENTS AND PHOTOMULTIPLIERS

IZMERITEL'NAYA TEKHNIKA in Russian No 6, 1979 pp 71-73

[Article by L. I. Andreyeva, S. A. Kaydalov and B. M. Stepanov]

[Text] Domestic industry now produces over 200 types of photomultipliers and photoelectric cells, forming a foundation for many devices and systems used in optical and physical measurements in the many fields of science and technology. The physical principle underlying the operation of photoelectric cells and photomultipliers is the external photoeffect and secondary electron emission, (time-delay less than 10^{-13} sec., thermal agitation noise 10^{-12}-10^{-17} $A \cdot cm^{-2}$, photoelectric current gain up to 10^{8}); it makes it possible to design photoelectric cells and photomultipliers for measurement purposes that have subnanosecond time resolution and high sensitivity to discrete photons [1-6].

Photoelectric cells and photomultipliers are widely used to measurement technology as the primary measurement transducers and, to a significant degree, determining net measurement error. Metrologic characteristics of photoelectric cells, however, (1-3, 6-9 in Fig. 1) and photomultipliers (3-10 in Fig. 2) are not calibrated [7-10] and only the circuit diagram of their parameters is indicated [11,12]. Questions of metrologic support of photoelectric cells and photomultipliers are considered below based on R&D experience in measurement technology of photoelectric cells used in photoelectric colorimeters (FEK) and photomultipliers used in cathode ray devices (ELU) [1-6]. This problem is being tackled with unified methods and on a legislative basis by the promulgation of a state system of guarantee of measurement unity [14], positions of metrologic guarantee of the national economy [13] and creation of a unified system of state standards for power engineering photometry [15].

The creation of measurement photoelectric cells and photomultipliers presumes their development as means of measurement in conformity with test circuits and systems of the state standards in the form of a composite set of devices based on the principles of functional, design, metrologic compatibility and interchangeability in terms of the conditions and features of operation.

To allow for requirements, measurement photoelectric cells used in photoelectric colorimeters (FEK) and electron photomultipliers used in cathode ray devices (ELU) [1-6] have been developed as a constituent part of the set of photoelectric measurement transducers for engineering photometry and measurement of the parameters of high-speed processes in a spectral quantum energy emission range from 0.9 eV to 1.5 MeV, dynamic range of over 200 dB, with time resolution of up to 3 x 10^{-11} seconds. For interface with interactive links of measurement devices, the photoelectric cells of photoelectric colorimeters (FEK) and photomultipliers of cathode ray devices (ELU) have broad-band coaxial outputs with wave impedance of 50 and 75 ohms, and are provided with standard connectors and cables of types SR and RK [16] (1-5 in Fig. 3). To match the characteristics of measured emission fluxes and to assure the desired range of photoelectric conversion at the input to photoelectric cells and photomultipliers, standardized components are utilized: diaphragms, telescoping attachments, diffusers, selective and non-selective filters, lenses, photometric spheres and other components. According to operating conditions, photoelectric cells and photomultipliers may be used with or without auxiliary screened housings (6-11 in Fig. 3).

To guarantee measurement in an expanded spectral range, photoelectric cells and photomultipliers are built with input windows and photocathodes whose characteristics are cited in the table.

Measurement of parameters of powerful emission fluxes ranging from 10 to 10^2 watts is supported using photoelectric cells and additional attenuators. To raise their time resolution or expand their dynamic range, photoelectric cells used in photoelectric colorimeters (FEK) have increased field strength in the photocathode up to 1-10 kV/mm; the anode and cathode are made in the form of broad-band strip and coaxial lines with wave impedance of 50 and 75 ohms, anode assembly inductance is reduced to 10^{-9} H; and photocathodes have resistivity no greater than one ohm per square centimeter.

To reduce the effects of dielectric design component charging, especially the input window, screen electrodes and grids are employed. Parameters such as photocathode surface, anode-cathode distance, anode voltage distinguish the five type-sizes of photoelectric cells, assuring an optimum relationship between required current and tolerable stray capacitance. To reduce dark currents, increase the threshold of sensitivity and lengthen service life, the design of photoelectric cells envisages increased electrical insulation of electrode leads, assuring leakage current no greater than 10^{-9} nA at voltages measured from 1 to 10 kV; this is done by using methods of oil-free evacuation to 10^{-9} mm Hg and high vacuum getters. Mechanical and electrochemical treatment of high-voltage parts is carried out to the 10th class of purity. To stabilize parameters, photoelectric cells are technologically aged at increased gating voltages.

Measurements of parameters of average power emission fluxes in the range from 10^{-2} to 10^3 watts are assured by a group of photoelectric cells with increased sensitivity (FEK-PCh)(5 in Fig. 1) and photomultipliers with fewer dynodes. In the photoelectric cells FEK-PCh, photocathodes with negative electron medium based on GaAs and semiconductor silicon structures with gain of up to 103 are used. In the 5ELU-F type photomultiplier (4 in Figure 1) and 32ELU-F (8 in Fig.

2), electron multipliers with 1-5 stages and gain of 10 to 10^3 are used, while in the 36EU-F type photomultiplier (9 in Fig. 2), microchannel MKP multipliers with dark current of 2×10^{-11} A and gain of 2.5×10^4 are employed.

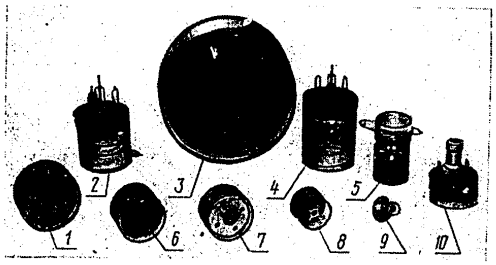

Figure 1

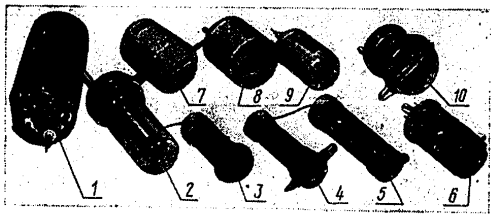

Figure 2

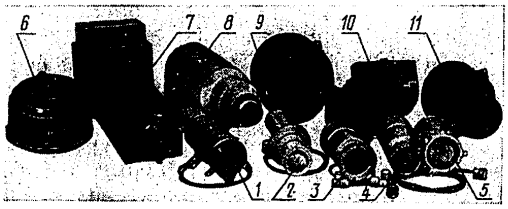

Figure 3

To measure weak emission fluxes in the range from 10^{-3} to 10^{-15} W on the basis of electron multipliers of cathode ray devices (ELU) [1], type ELU-F type photomultipliers have been developed. In terms of functions performed and design features, we can point out photomultipliers for measuring parameters of maximally weak emission fluxes, high-speed photomultipliers for pulsed photometry, photoelectric cells with log conversion and variable photomultipliers.

Photomultipliers (FEU) for measurement of maximally weak emission fluxes have several design technology features. Electron-optical systems of input chambers have precision focusing and provide selection of useful signal photoelectrons with a collection coefficients of at least 0.9. The first emitter has an increased

coefficient of secondary emission—at least 10-30—while the overall gain of multiple stage electron multipliers comprises 10^6 to 10^8. To reduce the effect of such noise components as leakage current, gas-discharge processes, auto-electron emission, ion and optical feedback,special mounting insulators, retaining rings, electrode screens, absorbent optical coatings and high-vacuum getters are used. The manufacture of the photocathode by the method of vacuum manipulator precludes the formation on the electrodes of the input chamber and insulators of photomultipliers of photosensitive and emission-active films. In these devices, the primary noises are induced by thermoelectronic emission, permitting measurements to be made at the level of photon noise of emission flux under conditions of pulse counting. Inherent photomultipliers noise comprises 0.1 to 10^3 pulse/second, according to the type of photocathode and operating temperature.

1 Спектральный диапазон, мкм	2 Входное окно	3 Катод	4 Чувствительность				
			$\eta(\lambda_m)$, эл/фот 5	$i_э(\lambda_m)$, А/Вт 6	$i_э(0{,}53)$, А/Вт 6	$i_э(1{,}06)$, А/Вт 6	$\Sigma_{св}$, А/лм 7
$1{,}2\cdot10^{-5}$—$8{,}1\cdot10^{-7}$	Al; Fe	CuAlMgO CuBeO	$1{,}5\cdot10^{-3}$	—	—	—	—
$4{,}1\cdot10^{-5}$—$8{,}1\cdot10^{-7}$	Be	CuAlMgO	$1{,}5\cdot10^{-3}$	—	—	—	—
0,11—0,22	MgF_2	CuI; CsI	0,1; 0,2	—	—	—	—
0,22—0,8	УТ—49	$Na_2K(Cs)Sb$	0,25	0,1	0,08	—	100
0,11—0,9	MgF_2	GaAs(Cs)	—	—	—	—	600
0,38—0,68	С52—1	$Cs_3Sb(O)$	0,15	0,05	0,03	—	80
0,38—0,8	С52—1	$Na_2K(Cs)Sb$	0,25	0,1	0,08	—	100
0,22—1,2	УТ—49	AgOCs	$(3—8)\cdot10^{-3}$	$(2—5)\cdot10^{-3}$	$(0{,}8—2)\cdot10^{-3}$	$(2—5)\cdot10^{-4}$	30
0,38—1,3	С52—1	AgOCs	$(3—8)\cdot10^{-3}$	$(2—5)\cdot10^{-3}$	$(0{,}8—2)\cdot10^{-3}$	$(2—5)\cdot10^{-4}$	30

[Key: 1. spectral range, microns; 2. input window; 3. cathode; 4. sensitivity; 5. electron/photon; 6. A/W; 7. A/lm.]

The 31ELU-F device (10 in Fig. 2) was developed for pulsed photometry. A distinctive feature of its design is the placement of the frame photocathode on a disc cold-conductor connected by a metal-glass weld with a thermoelectric cooler; this reduces its dark currents to 10^{-8} A at gains of 10^7 to 10^8 and retains the advantages of high-speed photomultipliers [4].

In high-speed photomultipliers, the electron-optical systems of the cathode chambers and secondary-electron emitters provide an electron dispersion of at least 0.5 ns, input lead inductance does not exceed 10^{-8} H and the circuits of the final emitters contain compensating capacitors of 10^{-9} to 10^{-8} farads capacitance. The output signal of the electronic multiplier is made inthe form of a screened broad-band coaxial-strip line with wave impedance of 50 and 75 ohms. To increase sensitivity and reduce noise currents, the photocathodes of high-speed photomultipliers of the 18ELU-F type (7 in Fig. 2) are manufactured with the vacuum manipulator.

To measure in the dynamic range 10^7 to 10^8 based on high-speed devices, photomultipliers are manufactured with log conversion, ELU-FL (6 in Fig. 2) and variable photomultipliers , ELU-FU and ELU-FS. Log conversion is done by limiting the current by a space charge in the intermediate or output stages of the secondary-electron multiplier by selecting the distribution of potentials on the electrodes.

In variable photomultipliers, a system of electrostatic control of photocurrent density with minimum potential is placed between the photocathode and the input stage of the electron multiplier; it is controlled by distribution on electrodes of the cathode chamber. Variable photomultipliers have transconductance of up to 1 A/V, suppression coefficient of 10^4 to 10^5 and working frequency band of up to 1.5 GHz.

In conformity with [14], metrologic characteristics of measurement devices are characteristics exerting an effect on results and measurement error. Certification of metrologic characteristics of photoelectric cells and photomultipliers lets us measure characteristics of test processes with desired error; to compare and select photoelectric cells and photomultipliers according to known conditions of measurement and required accuracy; and to estimate error of complex devices and sytems according to desired functions and structure.

The list of problems to be solved suggests how important it is to standardize the set of metrologic characteristics of photoelectric cells and photomultipliers as measurement devices. Apparently the set of standardized metrologic characteristics on one hand should not be extremely great, while on the other hand it should reflect the basic physical and technical properties of devices and be expressed in form and units permitting simple assessment of measurement results of parameters and their conformity to the standards. When photoelectric cells and photomultipliers are used as the primary measurement transducers, the measurement result will be affected by three groups of parameters. First of all, emission parameters at the input, matching of input window and photocathode with emission parameters. Measurement errors at the input may be caused, for example, by a partial miss of the photocathode by emission, multiple reflections, instability of three-dimensional arrangements and distribution of emission and other random factors. Secondly, parameters supported by photoelectric cells or photomultipliers themselves. Thirdly, parameters of processing and measurement devices for electrical signals at the output of photoelectric cells and photomultipliers, matching of impedance, amplitude and phase-frequency characteristic parameters.

From the viewpoint of creating and using measuring photoelectric cells and photomultipliers, the second group of parameters is most important. Despite the diversity of photoelectric cells and photomultipliers, it is possible to specify general methods of mathematical description of their characteristics, considering the aspects of photoelectric conversion independently of the principle of action and esign features. In mathematics, the term "statement" corresponds to the term "photoelectric conversion"; this establishes the relationship between the elements of the two sets and correlates each element of one set to some element of another set. From the mathematical viewpoint, photoelectric cells and photomultipliers having emission flux at the input and an electrical output,

are a realization of a photoelectric conversion statement, since a transient value of output electrical signal corresponds to each transient value of input photon flux. From the viewpoint of physical processes, spectral sensitivity $i_э(\lambda)$, is the statement of photoelectric conversion; it appears in the equation

$$I = i_э(\lambda)\,\Phi_э + I_0, \tag{1}$$

where I is output current; Φ is power emission flux striking the photocathode; and I_0 is noise current.

As was shown in studies [3, 15], only gradation and calibration of the device in energy units guarantees the unity of measurements in the entire spectral range of electromagnetic emission. Measurement error, in conformity with (1), may be represented in the form

$$\frac{\Delta\Phi_э}{\Phi_э} = \frac{\Delta i_э(\lambda)}{i_э(\lambda)} + \frac{i_0}{I} + \frac{\Delta I}{I}. \tag{2}$$

From (2), it follows that measurement photoelectric cells and photomultipliers should retain unchanged spectral sensitivity in the entire range of measured quantities in order to have a high signal-to-noise ratio and support adequate output currents with an error of ΔI.

As was shown in [3], the basic metrologic characteristics of photoelectric cells and photomultipliers, when measuring parameters of emission pulses using the method of high-speed oscillography, are connected by the relationship

$$\Phi_э = \frac{\int_0^T h(t)\,dt}{TjZi_э(\lambda)}, \tag{3}$$

where T is pulse repetition rate; h(t) is beam deflection on the oscillograph screen at time t; f is oscillation sensitivity; and Z is wave impedance of the measurement tract.

In conformity with (3), amplitude of beam deflection on the oscilloscope screen may be found by the formula

$$h(t) = IjZ$$

If d denotes the beam Ø on the screen, then it is possible to find the relative error of amplitude measurements with output current I:

$$I = d/IjZ.$$

On the other hand, relationship (3) does not explicitly take into account the dynamic characteristics of photoelectric cells and photomultipliers. It is therefore necessary to take both amplitude and time measurements with error δ_t on the time axis, whereas the standardized time resolution Δt of photoelectric cells and photomultipliers [3, 4, 17] also determines the accuracy of photoelectric conversion of emission pulses of desired width $t_и$:

$$\frac{\Delta t}{t_и} 100 < \delta_t. \tag{4}$$

As we know [17], time resolution is determined as a function of conditions of measurement of pulse characteristics, transient characteristics or the complex coefficient of transmission set by the amplitude-frequency and phase-frequency characteristics of the photoelectric cells and photomultipliers. It should be noted that according to classification in [14], photoelectric cells and photomultipliers can be related to the first subgroup of the first group of measurement devices. Thus in addition to the basic error components already considered, it is sometimes necessary to standardize functions of effect caused by the possible deviation of metrologic characteristics from rated values and determine additional error under varied operating conditions.

For certification of metrologic characteristics of photoelectric cells and photomultipliers, as was indicated above, it is necessary to eliminate reproduction error of parameters of emission at the input and measurement error at the output. This condition is satisfied using special meter devices of the appropriate testing circuits of state references. The purposeful elaboration and metrological certification of measurement photoelectric cells of photoelectric colorimeters (FEK) and photomultipliers of cathode ray devices (ELU) now assures the creation of new methods and means of optical-physical measurements with an error of photoelectric conversion no greater than 15 percent.

References

1. Andreyeva, L.I. and Stepanov, B.M., PTE No 3, 1962.

2. Andreyeva, L.I. and Stepanov, B.M., PTE No 5, 1962.

3. Andreyeva, L.I. and Stepanov, B.M., IZMERITEL'NAYA TEKHNIKA No 8, 1965.

4. Andreyeva, L.I. et al., in: Impul'snaya fotometriya [Pulsed Photometry] Mashinostroyeniye Publishers, 1972.

5. Andreyeva, L.I. et al., PTE No 3, 1970.

6. Andreyeva, L.I. et al., PTE No 6, 1976.

7. GOST 17485-77 "Photoelectric cells, electrical vacuum type. Basic specifications".

8. GOST 19798-74 "Photoelectric cells for general-purpose devices. General technical specifications".

9. GOST 20256-75 "Multipliers, photoelectronic, photoelectric cells. Terms, definitions".

10. GOST 17470-72 "Multipliers, photoelectronic. Basic specifications"

11. GOST 21316.0-75 "Multipliers, photoelectronic".

12. GOST 11612.0-75 through 11612.16-75 "Photoelectric cells. Methods of measurement of parameters".

13. GOST 1.25-76 "GSS. Metrologic Support. Basic Assumptions".

14. GOST 8.009-72 "GSI. Standardized metrologic characteristics of measurement devices"

15. Kotyuk, A.F. et al., IZMERITEL'NAYA TEKHNIKA No 3, 1976.

16. Spravochnik konstruktora radioelektronnoy apparatury [Handbook for Radio Engineering Designers], G. R. Varlamov, editor, Moscow, "Sov. radio", 1973.

17. Andreyeva, L.I. et al., in: Impul'snaya fotometriya, Leningrad, Mashinostroyeniye Publishers, 1975.

[249-8617]

8617
CSO: 1860

UDC 621.383.52

PHOTODIODES AND PHOTORESISTORS BASED ON GaSe

Moscow RADIOTEKHNIKA I ELEKTRONIKA in Russian No 7 1979 pp 1430-1432

[Article by G. B. Abdullayev, N. B. Zaletayev, A. Z. Mamedova, T. V. Rudobol and V. I. Stafeyev: "Photodiodes and Photoresistors based on GaSe"]

[Text] The study concerns research on the photosensitivity, noise and threshold characteristics of photodiodes and photoresistors based on monocrystals of gallium monosalenide.

The diodes were fabricated by fusing tin (the rectifying contact) at T = 500-600°C. Specimens of GaSe of the p-type with hole concentrations of 10^{15}-10^{16} cm^{-3} and mobility $\sim$30 $cm^2/v \cdot sec$ were used.

It is shown that the diodes have photosensitivity in the range of the spectrum λ= 0.36-0.65 mkm and the long-wave sensitivity threshold of diodes with an s-shaped volt-ampere characteristic reached 1 mkm.

The detector property D* at the maximum spectral sensitivity λ_{max} = 0.6 mkm of diodes with straight shift U = 10 v and T = 300°K achieved D* = 10^{11} cm $Hz^{\frac{1}{2}}$ vt^{-1}, which is a factor higher than with photoresistors of GaSe.

Among semiconductor compounds $A^{III}B^{IV}$ gallium monoselenide has a number of interesting properties: a significant photosensitivity to visible radiation, photo- and electroluminescence in the presence of induced radiation with rapid electron excitation and so on and, due to this, it may be used to create sources and receivers of radiation.

Earlier we have reported on some of the electrical properties of diodes based on gallium monoselenide (1).

In this study the resul-s are given of research on the photosensitivity, noise and threshold characteristics of diodes and photoresistors of gallium monoselenide at temperature intervals at 77-300°K.

For the base material of the diodes and resistors was used unalloyed and tin-alloyed specimens of gallium monoselenide of the p-type obtained by the Bridgeman method. The concentration and mobility of holes in the monocrystals of GaSe was $p = 10^{15}-10^{16}$ cm^{-3}, $\mu_p = 30$ cm^2/v·sec with 300°K. Wafers of gallium monoselenide were obtained by shearing from slabs of GaSe perpendicular to the direction of the "C" axis. As a result of this shearing a smooth, mirror surface was obtained which did not require further processing.

The diodes were manufactured by fusing tin (the p-n junction) at a temperature of 500-600°C and indium (the ohmic contact) at T = 200-300°K on different sides of the GaSe wafers. The specimens were illuminated on the side of the rectifying contact. The surface area of the diodes was S~0.5 - 1 mm^2.

Used in manufacturing the photoresistors were specimens of GaSe and GaSe alloyed with tin (Sn) with the dimensions 3 X 3 X 0.2 mm^3 at the end of which the ohmic contacts were developed by fusion with indium. The specific nonluminous resistance ρ_T of the GaSe photoresistors was on the order of 10^2-10^4 ohm·cm and of the photoresistors of GaSe(Sn)~10^5-10^6 ohm·cm.

Measurements were made with $R_{spec} \gg R_{load}$. The spectral characteristics were measured with a monochromator DMR-4. The integral photosensitivity was measured at a modulation frequency of 100 Hz and illumination of 100 lk from an incandescant light ("A" source). The photoresponse was recorded on an SI-19B oscillograph. The noise characteristics were measured with a selective micro-voltmeter with an effective band $\Delta f \sim 6$Hz.

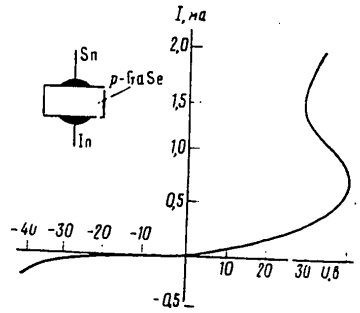

Figure 1. Nonluminous Volt-Ampere Characteristic of a Photodiode of GaSe

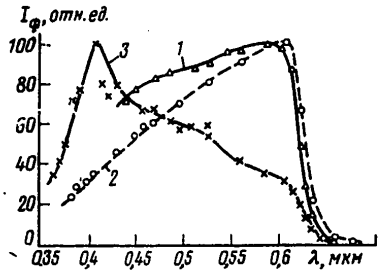

Figure 2. Spectral Characteristics at T = 300° K

1, 3 -- diode with forward and reverse bias;

2 -- photoresistor of GaSe

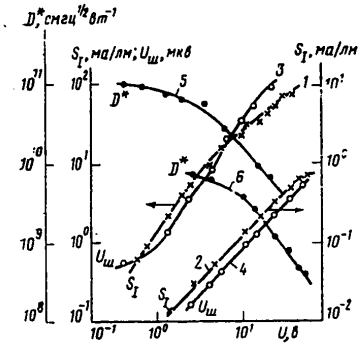

Figure 3. Dependences S_I, D* and $U_ш$ on Applied Voltage for Diodes (1,3,5) and Resistors (2,4,6)

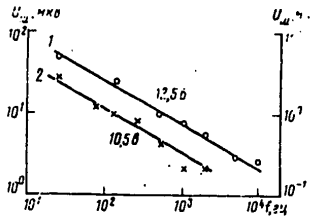

Figure 4. Noise Spectra for a Diode (1, Y-axis to the left) and a Photoresistor (2, Y-axis to the right) from GaSe with T = 300° K

On the straight leg of the volt-ampere characteristic (VAKh) sections of several diodes with negative differential resistance (ODS) of the s-type were observed. The voltage of the junction in the section with ODS amounted to 20-40 volts (fig. 1). Since the base of the diode was manufactured from high-ohm material the basic voltage gradient with forward bias fell within the base and not at the p-n junction. In connection with this, the voltage across the diode considerable exceeded the magnitude of the potential barrier at the p-n junction.

The diodes possessed photosensitivity in the range of the spectrum λ = 0.36-0.65 mkm (T = 300° K). The long-wave threshold of sensitivity of the specimens with s-shaped VAKh reached $\lambda \simeq$ 1 mkm. The maximum spectral sensitivity λ_{max} of the resistors and diodes with forward bias was found in the wavelength range λ_m = 0.56-0.6 mkm (fig. 2, curves 1 and 2). With reverse bias λ_m of the diodes was shifted to the short-wave range of the spectrum: λ_m = 0.44-0.5 mkm (fig. 2,curve 3).

The integral current sensitivity of the diodes and resistors S_1 increased linearly with the applied voltage (fig. 3, curves 1 and 2) and reached $5\text{-}10^2$ma/lm in diodes with forward bias and 1-10 ma/lm in the resistors. Thus, the diodes possessed higher sensitivity than the photoresistors of the same material.

The voltage of the noise $U_ш$ in the majority of diodes and photoresistors at room temperature was also increased almost linearly with an increase in applied bias (fig. 3, curves 3 and 4).

In all of the studies photoresistors and diodes in the frequency range f=25 - $2\cdot10^4$ Hz noise with a spectrum of the type 1/f was observed (fig. 4). When the temperature was lowered to 77° K the voltage of the noise was sharply reduced. The nature of the dependence of $U_ш$ remained unchanged here. The excess noise with a type 1/f spectrum in the photoresistors and diodes may be related to the process of manufacturing the contacts and processing the surface of the specimens.

The detector property at maximum of the spectral sensitivity $\lambda = 0.6$ mkm in diodes with forward bias U = 10v and T = 300° K reached 10^{11}-10^{12} cm $Hz^{1/2}vt^{-1}$ which corresponds to the cut-off power $P_m = (U_ш / R_ш)/S_1\sqrt{\Delta f} = 10^{-12}$-$10^{-13}$ $vt/Hz^{1/2}$. The value of the detector property in the photoresistors was approximately a factor lower.

BIBLIOGRAPHY

1. Aliyeva, M. Kh.; Mamedova, P. F.; Mamedova, A. Z.; and Muradova, G. A. DOKL. AN AzerSSR, 1972.

[272-8945]

8945
CSO: 1869

UDC 621.396

EFFECTIVE ALGORITHMS OF MAXIMALLY PROBABLE PROCESSING OF RADAR SIGNALS

Moscow RADIOTEKHNIKA in Russian Vol 34, No 7, 1979 pp 8-14

[Article by V. I. Chaykovskiy, submitted after revision 8 Sep 1978]

[Text] In many instances, radar searching (simultaneous detection and measurement of the parameters of useful signal) amounts to a maximally probable evaluation of these parameters and the verification of the truth of the hypothesis about the existence of the signal in the observed realization

$$y(t)=s(t,\alpha)+x(t),\quad t\in T, \tag{1}$$

where $s(t,\alpha)$ is the determined useful signal with a vector of unknown parameters α; $x(t)$ is the Gaussian noise with a known correlation function [1]. The above procedures can be performed on the basis of the processing of the complex envelope of the observed realization

$$\mathbf{Y}(t)=\mathbf{S}(t,\alpha)+\mathbf{X}(t),\quad t\in T \tag{2}$$

as a result of the formation and extreme analysis of the probability function or sufficient statistics of the vector of informational parameters of the signal component. The switching to the complex envelope of the realization of the band-pass signal being studied is particularly advantageous in digital processing systems. In this case, due to the low-frequency nature of the spectrum of the complex envelope, the quantification frequency and the aperture error of information quantization during analog-digital conversion decrease. Moreover, the complex nature of the representation of information is well in agreement with the functional characteristics of the procedures of digital spectral analysis which are used widely in modern processing systems.

Let us represent the complex envelope of the observed realization in the form of a column vector Y in a complex unitary space by the expression

$$\mathbf{Y}=\gamma\mathbf{S}_\beta+\mathbf{X}, \tag{3}$$

where the complex amplitude $\gamma=Ae^{i\varphi}$ allows for the influence of the random initial phase of the useful signal φ, the information parameters $\beta(\tau, \nu)$

are determined by the time shift of the signal τ and the displacement of its carrier frequency[1] ν, and the random vector X with a normal distribution law and a known covariance matrix

$$\Lambda = \mathrm{E}\{\mathbf{X}\overline{\mathbf{X}}^{T}\} \tag{4}$$

represents an additive interference. Here and hereafter, the line symbolizes the operation of complex conjugation. Having used a known expression for a normal distribution law of a random vector in a real unitary space [3] and having transformed it with consideration for the peculiarities of the scalar product in a complex unitary space, it is possible to obtain an expression for a probability function of a vector of information parameters β averaged over the area of variations of the interfering parameter (random phase φ)

$$L(\beta, \mathbf{Y}) = \frac{1}{2\pi}\int_{0}^{2\pi} \exp[\mathrm{Re}\{A\exp i\varphi \mathbf{S}_{\beta}^{T}\Lambda^{-1}\overline{\mathbf{Y}}\}]\,d\varphi = I_0\{A|\mathbf{S}_{\beta}^{T}\Lambda^{-1}\overline{\mathbf{Y}}|\}, \tag{5}$$

where $I_0\{\cdot\}$ is the Bessel function of the first kind of the zero order whose argument is the bilinear Hermite form of the vector S_β of the information part of the complex envelope of the useful signal and vector Y of the complex envelope of observation. The matrix Λ^{-1} of the bilinear form is formed by inversion of the covariance matrix (4). It is evident that the bilinear Hermite form is a sufficient statistic of the vector of informational parameters β and forms above the plane of its possible variance the surface

$$l(\beta, \mathbf{Y}) = |\mathbf{S}_{\beta}^{T}\Lambda^{-1}\overline{\mathbf{Y}}|, \tag{6}$$

whose extreme analysis is aquivalent to the analysis of the likelihood function (5). Consequently, in the practice of radar searching the maximally probable processing (MPO) oriented toward detection of a useful signal and the evaluation of its informational parameters can be reduced to the formation and subsequent extreme analysis of the surface of sufficient statistics $l(\beta, \mathbf{Y})$. Thus, (6) is a matrix form of a basic algorithm of maximally probable processing of a complex envelope of a radar signal with a random initial phase under the conditions of a Gaussian interference.

Having made use of the property of associativity of the multiplication of matrices, algorithm (6) can be represented in the form of a modular value of the scalar product of the vector of observation Y and a certain reference vector G_β

$$\mathbf{G}_{\beta}^{T} = \mathbf{S}_{\beta}^{T}\Lambda^{-1}, \tag{7}$$

formed by the products of known matrices S_β and Λ^{-1}*). Thus, the expression

1. In the general case, vector β can also allow for other parameters of a useful signal carrying useful information.

*Reference vector G_β can be considered as a solution of the system of linear equations $\Lambda G_\beta = S_\beta$.

$$l(\beta, Y) = |(G_\beta, Y)|, \tag{8}$$

representing each count of sufficient statistics in the form of a modulus of the coefficient of mutual correlation or scalar product of the vector of observation and a certain reference vector is true. Such an algorithm can be called an algorithm of correlation of copies in the space of complex envelopes. A simplified functional diagram of the MPO system on the basis of the correlation of copies is shown in Figure 1a, where symbol M designates the procedure of the decermination of modular values, and symbol H designates the procedure of the accumulation of pair products. As follows from (8), the formation of each count of sufficient statistics $l(\beta, Y)$ in an N-dimensional space is materialized as a result of the fulfillment of N operations of complex multiplication.

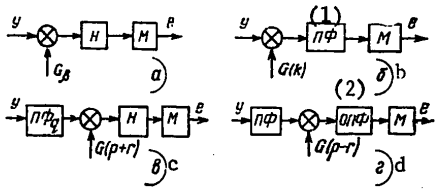

Key: 1. PF -- Fourier transformation
2. OPF -- inverse Fourier transformation

More economical MPO algorithms with respect to the amount of computations can be obtained if we represent vector S_β as a sequence of counts. If a signal with zero initial values of parameters τ and ν has a complex envelope S(t), then the complex envelope of the same signal with arbitrary values of these parameters is, as is known [4], equal to

$$S_\beta(t) = \exp[-i\nu(t-\tau)]\,S(t-\tau).$$

Let us assume, as it is taken in the theory of discrete Fourier transformation (DPF) [5], that W is the symbol of the latticed complex exponential function $\exp\left[i\frac{2\pi}{N}(\cdot)\right]$, and symbols r, k, q, and p respectively denote dimensionless values of the displacement of frequency ν, current time t, shift τ, and current frequency ω. Then, the following representation of vector S_β in an N-dimensional complex-valued space is true:

$$\mathbf{S}_\beta = \mathbf{W}^{-r(k-q)}\mathbf{S}(k-q), \quad k \in N.$$

The observation vector Y and interference vector X can be represented in an analogous form: $\mathbf{Y} = \mathbf{Y}(k)$, $\mathbf{X} = \mathbf{X}(k)$, $k \in N$. In this case, the elements of the covariance matrix Λ are defined by the expression

$$\lambda_{kl} = \mathrm{E}\{\mathbf{X}(k)\overline{\mathbf{X}}(l)\}, \quad k, l \in N$$

and, due to the stationary state of the interference, possess the properties of diagonal symmetry $(\lambda_{kl}=\bar{\lambda}_{lk})$ and invariance to shift $(\lambda_{kl}=\lambda_{(k+q)(l+q)})$. The elements of the matrix Λ^{-1} possess the same properties.

Having made use of the notations introduced above, let us represent the sufficient statistics (6) in the form of

$$l(r, q, Y)=|W^{rq}|\cdot|[W^{-rk}S(k-q)]^T\Lambda^{-1}\overline{Y}(k)|, \quad r, k\in N.$$

By virtue of the above-mentioned property of invariance of the elements of matrix Λ^{-1}, the following relation is true

$$l(r, q, Y)=|[W^{-rk}S(k)]^T\Lambda^{-1}\overline{Y}(k+q)|, \quad r, k\in N,$$

which can be represented in the form of a modulus of scalar product

$$l(r, q, Y)=|([W^{-rk}G(k)], Y(k+q))|, \quad r, k\in N, \tag{9}$$

where $G^T(k)=S^T(k)\Lambda^{-1}$ is a certain reference vector coinciding with the solution of the system of equations $\Lambda G = S$. By definition, a scalar product can be written in the form of sum of pair products

$$l(r, q, Y)=\left|\sum_k G(k)\overline{Y}(k+q)W^{-rk}\right|, \quad r, k\in N. \tag{10}$$

Consequently, the sufficient statistics coincides with the DPF modulus of the sequence of pair products of elements of the reference vector and the sliding vector of observation which, in technical applications, is called correlation product

$$l(r, q, Y)=|F[G(k)\overline{Y}(k+q)]|, \quad r, k\in N. \tag{11}$$

In this expression, $F=\|W^{-rk}\|$ is the DPF matrix.

The MPO algorithm represented by expressions (10) or (11), with respect to its informativeness, is equivalent to the algorithm of the correlation of copies (8) and amounts to the determination of modular values of the sequence of the DPF of correlation products of a fixed reference vector which is developing with time, and the vector of the complex envelope of observation at each step of its sliding. The Fourier transformation of each correlation product forms at points ν_r a latticed copy of the cross section of the surface of sufficient statistics $L(\beta, Y)$ parallel to the axis of the shifting of frequency ν with a fixed shift t_q. Algorithm (11) which accomplishes the MPO on the basis of spectral analysis of a correlation product can be called correlation-spectral algorithm. A simplified functional scheme which realizes such an algorithm is shown in Figure 1b, where symbol PF denotes the procedure of Fourier transformation, and the remaining notations coincide with those adopted earlier.

When the correlation-spectral algorithm is used in an N-dimensional space, first there forms an N-dimensional correlation product $G(k)\overline{Y}(k+q)$, on which N operations of complex multiplication are spent. Then the obtained sequence is transformed by means of the procedure of fast Fourier transformation (BPF) on which additional $0.5N \log_2 N$ of multiplication operations are spent. Thus, the total expenditure amounts to $N+0.5N \log_2 N$ such operations. Since as a result of this, there form N counts of sufficient statistics corresponding to various values of frequency shifts, then the proportionate expenditure of operations of complex multiplication per one its count are equal to

$$n = \frac{N + 0{,}5N \log, N}{N} = 1 + 0{,}5 \log_2 N < N$$

and always less than the corresponding expenditure when MPO is realized on the basis of direct correlation of copies. If instead of the BPF procedure the standard DPE procedure is used in calculations, the effectiveness of the algorithm is lowered approximately to the level of the effectiveness of the algorithm of direct correlation of copies.

Another economical MPO algorithm can be obtained by using expression (9). Since the operator of discrete Fourier transformation, by virtue of its orthogonality, is unitary, and, consequently, maintains the value of the scalar product [6], then the following relation is true:

$$l(r, q, Y) = |(F[W^{-rk}G(k)], F[Y(k+q)])|.$$

In accordance with the known [5] DPF theorems, the first co-factor of scalar product can be reproduced in the form of $F[W^{-rk}G(k)] = G(p+r)$, where index

r symbolizes the shifting of the vector $G(p) = FG(k)$ along the axis of frequencies. By definition, Fourier transform of the 2nd co-factor coincides with the sliding Fourier transformation (SPF) $Y_q(p)$ of the vector of observation [7]

$$F[Y(k+q)] = Y_q(p), \quad p, k \in N.$$

Thus, the sufficient statistics is equal to

$$l(r, q, Y) = |[G(p+r), Y_q(p)]|, \quad p \in N \tag{12}$$

and MPO is reduced to the sliding Fourier transformation of the vector of observation and determination of modular values of scalar products of the vector of the sliding spectrum $Y_q(p)$ and spectral images $G(p+r)$ of the reference vector G(k) with prescribed frequency shifts r. The procedure of the determination of scalar products is accomplished over the entire set of possible frequency shifts ν_r at each step q of the sliding of the vector of observation. As a result of this, there form latticed copies of sections of the surface of sufficient statistics analogous to those obtained in the realization of the correlation-spectral algorithm (11). Algorithm (12) which realizes MPO on the basis of SPF can be called spectral-correlational since, unlike (11), spectral analysis is realized during the first stage of processing, and the correlational product of spectral images is formed during the

second stage. A simplified functional scheme of the system realizing the processing on the basis of SPF is shown in Figure 1c, where the symbol PF_q denotes the SPF procedure.

For the formation of each count of sufficient statistics, when SPF is realized on the basis of effective recurrent procedures expending on each cycle of sliding analysis N operations of complex multiplication [7], it is necessary to perform only (1+Q) such operations where Q is the active dimensionality of the spectral image G(p) of the reference vector G(k). When processing radar signal with a small size of the base, this value is substantially smaller than N and the spectral-correlation algorithm is not any less effective than the correlation-spectral algorithm. The algorithm is particularly effective in processing simple audio signals (Q=1). In this case, the reference vector G(p) degenerates into a one-dimensional vector, which eliminates the necessity of the formation and summation of the elements of the correlation product in the spectral region. Thus, the structure of the processing system is simplified as a result of the elimination of the complex multiplication device and digital accumulator, and the number of complex multiplications spent on the formation of each count of sufficient statistics decreases to one.

The algorithms (11) and (12) examined above make it possible to form latticed copies of cross sections of the surface of sufficient statistics parallel to the axis of frequency shifting. Having used (11), it is possible to obtain the effective MPO algorithm forming cross sections parallel to the time-delay axis. As can be shown [5], the Fourier transform of the vector $[G(k)x\overline{Y}(k+q)]$ is equal to the convolution of the co-factor spectra. Since

$$FG(k) = G(p),\ FY(k+q) = W^{pq}Y(p),$$

then

$$l(r, q, Y) = \left|\sum_p G(p-r)\overline{Y}(p)W^{pq}\right| = |\overline{F}[G(p-r)\overline{Y}(p)]|. \qquad (13)$$

Thus, the sufficient statistics is defined as the modulus of the inverse Fourier transformation of correlation product of the reference vector G(k) and the vector of observation $\overline{Y}(k)$ in the spectral basis with all possible values of frequency displacement ν_r and shift t_q. The algorithm of MPO corresponding to such definition of sufficient statistics in the first stage amounts to the determination of the Fourier transformation of Y(p) of the observation vector and the formation of correlation products $[G(p-r)\overline{Y}(p)]$ by the set of the varying parameter of frequency shift r. The spectral image G(p) of the vector of the reference signal in this case is assumed to be known. The second stage of processing amounts to inverse Fourier Transformation of the formed correlation products. Each such transformation, after the determination of modular values, forms a cross section of the surface of sufficient statistics parallel to the axis of shifts q in entire interval of the determination of the vector of observation Y. Since the above algorithm realizes the Fourier transformation both in the first and second stages, it can be called spectral algorithm. A simplified functional scheme realizing such an algorithm is shown in Figure 1d where symbol OPF denotes the procedure of the inverse Fourier transformation.

In order to eliminate boundary distortions of the results of the processing on the basis of the spectral algorithm, the dimensionality M of the vector of observation must correspond to the full range of possible delays of the useful signal and, consequently, to be substantially greater than its dimensionality N. This lowers the effectiveness of the algorithm. Sectionalization of input information and its processing in mutually intersecting intervals remove the above-mentioned defect. Organization of sectionalized processing fully coincides with the known processing [8] oriented toward obtaining aperiodic convolution in a space of real samples and does not require additional explanations. The dimensionality of the vector of observation in sectionalized processing by the spectral algorithm usually is taken to be equal to 2N, so that for the formation of one count of sufficient statistics (13) with the use of the procedures of the fast Fourier transformation, approximately

$\left(\log_2 2N + \frac{Q}{N}\right.$ operations of complex multiplication are used, where Q is the

active dimensionality of the spectral image of the reference vector G(p). Thus, the spectral algorithm is somewhat less effective than the correlation-spectral algorithm, however, it always remains more economical than the algorithm of direct correlation of copies.

The four MPO algorithms for complex envelopes of radar signals are well suited for realization on the basis of the use of digital computers, since, all other things being equal, they minimize the aperture error of quantization and quantification frequency at the stage of analog-digital conversion. Three of the four algorithms make use in one or another form of spectral representations of information, which makes it possible, as a result of applying effective procedures of the fast Fourier transformation or recurrence analysis of the sliding spectrum, to reduce the volume of computations in comparison with that for the realization of the traditional algorithm of the correlation of copies. Moreover, the complex-valued nature of the input information agrees best with the functional peculiarities of various procedures of the Fourier transformation, which additionally lowers the computation and equipment expenses.

Since, as follows from the formulas representing effective algorithms, in the absence of an interference, the surface of sufficient statistics $l(r, q, S)$ coincides with the surface of the body of mutual ambiguity of useful signals (Woodworth [4]), such algorithms should be considered as algorithms of informationally complete representation of radar information. The completeness condition is always satisfied when the steps of quantification with respect to time and frequency are selected in accordance with the requirements of Kotel'nikov's sampling theorem.

Apart from a harmonic algorithm, the realization of a base algorithm (6) is possible in any other orthogonal base, for example, in the base of the Vilenkin-Krestenson step functions. However, preliminary analysis shows that in such a base there is practically no possibility of reducing computation expenditures in comparison with the algorithm of the correlation of copies.

It is advisable to use the above-mentioned considerations together with the obtained results of the synthesis of the algorithms in development and analysis of the effectiveness of systems of maximally probable processing of various radar signals.

Bibliography

1. Khelstrom, K. "Statisticheskaya teoriya obnaruzheniya signalov" [Statistical Theory of Signal Detection], Moscow, 1963.

2. Sakrison, D. "Lektsii ob analogovoy svyazi" [Lectures on Analog Communication], Mir, Moscow, 1974.

3. Anderson, T. "Vvedeniye v mnogomernyy statisticheskiy analiz" [Introduction to Multidimensional Statistical Analysis], Fizmatgiz, Moscow, 1963.

4. Frenks, L. "Teoriya signalov" [Theory of Signals], Sov Radio, Moscow, 1974.

5. Cooly, J. W.; Lewis, P. A., and Welch, P. D. TRANS IEEE, Vol AU-17, No 2, 1972.

6. Mal'tsev, A. I. "Osnovy lineynoy algebry" [Fundamentals of Linear Algebra], Nauka, Moscow, 1975.

7. Botnin, A. N., and Strashinin, Ye. E. AVTOMETRIYA [Autometry], No 1, 1975.

8. Gold, B., and Reyder, Ch. "Tsifrovaya obrabotka signalov" [Digital Processing of Signals], Sov Radio, 1973.

10,233
CSO: 1860

UDC 621.396.96

RADAR CONTRAST BETWEEN TWO OBJECTS

Kiev IZVESTIYA VYSSHIKH UCHEBNYKH ZAVEDENIY: RADIOELEKTRONIKA in Russian
No 6, 79 signed to press 13 Feb 79 pp 63-67

[Article by A. I. Kozlov]

[Text] Annotation

Concepts were obtained of dispersion matrices (MR) of two objects with one and the same polarization basis through characteristic values of these MR and a relationship was found between the radar contrast and the type of polarization of the radiating wave.

In a number of cases, the use of polarization effects in radar makes it possible to increase the value of the reflected power considerably by proper selection of the type of polarization of the radiating electromagnetic wave. For isolated targets, this gain may reach one-two and even three tens of decibels compared to the traditionally used linear polarized waves [1, 2].

For example, when scanning remote targets of the earth's surface, of interest is a comparison between signals reflected from two different sections (resolution components) for the purpose of selecting a kind of polarization at which the contrast between them is maximum (by contrast we mean the ratio between the powers of the indicated signals).

The given problem can be solved easily if the sought-for ratio is written using the respective components of dispersion matrices of the two sections, hereinafter called objects. However, in this case, it will be necessary to deal with 14 actual parameters: three complex parameters from each object and two describing the polarization of the incident wave. In this connection the problem arises of representing the dispersion matrices of the two objects on the same polarization bases through several invariants of these MR. In this case, naturally, the purpose is to impart to both MR the simplest symmetrical form. On Poincare's sphere (Fig. 1), let a pair of diametrically opposing points (1-1) represent the characteristic polarization basis (PB) of the first object and pair (2-2) -- of the

second. We will designate angle 102, which is invariant to changes of the bases, by $2\alpha_{12}$

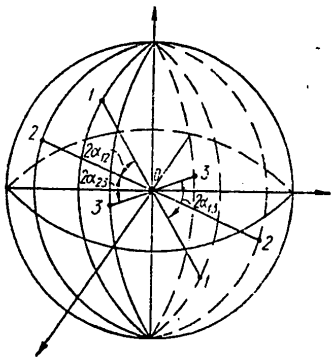

Fig. 1

In each of the indicated bases, one of the dispersion matrices is diagonal

$$\Lambda_{1-1}=\begin{bmatrix}\lambda_1 & 0\\ 0 & \lambda_2\end{bmatrix},\qquad P_{2-2}=\begin{bmatrix}p_1 & 0\\ 0 & p_2\end{bmatrix},$$

where λ_1 and λ_2, p_1 and p_2 -- characteristic values of dispersion matrices of the first and second objects respectively which, in the general case, are complex numbers. For definiteness, we will consider that $|\lambda_1|\geqslant|\lambda_2|$; $|p_1|\geqslant|p_2|$. Indices of Λ and P indicate the polarization basis used for consideration.

When changing over from one PB to another, the dispersion matrice, as is well known [1, 2], is subjected to congruent transformation by means of unitary matrix Q, consisting of four parameters: Φ, η, ξ, α, the general form of which is [3, 4].

$$Q=e^{i\Phi}\begin{bmatrix}e^{i\eta}\cos\alpha & -e^{-i\xi}\sin\alpha\\ e^{i\xi}\sin\alpha & e^{-i\eta}\cos\alpha\end{bmatrix}.$$

If two pairs of diametrically opposite points on Poincare's sphere show the old and the new basis, then the angle between corresponding diameters will be equal to half of angle α [4].

The geometrical interpretation of the remaining parameters Φ, ξ, and η is of no interest for the problem being considered.

The polarization bases represented by the points on the major circle, the plane of which is perpendicular to diameter (1-1) in Fig. 1, will be obtained from PB (1-1) at $\alpha = \pi/4$. Similarly PB, represented by points on the major circle, the plane of which is perpendicular to diameter (2-2), will be obtained from PB (2-2) also at $\alpha = \pi/4$. The basis which is represented by intersection points of the major circles considered, we will assign index (0-0) and will call it the zero basis.

The dispersion matrix of the first object on basis (0-0) will have the form:

$$\Lambda_{0-0} = Q_{10}\Lambda_{1-1}\tilde{Q}_{10}, \qquad (1)$$

and of the second --

$$P_{0-0} = Q_{20}P_{2-2}\tilde{Q}_{20}. \qquad (2)$$

Indices of Q designate from which to which basis the transfer is being made, for example, Q_{10} corresponds to transfer from (1-1) to (0-0).

From equalities (1) and (2) follow inverse formulas

$$\left.\begin{aligned}\Lambda_{1-1} &= \tilde{Q}^{*}_{10}\Lambda_{0-0}Q^{*}_{10}\\ P_{2-2} &= \tilde{Q}^{*}_{20}P_{0-0}Q^{*}_{20}\end{aligned}\right\}, \qquad (3)$$

where the basic property of a unitary matrix

$$Q\tilde{Q}^{*} = \begin{bmatrix}10\\01\end{bmatrix},$$

is taken into account, while symbols $\sim$ and $*$ designate correspondingly operations of transposition and complex conjugation.

On the other hand, in correspondence with transformations types (1) and (2) we have:

$$\left.\begin{aligned}\Lambda_{1-1} &= Q_{01}\Lambda_{0-0}\tilde{Q}_{01}\\ P_{2-2} &= Q_{02}P_{0-0}\tilde{Q}_{02}\end{aligned}\right\}. \qquad (4)$$

a comparison between (3) and (4) indicates that

$$\tilde{Q}^{*}_{10} = Q_{01}, \qquad \tilde{Q}^{*}_{20} = Q_{02}, \qquad (5)$$

from which it follows that

$$\alpha_{01} = \alpha_{10}, \quad \eta_{01} = -\eta_{10}, \quad \xi_{01} = \pi + \xi_{10}.$$

Using relationship (1) and requirement $\alpha_{10} = \pi/4$, we will write the form of the dispersion matrix of the first object on basis (0-0).

$$\Lambda_{0-0} = \frac{1}{2}\begin{bmatrix}\lambda_1 e^{2i\eta_{10}} + \lambda_2 e^{-2i\xi_{10}} & \lambda_1 e^{i(\eta_{10}+\xi_{10})} - \lambda_2 e^{-i(\eta_{10}+\xi_{10})}\\ \lambda_1 e^{i(\eta_{10}+\xi_{10})} - \lambda_2 e^{-i(\eta_{10}+\xi_{10})} & \lambda_1 e^{2i\xi_{10}} + \lambda_2 e^{-2i\eta_{10}}\end{bmatrix}. \qquad (6)$$

P_{0-0} has a similar form.

Matrix (6) contains little useful parameters η_{10}, ξ_{10}. It is important to express them by parameters which tie together PB (1-1) and PB (2-2), i.e., angle α_{12} and ξ_{12}, η_{12}.

The transfer from PB (1-1) to PB (2-2) can be made directly or in arrangement

$$(1-1)\rightarrow(0-0)\rightarrow(2-2),$$

which can be written

$$\Lambda_{2-2}=Q_{12}\Lambda_{1-1}\tilde{Q}_{12}=Q_{02}(Q_{10}\Lambda_{1-1}\tilde{Q}_{10})\tilde{Q}_{02}=\tilde{Q}_{20}^{\bullet}Q_{10}\Lambda_{1-1}\tilde{Q}_{10}Q_{20}^{\bullet},$$

where (5) is used. It follows from here:

$$Q_{12}=\tilde{Q}_{20}^{\bullet}Q_{10}=Q_{02}\tilde{Q}_{01}^{\bullet},$$

which produces

$$\left.\begin{aligned}\eta_{10}-\eta_{20}-\xi_{10}+\xi_{20}&=2\alpha_{12}\\ \eta_{10}-\eta_{20}+\xi_{10}-\xi_{20}&=2\eta_{12}\\ \eta_{10}+\eta_{20}+\xi_{10}+\xi_{20}&=2\xi_{12}+\pi\end{aligned}\right\}. \qquad (7)$$

Relationships (7) represent a system of three equations with four unknowns. We will write one of its symmetrical solutions:

$$\left.\begin{aligned}\eta_{10}&=\frac{\alpha_{12}+\eta_{12}+\xi_{12}}{2}+\frac{\pi}{4}\\ \xi_{10}&=\frac{\eta_{12}-\alpha_{12}+\xi_{12}}{2}+\frac{\pi}{4}\\ \eta_{20}&=-\frac{\alpha_{12}+\eta_{12}-\xi_{12}}{2}+\frac{\pi}{4}\\ \xi_{20}&=\frac{\alpha_{12}-\eta_{12}+\xi_{12}}{2}+\frac{\pi}{4}\end{aligned}\right\} \qquad (8)$$

We will substitute (8) in the general form (6) for dispersion matrix Λ on (0-0) basis

$$\Lambda_{0-0}=\frac{i}{2}\begin{bmatrix}(\mu_1-\mu_2)\,e^{i\alpha_{12}} & \mu_1+\mu_2\\ \mu_1+\mu_2 & (\mu_1-\mu_2)\,e^{-i\alpha_{12}}\end{bmatrix}, \qquad (9)$$

similarly

$$P_{0-0} = \frac{i}{2}\begin{bmatrix} (s_1 - s_2)\,e^{-i\alpha_{12}} & s_1 + s_2 \\ s_1 + s_2 & (s_1 - s_2)\,e^{i\alpha_{12}} \end{bmatrix}, \qquad (10)$$

where

$$\left.\begin{aligned} \mu_1 &= \lambda_1 e^{i(\eta_{12}+\xi_{12})} \\ \mu_2 &= \lambda_2 e^{-i(\eta_{12}+\xi_{12})} \\ s_1 &= p_1 e^{-i(\eta_{12}-\xi_{12})} \\ s_2 &= p_1 e^{i(\eta_{12}-\xi_{12})} \end{aligned}\right\}.$$

Relationships (9) and (10) give the sought for representations of the dispersion matrices of the two objects in the same PB, expressed by their characteristic values of each MR and the parameters tying together the characteristic polarizations of each object.

The following representations for Grave's power matrices follow from relationships (9) and (10):

$$\left.\begin{aligned} G_\Lambda &= \frac{1}{2}\begin{bmatrix} |\lambda_1|^2 + |\lambda_2|^2 & e^{-i\alpha_{12}}(|\lambda_1|^2 - |\lambda_2|^2) \\ e^{i\alpha_{12}}(|\lambda_1|^2 - |\lambda_2|^2) & |\lambda_1|^2 + |\lambda_2|^2 \end{bmatrix} \\ G_p &= \frac{1}{2}\begin{bmatrix} |p_1|^2 + |p_2|^2 & e^{i\alpha_{12}}(|p_1|^2 - |p_2|^2) \\ e^{-i\alpha_{12}}(|p_1|^2 - |p_2|^2) & |p_1|^2 + |p_2|^2 \end{bmatrix} \end{aligned}\right\}.$$

As may be seen, Grave's matrices depend, besides p and λ only on angle α_{12}.

We will now compare the powers of the signals reflected from the objects. We will write the orthogonal components of the incident elliptically polarized wave in PB (0-0) in the form

$$\left.\begin{aligned} E_{1\text{пад}} &= \cos\beta e^{i\varphi} e^{i\omega t} \\ E_{2\text{пад}} &= \sin\beta e^{-i\varphi} e^{i\omega t} \end{aligned}\right\},$$

where β and φ determine the form of the polarization ellipse. The value of the power reflected from the objects will be determined by relationships

$$\left.\begin{aligned}\Pi_{\Lambda} &= \tilde{E}^{*}_{\text{пад}} G_{\Lambda} E_{\text{пад}} \\ \Pi_{p} &= \tilde{E}^{*}_{\text{пад}} G_{p} E_{\text{пад}}\end{aligned}\right\}. \qquad (11)$$

where $\tilde{E}_{\text{пад}} = (E_{1\text{пад}} E_{2\text{пад}})$.

Relationships (11) make it possible to find the sought-for ratio of the powers of the signals reflected from the two objects depending upon the form of polarization (parameters β, φ):

$$q = \frac{\Pi_{\Lambda}}{\Pi_{p}} = \frac{\sigma_{\Sigma\Lambda}}{\sigma_{\Sigma p}} \frac{1 + k_{\lambda} \sin 2\beta \cos(2\varphi + \alpha_{12})}{1 + k_{p} \sin 2\beta \cos(2\varphi - \alpha_{12})}, \qquad (12)$$

where coefficients k_{λ} and k_{p} characterize the degree of polarization anisotropy of the objects

$$k_{\lambda} = \frac{|\lambda_1|^2 - |\lambda_2|^2}{|\lambda_1|^2 + |\lambda_2|^2}, \quad k_{p} = \frac{|p_1|^2 - |p_2|^2}{|p_1|^2 + |p_2|^2},$$
$$\sigma_{\Sigma\Lambda} = |\lambda_1|^2 + |\lambda_2|^2, \quad \sigma_{\Sigma p} = |p_1|^2 + |p_2|^2.$$

Sum $|\lambda_1|^2 + |\lambda_2|^2$, representing a spur of Grave's matrix, is invariant to bases (1) transformation. It is equal to the sum of all effective dispersion cross sections (EPR) with parallel and transverse polarizations and is called the full EPR of the target (5) (for horizontal and vertical polarizations $\sigma_{\Sigma} = \sigma_{\text{гг}} + \sigma_{\text{вв}} + 2\sigma_{\text{гв}}$).

External values are assumed by q, as follows from (12), when $\sin 2\beta = \pm 1$.

In this case:

$$q_1 = q\left(2\beta = \pm\frac{\pi}{2}\right) = \frac{\sigma_{\Sigma\Lambda}}{\sigma_{\Sigma p}} \frac{1 \pm k_{\lambda} \cos(2\varphi + \alpha_{12})}{1 \pm k_{p} \cos(2\varphi - \alpha_{12})}.$$

A further analysis shows that extremums are reached at

$$2\varphi = \pi - \arccos\left(\frac{k_p k_\lambda \sin 2\alpha_{12}}{\sqrt{k_\lambda^2 + k_p^2 - 2k_\lambda k_p \cos 2\alpha_{12}}}\right) - \\ - \operatorname{arctg}\left(\frac{k_p - k_\lambda}{k_p + k_\lambda} - \operatorname{tg}\alpha_{12}\right) + 2\pi n,$$

$$n = 0, \pm 1, \ldots$$

It may be seen from (12) that the sought-for value of q represents a product of two factors, one of which is a ratio of full EPR of objects independent of the form of the incident wave polarization, while the second -- takes into account the polarization anisotropy of the targets.

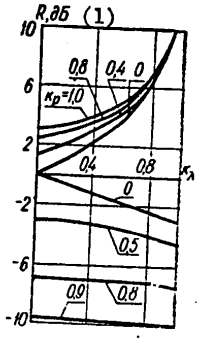

Fig. 2

1. db

Fig. 2 shows the relationship between the external values of the second factor, designated

$$R = q\frac{\sigma_{\Sigma p}}{\sigma_{\Sigma\lambda}},$$

and the value of k_λ for various k_p, with angle α_{12} assumed equal to $\pi/2$. The upper curves in Fig. 2 correspond to the maximum value of R and the lower -- to the minimum value of R. In other words, when the form of the incident wave polarization changes, the ratio of powers of reflected waves will change from

$$R_{\max}\frac{\sigma_{\Sigma\Lambda}}{\sigma_{\Sigma p}} \qquad \text{to} \qquad R_{\min}\frac{\sigma_{\Sigma\Lambda}}{\sigma_{\Sigma p}}.$$

In conclusion, we will turn our attention to one relationship. Let points (3-3) in Fig. 1 represent a polarization basis for making measurements. The dispersion matrices of objects in this PB will be assumed to be S and P. In this case, for k_λ and k_p the following [1, 2] is true:

$$k_\lambda = \sqrt{1-4\frac{|\det s|}{\sigma_{\Sigma\Lambda}}}, \qquad k_p = \sqrt{1-4\frac{|\det P|}{\sigma_{\Sigma p}}}.$$

If angles α_{13} and α_{23} are introduced as was done in Fig. 1, then

$$k_\lambda = \frac{\sigma_{11\Lambda}-\sigma_{22\Lambda}}{\sigma_{\Sigma\Lambda}\cos 2\alpha_{13}}, \qquad k_p = \frac{\sigma_{11p}-\sigma_{22p}}{\sigma_{\Sigma p}\cos 2\alpha_{23}},$$

where σ_{11} and σ_{22} are the EPR of two orthogonal polarizations.

BIBLIOGRAPHY

1. Kanareykin, D. B.; Pavlov, N. F.; Potekhin, V. A. "Polarization of Radar Signals." Moscow, SOVETSKOYE RADIO, 1966

2. Kanareykin, D. B.; Potekhin, V. A.; Shishkin, I. F. "Marine Polarimetry." Leningrad, "Sudostroyeniye," 1968.

3. Gorshkov, M. M. "Ellipsometry." Moscow, SOVETSKOYE RADIO, 1974.

4. Kozlov, A. I.; Demidov, Yu. M. "Certain Properties of Covariational Dispersion Matrices." RADIOTEKHNIKA I ELEKTRONIKA, 1976, 21, No 11, p 2415.

2291
CSO: 1860

UDC 621.396.96

THEORY OF NOISE-LIKE SPACE-TIME SIGNALS

Kiev IZVESTIYA VYSSHIKH UCHEBNYKH ZAVEDENIY: RADIOELEKTRONIKA in Russian No 7, 79 signed to press 28 Apr 78, after revision, 3 Nov 78 pp 3-10

[Article by A. I. Pogorelov]

[Text] Annotation

A definition of noise-like space-time signals is given and their classification is described. Problems of forming and processing phase-manipulated space-time signals were considered. An analysis is given of the output effect of an optimal system for processing such signals.

Space-time presentation of signals was found to be very fruitful in solving a great number of problems in radar, navigation, control and communications. At present, it has achieved a level where problems in the practical implementation of the optimal methods for transmitting data and measuring motion parameters can be solved successfully. However, unlike systems with "time" signals, the optimization and practical implementation of which are being developed in the direction of seeking the optimal structure of the signals, as well as finding optimal algorithms for their processing, in systems with space-time signals the solution of these problems is limited at present, as a rule, only to searching for the optimal procedure for processing space-time signals (PVS). This narrows considerably the area of using the space-time approach and makes it impossible to unveil and implement its possibilities fully because the problems of selecting the shape of the signal that determines the system structure, as well as its basic indicators, are some of the most important problems being solved in its design.

In synthesizing optimal time signals, attention was given to pseudorandom or noise-like signals (ShPS). A number of properties that were responsible for their wide dissemination and that predetermined great possibilities of the systems when they are used [1], provide a basis to consider that many problems of measuring motion parameters and transmitting data may be solved by using noise-like space-time signals (ShPVS).

Below problems of forming and processing ShPVS are considered for viewing a given comparatively wide sector of space.

The PVS may be represented in the form of a vertical or horizontal vector of electric field intensity with an angular density $s(t; \vec{\theta})$, where $\vec{\theta}$ -- angular coordinates of the PVS arrival direction. In the simplest case we will consider the PVS with a single-dimensional angular density $\vec{\theta} = \theta$. In this case, like the pseudorandom coding of signal $s(t; \vec{\theta})$ with respect to time, it is possible, by taking into account several limitations, to implement pseudorandom coding $s(t; \vec{\theta})$ and along space coordinate θ, where $\theta = \sin \vartheta$, ϑ -- angular coordinate. Such PVS $s(t; \theta)$, which has a noise-like structure along time, as well as space coordinates, we will call a noise-like space-time signal.

Like time noise-like signals, the ShPVS may be classified into signals with analog and discrete modulations, which may be formed as a result of their space-time modulation at intervals $|t| \ll T$ and $|\theta| \leq \theta_M$. In case analog modulation methods are used, the following expression can be written for the ShPVS:

$$s(t; \Theta) = \dot{S}(t; \Theta) \exp\{j(\omega_0 t + \varphi_0)\},$$

where $\dot{S}(t; \dot{\theta})$ -- complex envelope of signal

$$\dot{S}(t; \Theta) = |\dot{S}(t; \Theta)| \exp\{j\varphi(t; \Theta)\},$$

determined by the kind of modulation used, while φ_0 -- initial phase.

Any methods of time and space discrete coding can be used in principle for signals with discrete modulation. As an example, we will describe a discrete-coded signal using symmetrical cyclical coding which leads to some simplification of calculations, as well as simplifications of arrangements for practical implementation of systems with the ShPVS. In this case, modulation with respect to time t and space θ is done according to one and the same pseudorandom law, for example, according to the law of some pseudorandom sequence (PSP) which, in the case of using a linear antenna array, leads to the following expression for a discrete-coded signal:

$$s(t;\Theta)=\sum_{i=-\infty}^{\infty}\sum_{j=-\infty}^{\infty}\sum_{k=-m}^{m}\sum_{l=-n}^{n}S_l\exp\{j[(\omega_0+\omega_l)t+\varphi_l]\}\times$$
$$\times d_l\Pi\left[\frac{t-(l+k)\Delta t-i2T}{\Delta t}\right]f_k(\Theta)\,\Pi\left[\frac{\Theta-k\Delta\Theta-j2\Theta_M}{\Delta\Theta}\right], \qquad (1)$$

where N -- number of PSP elements, while $\Delta\Theta$ and Δt -- respectively values of the space and time elements of the PSP; S_l, ω_l, φ_l -- respectively values of the amplitude, frequency and phase in the l-th position; $d_l = +1, -1$, $f_k(\theta)$ -- determines the form of space PSP, $\Pi(X)$ -- cutting function determined in the following manner:

$$\Pi(x)=\begin{cases}1, & |x|<\frac{1}{2},\\ 0, & |x|>\frac{1}{2},\end{cases}$$

$$2m+1=\frac{2\Theta_M}{\Delta\Theta}=2n+1=\frac{2T}{\Delta t}=N, \qquad (2)$$

$$\Delta t=\Delta\Theta\frac{T}{\Theta_M}. \qquad (3)$$

In this case, the discrete-coded signals may be classified into amplitude-manipulated, phase-manipulated and frequency-manipulated, as well as signals with combined manipulation. The structure of phase-manipulated ShPVS when using for the space-time coding a seven-element Barker code (+++--+-) is shown in Fig. 1.

Forming a noise-like PVS structure with time coordinates is not difficult [1]. At the same time, in space coding, for example, it is difficult to form the required rectangular shape of the space element of the pseudo-random code $f_k(\theta)$, which leads to a peculiar space structure of the signal that differs from that ideal ShPVS structure shown in Fig. 1. These difficulties are caused basically by the limitation of the space frequency spectrum, due to the limited dimensions of the actual aperture of antenna systems.

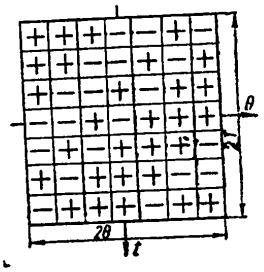

Fig. 1.

We will now consider the special features of noise-like space-time coding in which we will assume a given value $2\chi_м = 2X_м/\lambda$, of the space frequency spectrum, where $2X_m$ -- maximum linear aperture of the antenna system, while λ --working wavelength.

To form the ShPVS, we will utilize the well-known methods of forming complicated antenna radiation patterns (DN) for which the product of the width of space frequency spectrum $2\chi_м$ by the "duration" of space interval $2\theta_м$ scanned is considerably greater than unity [2, 3]. The formation of such DN, used basically in processing PVS, is based on the space-time modulation of the amplitude-phase distribution in the aperature of the antenna array. In this case, the formed PVS $s(t; \theta)$ may be represented thus:

$$s(t; \Theta) = s(t) F(\Theta; t), \qquad (4)$$

where $F(\theta; t)$ -- DN, determined by the amplitude-phase distribution $I(\chi; t)$ in the well-known way

$$F(\Theta; t) = \int_{-\chi_м}^{\chi_м} I(\chi; t) \exp\{-j2\pi\Theta\chi\}\, d\chi. \qquad (5)$$

As follows from (4), the space characteristics of the signal are fully determined by form of DN $F(\theta; t)$. Substituting DNin the form

$$F(\Theta;t) = |F(\Theta;t)| \exp\{i\varphi(\Theta;t)\} \qquad (6)$$

and formulating the condition for a uniform scan of the given space sector ($-\theta_м$; $\theta_м$) in the form

$$|F(\Theta;t)| = F_0 = \text{const}, \quad |\Theta| < \Theta_м, \qquad (7)$$

we, taking into account (5) - (7) and for a condition $2\Theta_м 2\chi_м \gg 1$, arrive at the following expression for DN:

$$F(\Theta;t) \simeq \sum_{k=-m}^{m} F_0 \exp\{j\varphi(k\Delta\Theta;t)\} \sin c\, 2\pi\chi_м(\Theta - k\Delta\Theta), \qquad (8)$$

where

$$\operatorname{sinc} x = \frac{\sin x}{x}; \quad \Delta\Theta = \frac{1}{2\chi_м} = \frac{\lambda}{2x_м}; \quad 2m+1 = 2\Theta_м 2\chi_м.$$

Determining $\varphi(k\Delta\Theta; t)$ as cyclic, 2T-periodic functions differing from each other only by a shift in the integral number of time intervals Δt, the number of which in interval 2T we select equal to the number of DN (8) discretization points in interval $2\theta_м$

$$\varphi(k\Delta\Theta;t) = \varphi_0\left(t - k\Delta\Theta\frac{T}{\Theta_м} - i2T\right), \qquad i = -\infty, \ldots, \infty,$$

we obtain from (8)

$$F(\Theta; t) = F_0 \sum_{i=-\infty}^{\infty} \exp\left\{j\varphi_0\left(t - \Theta\frac{T}{\Theta_M} - i2T\right)\right\} \simeq$$

$$\simeq F_0 \sum_{i=-\infty}^{\infty}\sum_{k=-m}^{m} \exp\left\{j\varphi_0\left(t - k\Delta\Theta\frac{T}{\Theta_M} - i2T\right)\right\} \operatorname{sinc} 2\pi\chi_M(\Theta - k\Delta\Theta). \quad (9)$$

The structural arrangement of the system that implements the algorithm for forming the ShPVS (4) may be represented in the form of a linear antenna array shown in Fig. 2, the radiation pattern forming the arrangement (DOS) of type

$$F(\Theta) = \sum_{k=-m}^{m} \operatorname{sinc} 2\pi\chi_M(\Theta - k\Delta\Theta),$$

Modulators (M) are installed at the input at each of its channels, controlled by signals of a modulating function oscillator (GMF) and performing in the general case frequency, as well as phase modulation of signals s(t) received through distribution device (RU) from the high frequency oscillator (GVCh).

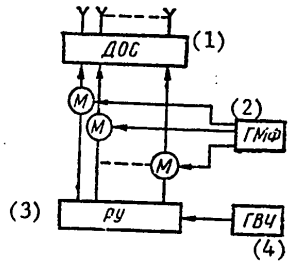

Fig. 2

1. DOS
2. GMF
3. RU
4. GVCh

When utilizing discrete-coded ShPVS, functions $\varphi(k\Delta\Theta;\ t)$ will be represented in the form of functions quantized by time and levels. Of great practical interest are functions $\varphi(k\Delta\Theta;\ t)$, that have only two quantizing levels, for example, 0 and π, the quantizing with respect to time of which is done according to a law for some PSP with 2n + 1 elements and a duration of $(2n+1)\tau_0 = 2T$. In this case

$$\exp\left\{i\varphi_0\left(t - k\Delta\Theta\frac{T}{\Theta_M} - i2T\right)\right\} = \sum_{i=-\infty}^{\infty}\sum_{l=-n}^{n} d_l\Pi\left[\frac{t-(l+k)\tau_0 - i2T}{\tau_0}\right],$$

and the formed phase-manipulated ShPVS has the form

$$s(t;\Theta) = \sum_{i=-\infty}^{\infty}\sum_{k=-m}^{m}\sum_{l=-n}^{n} S_0 e^{j\omega_0 t} d_l\Pi\left[\frac{t-(l+k)\tau_0 - i2T}{\tau_0}\right]\sin c2\pi\chi_M(\Theta - k\Delta\Theta). \tag{10}$$

The structure of signal (10) is very unusual. Thus, in any of fixed directions $\Theta_k = k\Delta\Theta$, coinciding with the DN discretization point, there is formed a signal

$$s(t;\Theta) = \sum_{i=-\infty}^{\infty}\sum_{l=-n}^{n} S_0 e^{j\omega_0 t} d_l\Pi\left[\frac{t-(l+k)\tau_0 - i2T}{\tau_0}\right],$$

differing from signals formed in other directions of discretization $\Theta_j = j\Delta\Theta$, only by a time shift of $\Delta t_{kj} = |k-j|\tau_0$.

In the directions that do not coincide with the directions of discretization of DN $\Theta_s \neq k\Delta\Theta$, a ShPVS is formed that represents an entire set of signals equal in structure (theoretically 2m + 1 signal), differing from each other in accordance with (10) only by a time shift, with an intensity and an initial phase (0 or π), which, when they are processed, makes it possible to limit oneself to a common filter matched with them.

However, in spite of such a complex structure of phase-manipulated ShPVS, formed in the scanning sector $(-\Theta_M;\ \Theta_M)$, the density of the signal power flow in any of directions $|\Theta| \leq \Theta_M$ in interval $|t| \leq T$ will be constant (7), (10).

Processing of the ShPVS. We will assume [4] that in intervals of time $[-T_{\text{прм}};\ T_{\text{прм}}]$ and space $[-\Theta_{\text{м прм}};\ \Theta_{\text{м прм}}]$ field $y(t, \chi)$ proceeds into the aperture of the receiving system $[-\chi_{\text{м прм}};\ \chi_{\text{м прм}}]$. This field has a distribution density along the angular coordinate

$$y(t; \Theta) = \sum_{i=1}^{n} s_i(t; \Theta)\,\delta(\Theta - \Theta_i) + n(t; \Theta),$$

representing a mixture of ShPVS (10) reflected by reradiated point objects or additive normal interferences with correlation function [5]

$$\langle n(t_1; \Theta_1)\, n^*(t_2; \Theta_2)\rangle = N_0\delta(t_1 - t_2)\,\delta(\Theta_1 - \Theta_2).$$

Below we will consider processing in those intervals of space and time where they are formed

$$(T_{\text{прм}} = T_{\text{прд}};\ \Theta_{\text{мпрм}} = \Theta_{\text{мпрд}}),$$

and will also assume that $\chi_{\text{мпрм}} = \chi_{\text{мпрд}}$.

By neglecting the delay of the signal envelope in the aperture and assuming that the angular signal spread $|\Theta_i - \Theta_j| \geqslant 1/2\chi_{\text{м}}$, we arrive at the following expression for the optimal effect of the processing system:

$$Y(\Theta) = \left| \int_{-T}^{T} \int_{-\Theta_{\text{м}}}^{\Theta_{\text{м}}} S_0 \exp\left\{-j\left[2\pi(f_0 t - \Theta\chi) - \varphi_0\left(t - \Theta\frac{T}{\Theta_{\text{м}}}\right) + \varphi_0\right]\right\} \times \right.$$

$$\left. \times\, y(t; \chi)\, dt d\chi = \left| \int_{-T}^{T} S_0 \exp\left\{-j\left[2\pi f_0 t - \varphi_0\left(t - \Theta\frac{T}{\Theta_{\text{м}}}\right) + \varphi_0\right]\right\} F_s(\Theta; t)\, dt \right| . \quad (11)$$

Function

$$F_s(\Theta; t) = \int_{-\chi_{\text{м}}}^{\chi_{\text{м}}} y(t; \chi) \exp\{j2\pi\Theta\chi\}\, d\chi = \int_{-\Theta_{\text{м}}}^{\Theta_{\text{м}}} y(t; \hat{\Theta})\, \text{sinc}\, 2\pi\chi_{\text{м}}(\Theta - \hat{\Theta})\, d\hat{\Theta}$$

which enters (11) in interval $|\theta| < \theta_м$ under condition $2\theta_м 2\chi_м \gg 1$ may be represented in the form of a series

$$F_s(\Theta; t) = \sum_{k=-m}^{m} F_s(k\Delta\Theta; t)\,\mathrm{sinc}\,2\pi\chi_{мпрм}(\Theta - k\Delta\Theta). \qquad (12)$$

Then, taking into account (12), we obtain for the optimum output effect

$$Y(\Theta) = \left| \sum_{k=-m}^{m} \mathrm{sinc}\,2\pi\chi_м(\Theta - k\Delta\Theta) \times \right.$$
$$\left. \times \int_{-T}^{T} S_0 \exp\left\{-j\left[2\pi f_0 t - \varphi_0\left(t - \Theta\frac{T}{\Theta_м}\right) + \varphi_0\right]\right\} F_s(k\Delta\Theta; t)\,dt \right|. \qquad (13)$$

The processing system, simulating algorithm (13), is shown in Fig. 3.

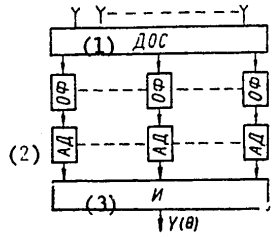

Fig. 3

1. DOS
2. AD
3. I

The radiation pattern arrangement (DOS) of the antenna array forms (2m + 1) partial DN. Oscillation from the k-th output of the DOS proceeds to the k-th channel of time processing, consisting of an optimal filter (OF) and amplitude detector (AD). Interpolator (I) implements the formation of $Y(\theta)$. Using cyclic coding in forming the ShPVS makes it possible to limit oneself in their processing to one optimal filter in each channel, because a set of signals equal in structure (10) proceeds to the input of the processing

system. In other coding methods, each channel of the antenna array must contain a full set of filters matched to each of the received signals.

We will consider separately the signal $Y_s(\theta)$ and interference $Y_n(\Theta)$ components of the output effect on the assumption that the single essential parameter of the signal received from direction θ_s

$$s(t;\Theta)=\sum_{i=-\infty}^{\infty}\sum_{k=-m}^{m}\sum_{l=-n}^{n}S_0\exp\{j(\omega_0 t+\varphi_s)\}\times$$
$$\times d_l\Pi\left[\frac{t-(l+k)\tau_0-i2T}{\tau_0}\right]\operatorname{sinc}2\pi\chi_{\text{мпрд}}(\Theta-k\Delta\Theta)\,\delta(\Theta-\Theta_s) \quad (14)$$

is the direction of its arrival. Then for $Y_s(\Theta)$ we obtain

$$Y_s(\Theta)=\Bigg|\sum_{q=-m}^{m}\operatorname{sinc}2\pi\chi_{\text{мпрм}}(\Theta-q\Delta\Theta)\int_{-T}^{T}S_0\exp\{-j(\omega_0 t+\varphi_0)\}\times$$
$$\times\sum_{l=-n}^{n}d_l\Pi\left[\frac{t-l\tau_0}{\tau_0}\right]dt\int_{-\Theta_M}^{\Theta_M}s(t;\hat{\Theta})\operatorname{sinc}2\pi\chi_{\text{мпрм}}(\hat{\Theta}-q\Delta\Theta)\,d\hat{\Theta}\Bigg|=$$
$$=\sum_{i=-\infty}^{\infty}\sum_{j=-n}^{n}\sum_{k=-m}^{m}\sum_{q=-m}^{m}\sum_{l=-n}^{n}S_0^2 2T e^{j(\varphi_s-\varphi_0)}d_l d_j\Pi\left[\frac{t-l\tau_0}{\tau_0}\right]\times$$
$$\times\Pi\left[\frac{t-(j+k)\tau_0-i2T}{\tau_0}\right]\operatorname{sinc}2\pi\chi_{\text{мпрм}}(\Theta-q\Delta\Theta)\times$$
$$\times\operatorname{sinc}2\pi\chi_{\text{мпрм}}(\Theta_s-q\Delta\Theta)\operatorname{sinc}2\pi\chi_{\text{мпрд}}(\Theta_s-k\Delta\Theta)\Bigg|. \quad (15)$$

Transforming (15), we finally obtain

$$Y_s(\Theta)=\Bigg|S_0^2 2T e^{j(\varphi_s-\varphi_0)}\sum_{k=-m}^{m}\Psi(t-k\tau_0)\times$$
$$\times\operatorname{sin}c2\pi\chi_{\text{мпрм}}(\Theta_s-\Theta)\operatorname{sinc}2\pi\chi_{\text{мпрд}}(\Theta_s-k\Delta\Theta)\Bigg|. \quad (16)$$

In (16) $\Psi(\tau)$ is the autocorrelation function PSP, according to the law of which the DN phase characteristic is coded.

The interference component $Y_n(\Theta)$ of the output effect is determined in a similar manner

$$Y_n(\Theta) = \left| \sum_{q=-m}^{m} \operatorname{sinc} 2\pi\chi_{\text{инпм}}(\Theta - q\Delta\Theta) \int_{-T}^{T} S_0 \exp\{-j(\omega_0 t + \varphi_0)\} \times \right.$$
$$\left. \times \sum_{l=-n}^{n} \left[d_l \Pi \frac{t - l\tau_0}{\tau_0} \right] dt \int_{-\Theta_M}^{\Theta_M} n(t; \hat{\Theta}) \operatorname{sinc} 2\pi\chi_{\text{инпм}}(\hat{\Theta} - q\Delta\Theta)\, d\hat{\Theta} \right| . \quad (17)$$

(17) represents a normal random process with a zero mathematical expectancy and a correlation function

$$\langle Y_n(\Theta_1) Y_n^*(\Theta_2) \rangle = \left| \sum_{k=-m}^{m} \sum_{q=-m}^{m} \sum_{l=-n}^{n} \sum_{j=-n}^{n} \operatorname{sinc} 2\pi\chi_M(\Theta_1 - k\Delta\Theta) \times \right.$$
$$\times \operatorname{sinc} 2\pi\chi_M(\Theta_2 - q\Delta\Theta) \int_{-T}^{T}\int S_0^2 \exp\{j\omega_0(t_1 - t_2)\}\, d_l d_j \Pi\left[\frac{t_1 - l\tau_0}{\tau_0}\right] \Pi\left[\frac{t_2 - j\tau_0}{\tau_0}\right] \times$$
$$\times dt_1 dt_2 \int_{-\Theta_M}^{\Theta_M}\int \langle n(t_1; \Theta_1)\, n^*(t_2; \Theta_2) \rangle \operatorname{sinc} 2\pi\chi_M(\Theta_1 - k\Delta\Theta) \operatorname{sinc} 2\pi\chi_M(\Theta_2 -$$
$$\left. - q\Delta\Theta)\, d\Theta_1 d\Theta_2 \right| \simeq \left| S_0^2 2T \frac{N_0}{2\chi_M} \operatorname{sinc} 2\pi\chi_M(\Theta_1 - \Theta_2)\, \Psi(t_1 - t_2) \right| . \quad (18)$$

With the assumption made above on neglecting the signal delay in the aperture, and the fixed direction of the signal arrival, the optimal space-time processing, as in case [5], separates into two independent processings: spatial, with algorithm of form

$$Y_s(\Theta; t) = \sum_{k=-m}^{m} \operatorname{sinc} 2\pi\chi_M(\Theta - k\Delta\Theta) \int_{-\chi_M}^{\chi_M} y(t; \chi) \exp\{j2\pi\Theta\chi\}\, d\chi,$$

and time --

$$Y_s(t) = \left| \int_{-T}^{T} S_0 \exp\{-j(2\pi f_0 t + \varphi_0)\} \sum_{l=-n}^{n} d_l \Pi\left[\frac{t - l\tau_0 - i2T}{\tau_0}\right] Y_s(\Theta; t)\, dt \right| .$$

The presence in the aperture of the receiving antenna of an entire set of signals arriving from one direction (14), leads to the fact that the echo of the system also contains a set of signals (16), formed by the basic and side lobes of the output effect. Fig. 4a shows the approximate shape of an envelope of the output effect when the signal arrives from direction $\theta_s=(k+\frac{1}{2})\Delta\theta$. (f) and in Fig. 4b -- from direction $\theta_s=k\Delta\theta$. The general shape of the signal component of the output effect for case $\theta_s=k\Delta\theta$ is shown in Fig. 4c.

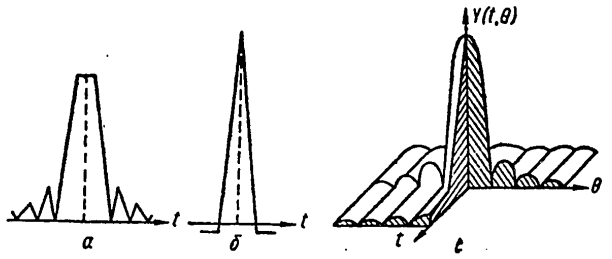

Fig. 4

As follows from (14), (16), as well as from Fig. 4, the processing system compresses signals $2\theta_м 2\chi_м$ times and provides a signal to noise ratio at its output (16), (18), equal to $S_0^2 2T 2\chi_м/N_0$.

The occurrence of several signals in the scanning zone leads to the formation of echoes at the processing system output (Fig. 3), the time position of which t_s, for matched coding along time and space coordinates, is uniquely related to the direction of signal arrival $t_s=\theta_s T/\theta_м$. When other data parameters are present in the received signal $s(t;\theta)$, the information for each one of them can be also separated in the course of processing the signal.

BIBLIOGRAPHY

1. Kuk, Ch.; Berifel'd, M. "Radar Signals. Theory and Application." Translated from English, V. S. Kel'zon editor. Moscow, SOVETSKOYE RADIO, 1971.

2. Drabovich; Orbi; Bonnas'ye. "Compressing the Radiation Pattern of an Antenna Array by the Space-Time Coding Method." "Zarubezhnaya radioelektronika, 1971, No 3.

3. Pogorelov, A. I. "Using Complex Radiation Patterns in Direction Finding Systems for Signal Resolution in a Wide Scanning Sector." In book: "Radiotekhnika," Khar'kov, "Vishcha shkola," 1976, issue 37.

4. Pogorelov, A. I.; Vititlov, L. L. "Certain Problems in Space-Time Signal Resolution." In book: "Radiotekhnika," "Vishcha shkola," 1977, issue 41.

5. Fal'kovich, S. Ye. "Evaluating Signal Parameters." SOVETSKOYE RADIO, 1970.

[269-2291]

2291
CSO: 1860

UDC 621.396.96

DOPPLER FILTERING IN SHORT-WAVE DIRECTION FINDING

Moscow RADIOTEKHNIKA I ELEKTRONIKA in Russian No 7 1979 pp 1444-1447

[Article by E. L. Afraymovich: "Doppler Filtering in Short-Wave Direction Finding"]

[Text] A method is described for measuring the arrival angles of a multimode shortwave radio signal by Doppler (frequency) separation of the modes. The results of experimental testing of the method accomplished by means of measurement of the arrival angles (in horizontal and vertical planes) on sloped distribution paths 3000 and 1200 km in length are given.

Measurement of the arrival angles of a multimode radio signal using classical radio direction finding equipment (amplitude and phase direction finders) is characterized by large interference errors and fluctuation of the direction finder indications (1). The method of time (pulse) separation of modes used in practice (see, for example, (2)) has, for a wide variety of reasons, a limited area of application. The problem of separating the modes of a continuous (narrow-band) radio signal at a fixed operating frequency is of considerable interest. One of the possibilities is based on the difference in the Doppler shift of modes distributed in the ionosphere on various paths. Experimental studies performed for various paths of the ionospheric distribution of radio waves has shwon that for a quiescent ionosphere this difference is located in the range 0.1-1.0 Hz (3,4). From this it follows that the modes of a signal may be separated according to the Doppler frequency shift if the relative instability of the transmitter signal frequency is no less than 10^{-8}-10^{-9} (which corresponds to the current standard for shortwave radiation) and the minimum duration of existence of the signal is no less than 10 seconds.

The phase direction finding with Doppler filtering method (FPDF) was formulated by the author in 1973 (5). The method was developed in a series of studies (6-8) and used for experimental research on Doppler and angular fluctuations with vertical sounding of the F_2 region of the ionosphere (8) as well as for measuring the arrival angles of a continuous multimode

signal in vertical and horizontal planes on paths 3000 and 1200 km in length (9). In 1976 patents were taken out in the USA (4) and the Federal Republic of Germany in which different variations were proposed for direction finders with Doppler filtering.

According to (5-8) the algorithm for FPDF in the simplest case may be described as follows:

1. A complex Fourier transform for a complex amplitude R(t) of the field of a radio wave recorded as the minimum at three points of the Earth's surface with Descartes coordinates (1,0), (0,d_x) and (0,d_y):

$$S(\omega)e^{i\Phi(\omega)} = \frac{1}{T}\int_0^T R(t)e^{-j\omega t}\,dt; \quad \omega = 2\pi F,$$

where $S(\omega)$ and $\Phi(\omega)$ are the amplitude and phase spectra; F is the Doppler frequency; i is the time and T is the interval of integration.

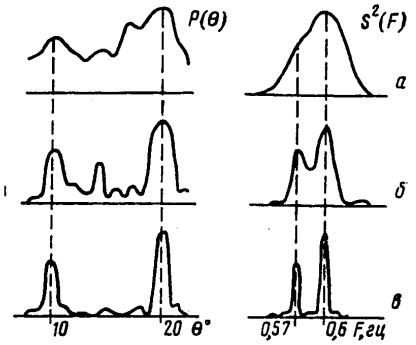

Figure 1. Doppler Spectra $S^2(F)$ and Elevation Distributions $P(\theta)$ obtained for a Test Signal by the FPDF Method with Various Integration Times: а--22 sec; б --41 sec; в -- 82 sec.

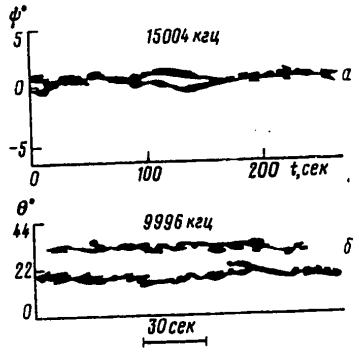

Figure 2. Patterns of Azimuthal P(Ψ) and Elevation P(θ) Distributions on Paths 3000 km (a) and 1200 km (б) in Length.

2. Calculation of the power spectrum $S^2(\omega)$ and the spectra of azimuthal angles $\Psi(\omega)$ and angles of location $\theta(\omega)$:

$$\operatorname{tg}\Psi(\omega)=\frac{\Delta\Phi_y(\omega)}{\Delta\Phi_x(\omega)}\frac{d_x}{d_y},$$

$$\cos\theta(\omega)=\frac{\lambda}{2\pi}\sqrt{\frac{\Delta\Phi_x^2(\omega)}{d_x^2}+\frac{\Delta\Phi_y^2(\omega)}{d_y^2}},$$

where $\Delta\phi_x$ and $\Delta\phi_y$ are the difference in phases between the center point and the peripheral points.

3. Construction of a weighted distribution of power of the spectral components $S^2(F)$ according to the arrival angles $P(\Psi)$ and $P(\theta)$.

The described procedure represents the simplest version for accomplishing the method and may be improved, especially by using an excess number (more than three) of antennas and also by smoothing and averaging operations in terms of known algorithms and estimates. In this case it is possible to optimize the characteristics of equivalent Doppler filters (the form of the frequency characteristics, the level of the side lobes) and the circuit for producing the weighted distribution P in accordance with the available means for actual implementation of the radiowave field.

Figure 1 illustrates the effect of increasing the accuracy of determination of the arrival angles by Doppler distribution of the modes (model calculations). On the right side of the illustration are the Doppler spectra S^2 (F) and on the left is the distribution $P(\theta)$. Given are two stationary sources of radiation with different amplitudes (4 and 6 of comparative units) with different Doppler frequency shifts (F = 0.57 Hz and F = 0.6 Hz) and different angular coordinates 10° and 20°. From figure 1 it

it is apparent that with an increase in the integration time (T = 22,41,82 sec) interference of components is eliminated and the accuracy in determination of θ is increased. Thus, the integration interval T is the most important parameter for analysis and, in the process of adaptive processing, it should generally be adjusted for actual field implementation.

It is natural that only an experiment may give an answer to the question of the extent to which the described procedure for processing the signal is adequate for an actual situation on paths of various lengths. In any case, however, the FPDF has a number of advantages among which the main one is multichannel narrow-band analysis with an equivalent band of an individual Doppler filter of 0.1-0.01 Hz (which is a factor of 3-4 less than the corresponding parameter for direction finders of the classical type (1,2). This ensures FPDF of excellent discrimination and increased noise-immunity.

Measurement of on a path 3000 km in length were performed in 1975 for the continuous signal of a correct-time station RKM (RID) (9). For reception were used VD type antennas 9.5 m in height placed in a straight line at an interval of 25 m perpendicular to the direction at the transmitter. Calibration of the system according to the procedure stated in (7) showed that the equipment accuracy of determination of Ψ was 0.25°. In figure 2a are presented typical dynamic azimuthal spectra P( ) obtained at an interval of integration T = 40 sec with shift at a time of 5 sec. Figure 2a illustrates the capability of FPDF to separate the components of a multimode signal; to obtain spectra of a similar type (with an angle of resolution on the order of 1°) using a phased antenna for the array, the latter should have an aperture of 2000 m.

Measurements of Ψ and θ on a path 1200 km in length were performed in 1977 for the continuous signal of a PVM station (9). Also used for reception were VD antennas placed in an azimuthal line with a base of 20 m and an elevation with bases of 10 m and 40 m. The presence of the two elevation bases made it possible to rule out multivalence in determining θ with retention of sufficient accuracy for the given experiment. In figure 2δ an example is given of elevation distribution $P(\theta)$ obtained with an integration time of 30 sec with a 5 sec shift. The values of the angles of location $\sim$30° and $\sim$16° apparently correspond to a one-hop version of distribution with a reflection from F_2 and E regions of the ionosphere (11). With a continuous signal, obtaining an elevation distribution of this type requires a phased antenna array with a height of $\sim$200-300 m.

Fhe first trial implementation of a phase direction finder with Doppler filtering showed that similar systems may be completely competitive with large multiantenna systems in doing special research and solving applied problems, especially under field conditions. For effective use of the method, modern high-speed-response processors must be included in the system along with data display devices to make it possible to process the signal in real time.

The phase direction finder with Doppler filtering may also be used for analyzing a modulated signal. In study (13) an analog-digital FPDF is described which makes it possible to process amplitude-modulated signals and results are given of measurement of the azimuthal arrival angles of a multimode signal on a path 2300 km in length.

BIBLIOGRAPHY

1. Kukes, I. S.; and Starik, M. E. "Osnovy radiopelengatsii" [Fundamentals of Radio Direction Finding], Izd. Sovetskoye radio, 1964.

2. Khmel'nitskiy, E. A. "Otsenka real'noy pomekhozashchishchennosti priyema signalov v KV-diapazone" [Analysis of the Actual Noise-Immunity of Signal Reception in the Shortwave Range], Izd. Svyaz', 1975.

3. Shepherd, R. A.: and Lomax, J. B. IEEE TRANS. COMMUN. TECHNOLOGY, COM-15, 2, 1967.

4. Bennett, S. M. USA Patent No 3.991.418, 9 IX, 1976.

5. Afraymovich, E. L. "Collection of Actual Questions of Distribution of Decimeter Radiowaves", section 3, IZMIRAN SSSR, 1973.

6. Afraymovich, E. L.; Bugmeyster, B. O.; and Korolev, V. A. "Collection of Studies on Geomagnetism, Aeronomy and Physics of the Sun", issue 32, Izd. Nauka, 1974.

7. Afraymovich, E. L and others. "Collection of Studies on Geomagnetism, Aeronomy and Physics of the Sun", issue 33, Izd. Nauka, 1975.

8. Afraymovich, E. L. and others. "Collection of Studies on Geomagnetism, Aeronomy and Physics of the Sun", issue 41, Izd. Nauka, 1977.

9. Afraymovich, E. L and others. GEOMAGNETIZM I AERONOMIYA, 18, 1978.

10. Helmut, H. et al. FRG Patent No 2 242 790, 21X, 1976.

11. Barabashov, B. G.; and Kalyadin, B. G. GEOMAGNETIZM I AERONOMIYA, 16, 1976.

12. Tvetin; and Khansaker. TIIER, 57, 4, 1969.

13. Afraymovich, E. L; and Panchenko, V. A. "Doppler Filtering in Shortwave Direction Finding. Analog-Digital Processing of a Modulated Signal", Preprint No 13 (217), IZMIRAN SSSR, 1978.

[272-8945]

8945
CSO: 1860

UDC 621.396.96:519.246

STATISTICAL CHARACTERISTICS OF ANGULAR COORDINATES OF A RADAR TARGET CENTER ABOVE THE DIFFUSING REFLECTING SURFACE

Moscow RADIOTEKHNIKA I ELEKTRONIKA in Russian No 6, 1979 signed to press 3 May 78 pp 1094-1102.

[Article by V. B. Razskazovskiy]

[Text] Abstract

A relationship was established between parameters of the distribution law of the angular coordinates of the instantaneous radar target center and the statistical characteristics of the object and the route under conditions of multibeam propagation. Evaluations were obtained of the mathematical expectancies and the scattering of angular coordinates for a route geometry for near radar and intensity of diffuse scattering. The strong dependence of these values was emphasized, characterizing the systematic and random error in coordinate measurements, on the relative level of the determined field components in reradiating the target.

Introduction

At present, systems of near radar (SBRL) are widely developed. A far from exhaustive list of such systems is cited in paper [1]. When such systems operate near the surface of the interface, errors originate in measuring the angular coordinates due to the effect of multibeam propagation, similar in nature to those considered in [2]. However, the conclusions of this paper are applicable only to installations using highly directional antenna systems, while antennas with wide radiation patterns are characteristic for the SBRL. The latter circumstance, as will be shown later, leads not only to quantitative, but also to qualitative differences in results.

In analyzing the statistical characteristics of angular coordinates, we will use the following premises:

1) the target is represented by a totality of a great number of reradiators with statistically independent varying signal amplitudes and phases, and one determined reradiator that has constant nonrandom scattering characteristics;

2) the interface surface is statistically uneven, flat on the average, with high irregularties compared to the wavelength, while reradiation in the entire considered region of angles of slide is fully diffused;

3) the radiation pattern of the goniometric antenna system is wider than the angular dimensions of the region, which includes the target and the reradiating zone of the interface surface.

The basis for the assumption of a diffuse nature of reradiation by the interface surface is the use in the SBRL radio waves of the centimeter and millimeter ranges because of which at the angle of slide of several degrees and more, the mirror reflection from actual dryland and sea routes is found to be practically fully destroyed.

1. Statistical Description of Angular Coordinates

The assumptions that angular coordinates of the instantaneous radar target center (MRTs) correspond to the direction of the normal to the phase front of the field at the reception point are statistically described in paper [3]. According to the latter, the distribution laws of the azimuth and elevation coordinates are, in the general case, the same and are described by expression*

$$(1)\qquad W(v)=W_0(v)\,e^{-(P_0/2)(1+\zeta)}\times \times\left\{(1+P_0\beta)I_0\left[\frac{P_0}{2}(1-\zeta)\right]+P_0\beta I_1\left[\frac{P_0}{2}(1-\zeta)\right]\right\},$$

$$(1a)\qquad W_0(v)=\frac{1}{2}[1+(q-v)^2]^{-3/2},$$

$$(1б)\qquad q=v^*-v_0,\quad \zeta=\frac{v^2}{1+(q-v)^2},\quad \beta=\frac{(1+q^2-qv)^2}{1+(q-v)^2},$$

where $I_0(x)$, $I_1(x)$ -- are Bessel functions of an imaginary argument.

* Designations of values in (1) were changed compared to those used in [3].

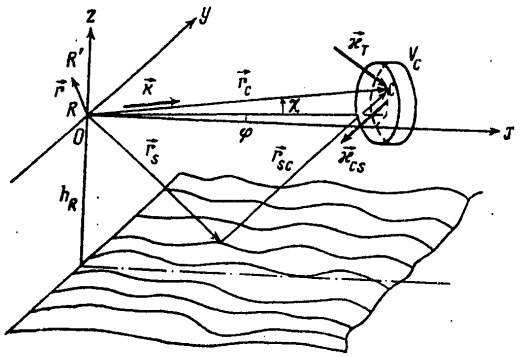

Fig. 1

Variable ν is a nondimensional angular coordinate of MRTs in the corresponding coordinate plane related to the azimuth φ and angle of place χ (see Fig. 1) by relationships

$$\nu_\varphi = \frac{\varphi}{\mu_\varphi}, \quad \nu_\chi = \frac{\chi}{\mu_\chi}, \tag{2}$$

$$\nu_{\varphi_0} = \frac{\varphi_0}{\mu_\varphi}, \quad \nu_{\chi_0} = \frac{\chi_0}{\mu_\chi},$$

where parameters $\mu_{\varphi,\chi}$ in their turn are expressed by the distribution of average flows of power along the arrival angles at the observation point (or the angular distribution of radio brightness) $S(\varphi, \chi)$:

$$\mu_\varphi^2 = \frac{1}{\sigma_\Sigma}\iint_\Omega (\varphi-\varphi^*)^2 S(\varphi,\chi)\,d\varphi\,d\chi, \tag{3}$$

$$\sigma_\Sigma = \iint_\Omega S(\varphi,\chi)\,d\varphi\,d\chi, \tag{4}$$

$$\varphi^* = \frac{1}{\sigma_\Sigma}\iint_\Omega \varphi S(\varphi,\chi)\,d\varphi\,d\chi, \tag{5}$$

$$\nu^* = \frac{\varphi^*}{\mu_\varphi}. \tag{6}$$

Similar relationships for angle χ are obtained by simple substitution $\varphi \to \chi$ in (3) - (6).

Obviously, parameters φ^*, χ^* and $\mu_{\varphi,\chi}$ have correspondingly, the meanings of the radio brightness center coordinates and of the effective angular dimension of the region of radiation coming to the observation point.

Parameter P_0 expresses the ratio at the observation point of the power flow density which is determined by the field component and the average of the total density of the random field flow, equal to (4), while angles φ_0 and χ_0 characterize the direction of the arrival of the determined wave.

We will note that the distribution of average power flows along the arrival angles are called by some writers, for example, [4], the angular density of the energy spectrum or the angular energy spectrum, because it is related to the Fourier transformation with a field correlation function along the spatial coordinates. In what follows, for the sake of briefness, we will use the latter name (abbreviated -- UES).

As noted in [5], dispersion does not exist for distribution laws of form (1) random values with the exception of case $P_0 \gg 1$, therefore, as a numerical characteristic of MRTs coordinate scattering with respect to the average position of $\langle\chi\rangle$ or $\langle\varphi\rangle$, we will use values

$$(7)\qquad \langle|\tilde{\Phi},\tilde{\chi}|\rangle=\mu_{\varphi,\chi}\int_{-\infty}^{\infty}|\nu_{\varphi,\chi}-\langle\nu_{\varphi,\chi}\rangle|W(\nu_{\varphi,\chi})\,d\nu_{\varphi,\chi},$$

$$\tilde{\Phi}=\varphi-\langle\varphi\rangle,\ \tilde{\chi}=\chi-\langle\chi\rangle.$$

2. Angular Field Energy Spectrum and Distribution Parameters

We will now determine UES taking into account the special features characteristic of near radar problems. As is well known, the field above the interface surface within direct sight limits is the sum of two components. The first component corresponds to the wave propagation reradiated by each element of the multiplexity that forms the target in free space; the second component is formed as a result of their scattering by the interface surface. Considering the case of a scalar field, it is possible to represent the latter in the vicinity of the observation point located at the start of the coordinates (Fig. 1) in the following form:

the field created directly by the target

$$(8a)\qquad U_{Rc}=\int_{V_c}\frac{a_c(\vec{r}_c,\vec{\varkappa}_T)\,U_T(\vec{r}_c)}{2\sqrt{\pi r_c}}\,e^{i[kr_c+\vec{k}(\vec{r}_c)\vec{r}]},$$

the field reradiated by the interface surface

$$(8б)\qquad U_{Rs}=\int_{S}\frac{a_s(\vec{r}_s,\vec{\varkappa}_{cs})\,U_c(\vec{r}_s)}{2\sqrt{\pi r_s}}\,e^{i[kr_s+\vec{k}(\vec{r}_s)\vec{r}]},$$

where $\vec{k}(\vec{r}_{c,s}) = -k(\vec{r}_{c,s}/r_{c,s})$ -- wave vectors of elementary waves; $U_T(\vec{r}_c)$ -- field irradiating the target, containing the random, as well as the determined components; $U_c(\vec{r}_s)$ -- field created on the interface surface by the target; $a_c(\vec{r}_c, \vec{\varkappa}_T)$, $a_s(\vec{r}_s, \vec{\varkappa}_{cs})$ -- complex scattering coefficients of target volume elements and of the target surface depending upon the directions of radiation and reradiation.

Integration in the first component is made over the area of the space containing the reradiating elements of the target and in the second component -- over the entire surface of the interface. We will note that the determined component is contained only in (8a) and it is equal to

$$U_{R\,\text{дет}}=\frac{1}{2\sqrt{\pi}\,r_{c0}}U_{\text{т дет}}(\vec{r}_{c0})\,a_{c0}(\vec{\varkappa}_{c0},\vec{\varkappa}_{\text{т}}), \qquad \text{ТД, eT = Tdet} \tag{8c}$$

where $U_{Tdet}(\vec{r}_c)$ -- determined component of the field $U_T(\vec{r}_c)$ radiating the target. Assuming that adjacent reradiators of the target and the interface surface are not correlated, i.e.,

$$\langle a_{c,\,s}(\vec{r}_1)\,\bar{a}_{c,\,s}(\vec{r}_2)\rangle=0 \quad \text{for} \quad \vec{r}_1\neq\vec{r}_2,$$

we will obtain, averaging over the set of numbers, the following expression for the correlation function of the field component at the reception point:

$$\langle U_R\bar{U}_R(\vec{\rho})\rangle=\langle U_{Rc}\bar{U}_{Rc}(\vec{\rho})\rangle+$$
$$+\langle U_{Rc}\bar{U}_{Rs}(\vec{\rho})\rangle-U_{R\,\text{дет}}\bar{U}_{R\,\text{дет}}.$$

Then changing over to polar coordinates and making the Fourier-transformations, we will determine the energy spectrum:

$$S(\varphi,\chi)=S_c(\varphi,\chi)+S_s(\varphi,\chi), \tag{9}$$

$$S_c(\varphi,\chi)=\frac{\cos\chi}{\pi}\Big[\int_{r_1}^{r_2}\sigma'(\vec{r}_c,\vec{\varkappa}_{\text{т}})\times \tag{9a}$$
$$\times S_{\text{т}}(\vec{r}_c)\,dr+\sigma_0(\vec{\varkappa}_{c0},\vec{\varkappa}_{\text{т}})\bar{S}_{\text{т}}(\vec{r}_{c0})\,\delta(\varkappa-\vec{\varkappa}_0)\Big],$$

$$S_s(\varphi,\chi)=\frac{1}{\pi}\rho_s^2(\vec{r}_s)\,S_s(\vec{r}_s,\vec{r}_{sc})\times \tag{9б}$$
$$\times\operatorname{ctg}\chi\sqrt{1+\operatorname{tg}^2\chi(\cos\varphi-\sin\varphi)^2},$$

where $\sigma_0 = 1/2\ a_{co}\bar{a}_{co}$ -- effective scattering surface (EPR) of the determined reradiator; $\sigma' = 1/2 \langle a_c \bar{a}_c \rangle$ -- unit volume of the EPR of the target; $\rho_s^2(\vec{r}_s) = 1/2 \langle a_s \bar{a}_s \rangle$ -- unit coefficient of diffuse scattering by the interface surface; $S_T(\vec{r}_c) = 1/2 \langle U_T \bar{U}_T \rangle_{\vec{r}}$ -- average density of the total flow of radiation to the target; $S_T(\vec{r}_{co})$ -- average density of the random component of target radiation; $S_c(\vec{r}_s, \vec{r}_{sc})$ -- average density of the total flow of radiation of the interface surface from the target.

For the case most frequently encountered in practice of target dimensions being small compared to the distance to the scattering region of the surface

$$S_c(\vec{r}_s, \vec{r}_{sc}) \simeq \frac{1}{4\pi r_{sc}^2}\left[\int_{V_c} S_T(\vec{r}_c)\sigma'(\vec{r}_c, \vec{\varkappa}_T, \vec{\varkappa}_{cs})\,dV + S_T(\vec{r}_{c0})\sigma_0(\vec{\varkappa}_T, \vec{\varkappa}_{cs})\right]. \tag{10}$$

It may be seen from (9) and (10) that in the general case the angular energy spectrum at the reception point and, therefore, the parameters of the angular coordinates distribution law (1) related to it depend on the spatial structure of the radiating field (function $S_T(\vec{r}_c)$, as well as the averaged indicatrix of the target reradiation.

We will now evaluate parameters (3) - (7) at situations characteristic for the SBRL. Since the vertical dimension of the target, as a rule, is considerably smaller than its height above the surface, on the basis of papers [6, 7], the radiation field of the target at diffuse scattering on the transmitter-target route may be considered uniform and it may be assumed that $S_T = \text{const}$. Then parameter P_0, which is the ratio of the determined field component power to the average flow of the random power component, will be

$$P_0 = \frac{U_{R\,\text{пот}}\bar{U}_{R\,\text{пот}}}{\iint_{\Omega} S(\varphi, \chi)\,d\varphi\,d\chi} = \frac{P_{0c}}{1 + (1 + P_{0c})(R_{dT} + R_d + R_{dT}R_d)}, \tag{11}$$

$$P_{0c} = \frac{\sigma_0}{\int_{V_c} \sigma'(\vec{r}_c)\,dV}. \tag{12}$$

here

$$R_d = \iint_{\Omega} \frac{\rho_s^2(\vec{r}_s)\,\mathrm{ctg}\,\chi\sqrt{1-\mathrm{tg}^2\chi(\cos\varphi-\sin\varphi)^2}\,d\varphi d\chi}{4\pi r_{sc}^2} \tag{13}$$

is, according to the terminology of papers [2, 6] the diffuse scattering coefficient, although it is more correct to call it the energy coefficient of diffuse scattering.

Parameter R_{dT}, determined as

$$R_{d\tau} = \frac{\bar{S}_\tau(\vec{r}_c)}{S_\tau(\vec{r}_c) - \bar{S}_\tau(\vec{r}_c)},$$

is obviously a similar characteristic for the transmission-target route.

Thus, the value of P_o at the reception point differs from the similar characteristic of the target (12) when there is not interface surface. In particular, for a characteristic, according to [6], for a wide region of angles of slide $R_d = R_{dT} \simeq 0.2$, even for a fully determined reradiation of the target (i.e., $P_{oc} = \infty$) the value $P_o \simeq 2.3$, i.e., the determined component of the power is only slightly higher than the random component. For $R_{dT} = o$ and $P_{oc} = \infty$, which, in particular, corresponds to measuring the coordinates of the radiation source, we obtain $P_o = R_d^{-1}$ and for the previous $R_d = 0.2$ now $P_o = 5$, i.e., it is more than double the value in the radar case.

Substituting (9) and (10) into (5), we will determine the elevation coordinate of the radio brightness center of the reradiating region:

$$\chi^* = \frac{\chi_c^*(1+R_{d\tau})+\chi_o P_{oc} R_{d\tau}+\chi_s^* R_d(1+R_{d\tau})(1+P_{oc})}{1+(1+P_{oc})(R_d+R_{d\tau}+R_d R_{d\tau})} \tag{14}$$

$$\chi_{s.s}^* = \frac{\iint_{\Omega} \chi S_{c.s}(\varphi,\chi)\,d\varphi d\chi}{\iint_{\Omega} S_{s.s}(\varphi,\chi)\,d\varphi d\chi}, \tag{14a}$$

where χ_o -- coordinate of the determined reradiator. In the particular case of $P_{oc} = o$, the coordinate distribution law (1) is symmetrical

with respect to χ and, therefore, the latter is an average coordinate of the instantaneous radar center of the target, i.e., $\langle\chi\rangle = \chi^*$. Its value in free space (i.e., $R_d = R_{dT} \to 0$) is equal to

$$\langle\chi\rangle = \chi_c^*,$$

and when an interface surface is present

$$\langle\chi\rangle = \frac{1}{1+R_d}(\chi_c^* + R_d\chi_s^*). \tag{15}$$

Since χ_s^* is always negative, it follows that the MRTs is shifted down due to the effect of the diffuse component of the average coordinate as compared to the case of free space by value, from (15)

$$\Delta\chi = -\frac{R_d}{1+R_d}(\chi_s^* - \chi_c^*). \tag{16}$$

For $P_{oc} \neq 0$, the value of $\langle\chi\rangle$ must be determined by numerical integration of (1); this case will be analyzed later. Substituting (9) and (10) into (3) we will obtain, taking into account equality

$$\iint_\Omega (\chi-\chi^*)^2 S(\varphi,\chi)\,d\varphi d\chi = \iint_\Omega \chi^2 S(\varphi,\chi)\,d\varphi d\chi - (\chi^*)^2 \iint_\Omega S(\varphi,\chi)\,d\varphi d\chi$$

the following expression for parameter μ_χ^2 :

$$(17)\qquad \mu_\chi^2 = \frac{\left[\mu_{c\chi}^2+(\chi_c^*)^2+(\chi_0)^2\frac{P_{0c}R_{d\tau}}{1+R_{d\tau}}+\mu_{s\chi}^2R_d(1+P_{0c})+(\chi_s^*)^2R_d(1+P_{0s})\right](1+R_{d\tau})}{1+(1+P_{0c})(R_d+R_{d\tau}+R_dR_{d\tau})}-(\chi^*)^2,$$

$$(17a)\qquad \mu_{c.s}^2 = \frac{\iint_\Omega(\chi-\chi_{c.s}^*)S_{c.s}(\varphi,\chi)\,d\varphi d\chi}{\iint_\Omega S_{c.s}(\varphi,\chi)\,d\varphi d\chi}.$$

For the azimuthal coordinates of the relationship, equivalents (14) - (17) are obtained by the simple replacement in the latter of variable χ by φ. Differences in results originate when special features of the angular energy spectrum are taken into account. In particular, for isotropic roughness in the interface surface, the energy spectrum with a point target is symmetrical with respect to plane $\varphi = \varphi^*$. Because of this $\langle\varphi\rangle = \varphi^*$, i.e., no shift occurs of the averaged coordinate of the MRTs. At $P_{oc} = o$, we obtain

$$(18)\qquad \mu_\varphi^2 = (\mu_{c\varphi}^2+\mu_{s\varphi}^2R_d)(1+R_d)^{-1}.$$

3. Quantitative Evaluation of Values

Thus, the calculation of statistical characteristics of angular coordinates with previous assumptions is reduced to finding parameters $M_{\varphi,\chi}, \varphi^*, \chi^*$ for the target proper and the interface surface. To establish the basic laws, we will evaluate the relationship between these parameters and the relationship berween quantitative distribution characteristic (1) and the route geometry and the value of R_d. In the calculations, we will assume a point target at height h, the same as that of the receiver, and lying in the coordinate plane (i.e., $\varphi^* = o$). The distribution law for the slopes of the irregularities we equally probably with maximum values of $\gamma_{max} = 0.1$. Calculation results of dependences of parameters $M_{s\varphi}, M_{s\chi}, |\chi_s^*|$ on the ratio of the height of the corresponding points to the distance D between them is shown in Fig. 2a. It may be seen from it that parameter χ_s^* (curve 1) is always greater than the angle if mirror reflection from the average plane (broken straight line), which indicates the prevailing role of the

half of the route nearest to the receiver. Parameter $\mu_{s\chi}$ (curve 2) remains almost unchanged in a wide range of h/D ratios, near their asymptotic value of 0.065. Parameter $\mu_{s\varphi}$ (curve 3) changes almost linearly with an increase in h/D from its initial value near $0.81/\gamma^2_{max}$. We will note that for a normal distribution law of irregularity slopes, the nature of the parameter changes remains the same as shown in Fig. 2a, and by selecting the effective value of the slopes properly, it is possible to obtain a good quantitative agreement. The relationship between $\mu_{s\varphi}$ and h/D makes it possible to make more precise the concept of "point target." If the following inequality is assumed as a criterion

$$\mu_{c\varphi} < (\mu_{c\varphi})_{min} \simeq 0{,}81\gamma^2_{макс},$$

then we will obtain for the angular size of the target, with an equally probably distribution of unit EPR along angle φ

$$\theta_\varphi = 2\sqrt{3}\mu_{c\varphi} < 2{,}8\gamma^2_{макс}.$$

For example, for $\gamma_{max} = 0.1$, $\theta_\varphi < 0.28$ mrad; obviously this condition is fulfilled for a wide class of targets.

Fig. 2b shows computer results of the values of $\Delta\chi$ (solid lines) of shifting in the angle of the place of the averaged position of the MRTs with respect to the direction to the target and $<|\tilde{\chi}|>$, which, as mentioned before, is a numerical scattering characteristic of the MRTs coordinates (broken lines). The calculation was made for the radar case at $P_{oc} = o$ (curves 1) and at $P_{oc} = \infty$ (curves 2), as well as for the case of a radiation source (curves 3) always assuming $R_d = R_{dT} = 0.2$. It may be seen from the figure that errors in measuring coordinates of an entirely "random target" (i.e., $P_{oc} = o$) exceed errors occurring in cases of determined reradiation by the target and the radiation source, while the shift in the averaged position of the MRTs differs most strongly (greater than three times). This law is preserved at least for $R_d \leq 0.5$, i.e., in the entire region of the actually observed values of the diffuse scattering coefficient. This may be seen in Fig. 3a which shows relationships between $\Delta\chi$ and $<|\tilde{\chi}|>$ and the value of R_d for cases of a fully random target (solid lines) and a radiation source (broken lines). Similar relationships for azimuthal coordinates are shown in Fig. 3b. Curves in Figs. 3a, b were plotted for h/D = 0.05, $\gamma_{max} = 0.1$.

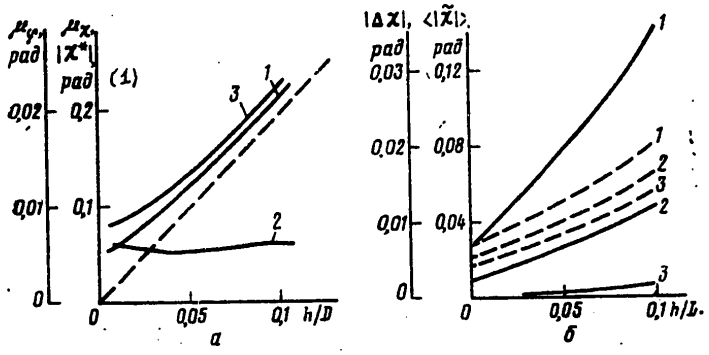

Fig. 2

1. rad

Fig. 3

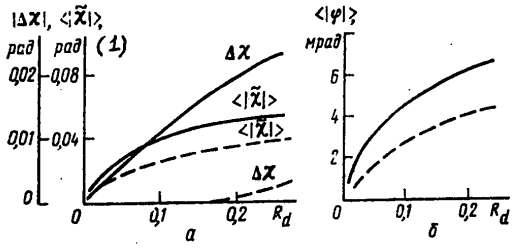

1. rad

Conclusions

Thus, the diffusion component of the field reflected by the interface surface is the reason not only for the instantaneous random deviations of the radar center of the "point target," but also for its average shift, which was not taken into account by the authors of the previous papers, in particular, of [2] . The value of errors, especially in the shift in the angular averaged position of the MRTs, changes considerably depending upon the powers of the determined and random components in the reradiation of the target. This means not only the necessity of taking into account the indicated target characteristic in calculated evaluations of errors, but also indicates certain limitations in experiemental methods of investigations, when the actual target is replaced by various kinds of imitations, in particular, by active responders or radiation sources.

BIBLIOGRAPHY

L. Kogan, I. M. "Theoretical Bases for Small Distance Radar, "Handbook Summaries of Science and Engineering. Radiotekhnika, vol. 13 pp 1-156, Izd. VINITI [All-Union Institute of Scientific and Technical Information] , 1976.

2. Barton, D. K. Proc. IEEE, 1974, 62, 6, 687.

3. Chayevskiy, Ye. V. Ukr. fiz. zh, 1968, 13, 4, 670.

4. Fal'kovich, S. Ye. "Evaluation of Signal Parameters," Izd. Sovetskoye radio, 1970.

5. Tikhonov, V. I. "Statistical Radio Technology," Izd. Sovetskoye radio, 1966.

6. Beckmann, P.; Spizzichino, A. "The Scattering of Electromagnetic Waves from Rough Surfaces," Oxford, Pergamon Press, 1963.

7. Bass, F. G.; Fuks, I. M. "Wave Scattering on a Statistically Rough Surface," Izd. Nauka, 1972.
[245-2291]

2291
CSO: 1860

UDC 621.396.965.4

CONSTRUCTION OF AN ELECTRONIC MODEL OF A MICROWAVE AIRCRAFT LANDING SYSTEM

Moscow RADIOTEKHNIKA in Russian No 6, 1979 pp 39-41 manuscript received 28 Oct 77

[Article by A.I. Nikitin]

[Text] Formulation of the Problem

The microwave landing system with beam scanning and time reading (MSP SLOV) operates in the data transmission channel time sharing (multiplexing) mode. The following data are transmitted to the aircraft in sequence over time: a) the position of the heading line and glide path in the direction of approach, b) the position of the heading line and glide path in a missed approach, c) the aircraft's bearing in the area of the airport, d) the position of the glide path for flattening out in landing and e) service information.

The MSP SLOV format represents a unified plan for space signals, making joint operation possible for a wide range of ground units and airborne equipment [1].

The transmitted information of the MSP format forms two alternating sequences which, for the purpose of improving noise rejection (eliminating synchronous interference), are separated at pseudo-random intervals. Data on each function of the system mentioned above in a) to e) are subdivided into preliminary (preamble) and main. The preamble contains information for identifying the function and the deviation scale factor, for selecting the airborne antenna, for tuning and calibrating the receiver, signs for "more to the left, more to the right" signals, etc. Preliminary information is coded by means of differential phase manipulation of a continuous carrier. Information in the main half is included in the time interval of $t_0 = t(\theta)$ between "back" and "forth" beam scanning signals received on board the aircraft (fig 1). Local objects (hangars, garages, aircraft at stations, refuelers, airfield equipment) in the effective area of a radio beacon cause re-echoed signals. Re-echoes take place also from the underlying surface.

The multibeam nature of the landing system's (SP's) channel exerts a considerable influence on its accuracy, i.e., on its classification category. The nature of the multibeam situation is determined by a considerable number of

factors specific to each individual airfield. In the process of designing new SP's an urgent problem is that of creating simulators of the actual radio engineering conditions of a landing channel for the purpose of estimating the degree of accuracy and noise immunity of airborne and ground equipment [1, 2].

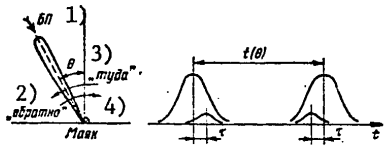

Figure 1.

Key:
1. BP [airborne subsystem]
2. "Back"
3. "Forth"
4. Beacon

Method of Modeling

The International Civil Aviation Organization (IKAO), in addition to flight tests of MSP's, has recommended that studies be conducted on modeling them [1]. A consolidated structural diagram of a modeling complex is shown in fig 2, where EIP is an electron re-echo simulator and BP MSP is the airborne MSP subsystem (receiver and automatic pilot). This model combines the merits of machine and semi-full-scale modeling. Among the merits of machine modeling can be named the high accuracy of computations and the ability to vary parameters of the airfield situation; among the merits of semi-full-scale modeling is the high speed of response and the ability as the result of this to monitor the airborne subsystem in real time. This modeling system makes it possible to realize a dynamic mode for the aircraft's approach for landing, taking into account the automatic pilot. The parameters of signals from the output of the electronic model of the MSP channel are determined by the computer on the basis of information entered into it on airfield conditions and of signals arriving on the space-time position of the aircraft. The processing of signals from the output of the MSP's airborne subsystem and comparison of their parameters with the assigned parameters make it possible to judge the influence of re-echoes in the MSP channel on the accuracy of the system.

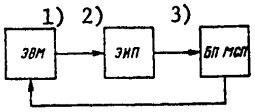

Figure 2.

[Key on following page]

Key:
1. Computer
2. EIP
3. BP MSP

Direct modeling of signals at the carrier frequency is not feasible, since because of the narrowband nature of signals all information is carried to the BP by means of double heterodyning to an intermediate frequency (PCh) without distortion. Modeling of only the envelope of the process excludes from consideration a substantial part of the BP--the logarithmic amplifier and detector. Modeling at the second PCh makes it possible to maintain the completeness of the investigation of the BP MSP and to preserve all informative traits of re-echoed and direct signals at its input [2, 3].

It is possible to improve the effectiveness of SP's by the optimal processing of re-echoed signals. It is obvious that the main difficulty in implementing this method of modeling involves constructing an electronic model of an MSP channel while taking into account the effect of re-echoes.

Electronic Simulator of MSP SLOV Re-Echoes

The direct signal in the input of the airborne receiver is described by the equation

$$u_{\text{пр}}(t) = U(t)\cos\omega_0 t, \tag{1}$$

where $U(t)$ is the signal's envelope and $\omega_0 = 2\pi f_0$ is the carrier frequency (for MSP SLOV, f_0 = 5 GHz).

In re-echoing from local objects or the underlying surface, the signal undergoes changes with respect to amplitude (p_i) and phase (ϕ_i). In addition, the direct and re-echoed signals have different Doppler increments ($\omega_{\text{д. пр}}$ and $\omega_{\text{д. отр}\,i}$) in frequency and are separated by time interval τ_i. At work in the input of the airborne receiver is an additive mixture of direct and reflected signals:

$$u_{\Sigma}(t) = U(t)\cos(\omega_0 + \omega_{\text{д. пр}})t + \sum_{i=1}^{n} p_i U(t-\tau_i)\cos[(\omega_0 + \omega_{\text{д. отр}\,i})t + \varphi_i]. \tag{2}$$

As can be concluded from (2), serving as modeling parameters are the reflection factor, the number of re-echoed signals, the Doppler frequency increments, the shape of the envelope, sudden changes in phase, ϕ_i, time shifts, τ_i, and also the time position of the signal in scanning, included in (2) in implicit form.

In fig 3 is given a functional diagram of an electronic simulator of MSP re-echoes, taking into account the following assumptions and conditions:

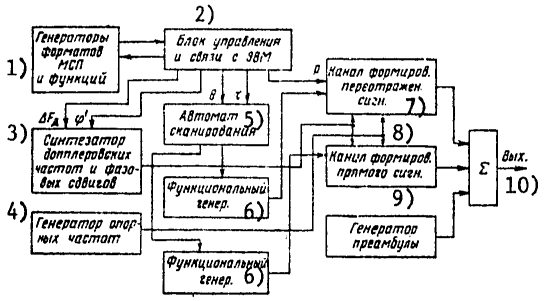

Figure 3.

Key:

1. MSP format and function generators
2. Unit for control and communication with the computer
3. Doppler frequency and phase shift synthesizer
4. Reference frequency generator
5. Automatic scanning unit
6. Function generator
7. Channel for forming re-echoed signal
8. Channel for forming direct signal
9. Preamble generator
10. Output

1. The number of re-echo factors within a beam equals one (which has been confirmed by the statistical analysis of the airfield situation at a number of USSR airfields). The number of re-echoes outside a beam can be specified at random.

2. The parameters of the model's signals reflect in the quantitative and qualitative respects the real radio engineering conditions of an MSP channel.

3. There is the capability of operating in combination with a computer and independently. The electronic simulator of MSP SLOV re-echoes represents a system for functional digital-analog processing of data according to an assigned algorithm [4, 5].

The sequence for the formation of output signals is determined by the format generator for the entire system and by function format generators for a specific kind of modeled signal. Communication between the model and the computer is accomplished by interrogation from the model, and in response to this from the computer in sequence through the communications unit codes for the parameters of modeled signals arrive and are recorded. Parameter codes can be assigned manually in the system's independent mode of operation.

The automatic scanning unit generates commands for triggering function generators for the envelope of MSP signals in keeping with codes for the angular position of direct and re-echoed signals. These function generators form an envelope according to the law employed for approximation of the directivity diagrams of the antennas of ground radio beacons.

The direct and re-echoed signals are formed in two separate channels. Information on the frequency ratios of direct and re-echoed signals with re-echoing inside the beam is contained in the difference (ΔF_d) of their Doppler components. The transfer of ΔF_d to the PCh is accomplished with intermediate conversion of the signal to 500 kHz. The value of the PCh is 10 to 25 MHz. The single sideband filtered by a band filter is modulated by the envelope signal, whereby the re-echoed signal is attenuated with an attenuator in keeping with the reflection factor code. The phase shift is introduced in the Doppler frequency synthesizer, representing a code-controlled frequency generator.

Conclusions

1. A model has been suggested for an MSP SLOV, according to the algorithm "Computer - EIP - BP MSP - Computer."

2. It is feasible to model MSP signals at the second PCh of the airborne receiver.

3. The utilization of this model in the planning stage makes it possible to select optimal methods of signal processing and to develop specifications for the MSP format; at the stage of testing and operating an MSP, the results of the joint operation of airborne equipment and the model in real time make it possible to evaluate the accuracy and noise immunity of the MSP to the effect of re-echoes.

Bibliography

1. "Analiz funktsionirovaniya mikrovolnovoy sistemy posadki. T. 1. Matematicheskiye modeli i ikh obosnovaniye" [Analysis of the Functioning of a Microwave Landing System. Vol 1. Mathematical Models and Their Substantiation], All-Union Center for Translations of Scientific and Technical Literature and Documentation, translation No Ts-91719, Moscow, 1976.

2. Talkin, A.P., Lapin, A.I. and Samoylov, A.G. "Modelirovaniye kanalov sistem svyazi" [Modeling of Communications System Channels], Moscow, Svyaz', 1979.

3. Korol'kov, G.V. ELEKTROSVYAZ', No 9, 1969.

4. Nikitin, A.I., Nikitin, O.R., Tararyshkina, L.I. and Fedorov, S.V. In "Povysheniye effektivnosti i nadezhnosti radioelektronnykh sistem" [Improving the Effectiveness and Reliability of Radio Electronic Systems], No 6, Leningrad, 1976.

5. Nikitin, A.I., Nikitin, O.R., Fedorov, S.V. and Chechetkin, V.D. "Avtomatizirovannyye sistemy upravleniya tekhnologicheskimi protsessami" [Automated Systems for Control of Technological Processes], Ryazan', RRTI, 1976.

[255-8831]

8831
CSO: 1860

UDC 621.396.967

ESTIMATION OF THE MAXIMUM EFFECTIVE RANGE OF A PULSED RADAR SET UNDER CONDITIONS OF RAIN

Moscow RADIOTEKHNIKA in Russian No 6, 1979 pp 31-33 manuscript received 24 Feb 78

[Article by V.N. Vetlinskiy]

[Text] In a number of applications (e.g., motor vehicle RLS's [radar sets]) it is necessary to detect and evaluate the parameters of both moving and stationary objects [1]. In these cases reflections from rain, which has a considerable complex dielectric constant, ε, unlike snow and dust, which are characterized by a low value of ε, limit the maximum effective range of a radar set.

In the published data [1-3] the reflecting properties of rain and the maximum effective range of an RLS, D_{pr}, are usually estimated on the basis of a Rayleigh approximation, which is valid with an RLS wavelength greater than the circumference of rain drops, $\lambda > \pi D_K$, where D_K is the diameter of a drop. The reflection properties of a great number of incoherently scattering elements are characterized by the reflection factor, η, representing the total effective scattering area (EPR) of a unit volume of space filled with scattering particles. The magnitude of η is determined as follows [2]:

$$\eta = \int_0^\infty n(\sigma)\,\sigma d\sigma = NM_\sigma.$$

where $n(\sigma)$ is the distribution law for the EPR of particles, σ; N is the number of particles in a unit volume; and M_σ is the mean value (MOZh) of the EPR of a particle.

In a Rayleigh approximation [2],

$$\eta = \frac{\pi^5}{\lambda^4}\left|\frac{\varepsilon+1}{\varepsilon-1}\right|^2 z.$$

For a drop of water,

is close to unity. With $t = 10°C$ and $\lambda = 10$ cm, $|K|^2 = 0.9313$.

The value of

$$z = \sum_{i=1}^{N} D_{ki}^6$$

is determined for rain from the experimentally gotten relationship $z = 200\rho^{1.6}$ in $мм^6/м^3$, where ρ is the intensity of rain in mm/h.

But the Rayleigh approximation is valid only in the range of centimeter or longer waves. Employing the distribution of sizes of water drops in rain of different intensity presented in [2], we determine the values of the mathematical expectations, $M_{D_K} = \Sigma D_K \rho(D_k)$, and the root mean square values, $\sqrt{D_{D_K}} = \sqrt{\Sigma(D_K - M_{D_K})^2 \rho(D_K)}$, of the dimensions of drops, where $\rho(D_K)$ is the discrete distribution of the diameter of drops. Computed values of M_{D_K} and $\sqrt{D_{D_K}}$ are given in the table.

Table

1) ρ, мм/ч	0,25	1,25	2,5	12,5	25	50	100	150
2) M_{D_K}, см	0,1	0,152	0,156	0,2	0,23	0,26	0,3	0,34
2) $\sqrt{D_{D_K}}$, см	0,038	0,058	0,066	0,076	0,085	0,1	0,105	0,11

Key:
1. mm/h
2. cm

Based on this table, curves have been plotted (fig 1) characterizing the boundaries of regions of different kinds of reflection as a function of the intensity of the rain and the wavelength.

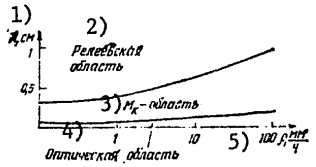

Figure 1.

Key:
1. λ, cm
2. Rayleigh region
3. M_K region
4. Optical region
5. ρ, mm/h

In the Mie (resonance) region with $1 < \pi D_K/\lambda < 10$, values of σ fluctuate with respect to the mean value of $M_\sigma = (\pi D_K^2/4)|K|^2$, and with an increase in D_K/λ the intensity of fluctuations is reduced. Since the variance in the dimensions of drops, characterized by $\sqrt{D_{D_K}}$, in the EHF wave band is commensurate with the wavelength, then in determining η in the optical and Mie regions it is possible to use the average value of

$$M_\sigma = \frac{\pi D_K^2}{4}|K|^2 \text{ и } M_\eta = \frac{\pi}{4}z|K|^2.$$

Utilizing expressions for the effective range of a pulsed RLS in free space and for the effective range of an RLS with a scattering cloud in the remote area of the antenna, we get the ratio of the signal power in the receiver's input, reflected from a target with an effective reflecting surface of σ_{ts} to the power reflected from the rain,

$$n = P_ц/P_д = 8A\sigma_ц/\pi D^2\lambda^2 c\tau\eta, \quad (1)$$

where A is the size of the antenna's aperture, σ_{ts} is the mean value of the target's EPR and τ is the length of the RLS's pulse.

Then the maximum range, D_{pr}, is determined from (1), with $n = n_п$, ensuring specific probability of detection and false alarm with a specific nature of fluctuations in the target's EPR,

$$D_{пр} = \frac{2}{\lambda}\sqrt{\frac{2A\sigma_ц}{\pi c\tau\eta n_п}}.$$

In motor vehicle, patrol and other radar sets, the permissible antenna aperture, A, is usually limited. Therefore, it is of interest to determine function $D_{pr} = f(\lambda)$ with $A = \text{const}$ and with rain of different intensity.

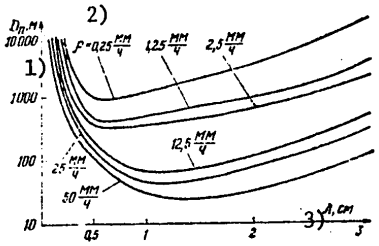

Figure 2.

Key:
1. D_{pr}, m
2. mm/h
3. λ, cm

In fig 2 is plotted the relationship $D_{pr} = f(\lambda)$ when $A = 0.1\ m^2$, $\sigma_{ts} = 5\ m^2$, $\tau = 0.1\ \mu s$ and $n_n = 10$. The values gotten for D_{pr} are valid on the condition that the energy parameters of the RLS make possible values of the detection range exceeding D_{pr} taking into account attenuation in the atmosphere and rain.

On the basis of the relationships obtained, it is possible to conclude that there is a value of $\lambda = \lambda_m$ at which D_{pr} is minimal.

With an increase in the intensity of the rain the value of $\lambda = \lambda_m$ shifts into the region of longer wavelengths, which is associated with an increase in the size of rain drops and a reduction of the region in which the Rayleigh approximation is valid.

Bibliography

1. Grims and Dzhons. TIIER, No 6, 1974.

2. "Spravochnik po radiolokatsii" [Radar Handbook], Vol 1, Moscow, Sovetskoye Radio, 1976.

3. Shirman, Ya.D. et al. "Teoreticheskiye osnovy radiolokatsii" [Theoretical Fundamentals of Radar], Moscow, Sovetskoye Radio, 1970.

8831
CSO: 1860

UDC 621.391

SUPERFAST SPECTRAL CONVERSION BY MEANS OF HAAR FUNCTIONS

Kiev IZVESTIYA VYSSHIKKH UCHEBNYKH ZAVEDENIY: RADIOELEKTRONIKA in Russian No 7, 79 signed to press 7 Mar 78; after revision, 9 Nov 78 pp 86-89

[Article by G. D. Tolstykh]

[Text] Below are considered algorithms for fast spectral conversion by means of Haar's functions (BPKh) that eliminate multiplication and reduce addition and subtraction considerably compared to algorithms of fast conversion by means of Walsh functions [BPU].

We will define Haar's sign functions on semisection (0, 1) as follows:

$$H_0(t) \equiv 1,$$

$$H_\alpha(t) = \begin{cases} +1 \text{ for } t \in \left[\alpha - \frac{1}{2^m};\ \alpha\right), \\ -1 \text{ for } t \in \left[\alpha;\ \alpha + \frac{1}{2^m}\right), \\ 0 \text{ at remaining points.} \end{cases} \qquad (1)$$

where α is a dual fraction; m is number of orders of α.

Haar's functions defined in this way are orthogonal, but are not normalized. We will take normalizing into account in summing spectral coefficients.

A signal may be represented by a spectrum for H_α (t) as follows:

$$U(t) = b_0 + \sum_\alpha 2^{m-1} b_\alpha H_\alpha(t), \qquad (2)$$

where

$$b_\alpha = \int_0^1 U(t)\, H_\alpha(t)\, dt.$$

Functions $H_\alpha(t)$ may be arranged with respect to α in three ways: arrange the dual fractions of α in the natural order of increasing; arrange α in the order of increasing the inverted code; group α in groups with the number of orders after the comma 1, 2, 3 etc., while within the group arrange the fractions in the order of increasing.

Like the arrangement of Walsh functions, we will call the first the Adamar arrangement, the second -- the dyad and the third -- the classical arrangement. Haar's functions in the Adamar arrangement are shown in Fig. 1a and in the dyad arrangement -- in Fig. 1b.

The Adamar arrangement of Haar's functions leads to the most optimal BPKh algorithms, but it is inconvenient to use spectra in the Adamar arrangement because, in such spectra, uniform convergence of partial sums is not provided for continuous functions, which are usually considered as signals.

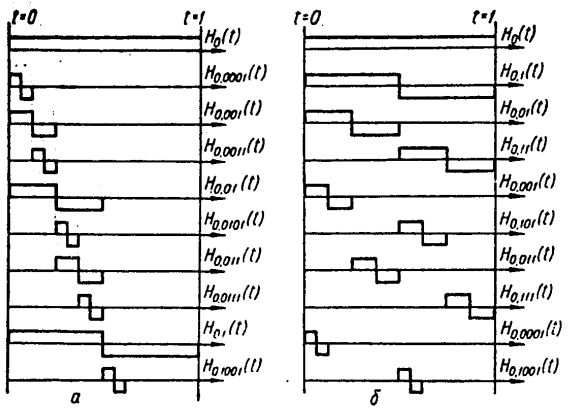

Fig. 1

As shown in [1], an approximation of continuous signals by partial sums of the spectrum is provided by the classical arrangement of Haar's functions. Since the dyad arrangement differs from the classical one only by the arrangement of functions within the groups, it also has this property. The dyad arrangement of Haar's functions provides greater uniformity of approximation because dropping the members of a series occurs not from one side, but uniformly in the entire determination region (Fig. 1b).

Whether Haar's functions belong to group (dyad) number m is determined by the number od digits after the comma in index α, equal to m. Each Haar's function of dyad m assumes nonzero values in the $\frac{1}{2}^{m-1}$ part of semisection (0, 1).

The requirements for fast spectral conversion algorithms consist, first of all, of the number of operations being minimal, simplicity of each operation and a minimum required volume of the internal memory.

In [2] BPU and PBKh algorithms were compared with respect to the number of addition-subtraction operations. While in the BPU algorithms $n.2^n$ addition-subtraction operations are required for spectral processing of the group of 2^n values of the initial signal, in the BPKh algorithms the required number of operations is reduced to $2(2^n-1)$. On this basis, it is proposed in [2] to use the PBKh algorithm for calculating the spectrum for Walsh functions with the following change to the spectrum for Walsh functions. The total number of operations in this case is found to be smaller than in the direct use of the BPU algorithm. In this paper, the BPKh algorithm in classical form was considered.

The Adamar arrangement of Haar's functions makes it possible to design a BPKh algorithm that does not require transactions at intermediate spectrum conversions which leads to considerable saving in internal memory. This algorithm is shown in Fig. 2. Data at each intermediate conversion step is taken from each pair of cells and the results are sent to the same pair of cells. The results of an elementary operation with a pair of values are their half-sum and half-difference. Summing is designated on the graphs by a solid line and subtraction by a broken line.

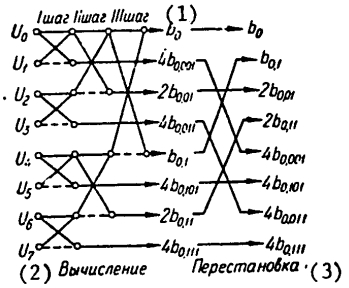

Fig. 2

1. Step
2. Calculation
3. Transposition

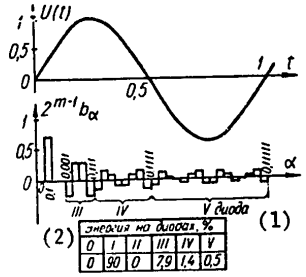

Энергия на диодах, %					
0	I	II	III	IV	V
0	90	0	7,9	1,4	0,5

Fig. 3

1. Dyad
2. Power on dyads, percent

The calculation of the half-sum and half-difference does not complicate the elementary operation because it is reduced to a shift. As a result of the calculation at each step of half-sums and half-differences, the spectral coefficients are obtained with normalizing multipliers, as is required in (2).

After calculating coefficients in Adamar's arrangement, they may be positioned in a dyad order. As shown in Fig. 2, this requires making a pair-by-apir transposition of coefficients.

Signal U(t) - sinπ t and its spectrum in Haar's functions in the dyad arrangement are shown in Fig. 3 as an example of spectral expansion. As the dyad number increases, i.e., with the decrease in the region of non-zero values of Haar's functions, spectral coefficients decrease. This is characteristic for the majority of signals used in practice.

When using spectral representations in approximation problems or in analyzing the analog-digital structures, it is possible to determine the root-mean-square error of representing a signal by the limited spectrum of Haar's functions. For a given determination of Haar's functions, Parseval's equation can be obtained from (2) by squaring and integrating over the (0, 1) half-section

$$\int_0^1 U^2(t)\,dt = \sum_\alpha \frac{(2^{m-1}b_\alpha)^2}{2^{m-1}} = \sum_\alpha 2^{m-1}b_\alpha^2.$$

The root-mean-square approximation error is

$$\delta = \sqrt{\int_0^1 U^2(t)\,dt - \sum_{\alpha=0}^{\alpha_k} 2^{m-1}b_\alpha}.$$

It is interesting to note the obvious property of spectral representation of the Walsh and Haar functions, which once more confirms the close relationship between these two systems of spectral decomposition. The accuracy of approximation of 2^k by Walsh and Haar functions is the same because the stepped functions of partial sums obtained in this case coincide.

Frequently for spectral evaluations, it is sufficient to indicate the accuracy of approximation of 2^k by Walsh and Haar functions for values of k. Then it is possible to calculate the power sums of spectral components from the dyads of the spectrum without using spectral coefficients. Such a calculation for the spectrum U(t) = sin $2\pi t$ is shown in Fig. 3.

The method considered above of spectral analysis using Haar's functions can be generalized naturally for a multidimensional case. Actually, a multidimensional Haar's function is defined as a product of single-dimensional functions, each of which depends only on its own coordinate

$$H_{\alpha,\beta}(t, U) = H_{\alpha}(t) H_{\beta}(U).$$

The problem of arranging multidimensional functions in accordance with dyads is solved exactly in the same way as for the single dimensional case. Dyad number m contains all the Haar functions that have non-zero values in the $\frac{1}{2}^{m-1}$ part of the multidimensional region of determination of Haar's functions, limited by (0.1) half-sections for all coordinates. True, the problem on the distribution of multidimensional functions within the dyads remain open. However, this problem will hardly have great practical importance because, in the multidimensional case, the number of spectral coefficients increases to the degree of the number of measurements. Therefore, a direct analysis of multidimensional spectrum coefficients is hardly worthwhile.

To evaluate spectra in the multidimensional case, it is necessary to utilize power evaluations over various spectral regions, in particular, over dyads. Even in the two-dimensional case, when it is still possible to represent the spectrum in a plane in the form of a matrix, power evaluation by dyads is much clearer than direct consideration of the spectrum.

The algorithm for fast spectral conversion for the multidimensional case may be obtained by successive use of a single dimensional algorithm, the first time along one coordinate (for example, lines), then the same algorithm is used for the second coordinate (columns), etc. for all coordinates [3].

In multidimensional problems advantages show up especially clearly of the minimal number of BPKh operation compared to all other fast spectral conversion algorithms, because the mass of input data increases considerably in the other algorithms. This fact prompted the turning of attention to the Haar functions.

It may be expected that in the very near future, the development of multidimensional spectral analysis will make it possible to solve many problems related to the analysis of analog-digital devices, facsimile transmission and holography where the very statement of the problem prompts its solution by multidimensional means, in particular, spectral.

BIBLIOGRAPHY

1. Sobol', I. M. "Multidimensional Quadratic Formulas and Haar's Functions." Moscow, "Nauka," 1969.

2. Fayn. "Relationships between Haar, Walsh and Adamar Conversions," TIEER, 1972, No 5.

3. Trakhtman, A. M.; Trakhtman, V. A. "Principles of the Theory of Discrete Signals on Finite Intervals." Moscow, SOVETSKOYE RADIO, 1975

[269-2291]

2291
CSO: 1860

- END -